A least invasive method to estimate the residual strain capacity of steel reinforcement in earthquake-damaged buildings

Giuseppe Loporcaro

A thesis submitted in partial fulfilment of the requirements for the Degree of
Doctor of Philosophy in Earthquake Engineering
at the University of Canterbury
Christchurch, New Zealand
May 2017

A mamma e papà

“I have no special talent. I am only passionately curious” Albert Einstein

ABSTRACT

Capacity design and hierarchy of strength philosophies at the base of modern seismic codes allow inelastic response in case of severe earthquakes and thus, in most traditional systems, damage develops at well-defined locations of reinforced concrete (RC) structures, known as plastic hinges. The 2010 and 2011 Christchurch earthquakes have demonstrated that this philosophy worked as expected. Plastic hinges formed in beams, in coupling beams and at the base of columns and walls. Structures were damaged permanently, but did not collapse.

The 2010 and 2011 Christchurch earthquakes also highlighted a critical issue: the reparability of damaged buildings. No methodologies or techniques were available to estimate the level of subsequent earthquakes that RC buildings could still sustain before collapse. No repair techniques capable of restoring the initial condition of buildings were known. Finally, the cost-effectiveness of an eventual repair intervention, when compared with a new building, was unknown. These aspects, added to nuances of New Zealand building owners' insurance coverage, encouraged the demolition of many buildings.

Moreover, there was a perceived strong demand from government and industry to develop techniques for assessing damage to steel reinforcement bars embedded in cracked structural concrete elements. The most common questions were: "Have the steel bars been damaged in correspondence to the concrete cracks?", "How much plastic deformation have the steel bars undergone?", and "What is the residual strain capacity of the damaged bars?" Minimally invasive techniques capable of quantifying the level and extent of plastic deformation and residual strain capacity are not yet available. Although some studies had been recently conducted, a validated method is yet to be widely accepted.

In this thesis, a least-invasive method for the damage-assessment of steel reinforcement is developed. Based on the information obtained from hardness testing and a single tensile test, it is possible to estimate the mechanical properties of earthquake-damaged rebars. The reduction in the low-cycle fatigue life due to strain ageing is also quantified.

The proposed damage assessment methodology is based on empirical relationships between hardness and strain and residual strain capacity. If damage is suspected from in situ measurements, visual inspection or computer analysis, a bar may be removed and more accurate hardness measurements can be obtained using the lab-based Vickers hardness methodology. The Vickers hardness profile of damaged bars is then compared with calibration curves (Vickers hardness versus strain and residual strain capacity) previously developed for similar steel reinforcement bars extracted from undamaged locations.

Experimental tests demonstrated that the time- and temperature-dependent strain-ageing phenomenon causes changes in the mechanical properties of plastically deformed steels. In particular, yield strength and hardness increases, whereas ductility decreases. The changes in mechanical properties are quantified and their implications on the hardness method are highlighted.

Low-cycle fatigue (LCF) failures of steel reinforcing bars have been observed in laboratory testing and post-earthquake damage inspections. Often, failure might not occur during a first seismic event. However, damage is accumulated and the remaining fatigue life is reduced. Failure might therefore occur in a subsequent seismic event. Although numerous studies exist on the LCF behaviour of steel rebars, no studies had been conducted on the strain-ageing effects on the remaining fatigue life. In this thesis, the reduction in fatigue life due to this phenomenon is determined through a number of experimental tests.

Acknowledgments

Firstly, I would like to acknowledge my supervisors Professor Milo Kral and Professor Stefano Pampanin, for the great opportunity given and for their constant feedback and motivation throughout the period of this research. I also would like to thank the late Professor Les Erasmus for the many helpful discussions, and Professor Normal Dowling from Virginia Tech for his unevaluable assistance during the low-cycle fatigue experimental tests.

I would like to express my gratitude to the Natural Hazards Research Platform and MBIE Building System Performance Branch for the financial support through the SAFER Structures Research Project. Also, I would like to thank Pacific Steel and Bruce Roberts for providing the steel rebars used in this research.

Assistance from the administration staff from both Mechanical and Civil and Natural Resources departments was highly appreciated. Special thanks to Linda Forbes, Annie Homewood and Elizabeth Ackermann for their great and professional assistance they provide to all the PhD students. I would like to acknowledge the Mechanical engineering technical staff, in particular Kevin Stobbs, Bruce Robertson, Scott Amies, Ken Brown, David Read, Paul Southward, Adam Latham and Mike Flaws. Thanks also to Joan Gladwyn for the thesis proofreading.

Special thanks to all the members of the Materials Engineering group (MEG). Thanks to my numerous officemates, colleagues and flatmates. Special thanks to Alberto Cuevas, Aaron Beardsley, Gabriele Granello, Claudio Cappellaro, Royce Liu, Adnan Rais, Karim Tarbali, Danilo Moretti, Mimmo Sclofani, Alessandro Palermo, and to Giulia, Emma, Erin and Fabio Parodi. I would like to thank the friends I met over the years in Christchurch, and those back in Italy.

A big thanks to my parents and brothers, I cannot imagine how hard must be for you to have me so far away. The biggest thanks to Chiara for the everyday support and love, we shared this journey together, without her this thesis would not have been possible.

Table of Contents

List of figures

List of tables

1 INTRODUCTION

1.1 RESEARCH MOTIVATION

1.1.1 Research project on residual capacity and repair technique

On 4 September 2010, the city of Christchurch, in Canterbury, New Zealand, was hit by a 7.1M_w earthquake. This event was followed by another, more devastating, earthquake on 22 February 2011. During this second seismic event, 185 people lost their lives (CERC, 2012a).

In the Central Business District (CBD) two reinforced concrete buildings collapsed, and many others were damaged to different extents. From an engineering point of view, many buildings performed as expected: damage concentrated in critical locations known as plastic hinges, which prevented collapse (Kam, Pampanin, & Elwood, 2011). The life safety target was achieved. Modern codes and the performance-based design objective matrix (Fig. 1-1) define as the life safety target required for "ordinary" buildings, a minimal life risk for building occupants in the event of a rare earthquake (SEAOC, 1995). Therefore, if minimum standard design is employed, damage is expected in the plastic hinge locations.

The Canterbury earthquakes highlighted a critical issue that emerged during the post-earthquake stage: the repairability of damaged buildings. No guidelines, methodologies or techniques could estimate the level of subsequent earthquakes that the reinforced concrete (RC) buildings could still sustain before collapse. No repair techniques were known to restore the initial condition of the buildings. Finally, the cost-effectiveness of an eventual repair intervention, compared with a new building, was unknown. These aspects, added to nuances of New Zealand building owners' insurance coverage, encouraged the demolition of many buildings.

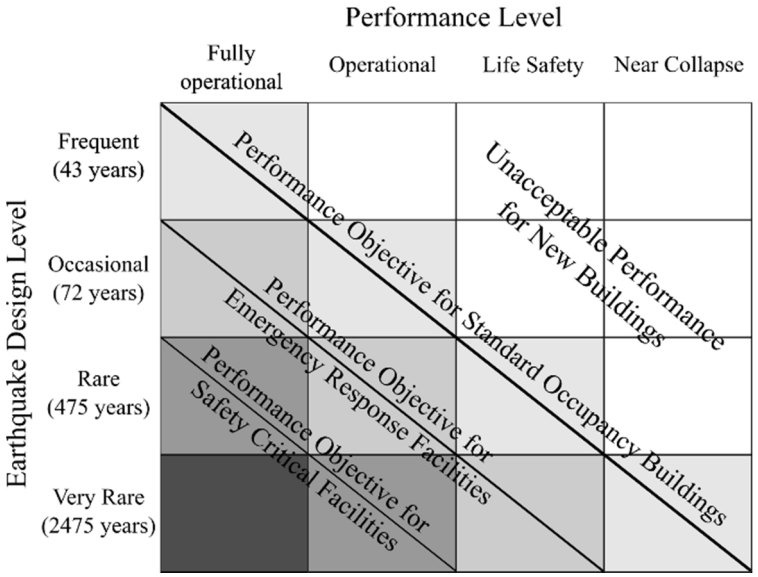

Fig. 1-1 Seismic performance-based design objective matrix as defined by the SEAOC Vision 2000 PBSE guidelines (SEAOC, 1995)

A residual capacity and repair technique project was conceived within this context. The wider residual capacity research project, known as "SAFER (Significant Advances for Earthquake Resistant) Concrete technology" (S. Pampanin et al., 2015), was funded by the Natural Hazard Research Platform (NHRP) and the Ministry of Business, Innovation and Employment. The main objective for the SAFER project is to provide end users, such as practitioner engineers, owners, territorial authorities and insurers, with guidelines for the assessment of the residual capacity of earthquake-damaged RC buildings, and the evaluation of the cost-effectiveness of repair techniques during the decision-making phase, post-earthquake.

At the University of Canterbury, three PhD students are contributing to the SAFER residual capacity project: Alberto Cuevas, who is investigating the residual capacity of RC frames, with a particular emphasis on beam-column joints and their fatigue life (Cuevas, 2013; Cuevas & Pampanin, 2016, 2017); Amir Malek, who is studying the seismic residual capacity of RC frames (Malek, 2014; Malek, Scott, Pampanin, & MacRae, 2015; Malek, Scott, Pampanin, MacRae, &

Hoult, 2016), focusing his interest on techniques to quantify the concrete degradation during a seismic event; and the author of this thesis, who investigated the residual strain capacity of damaged steel reinforcement (using hardness as a key parameter), and the detrimental effects of strain ageing on the monotonic and cyclic properties of steel reinforcing bars.

1.1.2 Canterbury Earthquake Royal Commission (CERC)

In April 2011, after the catastrophic collapse of the CTV and PGC buildings, the significant damage of many buildings in the Christchurch CBD, and 185 fatalities, the Canterbury Earthquake Royal Commission (CERC) was established. Operating from April 2011 to November 2012, the CERC inquiry delivered a final report in stages, divided into three parts and seven volumes, containing information about the performance of Christchurch buildings and recommendations to prevent or minimise the collapse of buildings due to earthquakes (CERC, 2012a). Section 8.1 of Volume 2 discusses the issue of strain ageing and strain level assessment in steel reinforcing bars. The testing method described for strain assessment is the Leeb hardness method. Leeb hardness measurements are conducted along the longitudinal length of the bar and then correlated to strain levels. The method aims to assess the extent of the plastic strain and the peak strain level in individual reinforcement bars.

The analysis of the Leeb hardness tests broached the critical issue that reinforcing bars crossing significant concrete cracks might not have sufficient residual strain capacity to sustain additional plastic deformation in subsequent earthquakes. This critical condition could be encountered in walls and plastic hinge zones of beams with a single large crack or widely-spaced cracks, and in wide cracks in floors (CERC, 2012b).

1.1.3 Residual strain capacity of steel reinforcing bars

It was deemed highly desirable to develop a practical technique to estimate the level of plastic deformation generated in steel reinforcement. The Leeb hardness method was quickly conceived and extensively employed immediately after the Christchurch earthquakes to estimate plastic deformation and to predict residual strain capacity ductility before fracture (Allington, 2011). However, no peer review articles or scientific publications exist in the open literature vetting the validity of the Leeb hardness residual capacity test method. Therefore, a comprehensive investigation including the method's advantages and limitations was required. Any method developed for residual capacity must be accepted widely to be useful.

Ideally, structural engineers who are called to assess the damage of RC structures would have access to a simple tool, able to identify the locations and extent of plastic deformation in steel reinforcing bars. Furthermore, such a tool would also supply mechanical properties, including yield stress and uniform elongation of the damaged region of the steel bars. Yield stress and uniform elongation are required in FEM (Finite Element Model) software to model the mechanical behaviour of the steel reinforcement. Therefore, updated steel mechanical properties are fundamentally important to analyse the residual ductility of RC structural elements and structures at the global and local levels. The motivation of this research is to fill the current gap in the literature and provide a reliable methodology that enables an estimation of the damage to the steel reinforcement and prediction of its residual ductility.

1.2 SCOPE AND RESEARCH QUESTIONS

The scope of this research is to propose a reliable, useful and least-invasive method to identify the location and extent of plastic deformation in steel reinforcing bars and predict the residual strain capacity using hardness as a key parameter. The results obtained by the method are intended to allow users to take informed decision upon the reparability of reinforced concrete structures.

The following research questions were formulated to design the methodology:

- What is the appropriate (available at the University of Canterbury (UC) engineering laboratories) hardness testing method in terms of practicality and measurement accuracy for the scope of this research?
- If hardness increases with plastic deformation, does this increase follow a specific pattern? Is this pattern predictable?
- Can hardness be used as a key parameter to identify steel damage?
- Can a unique relationship between hardness and plastic deformation be obtained for steels of similar grade?
- Can strain ageing affect the hardness and the residual ductility of steels? What is the impact on the hardness method?
- During earthquakes, steel reinforcing bars are subjected to reverse cyclic loading history. Do the number of cycles affect the hardness of steel?
- Does strain ageing also affect the fatigue life of steel reinforcing bars (rebars)?

1.3 HYPOTHESIS AND OBJECTIVES

To answer the research questions, a number of experiments were planned. Several objectives were set for each experiment:

a) Determine the most practical and accurate, within the range under investigation, hardness testing tool among those available at the UC laboratories. These are the static indentation Vickers and Rockwell hardness machines, and rebound Leeb hardness portable machine (Proceq Equotip).

b) Establish a standardised method to develop calibration curves for hardness versus pre-strain, and residual strain capacity versus hardness.

c) The calibration curves for hardness versus pre-strain, and residual strain capacity versus hardness developed monotonically might vary if the samples are previously subjected to a number of cycles. Quantify the effects of the number of cycles on the steel calibration curves.

d) The protrusions on the deformed bars, known as ribs, can represent stress concentrations points and might cause localised plastic strain. Quantify the increase in hardness observed at the root of the ribs and propose recommendations for hardness testing on steel rebars.

e) Determine and quantify the strain-ageing effects, in terms of change in mechanical properties, including hardness, for Grade 300E steel. Propose recommendations to allow for the change in mechanical properties of the damaged steel reinforcement.

f) Because of a vanadium content higher than 0.06% by mass, Grade 500E steel is unlikely to be prone to strain ageing at temperatures below 150°C. No changes in mechanical properties are expected. Verify whether this hypothesis is true and discuss implications on the hardness method.

g) Quantify and compare the changes in mechanical properties caused by natural strain ageing at 15°C and "accelerated" strain ageing at 100°C, using Hundy's relationship (Hundy, 1954).

h) While carbon atoms in Grade 500E do not cause any strain-ageing effects at temperatures below 150°C, changes in mechanical properties are also expected at higher temperatures. Determine and quantify the strain-ageing effects of Grade 300E and 500E when aged at 200°C.

i) Design and apply the "hardness method" to reinforced concrete buildings damaged during the 2010 and 2011 Canterbury earthquakes.

j) Develop a strain–life curve for Grade 300E steel and determine the change in the fatigue life caused by strain ageing. Use strain–life models to fit the experimental results.

1.4 THESIS OUTLINE

Chapter 2 summarises the research background of the thesis. A literature review of five main topics is presented. A summary of the 2010 and 2011 Canterbury earthquakes is included. Properties, features and production of New Zealand manufactured steel reinforcement are described. An important part of the chapter is dedicated to the hardness of metals: definitions, methodologies and relationships with other mechanical properties are discussed. The strain-ageing phenomenon and its implications on seismic design are discussed. Finally, an introduction to the low-cycle fatigue behaviour of metals and the analytical methods available to predict the fatigue life are presented.

In Chapter 3 the relationship between hardness and plastic strain is investigated. After a short introduction to the testing facilities available at the University of Canterbury, the experimental testing is presented and the results discussed. Different hardness methodologies are compared to find the most suitable technique. A standard procedure is devised, aimed at developing empirically-based mathematical relationships between Vickers hardness (HV) and pre-strain, and between residual strain capacity and Vickers hardness. Recommendations for hardness testing on rebars are proposed. Sections of this chapter were presented at the New Zealand Society of Earthquake Engineering (NZSEE) 2014 conference in Auckland. The paper title is: “Investigating the relationship between hardness and plastic strain in reinforcing steel bars” (Loporcaro, Pampanin, & Kral, 2014). A section of this chapter is also included in a paper submitted to the *ASCE Journal of Structural Engineering* currently under the second review process.

The effects of cyclic plastic deformation on the hardness of Grade 300E steel is discussed in Chapter 4. Constant strain-amplitude tensile tests are conducted on 12-mm diameter unmachined rebar samples. Calibration curves (HV versus pre-strain, and residual strain capacity versus HV)

for monotonically and cyclically deformed steel specimens are compared. The effects of number of cycles on hardness is quantified. Results of this chapter were briefly presented at the 1st Quakecore Annual meeting in Taupo (2016). The poster title is "Residual strain capacity of earthquake damaged reinforcing bars: damage assessment and remaining ductility prediction through Vickers hardness testing".

In Chapter 5, an introduction to the state of the art current hardness method is presented. The proposed method is then illustrated and applied to a number of buildings belonging to the Christchurch City Council (CCC) assets. An alternative and simplified methodology is also presented. The current limitations and suggestions for improvements conclude the chapter. Significant findings described in this chapter were presented at the NZSEE 2015 conference in Rotorua. The paper title is "Experimental validation of 'the hardness method' to estimate the residual ductility of plastically deformed steel reinforcement" (Loporcaro, Kral, & Pampanin, 2015). A subsequent paper, based on this chapter, was prepared and presented at the 16th World Conference of Earthquake Engineering (WCEE) in Santiago (Chile) as "A case study: application of the hardness method to estimate the residual capacity of reinforcement in an earthquake damaged building" (Loporcaro, Kral, & Pampanin, 2017). The paper submitted to the *ASCE Journal of Structural Engineering* (currently under review) also contains material from this chapter.

The effects of strain ageing on Grade 300E and Grade 500E steel are illustrated in Chapter 6. Results are presented from experimental tests conducted on the above-mentioned steel grades aged at 100°C. Changes in mechanical properties are quantified. Natural (at 15°C) and "artificial" (at 100°C) strain-ageing effects are compared. In conclusion, strain-ageing effects due to interstitial carbon atoms (at 200°C) are presented. Sections of this paper were presented at the NZSEE 2016

conference in Christchurch. The paper title is “Comparison between accelerated and natural strain ageing effects on New Zealand manufactured Grade 300E steel reinforcing bars” (Loporcaro, Pampanin, & Kral, 2016).

In Chapter 7, a least-invasive method, based on a universal calibration curve, is proposed and applied to Grade 300 steel rebars. The method has the advantage to reduce test invasiveness, time and costs. Only baseline and peak Vicker hardness and a baseline stress-strain curve are required to estimate lower yield strength, plastic deformation and residual strain capacity of earthquake-damaged rebars.

In Chapter 8, the low-cycle fatigue behaviour of reinforcing steel is discussed. Strain-controlled cyclic tests were performed and results are presented. A strain–life curve for Grade 300E steel is obtained and fitted using strain–life models. The fatigue-life loss due to the strain-ageing phenomenon was quantified. A paper based on this chapter will be submitted to the *ASCE Journal of Materials in Civil Engineering*.

In Chapter 9, final conclusions and recommendations for future studies are presented.

1.5 REFERENCE

Allington, C. (2011). *Materials testing in buildings of interest. Gallery Apartments, Westpac centre, IRD building.* (Report 107267-1 (v1.1) prepared for royal commission). Retrieved from HolmesSolution, Christchurch:

CERC. (2012a). *Final Report. Volume 1.The performance of Christchurch CBD buildings.* Retrieved from

CERC. (2012b). *Final Report. Volume 2: The performance of Christchurch CBD buildings.* Retrieved from

Cuevas, A. (2013). PhD research proposal. Seismic residual capacity of reinforced concrete frames. University of Canterbury.

Cuevas, A., & Pampanin, S. (2016). *Preliminary experimental and numerical inverstigation on the seismic residual capacity of reinforced concrete beam-column joints*. Paper presented at the The New Zealand Concrete Industry Conference 2016, Auckland.

Cuevas, A., & Pampanin, S. (2017). *Post-seismic capacity of damaged and repaired reinforced concrete plastic hinges extracted from a real building*. Paper presented at the 16th World Conference on Eartquake Engineering, Santiago Chile.

Hundy, B. B. (1954). Accelerated Strain Ageing of Mild Steel. *Journal of The Iron and Steel Institute, 178.*

Kam, W. Y., Pampanin, S., & Elwood, K. (2011). Seismic performance of reinforced concrete buildings in the 22 February Christchurch (Lyttelton) earthquake. *Bulletin of the New Zealand Society for Earthquake Engineering, 44*(4), 239-278.

Loporcaro, G., Kral, M. V., & Pampanin, S. (2015). *Experimental validation of "the hardness method" to estimate the residual ductility of plastically deformed steel reinforcement*. Paper presented at the NZSEE conference, Rotorua.

Loporcaro, G., Kral, M. V., & Pampanin, S. (2017). *A cause study: application of the hardness method to estimate the residual capacity of reinforcement in an earthquake damaged building*. Paper presented at the 16th World Conference of Earthquake Engineering, Santiago de Chile.

Loporcaro, G., Pampanin, S., & Kral, M. V. (2014). *Investigating the relationship between hardness and plastic strain in reinforcing steel bars*. Paper presented at the NZSEE conference, Auckland.

Loporcaro, G., Pampanin, S., & Kral, M. V. (2016). *Comparison between accelerated and natural strain ageing effects on New Zealand manufactured Grade 300E steel reinforcing bars*. Paper presented at the NZSEE, Christchurch.

Malek, A. (2014). PhD research proposal. Residual seismic capacity of reinforced concrete members. University of Canterbury.

Malek, A., Scott, A., Pampanin, S., & MacRae, G. (2015). *Assessment of post-earthquake in RC elements using low-invasive techniques.* Paper presented at the New Zealand Society of Earthquake Engineering 2015, Rotorua, New Zealand.

Malek, A., Scott, A., Pampanin, S., MacRae, G., & Hoult, N. A. (2016). *Damage assessment of RC beam using distributed fibre optics strain sensors.* Paper presented at the New Zealand Society of Earthquake Engineering 2016, Christchurch, New Zealand.

Pampanin, S., Cuevas Ramirez, A., Kral, M. V., Loporcaro, G., Scott, A., & Malek, A. (2015). *Residual capacity and repairing options for reinforced concrete buildings*. Retrieved from

SEAOC. (1995). *Vision 2000 committee. Performance-based seismic engineering of buildings*. Retrieved from Sacramento, California:

2 LITERATURE REVIEW

The scope of this thesis investigation lies in the common ground shared by the structural and mechanical (or metallurgy) engineering fields. Some of the topics discussed might be more familiar to structural engineers; others, to mechanical engineers. In this literature review, basic concepts from both disciplines, required to understand the key aspects of the thesis, are reviewed. This will help the reader to understand the main topics discussed in the thesis.

As introduced in Chapter 1, the Christchurch 2010 and 2011 earthquakes highlighted the limits of the traditional earthquake engineering design concerning the post-quake assessment of damaged reinforced concrete (RC) buildings, and the estimation of their residual capacity. This is the ability of structures to withstand subsequent aftershocks before collapse. Therefore, the chapter starts with an overview of the Christchurch seismic events and the damage observed on the RC structures. The concepts of capacity design and hierarchy and its implications on the steel's properties are reviewed. Mechanical properties and the manufacturing process of steel reinforcing bars are presented. Experimental tests on rebars extracted from buildings constructed in New Zealand throughout the twentieth century are discussed later in the thesis; therefore a brief summary of the historical steel material codes is presented. Finally, the three most important topics of this research are reviewed: hardness, strain ageing and low-cycle fatigue. Hardness is the key parameter on which the methodology developed is based; strain ageing is a phenomenon that affects the mechanical properties of some steel grades that have been previously plastically deformed; and low-cycle fatigue is a failure mode often observed during post-quake reconnaissance activities.

2.1 2010/2011 CHRISTCHURCH EARTHQUAKES

2.1.1 Seismic intensity and response spectra

On 4 September 2010, a moment magnitude M_w7.1 earthquake with epicentre in Darfield, approximately 35 km from the city centre, hit the city of Christchurch. Five months later, a more destructive M_w6.3 moment magnitude earthquake hit Christchurch again. The hypocentre was located in Lyttlelton, approximately 10 km south-east of Christchurch CBD and only 5 km deep (Bradley, 2012; Kam & Pampanin, 2011). The accelerations recorded during the September earthquakes were close to, and sometimes higher than, those predicted by the 500-year design spectrum. Fig. 2-1 shows the inelastic acceleration spectra (5%-damped) obtained from four records in the Christchurch CBD and the 500-year design spectrum as defined by the NZS1170:5 code (2004) for Christchurch (PGA=0.22g), soil class D and distance to the nearest fault (R) of 35 km. For short-period structures, the seismic demand, caused by the earthquake, was below or close to that defined by code (NZS 1170.5:2004). However, for longer-period structures, the seismic demand was above the design spectrum. As a consequence, high-rise buildings were likely subjected to significant seismic accelerations (Kam, Pampanin, Dhakal, Gavin, & Roeder, 2010).

The February earthquake induced an even higher seismic demand in the east-west direction, this being the principal component of the horizontal shaking. In Fig. 2-2, the elastic acceleration spectra derived from four ground motions recorded in the Christchurch CBD are compared to the 500-year and 2500-year design spectra for Christchurch (PGA = 0.22g), soil class D and R = 20 km. Seismic accelerations were well beyond those predicted by the 500-year design spectrum typically used for the design of “ordinary” (importance level 2) buildings. The accelerations matched and sometimes exceeded the 2500-year design spectrum (Kam et al., 2011).

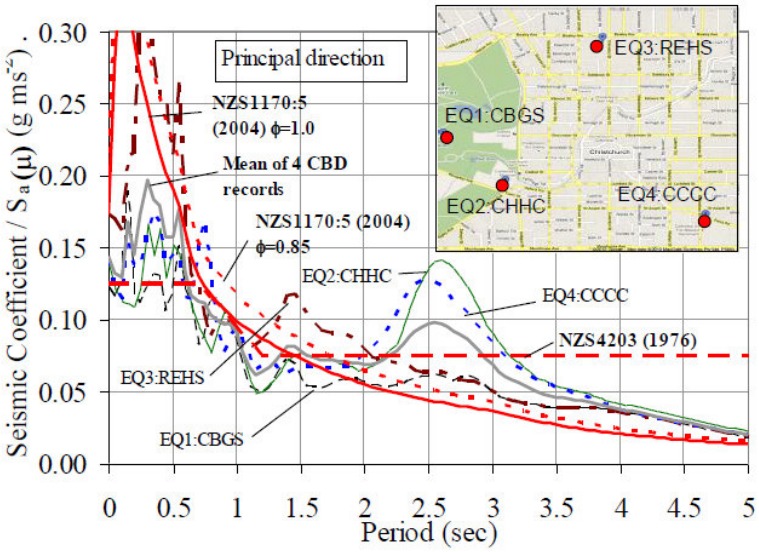

Fig. 2-1 September 4th 2010 Mw7.1 earthquake: comparison of inelastic spectra of four records in the Christchurch CBD and the NZS1170:5 design spectra (red solid) for Christchurch (soil class D, R=35 km), reduced assuming limited-ductility frames (μ=3 and Sp=0.7) (Kam et al., 2010).

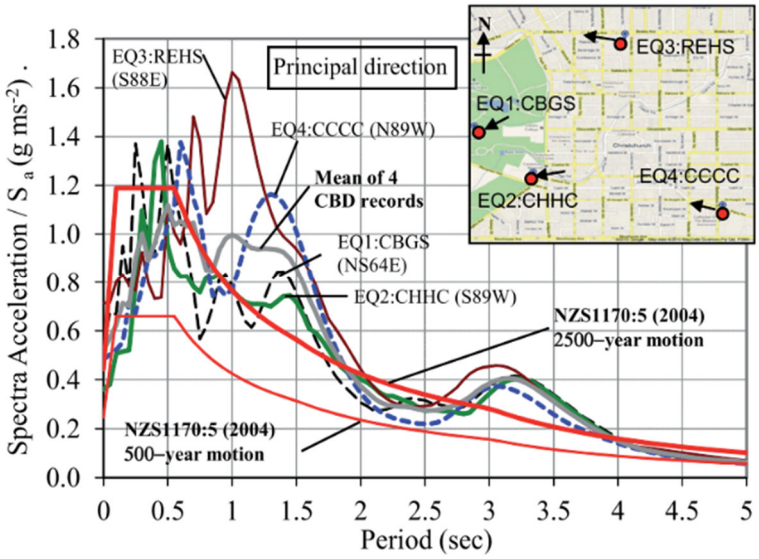

Fig. 2-2 February 22nd 2011 Mw6.2 earthquake: elastic acceleration response spectra (5% damped) in the Christchurch CBD after the 22 February event and the NZS1170:5 design spectra (solid red line) for Christchurch (soil class D, R=20 km) in the principal direction (generally east-west component) (Kam et al., 2011).

2.1.2 Capacity design and hierarchy of strength design philosophy

The design philosophy for the basis of modern seismic codes allows for the damage of structures subjected to major earthquakes. At the ultimate limit state, "ordinary" structures, buildings designed to importance level 2 AS/NZS 1170.0 (2002), are designed to prevent collapse during seismic events that have a 10% probability of being exceeded in their designed life (for a 50-year design, this is equivalent to a 500-year return period). It is not economically viable for structures designed for life safety to remain elastic when subjected to a 500-year return period seismic event. Therefore, designers are allowed to reduce the seismic forces based on the overall ductility and redundancy of the entire structural system. As a result, structures are expected to survive to the design-level earthquake at the cost of permanent damage as a consequence of large inelastic deformation and energy dissipation of the structural materials (Paulay & Priestley, 1992).

Based on the capacity design and the hierarchy of strength philosophy, designers are encouraged to strategically locate and detail structural member regions, termed plastic hinges, that will dissipate energy during high-intensity earthquakes and prevent brittle shear failure. The capacity design and hierarchy of strength concepts are traditionally explained using the chain analogy. The chain in Fig. 2-3 is made from a number of brittle links and a single ductile link. The strength of a chain corresponds to the strength of its weakest link. If all links are designed to have the same strength, it is highly probable that a brittle failure of the chain would occur. Therefore, the chain will have no ductility. However, if the brittle link is designed in excess of the maximum strength of the ductile link, taking account the material strength uncertainties and strain hardening, then brittle failures would be prevented and the ductility of the chain will be mainly dictated by the ductility of the weakest link (Paulay & Priestley, 1992).

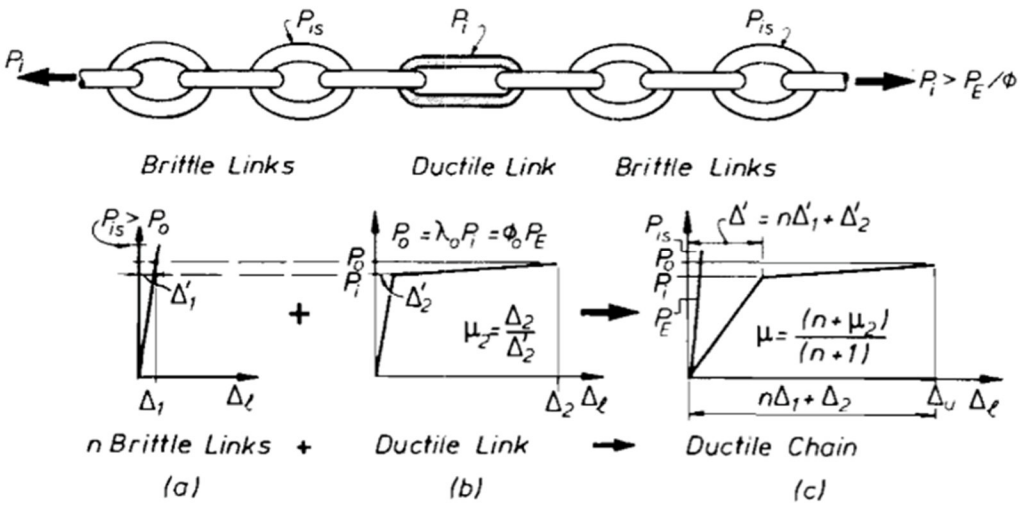

Fig. 2-3 Chain analogy for capacity design (Paulay & Park, 1975).

In lateral resistant systems the weakest link is represented by the plastic hinges. In reinforced concrete (RC), the ductility of a plastic hinge is achieved by designing the proper amount of steel reinforcement compared with the entire concrete cross section, allowing ductile behaviour of the section in case of failure.

The role of dissipating the energy originating from an earthquake is assigned to the steel reinforcement, which has the ability to sustain load cycles that induce high plastic deformation without a reduction in strength. For a well-designed structure subjected to severe lateral displacement, plastic hinges form at the base of columns and walls, in the beam ends, in beam-column joints and in coupling beams (see Fig. 2-4 and Fig. 2-5). Plastic hinges undergo high levels of cyclic plastic rotations that induce large flexural compressive and tensile stresses in the RC materials. The expected result, as observed by numerous laboratory tests, is a uniform crack distribution pattern (Fig. 2-6 and Fig. 2-7), bond deterioration and plastic deformation in the steel, spread over the plastic hinge zone (Bull, 2013; Stefano Pampanin, 2012). At ultimate limit state (ULS), the cover concrete is expected to be crushed; however, the member and the overall structure

maintain their integrity without losing excessive moment- and shear-resisting capacity. During the Christchurch earthquake, the distributed cracking pattern was not always observed (Bull, 2013).

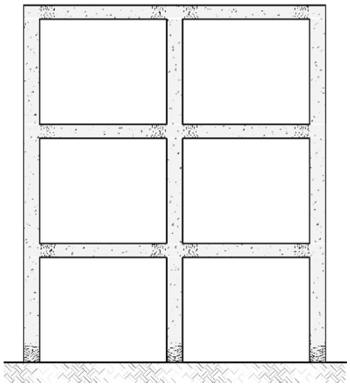

Fig. 2-4 Elevation view of a RC frame with plastic hinges formed in beam ends and column bases.

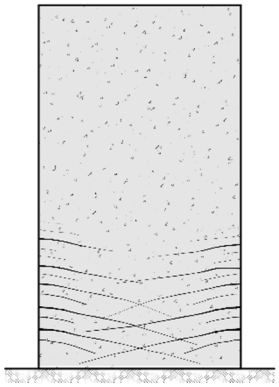

Fig. 2-5 Elevation view of a RC wall with plastic hinge at the base.

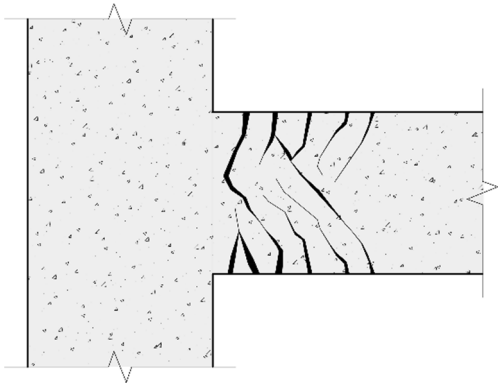

Fig. 2-6 Elevation view of a typical crack pattern expected in a beam-column joint plastic hinge subjected to reversed cyclic loads.

Fig. 2-7 Beam plastic hinges in a 22-storey reinforced concrete building constructed in mid-end 1980s (Stefano Pampanin, 2012).

2.1.3 Summary of damage of ductile reinforced concrete (RC) moment-resisting frames

Because of the proximity to the city and the acceleration produced, the 22 February 2011 earthquake was the most destructive. During the after-event building survey, 50% of the RC buildings in the Christchurch CBD were tagged either red (no entry) or yellow (restricted entry to retrieve essential records, files or equipment, or, under special circumstances, limited work/function is able to continue) (Kam et al., 2011). The Canterbury Earthquakes Royal Commission (CERC) reported that, in total, about 1100 CBD buildings were expected to be demolished (CERC, 2012a).

Pre-1970s buildings, designed before the introduction of capacity design and ductile detailing concepts, performed poorly. Structural deficiencies, typical of those buildings, such as lack of steel confinement in vertical members, use of plain reinforcing bars, inadequate anchorage details, insufficient reinforcement, and irregular plan and elevation configurations, caused a series of brittle failure mechanisms (see Fig. 2-8 and Fig. 2-9) (Kam et al., 2011).

On the other hand, ductile buildings designed according to the "modern" codes (NZS 4203 (1976) and NZS 3101:1982 (1982) performed as expected in the case of severe earthquakes. Plastic hinges formed in the desired locations (beam ends, column and wall bases and coupling beams) and no damage was observed in columns and in beam-column joints (Kam et al., 2011). In some cases, instead of the uniformly distributed cracking patterns expected from laboratory testing, a few large cracks were found (Bull, 2013) (CERC, 2012b). This unexpected behaviour could potentially cause a localised peak strain in a short length of the steel reinforcement, a reduction in ductility and decrease in hysteresis energy dissipation (Morris, Bull, & Bradley, 2014). The discrepancy between the laboratory and field observations might be attributed to a number of factors such as test protocols and loading rate during laboratory testing, and to material properties,

in particular concrete strength and amount of the steel reinforcement (Morris et al., 2014; SESOC, 2011).

Other types of damage in RC structures were also observed. Displacement incompatibility between lateral resisting systems and precast floor, due to beam elongation effects, produced significant cracking at the interface between floor diaphragms and supporting beams, almost causing loss of the floor support (Fig. 2-10). This unfavourable structural behaviour was identified as a structural issue after the 2011 earthquake (Kam et al., 2011).

Plan and elevation irregularities, caused by non-uniform mass and stiffness distribution, triggered higher seismic demands on structural members in addition to torsional effects. Severe basement column shear-axial failures and transfer slab failures were recorded (Kam et al., 2011). Many slender and lightly reinforced RC walls, detailed for flexural load, failed due to brittle shear-compression mechanism, steel reinforcement fracture and web buckling (Fig. 2-11). Fractured reinforcing bars were observed in a number of walls, the cause of which might be attributed to the inadequate amount of steel and the wide spacing of horizontal reinforcement, which allowed the bars to buckle, leading to fatigue fracture (Fig. 2-13 and Fig. 2-14). Core concrete crushing was also observed outside the boundary zones of many walls (Kam et al., 2011).

Fig. 2-8 Column shear failure in a pre-1970s building. (Kam et al., 2011)

Fig. 2-9 Compression zone failure of pre-1970s RC wall. (Kam et al., 2011)

Fig. 2-10 Damage of floor diaphragm due to beam elongation. (Kam et al., 2011)

Fig. 2-11 Severe wall damage with local buckling. (Buchanan et al., 2011)

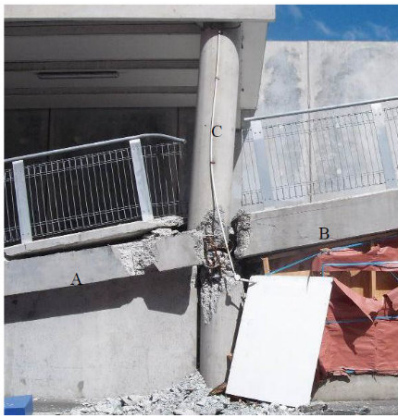

Fig. 2-12 Lack of displacement allowance leading to a column shear failure. (Kam et al., 2011)

Fig. 2-13 Bar buckled and fracture in a lightly reinforced, slender RC shear wall. (Kam et al., 2011)

Fig. 2-14 Fractured rebars in a shear wall. (Buchanan et al., 2011)

Fig. 2-15 Collapse of a precast staircase in a multistorey building. (Kam et al., 2011)

Damage was also observed in precast concrete structures: punching shear of post-tensioned slabs causing “pancake” failure; collapse of simply supported ramps due to insufficient seating; and damage, total or partial, of staircases in high-rise buildings (Fig. 2-15) (Kam et al., 2011).

The 22 February earthquake caused the catastrophic collapse of two buildings: the Canterbury Television (CTV) and the Pyne Gould Corporation (PGC) buildings. A total of 185 people lost their life during this earthquake, and many others were seriously injured.

2.2 STEEL REINFORCING MATERIAL

2.2.1 Introduction to reinforced concrete (RC) materials

Concrete is not a recently discovered material. A first version of concrete (*opus caementicium*), made by mixing sandy volcanic ash and lime mortar, was wisely used in construction by the Romans by the third century BC. An example is the Pantheon (Fig. 2-16) located in Rome (Italy). Modern concrete, made of Portland cement and coarse aggregate, was produced from the beginning of the1800s. The large-scale manufacture of steel was not introduced until the industrial revolution (from the eighteenth century).

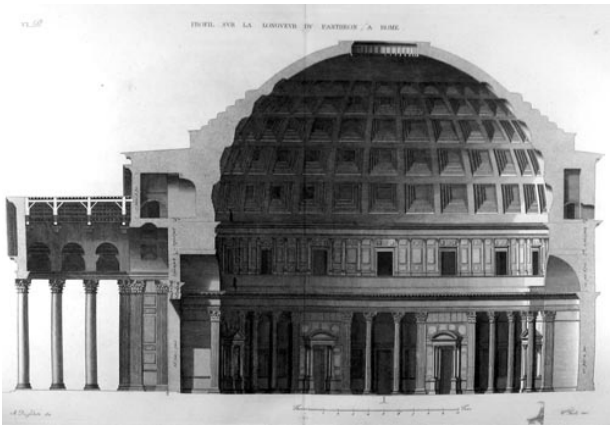

Fig. 2-16 Section view of the Pantheon in Rome

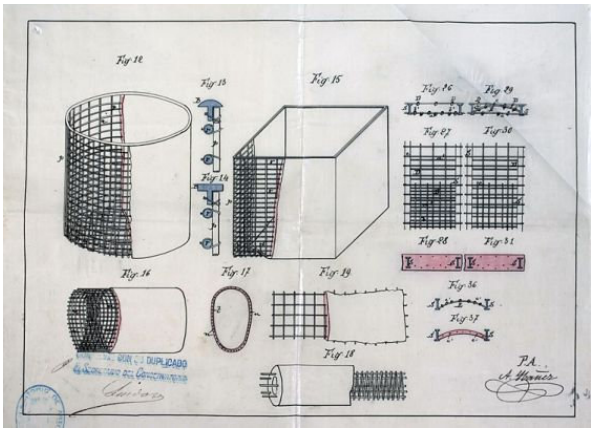

Fig. 2-17 Drawings of Monier’s RC patent

The invention of reinforced concrete can be attributed to Joseph Monier, who patented the idea of combining concrete and round steel bars in flexural members in 1877 (see Fig. 2-17) (Mezzina, 2001). The success of this invention in the construction industry was certainly due to its resistance to fire and the ability to obtain slender structures able to span long distances. However, it is the French constructor François Hennebique who gave the biggest impulse to the spread of reinforced concrete in construction.

The complementarity between concrete and steel reinforcing bars makes reinforced concrete a reliable material to be used in construction. Concrete has a good compressive strength, great fire resistance, low maintenance cost, and shape flexibility (it can assume almost any shape required). However, it has the big disadvantage of being a brittle material with poor tensile strength. Steel, conversely, is a high strength material with large ductility capacity; this implies that even a small quantity of steel can provide adequate resistance. The poor fire resistance, the sensitivity to corrosion and the low buckling resistance are the main disadvantages of steel. Therefore, the two materials combined together represent a great composite material with high strength, either in compression or tension, good fire resistance and relatively low production costs.

Reinforcement was originally manufactured in the shape of plain round reinforcing bars (Fig. 2-18); later (around the 1960s) deformed (with ribs) bars (Fig. 2-19) were introduced to improve the bond between the steel and the concrete. When the bars are subjected to tension, compressive stress is transferred from the reinforcement to the concrete through the ribs. The ribs' geometry is prescribed by the current AS/NZS 4671:2001 standards (Standards, Australia and New Zealand, 2001) .

Fig. 2-18 A plain round reinforcing bar removed from a RC building

Fig. 2-19 A 16 mm diameter reinforcing bar as received from the supplier

2.2.2 Steel reinforcement: microstructure and production

Steel used in reinforcing bars is an iron-carbon alloy known as low-carbon steel, whose carbon content is less than 0.25 wt%. It can also contain other elements such as vanadium, manganese, silicon, and copper (Callister & Rethwisch, 2014) (see also Appendix B). Low-carbon steels are relatively soft and weak (yield strength is about 300 MPa), but very ductile. Small additions of other elements such as vanadium can provide these steels with higher tensile strength; this is the case of the New Zealand-manufactured Grade 500E MA (micro alloy) reinforcing bars (Pacific Steel Ltd, 21 Beach Road, Auckland, www.pacificsteel.co.nz). The steel microstructure consists of ferrite and perlite (Fig. 2-20).

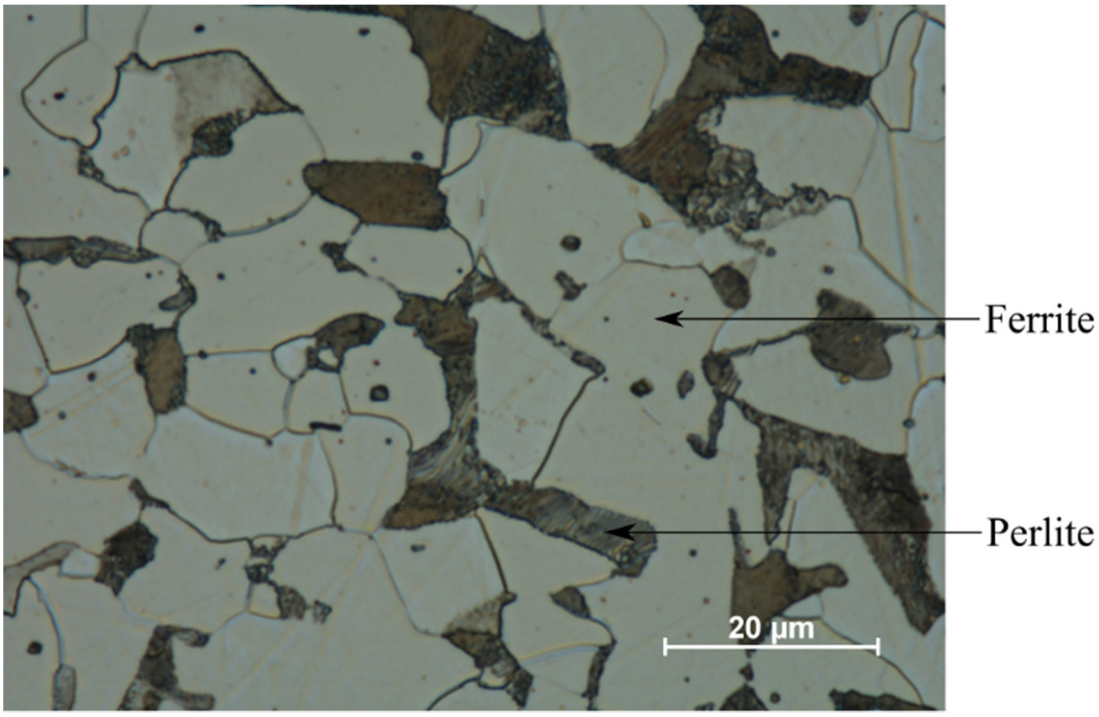

Fig. 2-20 Photomicrograph showing the microstructure of low-carbon steel reinforcement. Ferrite and perlite are indicated.

Steel for reinforcing bars is often obtained from melting scrap metal in electric arc furnaces (EAC). Each EAC operation produces batches of molten steel known as “heats”. Therefore, steel obtained from the same EAC operation (or batch) is said to be from the same heat (also known as “cast”).

From 1962 until 2015, the local New Zealand company Pacific Steel (21 Beach Road, Otahuhu, Auckland 2024), made reinforcing steel from scrap metal (Roberts, 2016). The metal was collected from different sources and graded into different piles. In order to produce a specific steel grade, specific amounts of steel from the different steel piles were put into the EAC for melting. The EAC has three electrodes that melt the scrap at about 1600°C; during the melting process, steel is separated from its impurities, which form a liquid known as slag. The slag floats on the top of the molten steel. To remove other impurities that are not removed when the slag

initially forms, a refining process takes place. Oxygen is blown into the furnace and reacts with the impurities forming oxides which are then absorbed into the slag. Once the desirable chemical composition of the molten steel is obtained, the slag is removed from the furnace during an operation called de-slagging. The final slag is the result of the melting and the refining process. The molten steel of the right composition and temperature is transferred to a ladle for the tapping operation. In this phase, an additional refining process takes place. All the other steel alloys (carbon, manganese, and for high strength steel, vanadium) are added to obtain the required chemical and mechanical properties for that particular grade of steel.

Fig. 2-21 Stocked billets ready to be hot rolled. The cast number is written on their sides.

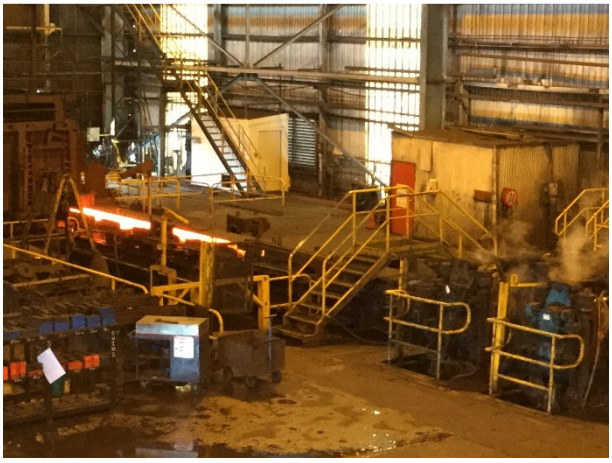

Fig. 2-22 Hot billet coming out from re-heat furnace, now on the way to the rolling process.

The liquid steel obtained is then poured continuously into cooled moulds, forming, when solidified, square billets of dimensions 150 x 150 mm and approximately 10 m long. These billets, coming from the same steel-making process (cast), are stored together. The billets are stored until the final hot rolling phase starts (Fig. 2-21). By this stage, the chemical composition of the steel has been monitored already – in the furnace, during the melting process, into the ladle when the alloys are added, and during the casting. In the final phase, the billets are softened by heating at 1000°C–1100°C for the rolling phase, which is conducted in the roughing mill (Fig. 2-22). The

hot billets are moved into a first set of rolls encased in a steel frames known as a "stand". The rolls are made in cast iron and their grooves have different shapes and geometries depending on the bars that are manufactured (Fig. 2-25). Then, the billets are gradually shaped into the desired bar size and geometry as they go through each stand. The reduction in area in each stand is about 30–35% (Fig. 2-23). Once the bars have undergone all the stands and reached the desired aspect, they are delivered into a cooling bed and slowly air cooled (Fig. 2-24). Once cooled, the bars are cut into specific lengths and collected in bundles. For sizes equal to or smaller than 12 mm, the bars are produced in coils and then straightened (Fig. 2-26) (Roberts, 2016).

Fig. 2-23 Hot rolling process. The billet goes through a series of "stands". In each stand the material size is reduced by the 30-35%.

Fig. 2-24 At the end of the rolling process, the reinforcing bars are left to air-cool evenly spaced on a cooling bed.

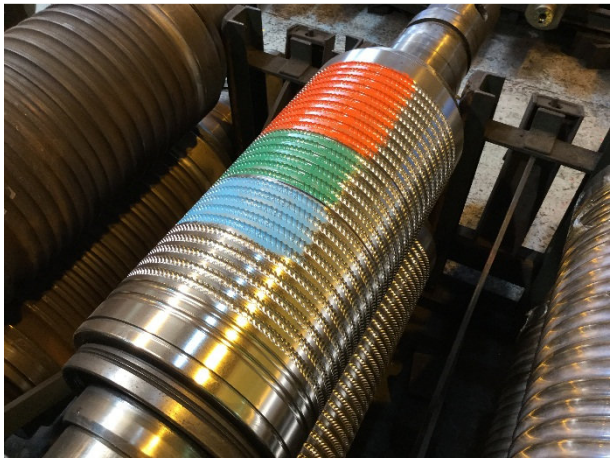

Fig. 2-25 Rolling turning lathe. Grooves are designed to reproduce the desired rebar geometry.

Fig. 2-26 Bundle of coiled rebars.

2.2.3 Steel reinforcement mechanical properties and chemical composition

Specifications about the chemical composition and the mechanical and geometrical properties of steel reinforcing bars, wire and mesh are contained in the Australian and New Zealand joint standard AS/NZS 4671 (2001). The standard considers three steel strength grades: 250 MPa, 300 MPa and 500 MPa. The grade refers to the lower characteristic value of the yield strength. In New Zealand, only grades 300 MPa and 500 MPa are permitted. Because Australian and New Zealand RC buildings are required to possess different limits of ductility, AS/NZS 4671:2001 introduces three ductility classes: "L" low, "N" normal and "E" earthquake. In terms of mechanical properties, they indicate specific limits to the uniform elongation and the ratio between ultimate tensile strength (UTS) and yield strength. The ductility class identification letter is placed after the strength-grade number. Only ductility class "E" is allowed in New Zealand. In conclusion, only two steel grades are available in New Zealand: Grade 300E and Grade 500E.

In addition, reinforcing bars can be plain (with no ribs on the surface), identified with the letter "R" (standing for Round) or deformed (with ribs), identified by the letter "D" (standing for

deformed). The standard also prescribes limits in the chemical composition of steel in terms of percentages by mass of the nonferrous elements such as carbon (C), phosphorus (P) and sulfur (S) (see Table 2-1). Carbon equivalent (C_{eq}) limits are also established. C_{eq} is determined by the following equation:

$$C_{eq} = C + \frac{Mn}{6} + \frac{Cr + Mo + V}{5} + \frac{Ni + Cu}{15} \quad \textbf{(2-1)}$$

The mechanical properties' limits set by the standard are presented in Table 2-2.

In order to determine the yield stress and (ultimate) tensile strength, AS/NZS 4671:2001 refers to AS1391 (2007); uniform elongation is defined as the percentage of elongation at maximum force (see Fig. 2-27 and Fig. 2-28).

Table 2-1 Chemical composition of steel reinforcement. Adapted from AS/NZS 4671 (2001).

Type of analysis	**Chemical composition, % max**							
	All grades			Carbon equivalent value (C_{eq}) for standard grades				
	C	P	S	250N	500L	500N	300E	500E
Cast analysis	0.22	0.050	0.050	0.43	0.39	0.44	0.45	0.49
Product analysis	0.24	0.055	0.055	0.45	0.41	0.46	0.45	0.51

Table 2-2 Typical mechanical properties of reinforcing steel. Adapted from AS/NZS 4671 (2001).

Property	250N	500L	500N	**300E (Seismic)**	**500E (Seismic)**
Yield stress (MPa)					
Lower characteristic value	≥ 250	≥ 500	≥ 500	**≥ 300**	**≥ 500**
Upper characteristic value		≤ 750	≤ 650	**≤ 380**	**≤ 600**
Ratio tensile strength/yield stress	≥ 1.08	≥ 1.03	≥ 1.08	**≥ 1.15** **≤ 1.50**	**≥ 1.15** **≤ 1.40**
Uniform elongation	≥ 5.00	≥ 1.5	≥ 5.0	**≥ 15.0**	**≥ 10.0**

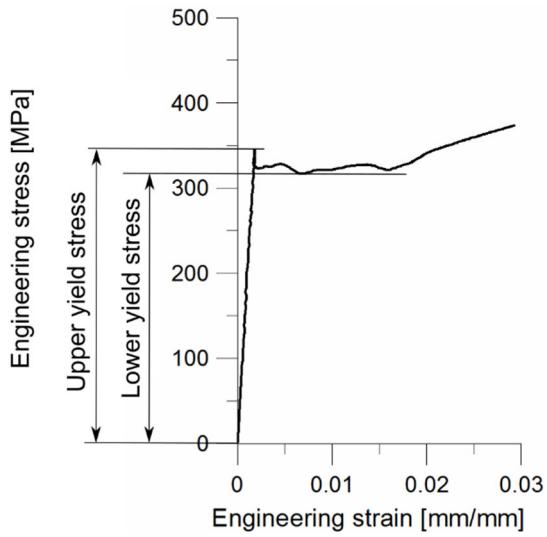

Fig. 2-27 Stress–strain curve illustrating upper–lower yield stress.

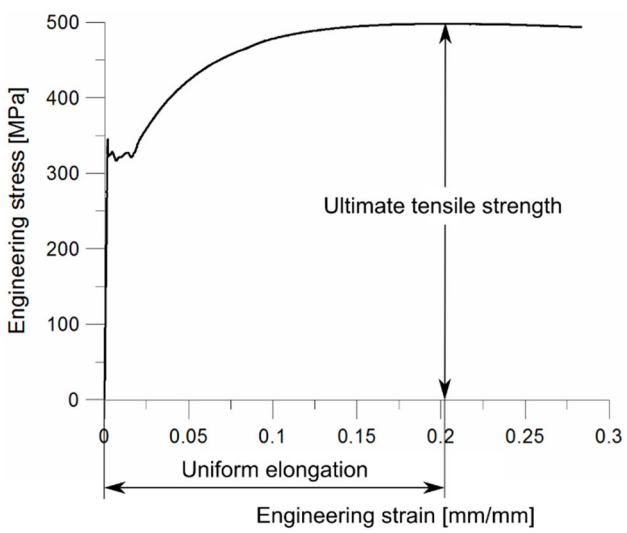

Fig. 2-28 Stress–strain curve illustrating ultimate tensile strength and uniform elongation.

2.2.4 History of New Zealand standards of steel reinforcing materials

The first New Zealand standard to regulate the mechanical properties of steel bars for reinforcing concrete is probably NZS 197:1949 (based on BS 785:1938) “Rolled steel bars and hard drawn steel wire” (Standards, New Zealand 1949). This standard only referred to plain round bars. Before 1949, there was apparently no specific national standard to cover reinforcing steel properties. Deformed bars were introduced in 1963 with the NZSS 1693:1962 “Deformed steel bars of structural grade for Reinforced Concrete” (Standards, New Zealand 1963) . A 227 MPa (33000 psi) yield stress steel bar grade was first introduced and then replaced in 1968 (Amendment 1 of NZSS 1693:1962) by a 275 MPa (40,000 psi yield stress steel bar) steel grade. It can be reasonably assumed that plain round bars were used in concrete buildings at least until the mid-1960s.

In 1964, another standard regulating deformed steel bars was issued: NZSS 1879:1964 “Hot rolled deformed bars of HY 60 (High yield 60,000 psi) for Reinforced Concrete” (Standards, New Zealand, 1964) . This standard introduced a higher yield steel grade: 414 MPa (60,000 psi). In this

period, there were three standards for steel reinforcing bars: one for plain round bars (NZS 197) and two for deformed bars (NZSS 1693 and NZSS 1879). In 1972, the old NZSS 197 was replaced by a temporary standard NZS 3423P:1972 “Hot rolled plain round steel bars of structural grade for reinforced concrete” (Standards, New Zealand, 1972) , which was only valid for a year.

In 1973, all three standards NZSS 1693:1962, NZSS 1879:1964 and NZS 3423P were superseded by NZS 3402P:1973 “Hot rolled steel bars for the reinforcement of concrete”(Standards, New Zealand, 1973) , and this regulated both plain round and deformed bars. Metric units for steel bars were slowly introduced in 1974 and became the only units used by New Zealand steel manufacturers from 1976 onwards. Steel grades used at that time were Grade 275 and Grade 380. In 1989, NZS 3402P was superseded by NZS 3402:1989 (Standard, New Zealand, 1989) . This replaced Grades 275 and 380 with the new Grades 300 and 430. In 2001, the current version of the standard for steel reinforcement was introduced: AS/NZS 4671:2001 (Standards, Australia and New Zealand, 2001) . Steel grades proposed for New Zealand in this standard were Grade 300E (Earthquake ductility) and Grade 500E. Table 2-3 summarises the evolution of these standards. More tables summarising prescriptions from historical New Zealand standards on steel reinforcement materials can be found in Appendix A.

Table 2-3 Evolution of reinforcing steel material standards in New Zealand

<table>
<tr><th>1949</th><th>1962</th><th>1964</th><th>1968</th><th>1972</th><th>1973</th><th>1989</th><th>2001</th></tr>
<tr><td colspan="4">NZS 197:1949 (BS 785 - 1938)
Rolled steel bars and drawn steel wire for concrete reinforcement (Yield stress varied with diameter, minimum value was 227 MPa, Refer to Appendix A)</td><td>NZS 3423P:1972
Hot rolled plain round steel bars of structural grade for reinforced concrete "Grade" 40,000 psi (275 MPa)</td><td rowspan="4">NZS 3402P:1973
Hot rolled steel bars for the reinforcement of concrete
Grade 275 MPa
Grade 380 MPa</td><td rowspan="4">NZS 3402:1989
Steel bars for the reinforcement of concrete
Grade 300 MPa
Grade 430 MPa</td><td rowspan="4">AS/NZS 4671:2001
Steel reinforcing material
Grade 300 MPa
Grade 500 MPa</td></tr>
<tr><td></td><td colspan="2">NZSS 1693:1962
Deformed steel bars of structural grade for reinforced concrete "Grade" 33,000 psi (227 MPa)</td><td colspan="2">NZSS 1693:1962 (Amendment 1:1968)
Deformed steel bars of structural grade for reinforced concrete "Grade" 40,000 psi (275 MPa)</td></tr>
<tr><td></td><td></td><td colspan="4">NZS 1879:1964
Hot rolled deformed bars of HY 60 (High Yield 60,000 psi) for reinforced concrete
"Grade" 60,000 psi (415 MPa)</td></tr>
</table>

2.3 HARDNESS OF METALS

2.3.1 Definition and testing methods

The definition of hardness has been, and still is, a matter of discussion. O'Neill described the hardness of metals "like the storminess of seas, is easily appreciated but not readily measured" (O'Neill, 1967, p, 1). In his book "Mechanical Metallurgy", Dieter affirms that hardness assumes different meanings "depending upon the experience of the person involved" (Dieter, 1976, p. 389). In general terms, hardness provides information about the resistance of a metal to permanent or plastic deformation. In material testing, hardness is the resistance of a metal against the penetration of an indenter made of a harder material, such as diamond or a hard steel ball. Meanwhile in engineering applications, hardness is an easy and practical measure of the deformation resistance and provides insight to the thermomechanical history of a metal (Dieter, 1976).

Depending on the type of the test conducted, hardness measurements fall into three categories:

- scratch hardness
- static indentation hardness
- rebound or dynamic hardness.

The first category is of interest to mineralogists, while from an engineering point of view, the the indentation and the rebound methods are more interesting. The traditional hardness testing method is the static indentation method. An indenter is pressed into the surface of a metal sample under a specific load; when equilibrium is reached, the indentation dimensions are measured. Hardness is then calculated as the ratio between load applied and area of indentation made on the surface sample. Depending on the geometry of the indenter, the load applied and the testing procedure, different types of static indentation tests and hardness scales are available. For example the Brinell test uses a spherical hard steel indenter, the Vickers test uses a square-based pyramid

diamond indenter (Fig. 2-31), and finally, the Rockwell employs either a conical or spherical indenter (Fig. 2-30). In the Brinell and the Vickers test, hardness is measured in the Brinell (H_B) and Vickers (H_V) scales respectively. While in the first case the hardness number is a function of the size of the indenter, in the Vickers test the hardness is independent of the dimension of the diamond indenter and is calculated as:

$$H_V = \frac{P}{A} = \frac{1.854P}{d^2} \quad (2\text{-}2)$$

where P is the load applied during the test; A is the square indentation area; and d is the mean diagonal length of the square indentation area.

Traditionally the static test methods employ conventional workbench hardness testers. In a Vickers hardness test, generally a 30 kg load (different loads are also available) is applied to a specimen through the pyramid-shaped diamond indenter; once equilibrium is reached, the load is automatically removed and a permanent indentation is obtained on the sample surface. Both diagonal lengths of the square indentation area are measured through an optical microscope (Fig. 2-29). The accuracy of the size indentation measurement depends also on the operator's skill. Vickers indentations can be also conducted by applying very small loads from 0.001 kg to a maximum 1 kg: this is known as microhardness. See Fig. 2-30 for a micro hardness indentation.

Another hardness testing technique commonly used in the industry is the Rockwell hardness test, named after its inventor. Over the years, this hardness methodology was improved by its first manufacturer, Charles H. Wilson. He introduced, besides the original 1/16 inch steel ball indenter, a "smoothed" tip conical indenter known as a "Brale" penetrator. Depending on the load applied (60, 100 or 150 kg) and on the type of indenter (Brale, 1/2 in, 1/4 in, 1/8 in, 1/16 in ball) different Rockwell scales are defined. In general, the most common for steel hardness testing are Rockwell

scales B and C. The first, suitable for soft steels (the steel used for manufacturing steel reinforcing), requires a 1/16 inch steel ball and 100 kg load. Meanwhile, the second, which is more appropriate for harder steel, requires a Brale indenter and a 150 kg load. During a Rockwell hardness test a small load of 10 kg is first applied on the metal sample in order to define the "zero" hardness. Then, the required testing load (100 kg for Rockwell B or 150 for Rockwell C) is progressively applied through the indenter which penetrates into the sample. The Rockwell hardness is a measure of the penetration depth when the testing loading is applied. One hardness point is representative of a 0.002 mm penetration depth. The hardness measurement is shown on a calibrated dial gauge attached to the machine (Vander Voort, 1999).

The rebound or dynamic hardness technique such as the Leeb hardness (H_L) test is an indirect method to measure metal hardness through the loss of energy of a spherical impact body during the impact (see Fig. 2-32). The impact body, for example a tungsten carbide, silicon nitride or diamond ball, is dynamically applied by a spring on the metal test surface at a defined speed. During the collision the spherical body loses part of its initial velocity due to energy dissipation that is related to the plastic deformation of the metal (the softer the material, the greater the velocity loss will be). The velocity before (impact velocity) and after (rebound velocity) the impact is measured and used to determine the Leeb hardness (named after its inventor) (ASTM, 2012a) (Frank & Technologies, 2005):

$$H_L = \frac{rebound\ velocity}{impact\ velocity}\ x\ 1000 \qquad (2\text{-}3).$$

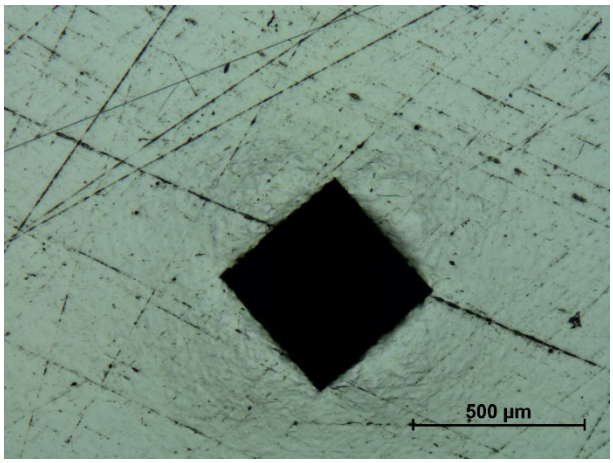

Fig. 2-29 Pyramidal Vickers indentation on a metal surface (50x magnification).

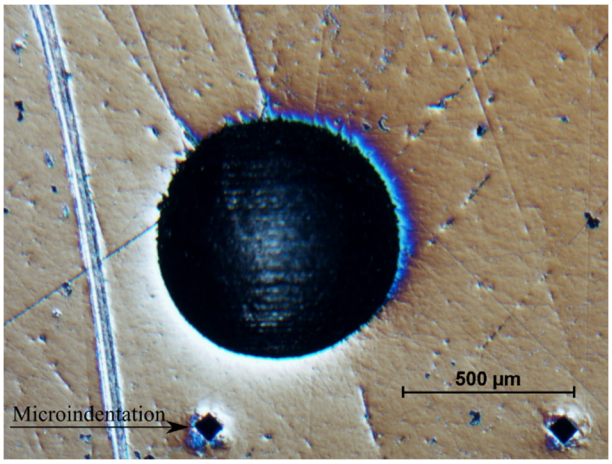

Fig. 2-30 Round indentation of a Rockwell spherical indenter. On the bottom of the picture it is possible to see the Vickers Micro-indentations (50x magnification).

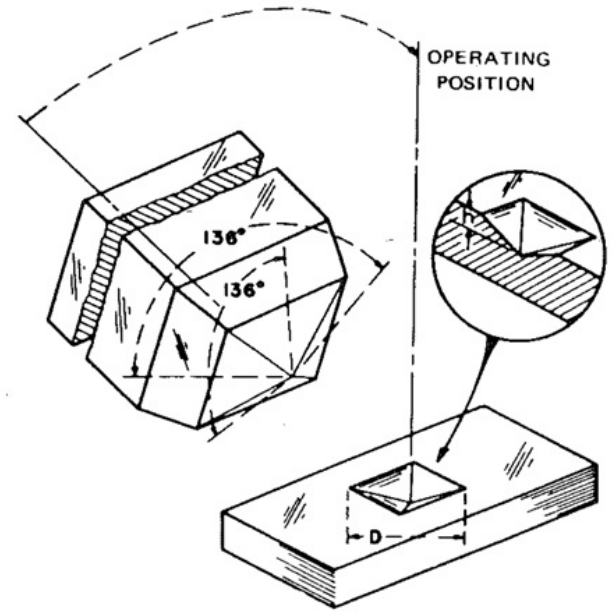

Fig. 2-31 Schematic representation of the Vickers indentation (Vander Voort, 1999).

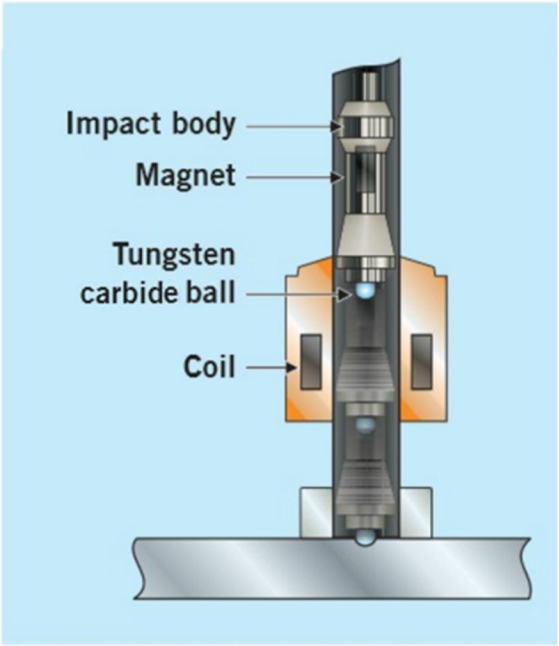

Fig. 2-32 Cross-sectional representation of a rebound portable tester. Adapted from(Frank & Technologies, 2005)

2.3.2 Relationship between hardness and mechanical properties

Because of its cost effectiveness and versatility characteristics, hardness is used as a fast and direct method to quantify some mechanical properties of steels. Since the beginning of the twentieth century many studies were conducted to find a correlation between hardness and a metal's mechanical properties such as ultimate tensile strength and yield strength (Hutchings, 2009). Many relationships have been documented that correlate hardness to yield and ultimate tensile strength (Cahoon, Broughton, & Kutzak, 1971; Lee & Song, 2006; O'Neill, 1967; Pavlina & Van Tyne, 2008, 2014; Tabor, 1951b). Probably a first empirical correlation between Brinell hardness (H_B) and ultimate tensile strength (σ_u) for different types of steel was derived by Brinell himself (Wahlberg, 1901). He found the following relationship:

$$\sigma_u = 0.346\, H_B \qquad (2\text{-}4)$$

One of the most significant contribution to the science of hardness indentation was given by David Tabor. In his book *The Hardness of Metals* (Tabor, 1951b), he develops a semi-empirical theory of hardness. Hardness is the ratio between a load and the indentation surface area and consequently has the dimensions of pressure. Relative to spherical indentation (Brinell hardness), from several researchers (Davies, 1949; Timoshenko, 1970) (Davies, 1949) (Tabor, 1951a) it can be shown that as the load is applied on the metal surface, the region of the metal below the indenter starts to deform plastically. As the load increases, the plastic region increases as well, and so does the pressure on the metal surface. This pressure will finally reach a constant upper limit P. This value of P, also known as Meyer hardness or mean pressure, for "ideal" plastic metals (those that do not work harden) is approximately three times the elastic limit (or yield stress) of the metal itself (Y_r).

Further experiments on heavily work-hardened metals showed that the ratio between mean pressure and yield stress was equal to 2.8, therefore:

$$P = 2.8\,\mathrm{Y}_r \qquad (2\text{-}5)$$

Similar results can be extended to materials that undergo work hardening, such as low-carbon steels. The major difference is that when the indenter penetrates the metal surface the amount of work hardening occurring in the metal region below the indenter is not constant but varies from one point to another. As result, the yield stress varies accordingly. Tabor assumed, therefore, that a representative yield stress Y_r is correlated to the mean pressure through a constant approximately equal to 3. The value of Y_r was obtained by introducing a representative strain function of the chordal diameter of the projected area of the indentation (d) and the diameter of the spherical indenter (D). This representative strain, if expressed in percentage, was semi-empirically found to be equal to:

$$\varepsilon_r = 20\left(d/D\right) \qquad (2\text{-}6)$$

As the representative stress is a function of the representative yield stress, for different combinations of chordal and indenter diameter, it means that for similar geometrical indentation it was possible to correlate the mean pressure of the metal to its stress–strain curve. For example a 5-mm chordal diameter indentation caused by a 10-mm diameter spherical indenter will produce a representative strain equal to 10%. Therefore, the representative yield stress, which is the stress at 10%, will be equal to P divided by 2.8. Based on this relationship, using different indenters, Tabor was able to experimentally observe a close agreement between the stress–strain curve (multiply by the constant 2.8) and hardness of mild steel, annealed copper and partially annealed aluminium within the strain range 0% to 20% (see Fig. 2-33).

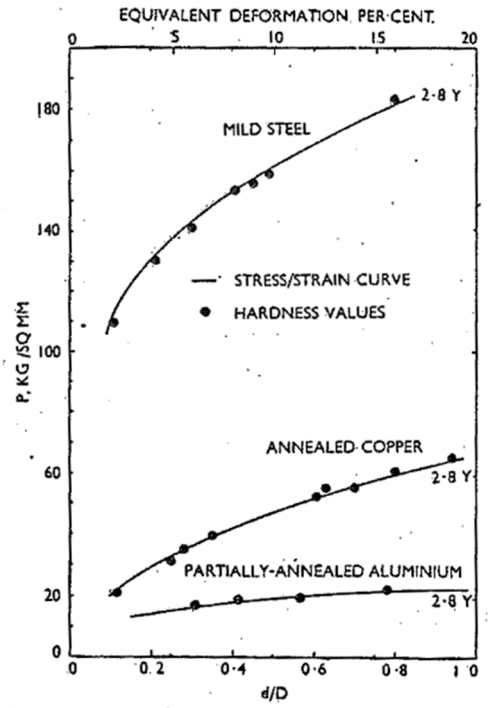

Fig. 2-33 Correlation of stress/strain curves with hardness values of steel, copper and aluminium (Tabor, 1951a).

Tabor developed the same analysis for conical (Ludwik hardness) and pyramidal indenters (Vickers hardness). For these indenter geometries the shape of the indentations remained the same and consequently the stress and the strain of the metal below the indenter was constant, independent of the size of the indentation. This meant that the representative strain was constant and did not depend on the properties of the indenter and the indentation size.

Furthermore, Tabor developed a linear relationship between Vickers hardness (H_V) and a "representative yield stress":

$$H_V = 2.8\,\mathrm{Y}_r \tag{2-7}$$

where the representative yield stress Y_r is the stress at the experimentally observed representative strain of 8%.

Other equations that correlate hardness with yield and ultimate tensile strength were developed. For example, Roessle and Fatemi (2000) correlated Brinell hardness (H_B) and ultimate tensile strength (σ_u) using the following second-order polynomial equation:

$$\sigma_u = 0.0012\ H_B^2 + 3.3\ H_B \quad (2\text{-}8)$$

Based on a series of experimental tests on a number of steels with yield strength ranging from 300 MPa to 1700 MPa, Pavlina and Van Tyne (2008) derived two empirical equations that relate Vickers hardness (H_V) to the yield strength (Y_S) (2-9) and to the ultimate tensile strength (T_S) (2-10):

$$Y_S = -90.7 + 2.876\ H_V \quad (2\text{-}9)$$

$$T_S = -99.8 + 3.734\ H_V \quad (2\text{-}10)$$

Equation (2-9) had a standard error of 102 MPa, while equation (2-10) had a standard error of 112 MPa.

In a subsequent work, the same authors (Pavlina & Van Tyne, 2014) determined an empirical relationship between Vickers hardness (H_V) and uniform true strain (ε_y):

$$\varepsilon_u = 0.479 + 0.450\ (1 - e^{-0.00765 H_V}) \quad (2\text{-}11)$$

Lopez and Fatemi (2012) also found a correlation between yield strength (σ_y) and Brinell hardness (H_B) in the form of a second-order polynomial equation:

$$\sigma_y = 0.0039\ {H_B}^2 + 1.62\ H_B \quad (2\text{-}12)$$

where the yield strength is expressed in MPa.

A summary of other relationships between hardness and mechanical properties can be found in the study by Lee and Song (2006).

Research was also conducted to derive stress–strain curves for different metals from hardness measurements (Choi, Park, Kim, Choi, & Min, 2000; Lee & Song, 2006; Pavlina & Van Tyne, 2014; Zhang, Li, & Wang, 2013).

In summary, there are many semi-empirical expressions relating hardness to yield strength and other mechanical properties of specific materials, but with relatively large errors.

2.4 STRAIN AGEING

2.4.1 The phenomenon

The mechanical properties of many carbon steels exhibit a time- and temperature-dependent "strain-ageing" effect after being subjected to plastic strain (Baird, 1971; Erasmus & Pussegoda, 1977; Hall, 1951). This phenomenon causes a significant time- and strain-dependent change in the mechanical properties of steel during and after plastic deformation, termed dynamic strain ageing and static strain ageing respectively (Leslie, 1981). This process is related to the diffusion of interstitial nitrogen and carbon atoms, which lock mobile dislocations in new positions after the steel has been strained. The locking effect is weak when the interstitial content of these elements is low and/or during the initial stage of the process; however, it becomes stronger as the ageing time increases, and with higher nitrogen and carbon interstitial content (Pussegoda & Erasmus, 1977).

The strain-ageing phenomenon can be divided in three distinct processes: strain ageing, strain-ageing hardening, and strain-ageing embrittlement. An example is illustrated in Fig. 2-34 using Grade 300E supplied by Pacific Steel. Consider the case where steel with a strain-ageing tendency is strained in tension beyond its elastic limit up to stress A. If the specimen is unloaded and then immediately reloaded, the specimen will show elastic behaviour up to stress A, and strain hardening will continue as if the test had not stopped. However, if the specimen is unloaded, aged

and reloaded, the discontinuous yield point phenomenon not only reappears, but it does so at a higher stress (point B); this is strain ageing. In addition, the tensile strength is higher and ductility is reduced – strain-ageing hardening. Strain ageing also causes an increase in transition temperature – strain-ageing embrittlement (Erasmus & Pussegoda, 1977).

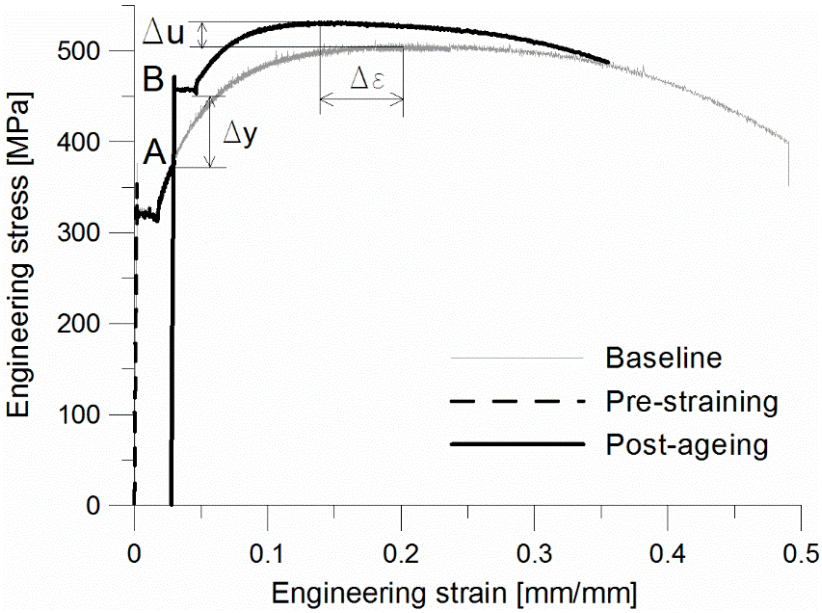

Fig. 2-34 Stress–strain curve of NZ Grade 300E subjected to strain ageing (Adapted from Erasmus and Pussegoda, 1977).

As mentioned, carbon and nitrogen play a significant role as a cause of strain ageing and it can be explained by recalling the discontinuous yielding phenomenon common in low-carbon steels. Carbon and nitrogen are present in the austenite and ferrite matrix as interstitial solute atoms. The interstitial sites are considerably smaller than the carbon and nitrogen atoms. This causes the lattice to be elastically strained. Dislocations, where the lattice is dilated, are ideal sites for interstitial clustering (Erasmus, 1987). Nitrogen and carbon interstitial atoms relieve the stress around a dislocation, causing an equilibrium "atmosphere" known as "Cottrell atmosphere". These, in most

instances, evolve to precipitations of nitrides and carbides. Both Cottrell atmospheres and precipitates lock the mobile dislocations, causing the discontinuous yielding point usually seen in annealed steels. The upper yield point is the stress at which the dislocations are unlocked from their Cottrell atmospheres of interstitial atoms (Cottrell & Bilby, 1949).

The upper yield strength is affected by strain rate, surface finish, geometrical details, axiality of straining, machine stiffness, and imperfections that cause stress concentrations (AS1391, 2007; Pussegoda, 1978). During a tensile test, at the upper yield point, a series of typically 45° lines (from the tensile stress) are starting to form; these are known as Lüders bands (Dieter, 1976). They first appears at a stress concentration and then propagate along the entire length of the steel sample. Once these bands have covered the entire sample, normal strain hardening starts to occur (see Fig. 2-35 and Fig. Fig. 2-36). The lower yield stress is the stress necessary for the band to propagate.

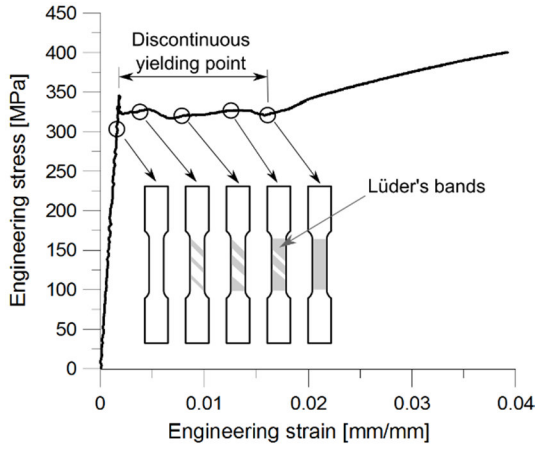

Fig. 2-35 Schematic development of Lüders bands as deformation increases.

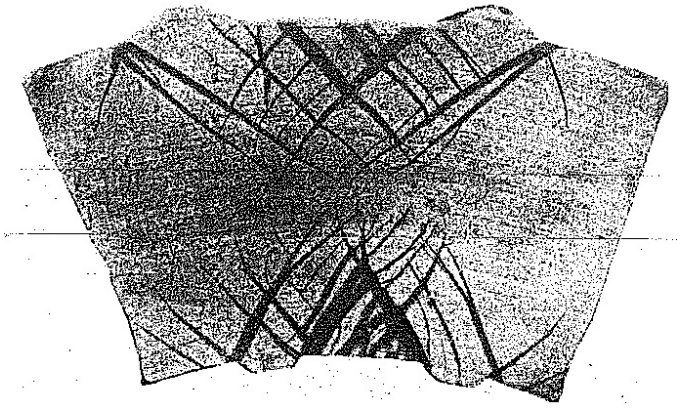

Fig. 2-36 Localised plastic deformation start from stress concentration at the rib roots. Dark bands represents the Lüders bands (Erasmus & Pussegoda, 1978).

Static strain ageing can occur when the test is interrupted and time is allowed for carbon and nitrogen atoms to diffuse from the lattice matrix to the dislocation locations, creating new atmospheres and re-locking the dislocations. Baird (1971) demonstrated that at temperatures below

100°C and 150°C, nitrogen is the most significant cause of strain ageing; carbon starts to play its role above these temperatures. Even very low interstitial carbon and nitrogen content causes the locking effect on dislocations. Strain-ageing effects can be easily observed in steel with a nitrogen content of 0.001% and can even be detectable in steel with a nitrogen content of 0.0001% (Baird, 1963). At temperatures below 100°C, strain ageing is almost entirely caused by "active" nitrogen (Leslie, 1981) because the low diffusivity of carbon at these temperatures does not cause any significant ageing effects. Natural strain ageing at ambient temperature is slow and increases with temperature (Hundy, 1954).

2.4.2 Previous studies on strain ageing of steel reinforcing bars

Strain ageing is not a new phenomenon but often unknown to many engineers. Evidence of research into the phenomenon are found in an article published in 1874 by John Fritz, who observed that processes such as straightening, punching or notching cause steel embrittlement; in the same journal W.A. Sweet affirms that "It is an established fact that punching holes for fish-plate bolts weakens the rail 75%" (Leslie, 1981, p.82). In 1932 and 1965 other examples of brittle failure of steel members were attributed to strain ageing (Leslie, 1981).

The generally accepted theory of strain ageing is attributed to a study conducted by Cottrell and Bilby (1949). Their theory is able to explain the return of the discontinuous yield point (also known as Lüders strain) and the increase of yield strain; however, it does not apply to the other strain-ageing effects normally observed: increase in ultimate tensile strength and rate of work hardening, and decrease in ductility. These property changes were explained by Baird as being caused by precipitations on dislocations (Baird, 1963).

Although in their paper Cottrell and Bilby (1949) mentioned the migration of carbon atoms to free dislocations as being the only cause, later it was shown that nitrogen also plays a very

important role (Hundy, 1954). A comprehensive study of the strain-ageing effects is found in two articles by Baird (1963, 1971).

Because strain ageing is more rapid at higher temperatures, Hundy (1954) demonstrated a relationship between the time of ageing at ambient temperature and the time of ageing at elevated temperatures:

$$\log_{10}\frac{t_r}{t} = H\left(\frac{1}{T_r} - \frac{1}{T}\right) - \log_{10}\frac{T}{T_r} \qquad (2\text{-}13)$$

where t_r is the strain-ageing time at ambient temperature T_r, and t is the time that produced the equivalent strain-ageing effect at an elevated temperature T (temperatures must be expressed in kelvin). H is 4,400 if it assumed that carbon atoms cause ageing, otherwise H is 4,000 if it assumed that nitrogen atoms cause ageing. Based on the relationship above, Hundy tabulated equivalent ageing times at room and at elevated temperatures (see Table 2-4).

Table 2-4 Equivalent ageing times at room temperature and at elevated temperatures (Hundy, 1954)

Temperature	15°C	21°C	100°C	120°C	150°C
Ageing time	1 year	6 months	4 hours	1 hour	10 min
	6 months	3 months	2 hours	30 min	5 min
	3 months	6 weeks	1 hour	15 min	2 ½ min
	1 month	2 weeks	20 min	5 min	
	1 week	4 days	5 min		
	3 days	36 hours	2 min		

A large contribution to the study of strain ageing on steel reinforcing bars was given by Professor Leslie Erasmus from the University of Canterbury, New Zealand. First papers discussed a series of brittle failures of rebars that were bent in and then re-straightened with a sledge hammer on site. These (cleavage) failures were caused by strain-ageing embrittlement and associated with

stress concentration represented by the ribs of the deformed bars (Erasmus & Pussegoda, 1977; 1978; Pussegoda, 1978)

A number of papers were then published suggesting the small additions of titanium or vanadium in order to minimise the effects of strain ageing (Erasmus & Pussegoda, 1980; Pussegoda, 1978; Pussegoda & Erasmus, 1977). The current NZ grade 500E MA is manufactured with the additions of vanadium (see certificate of test provided by the steel manufacturer with steel chemical composition, provided in Appendix B).

In 1994, Restrepo-Posada, Dodd, Park, and Cooke (1994) studied the strain-ageing effects of reinforcing bars pre-strained only by small amounts (in the Lüders strain regions and at the initiation of work hardening) and aged up to 147 days. An increase in yield strength, from 311 MPa to 356 MPa, was only observed on grade 300 pre-strained at the initiation of work hardening. Increase in ultimate tensile strength and reduction in ultimate strain were also observed. On the other hand, no strain ageing was observed in Grade 430. More recently, Momtahan, Dhakal, and Rieder (2009) discussed the effects of strain ageing on the mechanical properties of the current NZ grade 300E. Experiments were conducted on pre-strained specimens aged up to 50 days, and an increase in yield stress up to 25% was observed.

After the Christchurch earthquakes, the Royal Commission also required information about the influence of strain ageing on the steel reinforcement used in the CTV building that collapsed during the event (Allington, 2012).

2.4.3 Critical effects of strain ageing on reinforced concrete structures

Reinforced concrete moment-resisting frames are designed to avoid brittle failure of their members. This can be achieved by providing the structure with sufficient ductility capacity to absorb and dissipate energy through inelastic cycles during seismic events. The ductility of a

structure is obtained by the development of plastic hinges in specific locations (beams) where the inelastic dissipation occurs. The level of ductility required for a structure to withstand seismic cycles and dissipate energy is achieved by the arrangement and the mechanical properties of the steel reinforcement. During the design phase, it is also essential to ensure that the overstrength of beam plastic hinges is properly accounted for with respect to capacity design and hierarchy of strength principles, and thus develop a weak-beam, strong-column mechanism in case of major (design-level) earthquakes (Paulay & Priestley, 1992).

The increase in yield strength caused by the strain ageing of plastically deformed longitudinal bars could result in an increase in the flexural strength of (epoxy) repaired plastic hinges (Restrepo-Posada et al., 1994) and potentially change the hierarchy of strength of the structure in subsequent earthquakes, possibly leading to a soft-storey mechanism (Paulay & Priestley, 1992; Tasai, Otani, & Aoyama, 1988). In addition, in order to avoid brittle failure, RC members at the potential plastic hinge locations must have sufficient transverse reinforcement such as stirrups, to confine the core concrete and consequently prevent shear failure, to increase ductility, and to avoid longitudinal reinforcement buckling. For strain-ageing-susceptible steels, bends in stirrups, ties or hoops represents critical locations, as they are cold formed and have become more brittle. Therefore, in the eventuality of a strong earthquake, transverse reinforcement might be subjected to brittle failure, voiding its confining role (Pussegoda, 1978).

2.5 LOW-CYCLE FATIGUE BEHAVIOUR OF STEEL REINFORCEMENT

2.5.1 Low-cycle fatigue: introduction and definitions

The cyclic stress produced by repeated loads such as wind, car traffic or earthquakes can cause microscopic physical damage of the material involved. As the number of cycles increases, the microscopic damage accumulates and generates a crack that will eventually cause the material to fracture. This entire failure mechanism is called fatigue.

Depending on the level of the stress applied and the number of cycles to fracture, different types of fatigue failure can be distinguished:

1. High-cycle fatigue, when an element is subjected to a large number of repetitions, in the order of millions of cycles. In this case, the stress is low enough that yielding does not affect the material behaviour.
2. Low-cycle fatigue, when an element is subjected to a small number of repetitions, in the order of hundreds or thousands of cycles due to the effects of significant plastic deformation.
3. Ultra-low or extremely low-cycle fatigue, when an element is subjected to a very small number of repetitions, in the order of twenty or fewer cycles.

Fatigue problems are analysed using the following approaches or models currently available in literature: (a) a stress-based approach commonly used for problems of high cycle fatigue; (b) a strain-based approach useful for low-cycle fatigue analysis (Dowling, 2013) and extremely low-cycle fatigue analysis (Tateishi, Chen, & Hanji, 2008; Tateishi, Hanji, & Minami, 2007); and (c) a cyclic void growth model used in the case of ultra-low-cycle fatigue (Amiri, Aghakouchak,

Shahbeyk, & Engelhardt, 2013; Deierlein & Kanvinde, 2001; Kanvinde, 2004; Kanvinde & Deierlein, 2006, 2007).

Depending on the type of loads, the cyclic stress or strain histories can be either at constant or variable amplitude. Some basic definitions are presented:

- Stress or strain range is the difference between maximum and minimum stress $\Delta\sigma = \sigma_{max}$-$\sigma_{min}$ or strain $\Delta\varepsilon = \varepsilon_{max}$-$\varepsilon_{min}$.
- Mean stress or strain is the average of the maximum stress or strain and minimum stress or strain.
- Stress or strain amplitude, σ_a or ε_a is half the range $\sigma_a = \frac{\Delta\sigma}{2}$ and $\varepsilon_a = \frac{\Delta\varepsilon}{2}$.
- The stress or strain ratio R is a very common parameter; it represents the ratio between minimum and maximum stress or strain $R_\sigma = \frac{\sigma_{min}}{\sigma_{max}}$ or $R_\varepsilon = \frac{\varepsilon_{min}}{\varepsilon_{max}}$.

During seismic events in reinforced concrete structures, steel reinforcing bars are usually subjected to high levels of tension and compression strains and consequently a very small number of cycles are sufficient to cause failure. Therefore, in literature, the fatigue failure of reinforcing bars is analysed as a low- or ultra-low-cycle fatigue problem.

2.5.2 Strain–life and energy-based fatigue models

Low-cycle fatigue (LCF) problems are analysed by adopting the strain-based approach. This approach assumes that plastic yielding occurs in localised regions of the material, where fatigue cracks will eventually develop. Life estimation is performed using strain-fatigue life curves (Fig. 2-37). Strain and fatigue life are plotted on log-log coordinates with the number of cycles to failure (N_f) or half cycle ($2N_f$) on the x-axis, and the strain amplitude (ε_a) on the y-axis. The strain amplitude (ε_a) is made up of an elastic (ε_{ea}) and plastic part (ε_{pa}). These curves are obtained from

completely reverse ($R = -1$) strain controlled tests in which strain limits are constant (Dowling, 2013).

Several models to predict the low-cycle fatigue life of structural components can be found in literature. The most common, known as the Coffin–Manson relationship, was developed separately in two different studies during the late 1950s by Coffin (1954) and Manson (1953). The Coffin–Manson relationship allows the calculation of the number of cycles to failure N_f, for a given ε_a.

$$\varepsilon_a = \frac{\sigma'_f}{E}\left(2N_f\right)^b + \varepsilon_f\left(2N_f\right)^c \quad (2\text{-}14)$$

The materials constants σ_f, b, ε_f, c are obtained experimentally. The first term of the equation ($\frac{\sigma'_f}{E}\left(2N_f\right)^b$) corresponds to the elastic strain amplitude; meanwhile the second term ($\varepsilon_f\left(2N_f\right)^c$) corresponds to the plastic strain amplitude.

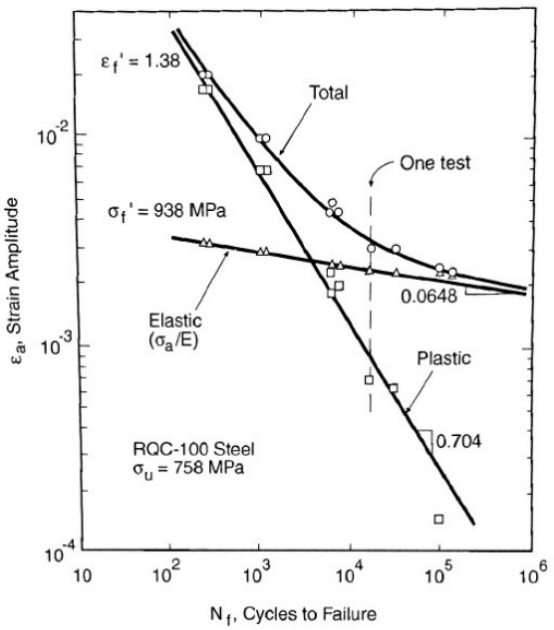

Fig. 2-37 Strain versus life curves for RQC-100 steel. For each test, elastic, plastic and total strain data points are plotted versus life, and fitted lines are also shown (Dowling, 2013).

A variant of the Coffin–Manson relationship that does not require the calculation of the elastic and plastic strain amplitude is the Koh and Stephens relationship (Koh & Stephens, 1991):

$$\varepsilon_a = M\left(2N_f\right)^m \quad (2\text{-}15)$$

M and *m* can be obtained by linear regression analysis.

As an alternative to the strain–life models, energy-based models were developed (Sugiura, Chang, & Lee, 1991; Tong, Wang, & Xu, 1989). These models use the energy dissipation as the fatigue damage parameter. They are developed from the Coffin–Manson relationship combined with the cyclic or total dissipation hysteresis energy (Tong et al., 1989).

Lefebvre and Ellyin (1984) affirmed that materials have the capacity to dissipate a specific energy amount before cracking and failure occur. The material energy dissipation represents the sum of the area of the hysteresis loop at each cycle. In some materials, hysteresis loops become stable after a few cycles until cracking propagates; this means that the energy dissipated in each cycle can be assumed to be constant during the material fatigue life (Lefebvre & Ellyin, 1984; Tong et al., 1989).

In cases of irregular cyclic load histories, such as seismic loads, fatigue life can be calculated by employing the Palmgren-Miner rule (Miner, 1945):

$$\frac{N_1}{N_{f1}} + \frac{N_2}{N_{f2}} + \frac{N_3}{N_{f3}} + \ldots = \sum \frac{N_j}{N_{fj}} = 1 \quad (2\text{-}16)$$

Assuming that $N_1, N_2, N_3, \ldots$ is the number of cycles that an element has already complete at a certain stress $\sigma_1, \sigma_2, \sigma_3, \ldots$ (or strain $\varepsilon_1, \varepsilon_2, \varepsilon_3, \ldots$) amplitude and $N_{f1}, N_{f2}, N_{f3}, \ldots$ is the number of cycles to failure at that specific stress (or strain) amplitude, the Palmgren-Miner rule says that

fatigue failure is expected when life fractions sum to 1. In other words, the ratio $\sum \frac{N_j}{N_{fj}}$ is a measure of the damage.

At a structural component scale, El-Bahy, Kunnath, Stone, and Taylor (1999b) used the Palmgren-Miner rule to estimate the cumulative damage experienced by laboratory-tested circular bridge columns subjected to different ground motion excitations. They stated that the calculated damage for some specimens, approximately equal to 0.8, was consistent with the damaged observed. The specimens were deemed unrepairable. Other cumulative damage models were introduced to predict the life of structural elements subjected to irregular strain histories such as the double linear damage rule and the damage curve concept (Manson & Halford, 1981). The above mentioned (strain–life and energy-based) models were used in several experimental studies to predict the fatigue life of steel reinforcing bars (Brown & Kunnath, 2004; Hawileh, Abdalla, Oudah, & Abdelrahman, 2010; Hawileh, Rahman, & Tabatabai, 2010; Hawileh, Tabatabai, Abu-Obeidah, Balloni, & Rahman, 2016; Mander, Panthaki, & Kasalanati, 1994). Details are in Section 2.5.3.

2.5.3 Previous experiments on steel reinforcing bars

Experimental tests on the low-cycle fatigue properties of steel reinforcing bars were conducted over the last 25 years. Mander et al. (1994) tested ASTM A615 grade 40 ordinary deformed steel reinforcing bars and ASTM A722 high strength thread bars. The research investigated the low-cycle fatigue behaviour of reinforcing bars subjected to a constant amplitude cyclic strain history in the range from yielding to 6% strain. Strain–life fatigue curves were developed. The results obtained were used to calibrate the Coffin–Manson, Koh–Stephens, Modified SWT, Lorenzo–Laird and the energy-based models. The samples used during the tests were tested unmachined as it was the intention of the experiment to capture the bars' inelastic buckling. A custom-built

extensometer was used to measure the axial strain over the gauge length of the central three bars' diameters. The extremes of the extensometer gauge length corresponded to the expected inflection points of a double curvature buckled specimen. Therefore, the extensometer was expected to measure an average strain along the buckled length of the specimen. As the specimens were tested unmachined, a special gripping technique was required to achieve high stresses.

Cyclic hardening was observed in the A615 grade 40 ordinary steel, while cycle softening was observed in the A722 high strength pre-stressing thread bars. Then, after a few cycles a stable behaviour was reached; this continued until cracking began and the stress at reversal dropped rapidly until complete fracture. The cycle when the stress-drop at reversal started was considered the failure. This concept can be observed looking at Fig. 2-39 (d): on the y-axis, the normalised stress at reversal (with respect to the stress at first reversal) is plotted against the number of cycles; the arrow indicates the points when the stress drops and the sample is considered "failed". This method was used to identify the fatigue life (N_f) for those samples tested at amplitudes smaller than 0.02 mm/mm. At larger strain amplitude, N_f was determined visually. The test results conformed with the strain–life and energy-based models adopted (Fig. 2-39).

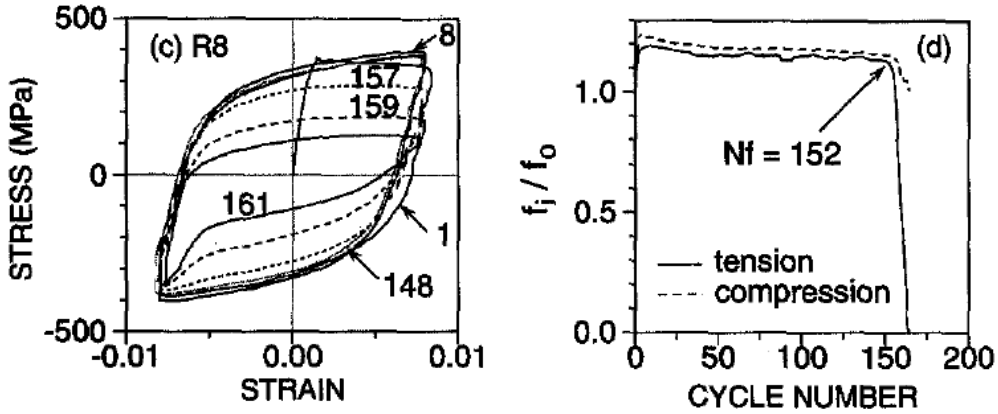

Fig. 2-38 Cyclic stress–strain results of an example specimen tested by Mander et al. (1994). On the left, the hysteresis loop; on the right a stress versus life plotted.

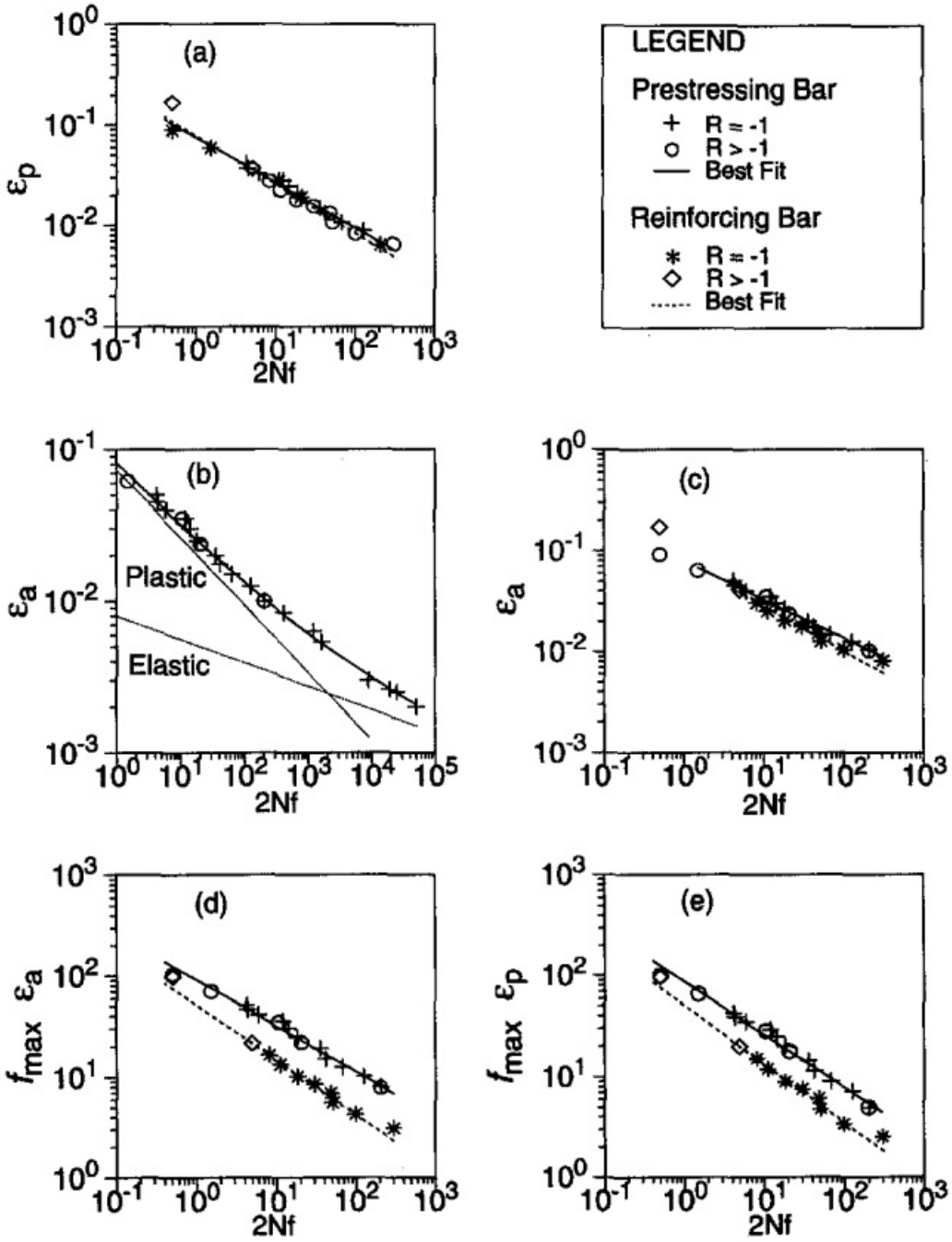

Fig. 2-39 “Experimental Data Fit to Existing Fatigue Models: (a) Coffin–Manson Model for Plastic Strain; (b) Coffin–Manson Model for Total Strain; (c) Koh–Stephens Model; (d) Modified SWT Model; and (e) Lorenzo–Laird Model” (Mander et al., 1994).

In the early 1990s, Restrepo-Posada and Dodd (1994) conducted a series of tests on Grade 300 and Grade 430 reinforcing bars in order to observe the effects of same variables such as bar deformations, strain rate and strain ageing on the cyclic behaviour (1994). A year later, they also provided a model for predicting the bar's cyclic behaviour (Dodd & Restrepo-Posada, 1995). They observed that, provided that buckling was precluded, the deformations did not affect the cyclic behaviour (in terms of hysteresis loop shape) of the rebars. Instead, an increase in strain rate caused an increase in upper and lower yield strength, ultimate tensile strength, and also strain at the onset of strain hardening. The effects of natural strain ageing (37 and 147 ageing days) were observed in terms of an increase in yield strength when the bars where pre-strained monotonically or cyclically. The increase in yield strength was observed only on Grade 300 and not on Grade 430.

Low-cycle fatigue life of reinforcing steel bars (ASTM Grade 60 reinforcement) was also investigated by Brown and Kunnath (2004). A similar approach to Mander's was adopted: reinforcing bars were tested under a constant amplitude, cyclic strain regime, then strain and energy models were employed to predict low-cycle fatigue life. A special test set-up was constructed in order to transfer the required axial force to plastically deform bars up to 25.4 mm (1 inch) diameter. The comparison between the analytical and experimental results showed that the Coffin–Manson and Koh–Stephens models gave more accurate results than the energy-based models. More recently, cyclic tests were conducted on a number of BS and ASTM reinforcing steel bars (Hawileh, Abdalla, et al., 2010; Hawileh, Rahman, et al., 2010; Hawileh et al., 2016). Tests were performed under indirect strain and displacement-controlled constant axial loading on unmachined bar specimens and experimental results were compared with the analytical ones obtained from the Coffin–Manson and the Koh–Stephens models. As in the previous

investigations, this series of experimental tests demonstrated that strain-based models can accurately predict the fatigue life of reinforcing steel bars.

Ultra-low-cycle fatigue problems (when the fatigue life is less than 20 cycles) were investigated by, Deierlein and Kanvinde (2001), Kanvinde (2004), and Kanvinde and Deierlein (2007) using the cyclic void growth model (CVGM), an extension of the void growth model (VGM) (Kanvinde & Deierlein, 2006). The VGM is based on the physical process of void nucleation, void growth, coalescence and macrocracking formation. Fracture is expected to occur when the void growth index ($VGI_{monotonic}$) reaches a critical value ($VGI_{monotonic}^{critical}$), which is a function of the mean and effective stresses. From a practical point of view, the $VGI_{monotonic}^{critical}$ corresponds to the necking stage; that is when voids reach a critical size that corresponds to the onset of coalescence and macrocracking. In the case of cyclic loads, the VGI needs to take into account that void size increases and decreases depending on the strain history. A new index was introduced, the cyclic void growth index VGI_{cyclic} and its critical value $VGI_{cyclic}^{critical}$. The model was capable of predicting the crack initiation in terms of cumulative plastic strain capacity with an error of less than 25%. This methodology worked better when the number of cycles to failure were smaller, that is, when the failure process follows the mechanism of void nucleation, void growth, coalescence and cracking. Conversely, when the number of cycles increases because the strain amplitude decreases, the prediction was less accurate; this discrepancy was attributed to other low-cycle fatigue mechanism, different from void growth and coalescence.

2.6 REFERENCES

Adeyemi, M. B., Stark, R. A., & Modlen, G. F. (1980). Isothermal stress relief of cold-extruded mild steel rods. *Studies in Surface Science and Catalysis*, 122-125.

Allington, C. (2011). *Materials testing in buildings of interest. Gallery Apartments, Westpac centre, IRD building.* (Report 107267-1 (v1.1) prepared for royal commission). Retrieved from HolmesSolution, Christchurch:

Allington, C. (2012). *Report prepared for Royal commission. Investigation into the influence of strain-ageing on the seismic performance of the reinforcing steel from the CTV building.* Retrieved from

Amiri, H. R., Aghakouchak, A. A., Shahbeyk, S., & Engelhardt, M. D. (2013). Finite element simulation of ultra low cycle fatigue cracking in steel structures. *Journal of Constructional Steel Research, 89*, 175-184.

ASTM. (2011a). E8/E8M - 11 *Standard Test Method for Tension Testing of Metallic Materials*. West Conshohocken, PA, United States.

ASTM. (2011b). E384 - 11$^{\varepsilon 1}$ *Standard Test Method for Knoop and Vickers Hardness of Materials*. West Conshohocken, PA, United States.

ASTM. (2012a). A956 - 12 *Standard test method for Leeb hardness testing of steel products*. West Conshohocken, PA, United States.

ASTM. (2012b). E18-12 *Standard test methods for Rockwell hardness of metallic materials*. West Conshohocken, PA, United States.

ASTM. (2012c). E606/E606M *Standard Test Method for Strain-controlled Fatigue Testing*. West Conshohocken, PA, United States.

Baird, J. (1963). Strain-ageing of steel - A critical review. *Iron and Steel, 36*, 186,326,368,400,450.

Baird, J. (1971). The effects of strain-ageing due to interstitial solutes on the mechanical properties of metals. *Metallurgical Reviews, 16*(1), 1-18.

Bradley, B. A. (2012). Strong ground motion characteristics observed in the 4 September 2010 Darfield, New Zealand earthquake. *Soil Dynamics and Earthquake Engineering, 42*, 32-46.

Brown, J., & Kunnath, S. K. (2004). Low-cycle fatigue failure of reinforcing steel bars. *ACI materials journal, 101*(6).

Buchanan, A. H., Bull, D. K., Dhakal, R., MacRae, G., Palermo, A., & Pampanin, S. (2011). *Base isolation and damage-resistant technologies for improved seismic performance of buildings. A report written for the Royal Commision of Inquire into building failure caused by the Canterbury earthquake*. Retrieved from Christchurch:

Bull, D. K. (2013). Earthquakes and the effects on structures: Some of the lessons learnt. *Australian Journal of Structural Engineering, 14*(2), 145-165.

Cahoon, J., Broughton, W., & Kutzak, A. (1971). The determination of yield strength from hardness measurements. *Metallurgical Transactions, 2*(7), 1979-1983.

Callister, W. D. J., & Rethwisch, D. G. (2014). *Materials science and engineering. An introduction*: Wiley.

CERC. (2012a). *Final Report. Volume 1.The performance of Christchurch CBD buildings.* Retrieved from

CERC. (2012b). *Final Report. Volume 2: The performance of Christchurch CBD buildings.* Retrieved from

Choi, Y., Park, J. H., Kim, B. M., Choi, J. C., & Min, B. H. (2000). Estimation of relation between effective strain and hardness by rigid-plastic FEM. *Metals and Materials, 6*(2), 111-116.

Coffin, J. (1954). A Study of the Effects of Cyclic Thermal Stresses on a Ductile Metal. *Trans. of the American Society of Mechanical Engineers, 76*.

Cottrell, A. H., & Bilby, B. A. (1949). Dislocation theory of yielding and strain ageing in iron. *Proceedings of the Physical Society. Section A, 62*(1).

Cuevas, A. (2013). PhD research proposal. Seismic residual capacity of reinforced concrete frames. University of Canterbury.

Cuevas, A., & Pampanin, S. (2016). *Preliminary experimental and numerical inverstigation on the seismic residual capacity of reinforced concrete beam-column joints*. Paper presented at the The New Zealand Concrete Industry Conference 2016, Auckland.

Cuevas, A., & Pampanin, S. (2017). *Post-seismic capacity of damaged and repaired reinforced concrete plastic hinges extracted from a real building*. Paper presented at the 16th World Conference on Eartquake Engineering, Santiago Chile.

Davies, R. M. (1949). The Determination of Static and Dynamic Yield Stresses Using a Steel Ball. *Proceedings of the Royal Society of London. Series A, Mathematical and Physical Sciences, 197*(1050), 416-432.

Deierlein, G. G., & Kanvinde, A. M. (2001). *Micromechanical simulation of earthquake-induced fractures in steel structures.* Paper presented at the Proceedings U.S.-Japan Joint Workshop and Third Grantees meeting.

Dieter, G. E. (1976). *Mechanical metallurgy* (Vol. 3): McGraw-Hill New York.

Dodd, L., & Restrepo-Posada, J. (1995). Model for Predicting Cyclic Behavior of Reinforcing Steel. *Journal of Structural Engineering, 121*(3), 433-445.

Dowling, N. E. (1977). Crack growth during low cycle fatigue of smooth axial specimens. *Stress strain and plastic deformation aspects of fatigue crack growth, ASTM STP 637*, 97-121.

Dowling, N. E. (2013). *Mechanical behavior of materials: engineering methods for deformation, fracture, and fatigue* (Fourth Edition ed.): Pearson.

Dowling, N. E. (2016). [Personal Communication].

El-Bahy, A., Kunnath, S., Stone, W., & Taylor, A. (1999b). Cumulative seismic damage of circular bridge columns: Variable amplitude tests. *ACI Structural Journal, 96*(5).

El-Bahy, A., Kunnath, S., Stone, W. C., & Taylor, A. W. (1999a). Cumulative seismic damage of circular bridge columns: Benchmark and low-cycle fatigue tests. *ACI Structural Journal, 96*(4).

Erasmus. (1964). Effect of small additions of Vanadium on the austenitic grain size, forgeability. and impact properties of steel'. *J. Iron Steel Inst, 202*, 128.

Erasmus. (1987). *Nitrogen in steel friend or foe?* Paper presented at the Australasian conference on materials for insutrial development, Christchurch, New Zealand.

Erasmus, & Pussegoda. (1977). Strain age embrittlement of reinforcing steels. *New Zealand Engineering, 32*(8).

Erasmus, & Pussegoda. (1980). The strain aging characteristics of reinforcing steel with a range of vanadium contents. *Metallurgical Transactions A, 11*(2), 231-237.

Erasmus, & Pussegoda, N. (1978). Safe bend radii for deformed reinforcing bar to avoid failure by strain age embrittlement. *New Zealand Engineering, 33*(8), 170.

Erasmus, L. A. (1981). Cold straightening of partially embedded reinforcing bars - A different view. *Concrete International*.

Frank, S., & Technologies, G. I. (2005). Mobile Hardness Testing. Application Guide for Hardness Testers *GE Inspection Technologies*.

Hall, E. (1951). The deformation and ageing of mild steel: III discussion of results. *Proceedings of the Physical Society. Section B, 64*(9), 747.

Hawileh, Abdalla, J., Oudah, F., & Abdelrahman, K. (2010). Low-cycle fatigue life behaviour of BS 460B and BS B500B steel reinforcing bars. *Fatigue & Fracture of Engineering Materials & Structures, 33*(7), 397-407.

Hawileh, Rahman, A., & Tabatabai, H. (2010). Evaluation of the Low-Cycle Fatigue Life in ASTM A706 and A615 Grade 60 Steel Reinforcing Bars. *Journal of Materials in Civil Engineering, 22*(1), 65-76.

Hawileh, Tabatabai, H., Abu-Obeidah, A., Balloni, J., & Rahman, A. (2016). Evaluation of the Low-Cycle Fatigue Life in Seven Steel Bar Types. *Journal of Materials in Civil Engineering, 28*(5).

Hundy, B. B. (1954). Accelerated Strain Ageing of Mild Steel. *Journal of The Iron and Steel Institute, 178*.

Hutchings, I. M. (2009). The contributions of David Tabor to the science of indentation hardness. *Journal of Materials Research, 24*(3), 581-589.

Kam, W. Y., & Pampanin, S. (2011). The seismic performance of RC buildings in the 22 February 2011 Christchurch earthquake. *Structural concrete, 12*(4), 223-233.

Kam, W. Y., Pampanin, S., Dhakal, R., Gavin, H. P., & Roeder, C. (2010). Seismic performance of reinforced concrete buildings in the September 2010 Darfield (Canterbury) earthquake. *Bulletin of the New Zealand Society for Earthquake Engineering, 43*(4), 340-350.

Kam, W. Y., Pampanin, S., & Elwood, K. (2011). Seismic performance of reinforced concrete buildings in the 22 February Christchurch (Lyttelton) earthquake. *Bulletin of the New Zealand Society for Earthquake Engineering, 44*(4), 239-278.

Kanvinde. (2004). *Micromechanical simulation of earthquake-induced fracture in steel structures.* (PhD), Stanford University.

Kanvinde, & Deierlein. (2006). The Void Growth Model and the Stress Modified Critical Strain Model to Predict Ductile Fracture in Structural Steels. *Journal of Structural Engineering, 132*(12), 1907-1918.

Kanvinde, & Deierlein. (2007). Cyclic void growth model to assess ductile fracture initiation in structural steels due to ultra low cycle fatigue. *Journal of Engineering Mechanics*(133), 701-712.

Koh, S., & Stephens, R. (1991). Mean stress effects on low cycle fatigue for a high strength steel. *Fatigue & Fracture of Engineering Materials & Structures, 14*(4), 413-428.

Krauss, G. (2005). *Steels: heat treatment and processing principles*. Ohio: ASM International.

Lee, K.-S., & Song, J.-H. (2006). Estimation methods for strain-life fatigue properties from hardness. *International Journal of Fatigue, 28*(4), 386-400.

Lefebvre, D., & Ellyin, F. (1984). Cyclic response and inelastic strain energy in low cycle fatigue. *International Journal of Fatigue, 6*(1), 9-15.

Leslie, W. C. (1981). *The physical metallurgy of steels* (M.-H. B. Company Ed.). Washington.

Lim, W. T. (1991). *Statistical analysis of reinforcing steel properties.* (Master of engineering), University of Canterbury, Christchurch.

Lopez, Z., & Fatemi, A. (2012). A method of predicting cyclic stress–strain curve from tensile properties for steels. *Materials Science and Engineering: A, 556*(0), 540-550.

Loporcaro, G., Kral, M. V., & Pampanin, S. (2015). *Experimental validation of "the hardness method" to estimate the residual ductility of plastically deformed steel reinforcement*. Paper presented at the NZSEE conference, Rotorua.

Loporcaro, G., Kral, M. V., & Pampanin, S. (2017). *A cause study: application of the hardness method to estimate the residual capacity of reinforcement in an earthquake damaged building*. Paper presented at the 16th World Conference of Earthquake Engineering, Santiago de Chile.

Loporcaro, G., Pampanin, S., & Kral, M. V. (2014). *Investigating the relationship between hardness and plastic strain in reinforcing steel bars*. Paper presented at the NZSEE conference, Auckland.

Loporcaro, G., Pampanin, S., & Kral, M. V. (2016). *Comparison between accelerated and natural strain ageing effects on New Zealand manufactured Grade 300E steel reinforcing bars*. Paper presented at the NZSEE, Christchurch.

Malek, A. (2014). PhD research proposal. Residual seismic capacity of reinforced concrete members. University of Canterbury.

Malek, A., Scott, A., Pampanin, S., & MacRae, G. (2015). *Assessment of post-earthquake in RC elements using low-invasive techniques.* Paper presented at the New Zealand Society of Earthquake Engineering 2015, Rotorua, New Zealand.

Malek, A., Scott, A., Pampanin, S., MacRae, G., & Hoult, N. A. (2016). *Damage assessment of RC beam using distributed fibre optics strain sensors.* Paper presented at the New Zealand Society of Earthquake Engineering 2016, Christchurch, New Zealand.

Mander, J., Panthaki, F., & Kasalanati, A. (1994). Low-cycle fatigue behavior of reinforcing steel. *Journal of Materials in Civil Engineering, 6*(4), 453-468.

Mander, J., & Rodgers, G. (2015). *Analysis of low cycle fatigue effects on structures due to the 2010-2011 Canterbury Earthquake Sequence.* Paper presented at the Tenth Pacific Conference on Earthquake Engineering, Sydney, Australia.

Manson. (1953). *Behavior of materials under conditions of thermal stress*: NACA TN 2933.

Manson, & Halford. (1981). Practical implementation of the double linear damage rule and damage curve approach for treating cumulative fatigue damage. *International Journal of Fracture, 17*(2), 169-192.

Matsumoto, Y. (2009). Study on the residual deformation capacity of plastically strained steel *Behaviour of Steel Structures in Seismic Areas*: CRC Press.

Mezzina, M. (2001). *Costruire con il cemento armato*. Torino.

Miner, M. A. (1945). Cumulative Damage in Fatigue, Transactions of the ASCE. *Cumulative Damage in Fatigue. Transactions of ASME, 67*, A159-A164.

Momtahan, A., Dhakal, R., & Rieder, A. (2009). Effects of strain-ageing on New Zealand reinforcing steel bars. *Bulletin of the New Zealand Society for Earthquake Engineering, 42*(2).

Morris, G. J., Bull, D. K., & Bradley, B. A. (2014). *Reviewing uncertainties in seismic experimentation following the unexpected performance of RC structures in the 2010-2011 Canterbury earthquakes.* Paper presented at the NZSEE 2014, Auckland.

Nakane, M., Kanno, S., Kurosake, Y., Takagi, Y., Komotori, J., & Ogawa, T. (2010). Accuracy of Plastic Strain Estimated by Hardness to Assess Remaining Fatigue Lives. *Material Properties Measurement*.

Nashid, H., Ferguson, W. G., Clifton, C., Hodgson, M., Battley, M., Seal, C., & Choi, J. H. (2014). Non-destructive method to investigate the hardness-plastic strain relationship in cyclically deformed steel structural steel elements. *Bulletin of the New Zealand Society for Earthquake Engineering, 47*(3), 181-189.

New Zealand Standards. (1949). NZS 197:1949 *Rolled steel bars and drawn steel wire for concrete reinforcement*. Wellington New Zealand.

New Zealand Standards. (1963). NZSS 1693:1962 *Deformed steel bars of structural grade for reinforced concrete*. Wellington New Zealand.

New Zealand Standards. (1964). NZSS 1879:1964 *Hot rolled deformed bars of HY 60 (High Yield 60000 psi) for reinforced concrete*. Wellington New Zealand.

New Zealand Standards. (1972). NZS 3423P:1972 *Hot rolled plain round steel bars of structural grade for reinforced concrete*. Wellington New Zealand.

New Zealand Standards. (1973). NZS 3402P:1973 *Hot rolled steel bars for reinforcement of concrete*. New Zealand Wellington.

New Zealand Standards. (1976). NZS 4203:1976 *Code of practice for general structural design and design loading for buildings*. Wellington, New Zealand.

New Zealand Standards. (1982). NZS 3101:1982 *Concrete structures standard - Code of practice for the design of concrete structures*. Wellington, New Zealand.

New Zealand Standards. (1989). NZS 3402:1989 *Steel bars for the reinforcement of concrete*. Wellington New Zealand.

New Zealand Standards. (2004). NZS 1170.5:2004 *Structural design actions. Part 5: Earthquake actions - New Zealand*. Wellington, New Zealand.

New Zealand Standards. (2006). NZS 3101:2006 *Concrete structures standard*. Wellington.

NZTA. (2016). Bridge manual (SP/M/022).

O'Neill, H. (1967). *Hardness measurement of metals and alloys* (Second edition ed.): Chapman and Hall.

Office of the Auditor General. (2017). *Canterbury Earthquake Recovery Authority: Assessing its effectiveness and efficiency*. Retrieved from http://www.oag.govt.nz/2017/cera/docs/cera.pdf

Palermo, A., Liu, R., Rais, A., McHaffie, B., Andisheh, K., Pampanin, S., . . . Wotherspoon, L. (2017). Performance of road bridges during the 14 November 2016 Kaikoura earthquake. *Bulletin of the New Zealand Society for Earthquake Engineering (under review)*.

Pampanin, S. (2012). *Reality-check and Renewed challenges in Earthquake Engineering: Implementing low-damage structural Systems–from theory to practice.* Paper presented at the 15th World Conference on Earthquake Engineering.

Pampanin, S., Cuevas Ramirez, A., Kral, M. V., Loporcaro, G., Scott, A., & Malek, A. (2015). *Residual capacity and repairing options for reinforced concrete buildings*. Retrieved from

Paulay, T., & Park, R. (1975). *Reinforced concrete structures: R. Park and T. Paulay*. New York: Wiley.

Paulay, T., & Priestley, M. J. N. (1992). *Seismic design of reinforced concrete and masonry buildings*. New York: John Wiley & sons, inc.

Pavlina, E., & Van Tyne, C. (2008). Correlation of Yield Strength and Tensile Strength with Hardness for Steels. *Journal of Materials Engineering and Performance, 17*(6), 888-893.

Pavlina, E., & Van Tyne, C. (2014). Uniform Elongation and the Stress-Strain Flow Curve of Steels Calculated from Hardness Using Empirical Correlations. *Journal of Materials Engineering and Performance, 23*(6), 2247-2254.

Priestley, M. J. N., Calvi, G. M., & Kowalsky, M. J. (2007). *Displacement-based seismic design of structures*. Pavia, Italy: IUSS Press.

Proceq. (2007). Equotip 3 Portable hardness tester. Operating instructions.

Pussegoda. (1978). *Strain age embrittlment in reinforcing steels.* (Doctor of Philosophy), University of Canterbury, Christchurch.

Pussegoda, & Erasmus. (1977). *The effect of titanium on the strain ageing characteristics of a carbon manganese structural steel*. Paper presented at the 6th Australas Conf on the Mech of Struct and Mater, Christchurch.

Restrepo-Posada, J., Dodd, L., Park, R., & Cooke, N. (1994). Variables Affecting Cyclic Behavior of Reinforcing Steel. *Journal of Structural Engineering, 120*(11), 3178-3196.

Roberts, B. (2016). [Personal communication].

Roessle, M. L., & Fatemi, A. (2000). Strain-controlled fatigue properties of steels and some simple approximations. *International Journal of Fatigue, 22*(6), 495-511.

SEAOC. (1995). *Vision 2000 committee. Performance-based seismic engineering of buildings*. Retrieved from Sacramento, California:

SESOC, S. e. s. N. Z. (2011). *Preliminary observations from Christchurch Earthquakes*. Retrieved from

Standards Australia. (2007). AS 1391-2007 *Metallic materials - Tensile testing at ambient temperature*. Sydney.

Standards Australia and New Zealand. (2001). AS/NZS 4671:2001 *4671:2001 Steel reinforcing materials*. Wellington, New Zealand.

Standards Australia and New Zealand. (2002). AS/NZS 1170.0:2002 Structural design action *Part 0: General principles*. Sydney NSW 2001, Wellingrton 6140 NZ.

Stephens, R. I., & Koh, S. K. (1988). Improvements in empirical representation of A356-T6 cast aluminum alloy round-robin low cycle fatigue data. *SAE SP-760*, 29-38. doi:10.4271/881702

Sugiura, K., Chang, K. C., & Lee, G. C. (1991). Evaluation of Low-Cycle Fatigue Strength of Structural Metals. *Journal of Engineering Mechanics, 117*(10), 2373-2383.

Surajit Kumar, P., Pritam Kumar, R., Debdulal, D., Sanjay, C., & Saurabh, K. (2014). High and low cycle fatigue performance comparison between micro-alloyed and TMT rebar. *Construction and Building Materials, 54*, 170-179.

Tabor, D. (1951a). The hardnes and strength of metals. *Journal of the Institute of Metals, 59*.

Tabor, D. (1951b). *The hardness of metals*: Oxford University Press.

Tasai, A., Otani, S., & Aoyama, H. (1988). Resistance of reinforced concrete component repaired with epoxy resin. *Journal of the faculty of engineering, the University of Tokyo (B), XXXIX*(3), 345-359.

Tateishi, K., Chen, T., & Hanji, T. (2008). Extremely low cycle fatigue assessment method for un-stiffened cantilever steel columns. *Structural Eng./Earthquake Eng., JSCE, 25*(1).

Tateishi, K., Hanji, T., & Minami, K. (2007). A prediction model for extremely low cycle fatigue strength of structural steel. *International Journal of Fatigue, 29*(5), 887-896.

Tilly, G. P. (1979). Fatigue of steel reinforcement bars in concrete: a review *Fatigue & Fracture of Engineering Materials & Structures, 2*(3), 251-268.

Timoshenko, S. (1970). *Theory of elasticity*. New York: McGraw-Hill.

Tong, X.-y., Wang, D.-j., & Xu, H. (1989). Investigation of cyclic hysteresis energy in fatigue failure process. *International Journal of Fatigue, 11*(5), 353-359.

Vander Voort, G. F. (1999). *Metallography: principles and practices*: ASM International.

Wahlberg, A. (1901). Brinell's method of determining hardness and other properties of iron and steel. *The journal of the iron and steel institute, 59*.

Wilson, D. V., & Russell, B. (1960). The contribution of precipitation to strain ageing in low carbon steels. *Acta Metallurgica, 8*(7), 468-479.

Zhang, C., Li, F., & Wang, B. (2013). Estimation of the elasto-plastic properties of metallic materials from micro-hardness measurements. *Journal of Materials Science, 48*(12), 4446-4451.

3 ROBUSTNESS OF THE RELATIONSHIP BETWEEN HARDNESS AND PLASTIC STRAIN

3.1 INTRODUCTION

The objective of this thesis is to find a simple and reliable technique to determine the amount of damage (plastic deformation) of steel reinforcement in earthquake-damaged buildings and to estimate the residual ductility. Prior to the Canterbury earthquakes, very little work had been published on techniques aimed to address this issue. The few applications found in the literature are based on hardness testing, since plastic deformation increases yield strength and yield strength can be correlated to hardness of metals in deformed regions (Cahoon et al., 1971; Dieter, 1976; Vander Voort, 1999).

Since hardness testing is a fast and practical method to estimate the mechanical properties of many metals, the author explored the possibility of employing the hardness technique during this research. Therefore, if hardness can be used as a parameter to detect plastic deformation in steel reinforcement, a robust mathematical relationship between hardness and strain must be identified. This relationship must be determined as accurately as possible by performing interrupted tensile tests, at defined strain limits, and subsequently measuring the Vickers hardness.

Previous attempts did not provide sufficient information to support such a strong correlation for steel reinforcement (Allington, 2011). To achieve the strong correlation, some objectives need to be achieved:

- define the specimen geometry for combined hardness and tensile testing
- determine the most reliable hardness testing technique
- define the specimen surface finishing

- establish the strain range of interest
- determine amount and type of steel material required
- establish a fast and practical strain-ageing procedure.

In this chapter, the results from a series of experimental tests, conducted to achieve the objectives listed above and to prove the main hypothesis, are presented and critically discussed.

3.1.1 Testing facilities

All experimental testing was conducted in the Mechanical Engineering laboratories of the University of Canterbury. Depending on the load requirement and specimen geometry, tensile testing was carried out using a servo-hydraulic MTS 810 testing system with 100 kN load capacity or a universal testing machine SATEC system with 1000 kN load capacity (see Fig. 3-1 and Fig. 3-2).

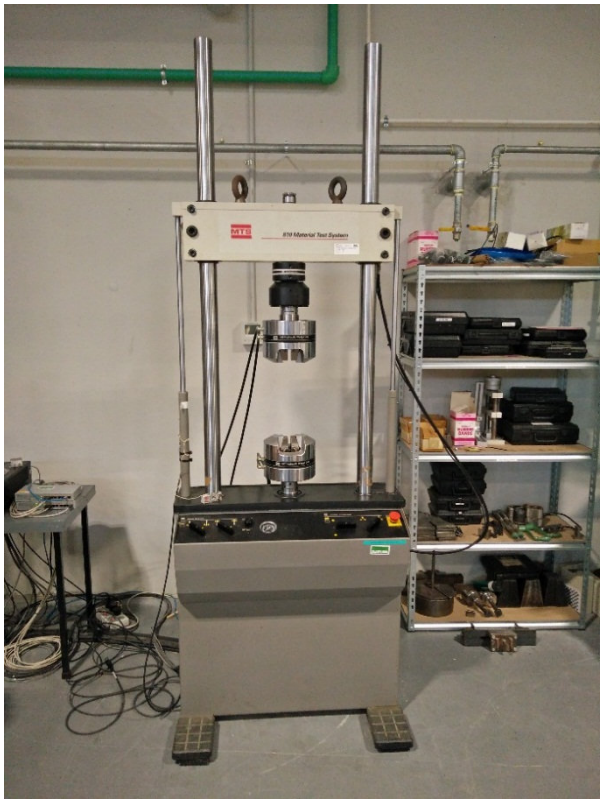

Fig. 3-1 MTS 810 servo-hydraulic testing machine.

Fig. 3-2 SATEC system testing machine.

The specimen elongation (strain) was captured using either a 25 mm or 50 mm gauge length MTS extensometer. The extensometer was attached at the centre of the reduced section of the testing sample with the aid of rubber bands (see Fig. 3-3 and Fig. 3-4).

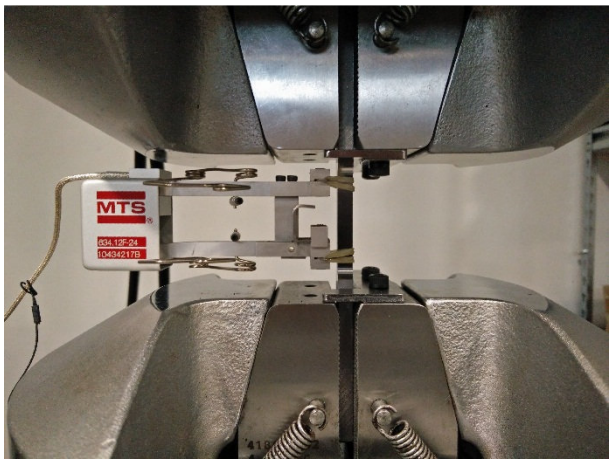

Fig. 3-3 Twenty-five mm gauge length extensometer settings on a flat-shape tensile specimen.

Fig. 3-4 Fifty mm gauge length extensometer settings on a round-shape tensile specimen.

Hardness testing was conducted using a conventional Vickers workbench testing machine with a diamond pyramidal indenter, 2/3" objective and 30 kg load (Fig. 3-5 and Fig. 3-6); and a Rockwell workbench testing machine. In the case of the Vickers testing, the indentation diagonal lengths were measured with the aid of a microscope and then converted using appropriate converting tables, to Vickers hardness (HV_{30}). In the case of Rockwell hardness testing, the measurement was obtained from a gauge incorporated in the machine (Fig. 3-7). A Proceq Equotip portable device was also used to measure the hardness on the Leeb scale (Fig. 3-8).

Fig. 3-5 Conventional workbench hardness testing machine.

Fig. 3-6 Diamond indenter of the Vickers hardness machine.

Fig. 3-7 Gauge of a Rockwell hardness machine.

Fig. 3-8 Proceq Equotip 3 portable Leeb hardness tester.

3.2 EMPIRICAL RELATIONSHIP BETWEEN HARDNESS AND STRAIN: EXPERIMENTAL TEST

3.2.1 Procedure

Preliminary tests were conducted to establish the standard procedure for developing the empirically-based mathematical hardness versus strain calibration curves and achieve the objectives listed in the introduction section of this chapter. Tests were conducted on steel samples machined from locally obtained Grade 300E and Grade 500E 25 mm in diameter reinforcing bars. Chemical composition and average tensile properties are summarised in Table 3-1 and Table 3-2.

Table 3-1 Chemical composition data (wt %) from Mill Certification Sheet

Material	C	Mn	Si	S	P	Ni	Cr	Mo	Cu	Sn	V	Ceq
300E	0.18	0.78	0.22	0.024	0.013	0.09	0.09	0.017	0.28	0.018	0.003	0.36
500E	0.18	1.27	0.35	0.032	0.017	0.07	0.11	0.013	0.26	0.017	0.085	0.46

Table 3-2 Average tensile properties of reinforcing steel

Material	Yield strength (MPa)	Ultimate tensile strength (MPa)	Uniform elongation (%)
300E	323	515	19.3
500E	524	684	13.1

In the first instance, two specimen geometries were selected: cylindrical and flat-shape "dog-bone". Flat-shape specimens were selected since hardness can be easily and accurately carried out on flat surfaces. In addition, the MTS wedge grips were only compatible with flat specimens. On the other hand, cylindrical samples were selected since larger-diameter specimens could be tensile tested in the 1000 kN load capability SATEC Universal Testing Machine (UTM). Flat-shape (Fig. 3-10) and cylindrical (Fig. 3-11) specimens were both machined according to ASTM E8/E8M – 11 standard (ASTM, 2011a).

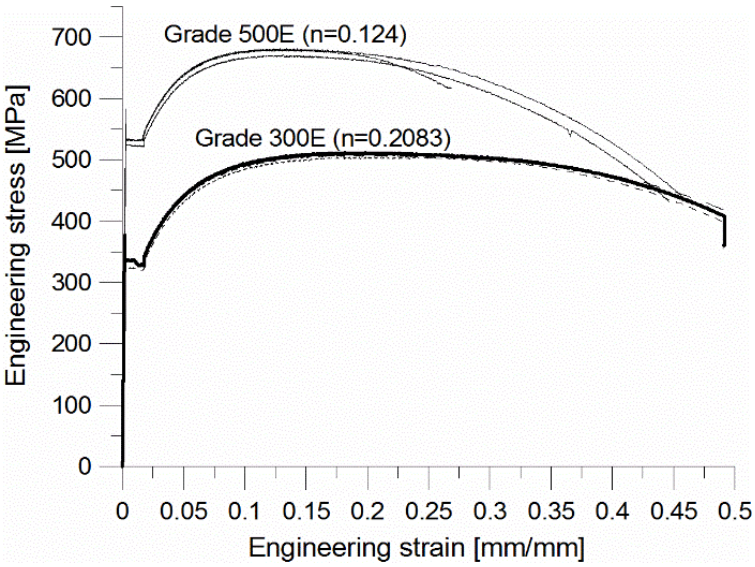

Fig. 3-9 Grade 300E and 500E stress–strain curves from six samples tested.

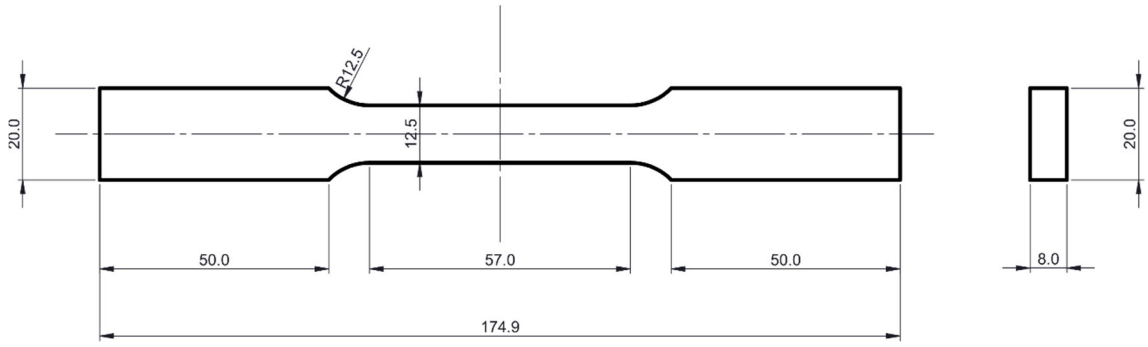

Fig. 3-10 Flat “dog-bone” steel specimen (type 2) samples, dimensions in mm.

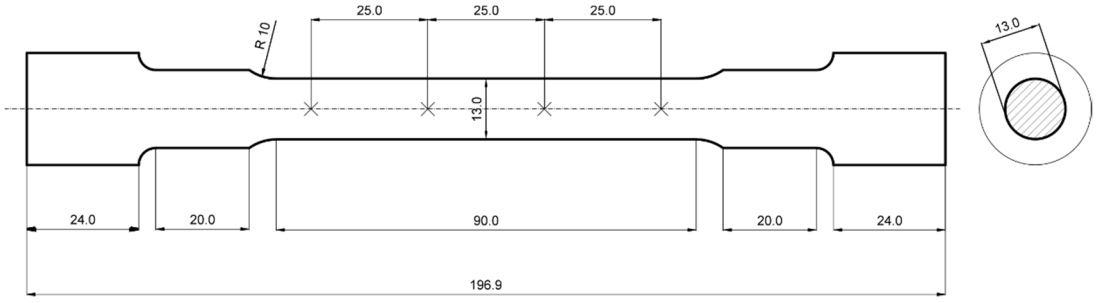

Fig. 3-11 Cylindrical “dog-bone” steel specimen samples drawing, dimensions in mm.

Knowing the strain at ultimate tensile strength (also named as uniform elongation or ultimate strain), the interrupted tensile tests were conducted. The interruption limits selected were: 1, 2, 4, 6, 8, 10, 14 and 18% strain, for seismic Grade 300E; and 1, 2, 4, 6, 8, 10, 12 and 14%, for seismic Grade 500E. The largest limit was selected at (or below) the ultimate strain since this point corresponds to the onset of necking, any further deformation occurring will be concentrated only at this location.

In order to take into account the strain-ageing effects for Grade 300E, after the interrupted tensile tests, the samples were immersed in boiling water for 4 hours, which is reported to simulate one year of ageing at about 15 °C (Hundy, 1954). Due to a relatively high vanadium content (about 0.085%), Grade 500E was not expected to be prone to strain ageing (Erasmus, 1964; Erasmus & Pussegoda, 1980). This assumption was then verified with another series of tests. Details are presented in Chapter 6.

Subsequently, Vickers and Rockwell hardness tests were carried out according to ASTM Standard E384 - $11^{\varepsilon 1}$ (ASTM, 2011b) and E18 – 12 (ASTM, 2012b) using conventional workbench Vickers and Rockwell hardness machines. The Vickers method requires the user to optically measure, through a microscope, the diagonal lengths of the indentation produced by a diamond indenter on the sample. In contrast, the Rockwell test requires the application of a 100 kg load through a 1/8 inch steel ball indenter. The indenter penetrates into the sample. The Rockwell hardness corresponds to the difference in the depth of the indenter at two specific times during the testing cycle (when a minor load of 10 kg and when the testing load of 100 kg are applied) (Vander Voort, 1999). The Rockwell hardness can be easily read from the machine dial gauge. To facilitate the hardness testing procedure, the shoulder ends of the “dog-bone” specimens were cut off and the round surface was ground flat. This operation was not required for the flat-shape specimens.

The flat surface was then sequentially ground from 240 to 600 grit and polished with 9-, 3- and then 1-micron diamond paste to reduce errors during the Vickers optical indentation measurements. Vickers indentations were performed on the deformed samples at 5 mm intervals along the gauge length. Approximately 16 to 18 measurements were made both in the Vickers and Rockwell B scales. The mean hardness and standard deviation were calculated and correlated to the amount of true plastic strain ($\tilde{\varepsilon}$), calculated as the natural logarithm of the ratio between original area *(A_i)* and current cross-sectional area *(A)* (Dowling, 2013):

$$\tilde{\varepsilon} = ln\frac{A_i}{A} \tag{3-1}$$

It is then possible to convert the true plastic strain to a more practical engineering plastic strain using the relationship:

$$\tilde{\varepsilon} = \ln(1 + \varepsilon) \tag{3-2}$$

ε is the engineering plastic strain.

3.2.2 Results

As expected, the results showed an increase in hardness with an increase of plastic strain for both steel grades. All data sets were fitted with a power-law curve as shown in Fig. 3-12 and Fig. 3-13:

$$HV = K\varepsilon^c \tag{3-3}$$

where *HV* is the Vickers hardness number, ε is the engineering plastic strain in mm/mm, and *K* and *c* are two material-dependent constants. The standard deviation for hardness measurements was approximately 2.5 HV for strains over 2% in both steels. The standard deviation for strains as low as 1% (i.e., within the Lüders extension) was 7 HV.

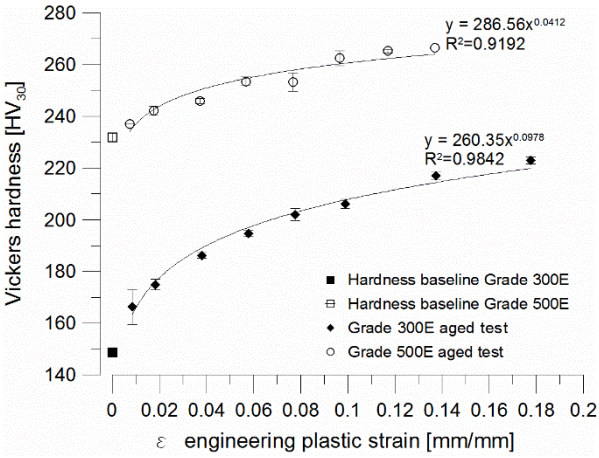

Fig. 3-12 Vickers hardness versus engineering plastic strain for aged seismic Grade 300E and aged seismic Grade 500E (although significant strain-ageing effects were not observed for Grade 500E).

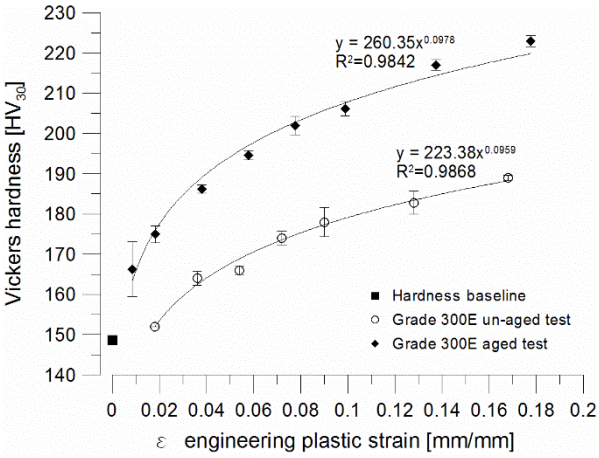

Fig. 3-13 Vickers hardness versus engineering plastic strain for un-aged Grade 300 steel and for Grade 300 steel with simulated strain ageing of one year.

3.2.3 Discussion

Initial observations, specimen geometry and strain ageing

In the literature, hardness is usually related to true stress or true strain (Tabor, 1951b); however for structural engineering applications, engineering stress and engineering strain are more practical and universally used. Therefore, the latter will be used in the rest of the research.

In the range between 0% and 2% plastic strain, the hardness standard deviation is higher compared with the other plastic strain limits. In this strain range, known as the discontinuous yielding point, plastic strain is localised. Lüders bands start to form at the upper yield stress and eventually extend over the entire length of the specimen until uniform strain hardening starts. In the discontinuous range, hardness increases only where the Lüders bands have formed (see Fig. 3-14).

Calibration curves were not affected by the specimen geometry (see Fig. 3-16), cylindrical specimens required a further machining process: shoulder ends needed to be cut before hardness

testing. Flat-shape specimens were more practical because the initial machining operation on its own is sufficient.

The “accelerated” strain-ageing procedure in boiling water (100°C) for four hours caused an increase in hardness, as can be observed from Fig. 3-13. The increase in hardness is due to the increased resistance to further plastic deformation. As discussed by Tabor (1951b), hardness is a measure of the yield strength of a metal; therefore, if strain ageing increases the yield stress of a steel, hardness increases consequently. Note that in Fig. 3-15 an increase in yield stress occurred when the sample was reloaded from 0.16 % strain during the interrupted tensile test. This discontinuity in behaviour occurred because the specimen was allowed to rest for 2 to 3 days at ambient temperature. During this time period, strain ageing took place and the effects were evident from the stress–strain curve. Therefore, it is recommended to include this procedure in the standard methodology. Further investigation on strain-ageing effects is conducted in Chapter 6.

From Fig. 3-17 it can also be observed that the hardness increase relative to the amount of plastic strain in Grade 300E is more significant compared with Grade 500E. This can be explained by the strain-hardening exponent (n) for Grade 300E (0.2083) being higher than for Grade 500E (n=0.124) (see Fig. 3-9).

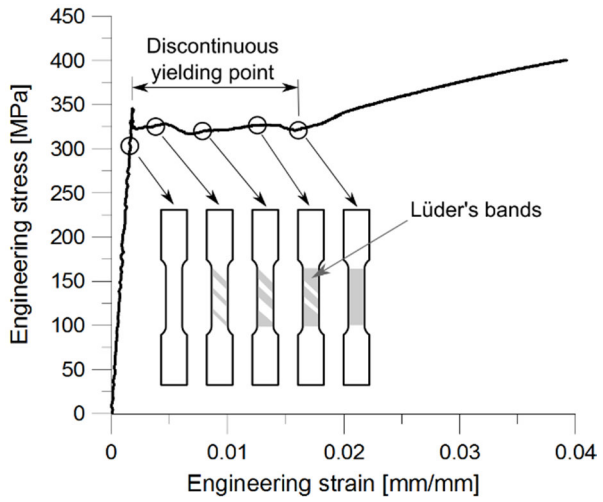

Fig. 3-14 Schematic development of Lüders bands as deformation increases.

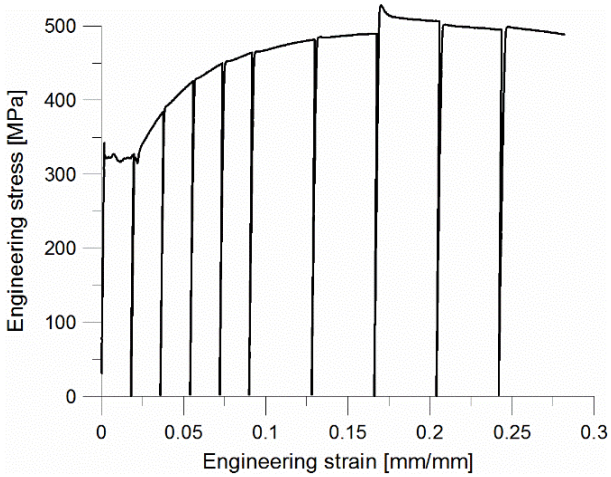

Fig. 3-15 Example of an interrupted stress–strain curve. Note the discontinuity at 0.16 mm/mm strain.

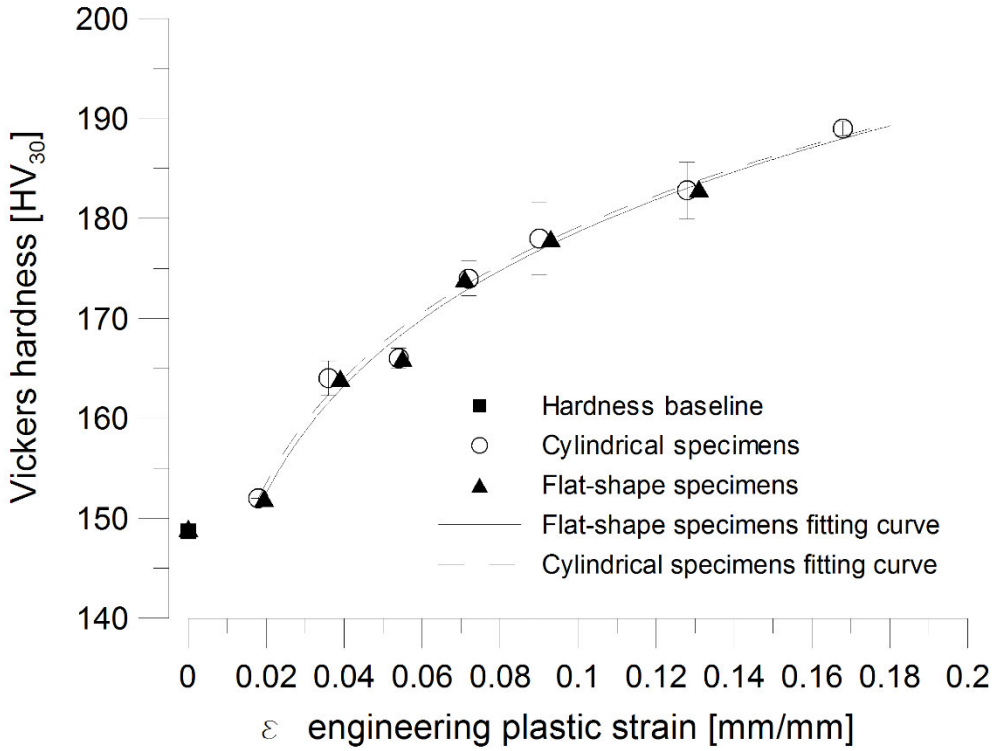

Fig. 3-16 Comparison of HV_{30} vs. ε curves for flat-shape and cylindrical specimens.

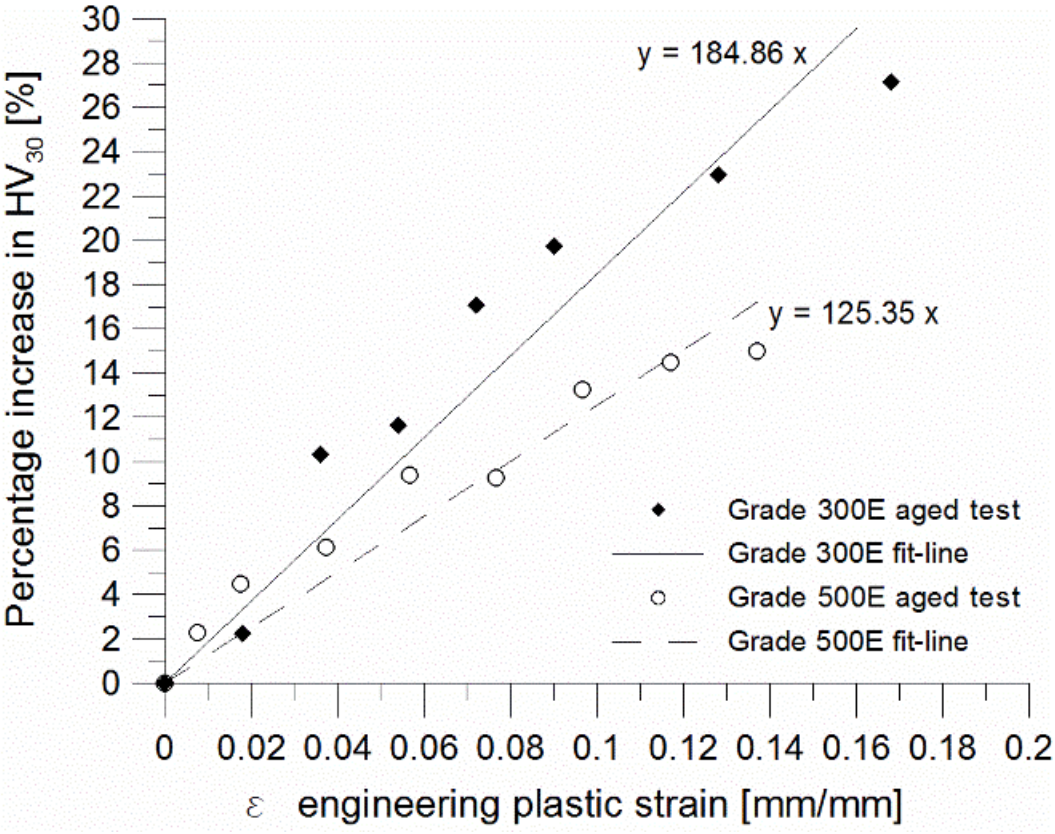

Fig. 3-17 Percentage increase in Vickers hardness (HV_{30}) versus engineering plastic strain for Grade 300E and 500E.

Hardness testing methodologies comparison: Vickers, Rockwell and Leeb

The preliminary tests provided also information about the most suitable hardness test method. The Vickers, Rockwell B and Leeb hardness methodologies were evaluated on their ability to reliably detect changes in hardness that were obtained by applying varying levels of strain to tensile specimens. First, Vickers and Rockwell B were compared. One tensile sample was prepared for each pre-strain level: 0.02, 0.04, 0.06, 0.08 and 0.10 mm/mm. Samples were aged at 100°C for four hours after straining. Ten hardness measurements were obtained along the gauge length for each sample, for each method. Second, Vickers and Leeb hardness methods were compared. Ten tensile samples were prepared for each pre-strain level: 0.02, 0.04, 0.06 and 0.08 mm/mm. Ten

hardness measurements at 5 mm spacing were obtained for each sample along the gauge length. All samples were tested with a ground surface finish.

It should be noted that Leeb measurements are dependent on the weight and thickness of the sample tested. ASTM A956-12 (ASTM, 2012a) suggests a minimum test piece weight of 1.5 kg and a minimum thickness of 1 mm. Test pieces smaller than the minimum weight or thickness require a rigid support. Initially, as a support, three materials were evaluated: steel, wood and concrete. The Leeb hardness value for the same steel specimens varied substantially (see Table 3-3). Since Leeb hardness measurements are dependent on the material elastic modulus (Frank & Technologies, 2005), it is convenient to couple the specimen with a material that has the same elastic modulus. Therefore, in this case a 20 mm-thick mild steel plate with a ground surface, of dimensions approximately 300 x 200 mm, was used. The Leeb portable hardness manufacturers propose guidelines and specific coupling pastes to conduct Leeb measurements on small test pieces (Proceq, 2007); the present work used petroleum jelly.

Table 3-3 Leeb hardness results of a steel specimens varying the support.

Supporting material	**Leeb hardness (HLDL)**
Steel	630
Wood	427
Concrete	502

Fig. 3-18 and Fig. 3-19 show the Vickers hardness and Rockwell hardness comparison, and Vickers and Leeb hardness comparison for Grade 300E steel over a range of tensile pre-strains. The average hardness for each strain level and each hardness method was fitted to a power-law function, since increasing pre-strain is analogous to strain hardening. In the strain range analysed (0 to 0.10 mm/mm), the Rockwell hardness scale showed a limited sensitivity in comparison with Vickers. Even though the standard deviation for the Leeb method was significantly higher than the

other two methods, the most important difference was the power-law exponent. With a near-zero exponent, the Leeb method has relatively poor ability to resolve small differences in pre-strain (in the order of 0.02 mm/mm). It should also be noted that when Leeb is used in the field, the surface finish and flatness that can practically be achieved are generally variable, which would degrade the results further. Both the portable Leeb method and lab-based Rockwell B hardness methods have been used previously in the context of earthquake-damaged material, mainly for ease of use and practicality. Although it would still be desirable to use the Leeb or Rockwell methods for continuity with previous work as well as ease of use, convenience, or even in situ measurements, the present results demonstrate that the Vickers method is superior in terms of detecting small changes in hardness

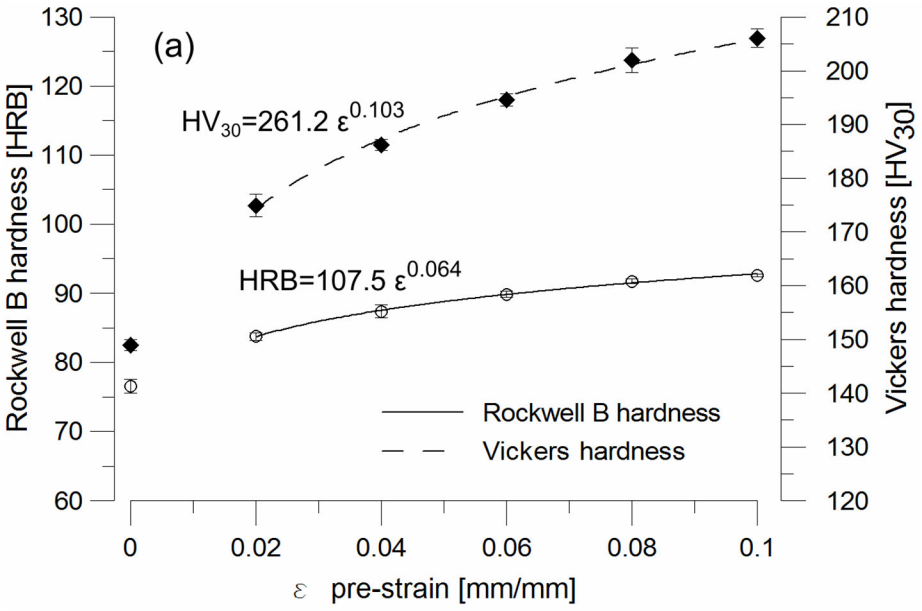

Fig. 3-18 Rockwell B and Vickers hardness versus pre-strain calibration curves for Grade 300E steel reinforcing bar.

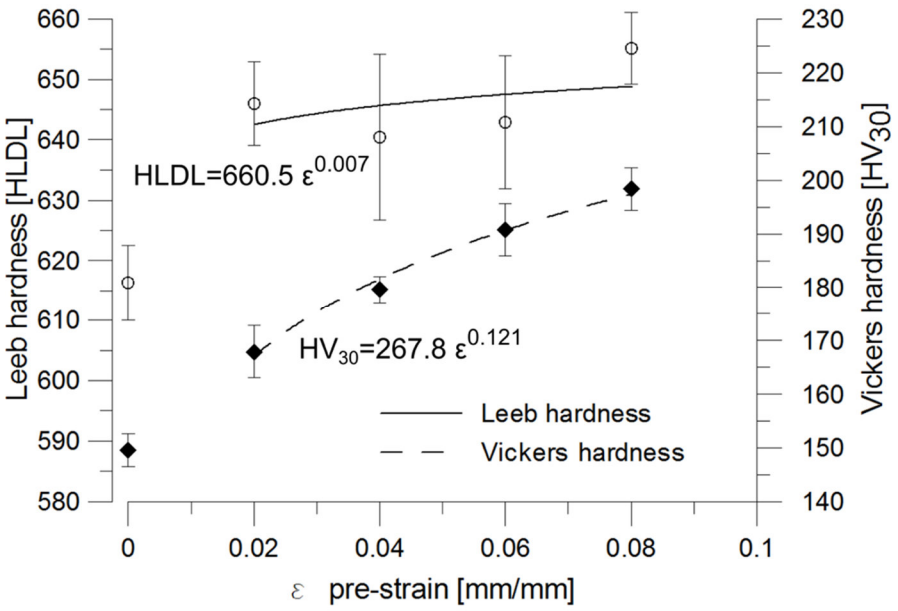

Fig. 3-19 Leeb and Vickers hardness versus pre-strain calibration curves for Grade 300E steel reinforcing bar.

Surface finish comparison test

Preliminary hardness tests were conducted in the laboratory also on steel reinforcing bars removed from earthquake-damaged reinforced concrete buildings (Fig. 3-20). The bars mentioned were taken from parts of structural elements near to cracks in the surrounding concrete. More details regarding hardness testing on specimens removed from damaged buildings are given in Chapter 5.

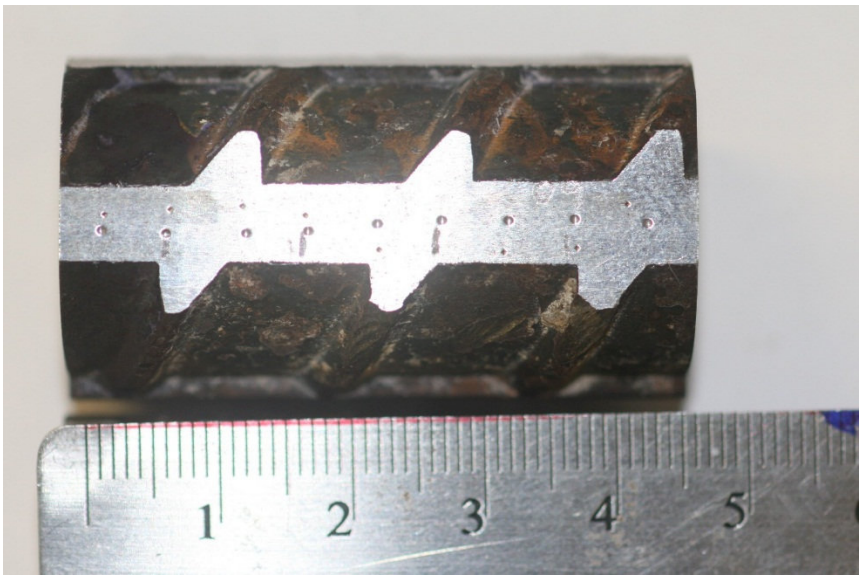

Fig. 3-20 Rockwell indentation on a ground flat surface of a deformed reinforcing steel bar.

These samples were used to define the surface preparation standard methodology to adopt. In the first instance, rib deformations were removed and, as recommended by Vander Voort (1999), two opposite parallel flat surfaces were machined to avoid tilting problems. In addition, a minimum thickness should be guaranteed to avoid the indenter producing a bulge or a mark on the opposite face of the test sample.

Vander Voort recommends either a smooth-ground or polished surface finish, which allow estimation of the Vickers indentation diagonal length to the nearest 0.0002 mm. Smooth-ground surfaces were compared with polished surface. These were obtained using silicon carbide grinding papers from 180 to 600 grit (Fig. 3-21); the polished finish was obtained by performing an extra step with diamond paste up to 9 micron (Fig. 3-22).

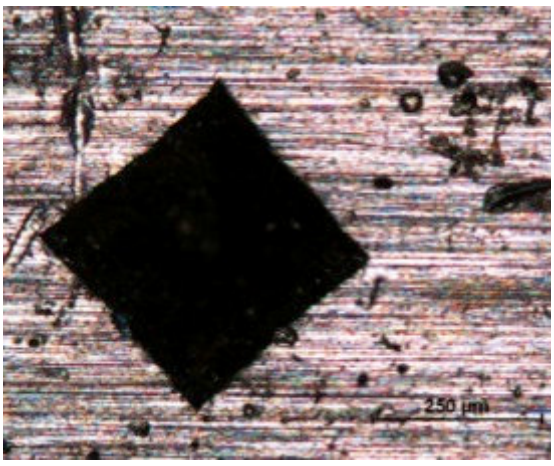

Fig. 3-21 Vickers indentation on a smooth-ground surface finish.

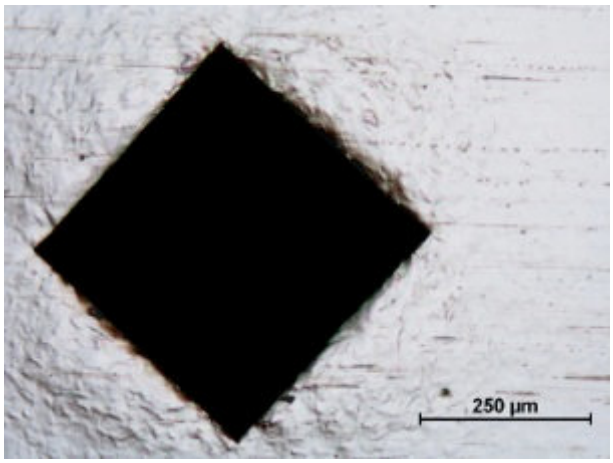

Fig. 3-22 Vickers indentation on a polished surface finish.

Fig. 3-22 shows clearly the benefits of performing the extra polishing step when compared with Fig. 3-21. A better contrast between the indentation impression and the rest of the material surface is evident. The vertices of the pyramidal indentation are easily detectable. Therefore, the error during the measurement of the diagonal length is reduced. The polishing step only requires approximately 2 minutes of extra work per sample. In conclusion, it is highly recommended to provide a polished surface to improve the optical measurements of the Vickers hardness.

3.3 THE STANDARD METHODOLOGY TO DETERMINE THE HARDNESS CALIBRATION CURVES

3.3.1 Application on the current NZ-manufactured Grade 300E

The standard methodology to develop calibration curves is described in this section through the application on the current NZ-manufactured Grade 300E. Certified Grade 300E deformed steel reinforcing bars were used in the 25 mm diameter size from the same batch obtained from Pacific Steel Ltd (www.pacificsteel.co.nz) for the preliminary tests described in Section 3.2. Forty-three flat-shape "dog-bone" specimens were machined (Fig. 3-10). The surface of the samples was then sequentially ground using silicon carbide grinding papers up to 600 grit and polished to 9 micron with diamond paste, to reduce the errors due to the optical measurement of Vickers hardness indentations.

Ten out of the total of forty-three samples were randomly selected to obtain the baseline hardness. On each sample, ten indentations were carried out at a spacing of 5 mm along the longitudinal section, giving a total of 100 measurements. Hardness tests were carried out using the Vickers hardness tester (ASTM, 2011b). The baseline hardness of as-received Grade 300E was found to be 150 HV_{30} (Vickers Hardness with a 30 kg load) with a standard deviation (SD) of 3.0 HV_{30}. Three samples were tested until failure to obtain the baseline tensile properties (Table 3-4)

Tensile tests were all performed with the MTS 810 tensile machine and the MTS 25 mm gauge length extensometer. This extensometer was selected for the best combination of gauge length and extension, to ensure that the ultimate tensile stress and strain were captured. Chemical composition, from the certificate of origin, is provided in Table 3-1.

Table 3-4 Benchmark mechanical properties of the steel reinforcing bars.

Sample	Upper yield strength (MPa)	Lower yield strength (MPa)	Ultimate tensile strength (UTS) (MPa)	Strain at UTS (mm/mm)
1	345	321	498	0.205
2	354	321	505	0.202
3	362	336	519	0.203

Knowing the benchmark mechanical properties, the hardness versus strain calibration curves were then developed. The first calibration curve, for un-aged steel, was obtained by pre-straining the samples up to the pre-identified level of strain and measuring the hardness immediately (within 1 hour). Four pre-strain limits were selected: 0.02, 0.04, 0.06 and 0.08 (mm/mm). Ten samples were prepared with each pre-strain. After reaching a specific strain limit, the tensile test was interrupted. The same approach used to calculate the hardness baseline was also used to obtain the average hardness on the pre-strained samples: ten hardness indentations at 5 mm spacing. The final average hardness used was the average hardness obtained from the 100 total measurements taken from the 10 samples. The standard deviation was also calculated. The calibration curve, consisting of average hardness (before ageing) versus pre-strain, is shown Fig. 3-23.

NZ Grade 300E is prone to strain ageing (Loporcaro et al., 2014, 2016). Therefore, to investigate and account for the strain-ageing effects, an accelerated ageing process was adopted by immersing the strained samples in boiling water (100°C) for four hours. After the accelerated ageing process, the samples were hardness tested again and the results are presented in Fig. 3-23

(after ageing). The empirically-based mathematical relationship between hardness and engineering plastic strain is approximated with a power-law curve (R^2 = 0.9891; 0.9928). The error bars represent the standard deviation. The hardness baseline is not included in the curve because the steel does not start to uniformly work harden until approximately 0.02 mm/mm strain (see Fig. 3-24). In the elastic region (between zero strain and approximately 0.00165 mm/mm), the hardness does not change at all. In the range of the discontinuous yielding (i.e., the Lüders extension from the elastic limit to the onset of the work hardening) the steel work hardens non-uniformly over the specimen length; therefore the hardness will not be uniform and the standard deviation is higher. Based on this observation it was consider justified to exclude the 0–0.02 mm/mm strain range in the fitting curve

Fig. 3-23 also shows the effect of strain ageing on hardness. In comparison, the strain-aged material has a larger strain-hardening exponent so two calibration curves were identified, one for the un-aged samples and one for the aged samples.

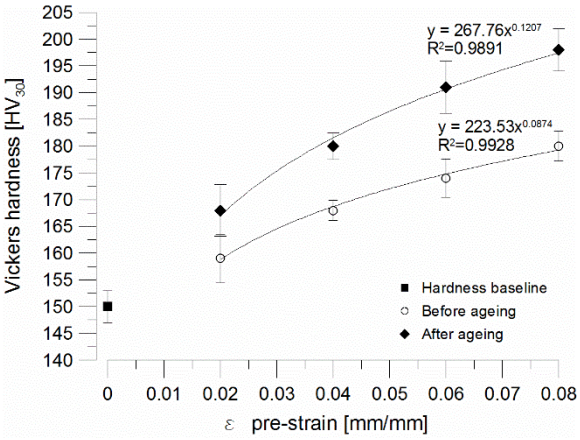

Fig. 3-23 Hardness versus pre-strain calibration curve for NZ Grade 300E steel.

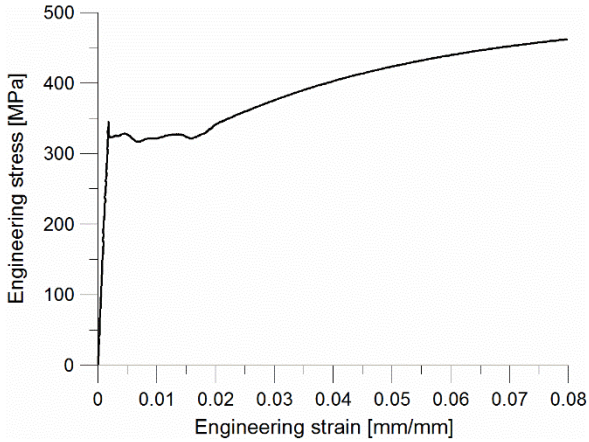

Fig. 3-24 Stress–strain curve of a NZ Grade 300E steel specimen in the strain range 0 to 0.08 mm/mm.

The final stage of the experiment consisted of tensile testing the pre-strained and aged samples beyond their ultimate tensile strength capacity to obtain the ultimate tensile strain (this property will be the residual strain capacity) and correlate it to the hardness. In general, the ultimate tensile

strain was obtained as the strain at maximum force. However, in some cases, since the stress–strain curve was almost horizontal at maximum stress (see Fig. 3-9), the data noise could potentially cause an incorrect determination of the ultimate strain. In this case, the stress–strain curve, within a strain range of 0.05–0.10 mm/mm in the neighbourhood of the expected maximum stress, was approximated as a polynomial function and the argument of the maximum (ultimate strain) was calculated. The outcome was a residual strain capacity versus hardness curve (Fig. 3-25), which can be used to quantify the residual strain capacity of earthquake-damaged and strain-aged steel bars of the same steel grade and bar diameter. A summary of the main mechanical properties of the pre-strained and aged Grade 300E is shown in Table 3-5.

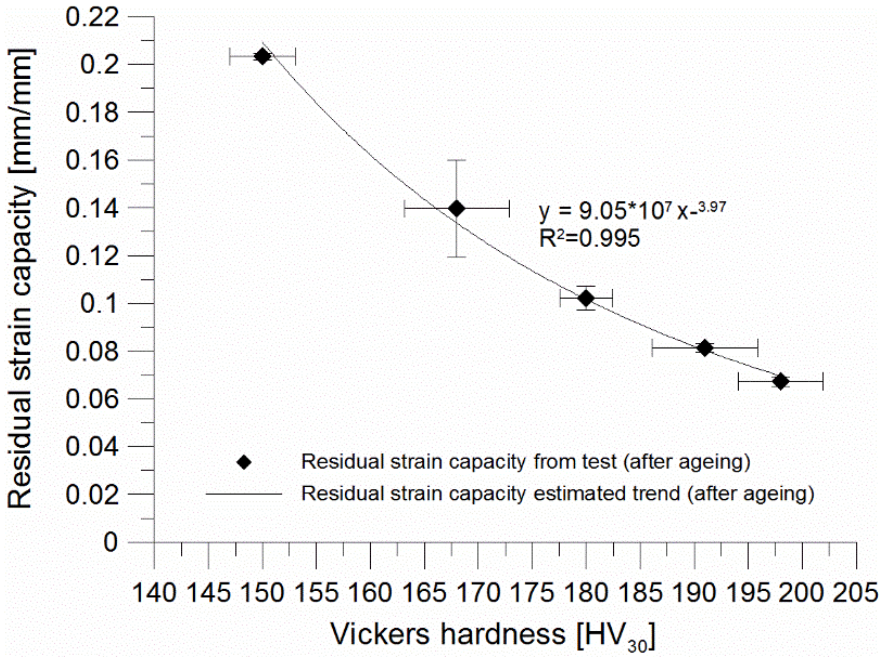

Fig. 3-25 Residual strain capacity versus Vickers hardness calibration curve for NZ Grade 300E steel.

Table 3-5 Mechanical properties summary of the pre-strained and aged steel samples.

Pre-strain [mm/mm]	**Vickers hardness [HV_{30}]**		**Lower yield strength [MPa]**		**Ultimate tensile strength (UTS) [MPa]**		**Strain at UTS (Residual strain capacity) [mm/mm]**		**Residual capacity compared to the initial [%]**
	Average	SD.	Average	SD.	Average	SD.	Average	SD.	
0	150	3.0	322	8.4	507	10.5	0.203	0.002	100
0.02	168	4.9	388	11.3	501	5.7	0.142	0.020	70
0.04	180	2.5	436	3.2	521	3.2	0.103	0.005	51
0.06	191	4.9	490	2.0	533	1.7	0.081	0.002	40
0.08	198	3.9	512	3.3	536	3.3	0.067	0.002	33

These laboratory-based experiments showed that Vickers hardness tests can be used to quantify the relationship between hardness and plastic strain (maximum standard deviation being 4.9 HV_{30}), and between hardness and residual strain capacity. Based on these results, it was possible to proceed to design the entire damage assessment methodology, which is illustrated in Chapter 5.

3.3.2 Application on historical NZ steel grades

Vickers hardness versus pre-strain, and residual strain capacity versus Vickers hardness were developed for different steel grades obtained from some reinforced concrete (RC) buildings in Christchurch. Through relationships with the Christchurch City Council (CCC), steel reinforcing bars were removed from earthquake-damaged RC building and brought to the University of Canterbury for testing. These reinforcing bars were then used to develop the calibration curves that were relevant to each specific building. It was not possible to obtain the steel certificate of origin or the manufacturer's company name. However, from tensile testing, average hardness of the material (in the undamaged region), existing drawings, construction date, bar mark indicating grade and relative steel reinforcing material standard it was possible to determine the steel grade.

Approximately six metres of steel reinforcement was obtained from each CCC building. This material was sufficient to machine about thirty steel specimens for calibration curves. Three specimens were tensile tested until failure to obtain the benchmark mechanical properties. Six pre-strain limits were selected: 1, 2, 3, 4, 5 and 10%, three specimens for each pre-strain were used for a total of eighteen specimens. The process employed was the same described in Section 3.3.1. A total of nine different steel types were obtained from various earthquake-damaged buildings and tested. Benchmark mechanical properties are presented in Table 3-6. Calibration curves for all steels are plotted in Fig. 3-26 to Fig. 3-43.

Table 3-6 Benchmark mechanical properties of the steels tested.

Steel type code	**Lower yield stress [MPa]**	**UTS [MPa]**	**Strain at UTS [mm/mm]**	**Strain-hardening exponent**	**HV_{30} baseline**
01	339	504	0.204	0.2002	151
02	315	480	0.207	0.2073	141
03	302	460	0.216	0.2082	136
04	323	470	0.205	0.1923	140
05	317	502	0.198	0.2089	146
06	463	630	0.149	0.1478	191
07	503	693	0.131	0.1085	221
08	532	700	0.126	0.1206	219
09	467	630	0.156	0.156	189

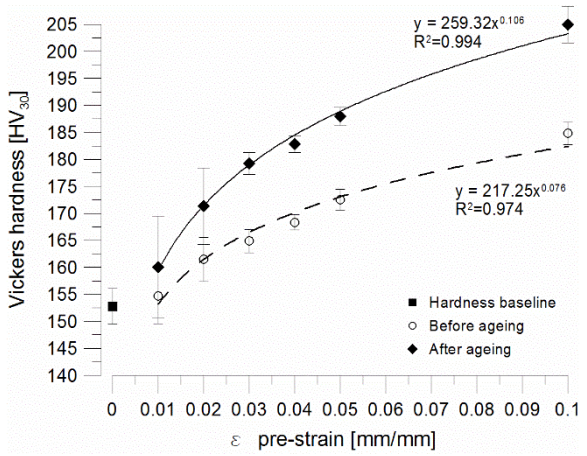

Fig. 3-26 Vickers hardness versus pre-strain calibration curve for steel type 01.

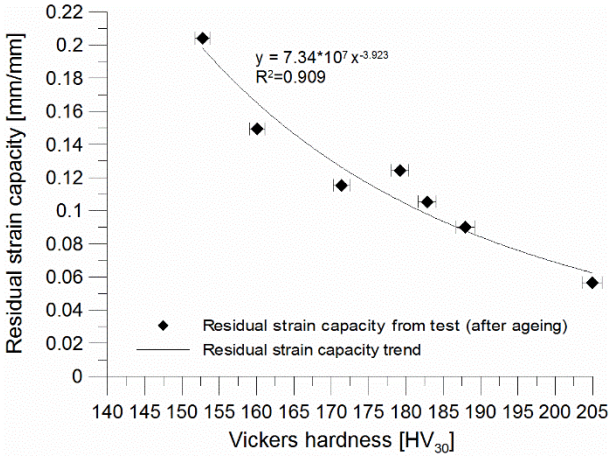

Fig. 3-27 Residual strain capacity versus Vickers hardness calibration curve for steel type 01.

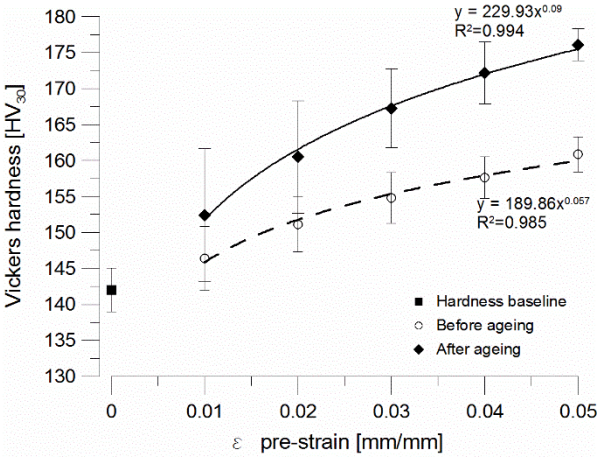

Fig. 3-28 Vickers hardness versus pre-strain calibration curve for steel type 02.

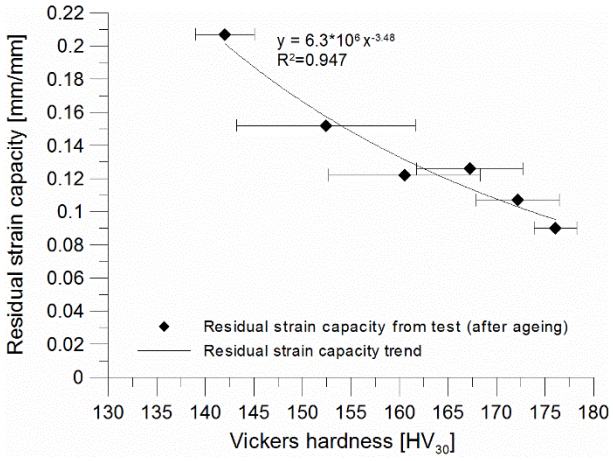

Fig. 3-29 Residual strain capacity versus Vickers hardness calibration curve for steel type 02.

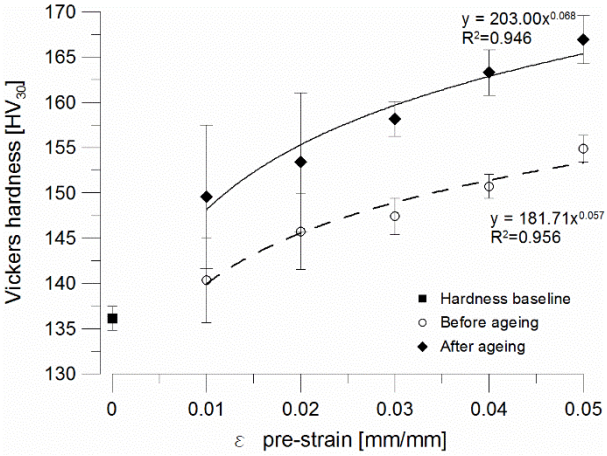

Fig. 3-30 Vickers hardness versus pre-strain calibration curve for steel type 03.

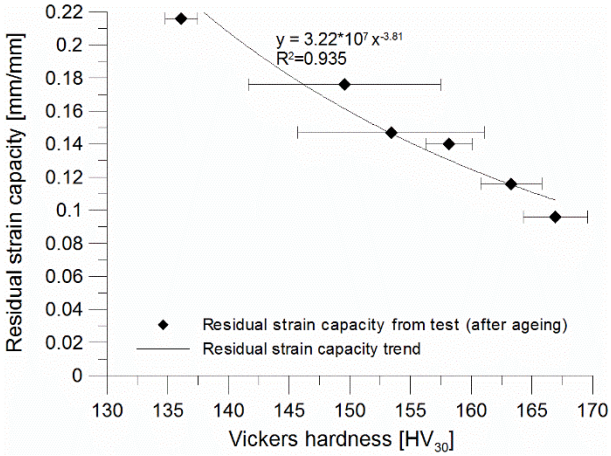

Fig. 3-31 Residual strain capacity versus Vickers hardness calibration curve for steel type 03.

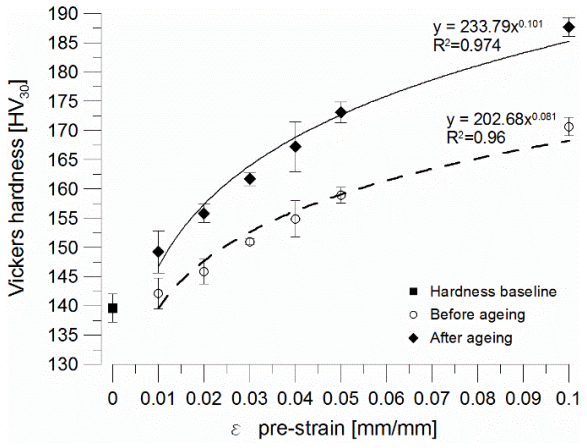

Fig. 3-32 Vickers hardness versus pre-strain calibration curve for steel type 04.

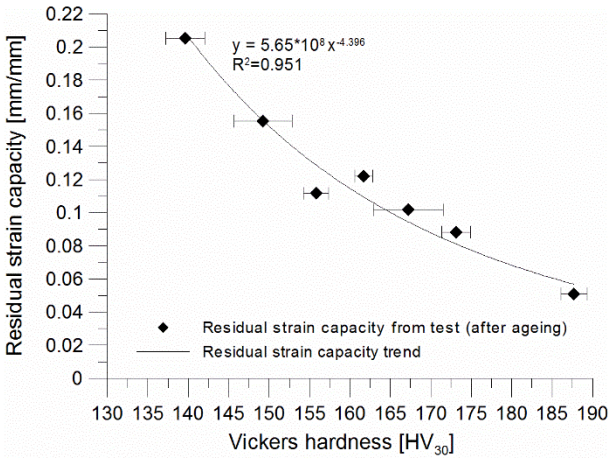

Fig. 3-33 Residual strain capacity versus Vickers hardness calibration curve for steel type 04.

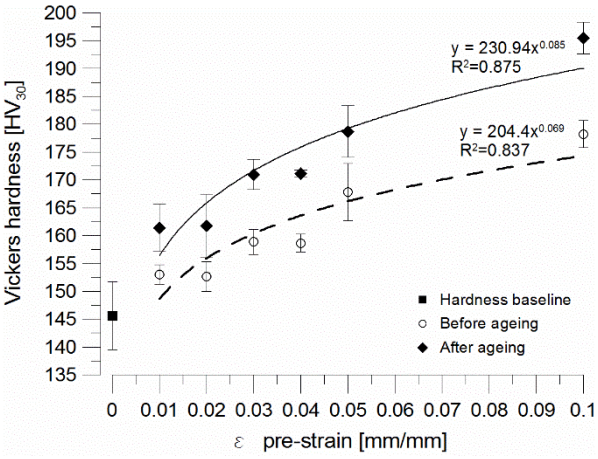

Fig. 3-34 Vickers hardness versus pre-strain calibration curve for steel type 05.

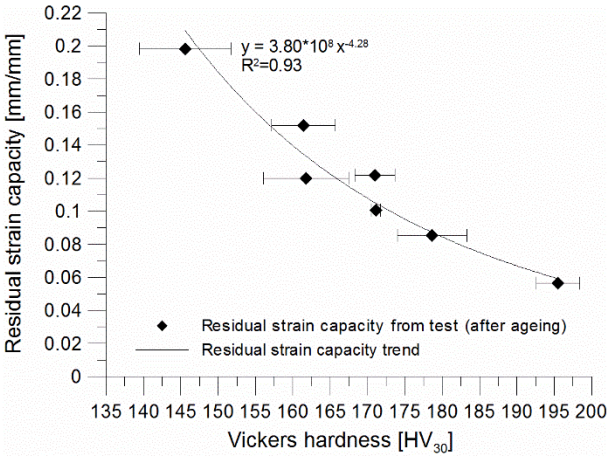

Fig. 3-35 Residual strain capacity versus Vickers hardness calibration curve for steel type 05.

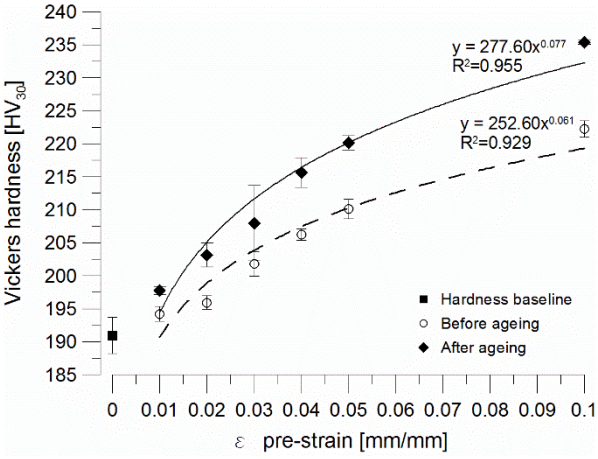

Fig. 3-36 Vickers hardness versus pre-strain calibration curve for steel type 06.

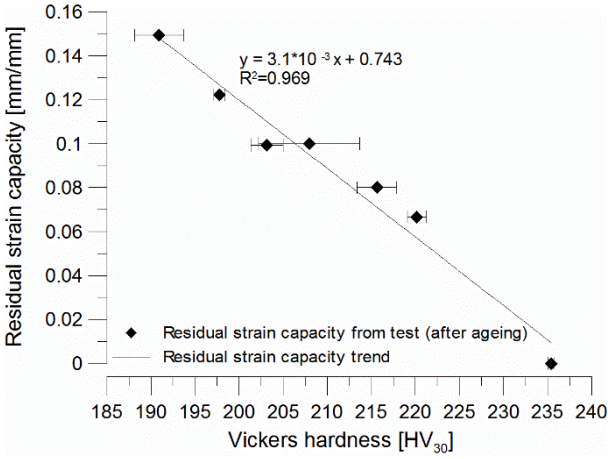

Fig. 3-37 Residual strain capacity versus Vickers hardness calibration curve for steel type 06.

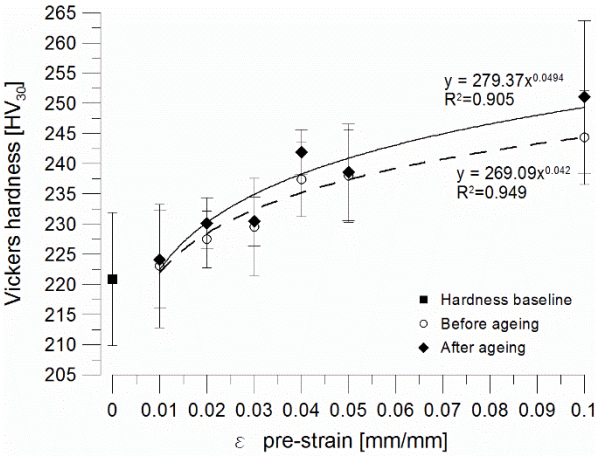

Fig. 3-38 Vickers hardness versus pre-strain calibration curve for steel type 07.

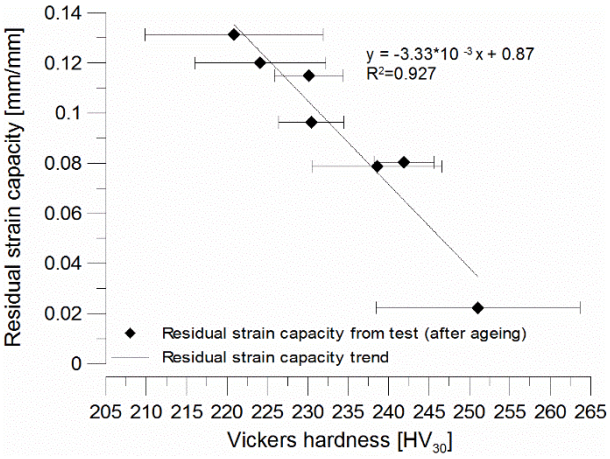

Fig. 3-39 Residual strain capacity versus Vickers hardness calibration curve for steel type 07.

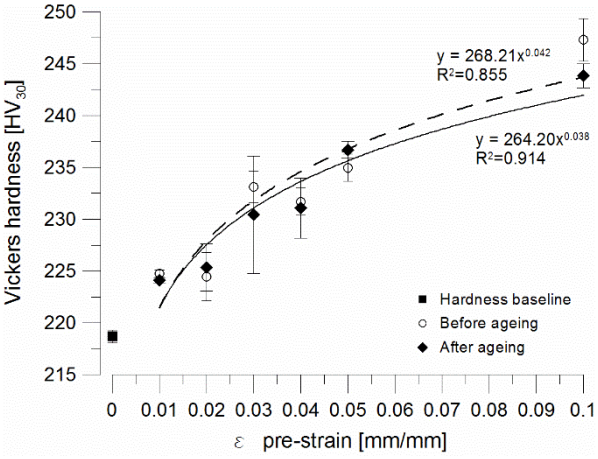

Fig. 3-40 Vickers hardness versus pre-strain calibration curve for steel type 08.

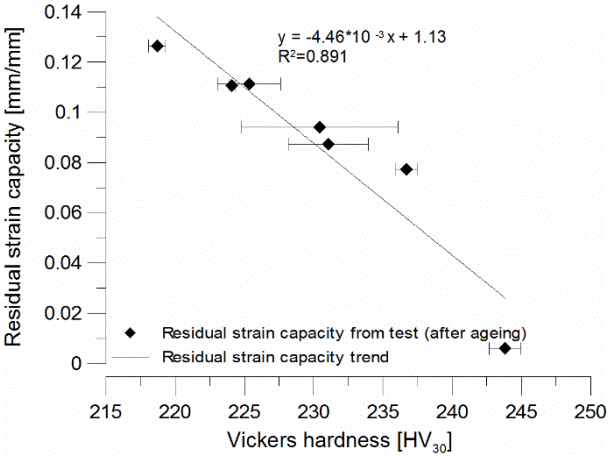

Fig. 3-41 Residual strain capacity versus Vickers hardness calibration curve for steel type 08.

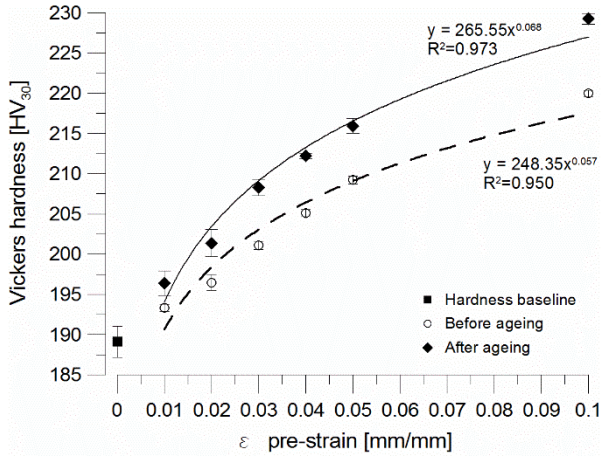

Fig. 3-42 Vickers hardness versus pre-strain calibration curve for steel type 09.

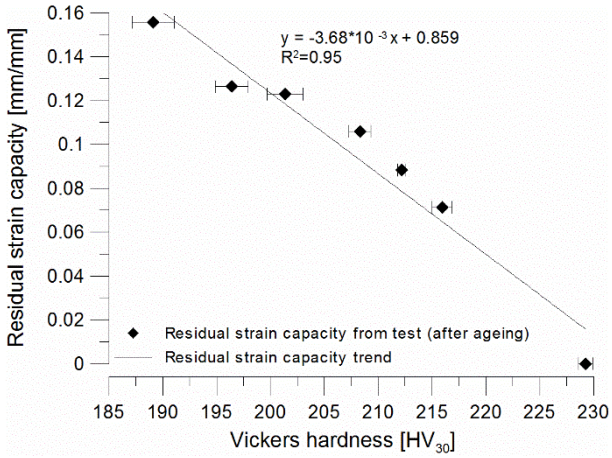

Fig. 3-43 Residual strain capacity versus Vickers hardness calibration curve for steel type 09.

3.3.3 Discussion

In Fig. 3-44, the calibration curves derived from 15 steels of different grade and diameter (including those presented in this Sections 3.3.1 and 3.3.2) are plotted, it is evident that the curves differ depending on the hardness baseline, the higher the yield strength, the higher is the hardness baseline. Moreover, in Fig. 3-45, calibration curves relative to the same steels are normalised with respect to the initial Vickers hardness baseline. The experimental data were fitted with a power-law curve:

$$HV_{30\,norm} = H\,\varepsilon_p^h \tag{3-4}$$

where $HV_{30\,norm}$ is the normalised hardness, ε_p is the plastic strain, h is a material exponent and H is a material coefficient.

The plot shows that a single unique relationship for all steel grades is not obtained. The curves that fit the experimental data have different "shapes" and consequently different exponents (h) depending on the work hardening capability of each steel. However, three groups of calibration curves are identified as a function of the steel grade: the lower is the (lower) yield strength (LYS),

the higher is the increase in hardness with increasing strain. This is because lower strength steels have larger strain hardening exponents and ratio UTS/LYS (see Table 3-7). From a microscopic point of view, work hardening (also known as strain hardening) is the increase in shear stress required to produce slip as the shear strain increases. During a monotonic tensile test, this is observed as an increase in force (or stress) required to produce more plastic deformation. The cause of this increase in stress is the interaction of the existing and forming dislocations with each other and with other obstacles, for example, foreign atoms and precipitates (Dieter, 1976). This justifies the fact that steels that have similar work hardening capability also have similar calibration curves.

Table 3-7 Mechanical properties of the 15 steels used for the normalised HV versus strain calibration curve.

Steel code	**HV_{30} baseline**	**LYS [MPa]**	**UTS [MPa]**	**Strain at UTS [mm/mm]**	**Ratio UTS/LYS**	**Strain-hardening exponent "n"**
G300.1	136	302	460	0.216	1.523	0.2709
G300.2	140	323	470	0.205	1.456	0.2562
G300.3	142	315	480	0.207	1.522	0.2682
G300.4	146	317	502	0.198	1.585	0.2689
G300.5	149	323	515	0.182	1.593	0.2636
G300.6	150	326	507	0.203	1.556	0.2619
G300.7	153	339	504	0.204	1.486	0.2597
G430.1	189	467	630	0.156	1.349	0.2051
G430.2	191	463	630	0.149	1.359	0.2052
G500.1	208	≈ 505	650	0.138	1.288	0.1544
G500.2	211	≈ 500	652	0.129	1.304	0.1611
G500.3	219	532	700	0.126	1.316	0.1771
G500.4	221	≈ 503	693	0.131	1.378	0.1708
G500.5	232	524	684	0.131	1.306	0.1773
G500.6	237	≈ 525	736	0.123	1.403	0.1564

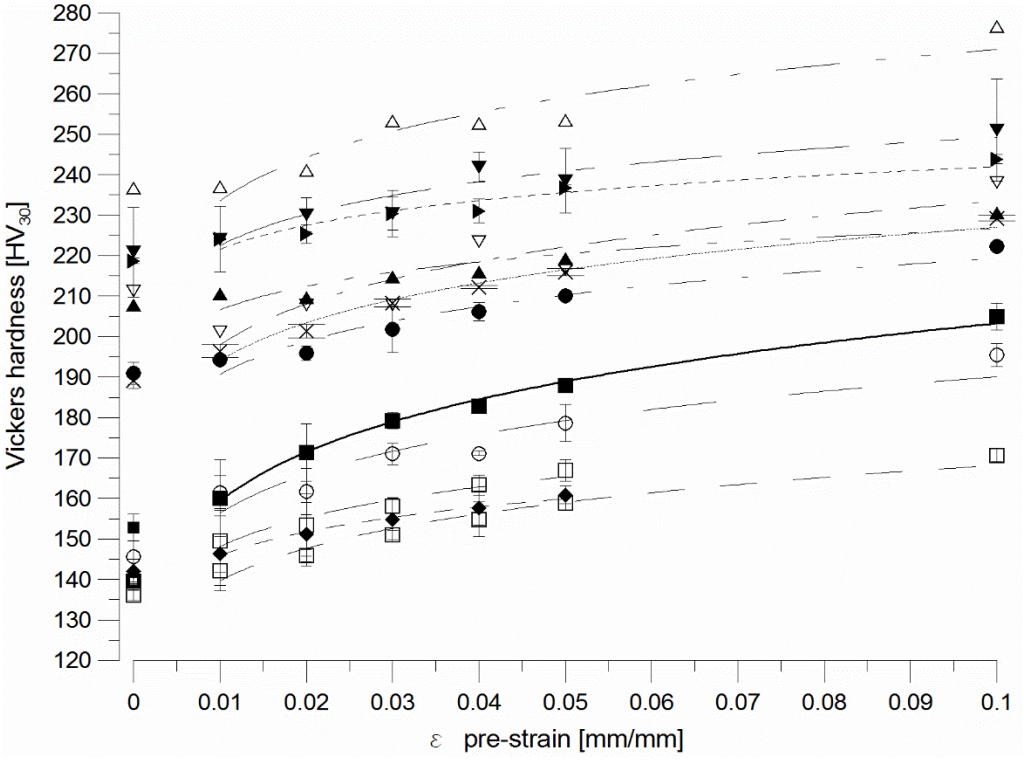

Fig. 3-44 Vickers hardness versus strain calibration curves from the 11 steels obtained (from tests in Sections 0 and 3.3) plotted together.

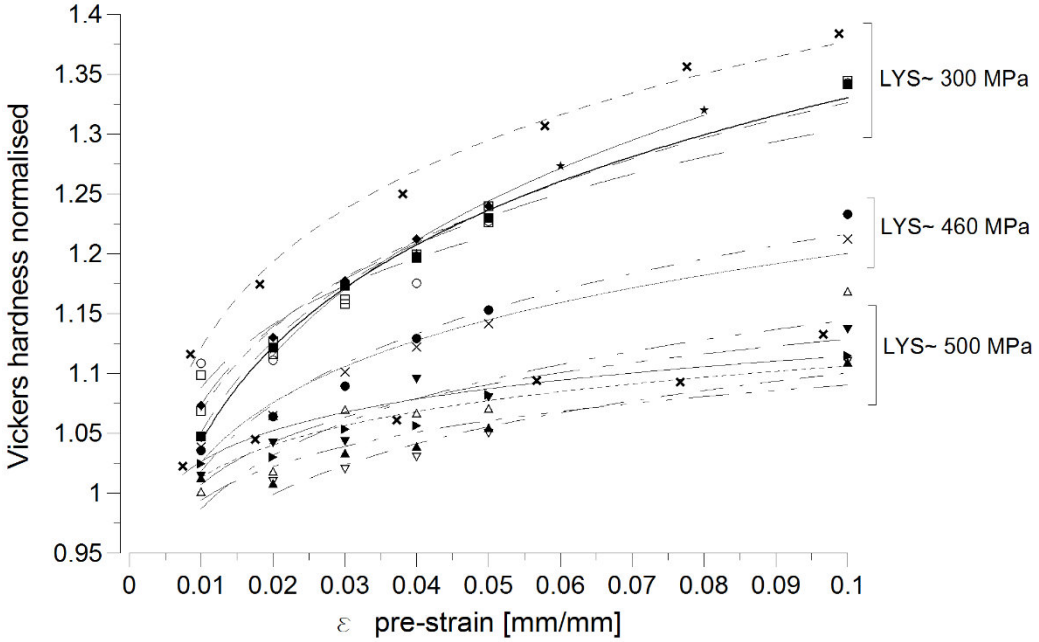

Fig. 3-45 Vickers hardness versus strain calibration curves from 15 steels normalised with respect to the hardness baseline.

The difference in the hardness calibration curves could also be explained by considering the material chemical composition, grain size, and second phase fractional amount. O'Neill (1967) defined the hardness as the resistance to the movement of dislocations. The dislocation movement can be impeded by pinning and blocking. The pinning effect is caused, for example, by nonmetallic inclusions such as carbon, nitrogen and trace of other elements. Additional obstacles to dislocation movement are represented by other dislocations (hardness increases with cold work as the dislocation density increases) and grain boundaries.

Hardness is also related to the yield stress (R_e) (Tabor, 1951b) that is expressed by the Hall-Petch equation:

$$R_e = \sigma_0 + K(1/D)^{\frac{1}{2}} \quad (3\text{-}5)$$

where σ_0 is the friction stress required to move a dislocation through various lattice resistance, K is the shear stress needed to release a locked dislocation and D is the average crystal size. Therefore, it follows that the smaller the grain size, the higher is the yield stress and consequently the hardness. The grain size can be controlled during the steel manufactured phase.

In summary, the hardness of a metal is a function of a number of microstructural properties (chemical composition, microstructure, cold work) that are controlled during the manufacturing process. Steels of different grades and originated from different sources are likely to possess different hardness baselines. In addition, it was also observed that steels with the same hardness baseline also have different calibration curves.

Moreover, the results obtained allowed additional observations and considerations:

- Steels of the same grade, but showing a different yield stress, in the order of approximately ± 35 MPa, had a difference in the Vickers hardness baseline in the order of ± 10 HV_{30},

which is not negligible. Using a calibration curve that has a lower baseline can overestimate the steel plastic deformation.

- Steels prone to strain ageing always showed two distinct calibration curves, before and after ageing. This aspect should not be neglected as it can underestimate the steel's plastic deformation.
- In the large majority of the cases (23 out of 27), the calibration curves (see Fig. 3-26 to Fig. 3-43) had a coefficient of determination (R^2) higher than 0.90, and often larger than 0.95 (13 out of 27). Only in a few cases (4 out of 27) was R^2 in the range from 0.83 to 0.87.
- Higher strength steels (Grade 430 or higher) pre-strained up to 10% and then aged, did not show any residual strain capacity. After reaching the elastic limit, the specimens almost immediately started to neck (see Fig. 3-46 and Fig. 3-47); the engineering stress versus engineering strain curve did not show any work hardening.
- Every steel has a unique calibration curve (see Fig. 3-44). Therefore, it is required to extract sufficient material from a building to develop the calibration curve(s) for each steel grade and diameter. Ideally, in order to reduce test invasiveness and testing time, it is very desirable to develop a methodology that allow to derive a unique calibration curve based on properties easily measurable such as Vickers baseline and strain hardening exponent (or steel grade). A universal calibration curve is proposed in Chapter 7.

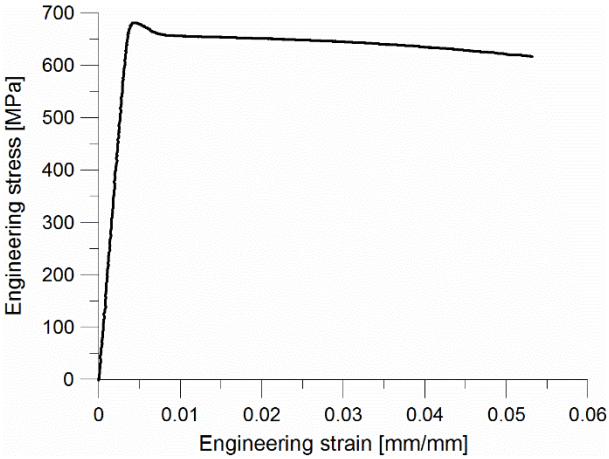

Fig. 3-46 Stress strain curve to failure of a high-strength steel sample (1) previously pre-strained to 10% and aged.

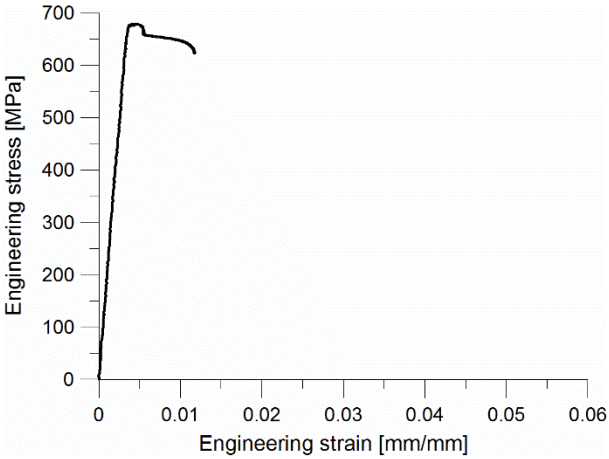

Fig. 3-47 Stress strain curve to failure of a high-strength steel sample (2) previously pre-strained to 10% and aged.

3.4 EFFECTS OF RIBS ON HARDNESS

From the 1960s, in order to improve the bond between concrete and steel, steel reinforcement was also produced as deformed bars. The protrusions on the deformed bars, known as ribs, represent stress concentrations and might cause localised plastic strain at the roots of the ribs as observed experimentally by Erasmus and Pussegoda (1978) (see Fig. 2-36), and through elasto-plastic finite element simulation by Surajit Kumar, Pritam Kumar, Debdulal, Sanjay, and Saurabh (2014). The following experiments were conducted on six unmachined reinforcing bars to determine the magnitude of the change in hardness associated with the plastic strain and provide recommendations about hardness testing on steel rebars. Combinations of bar diameter and grade (see Table 3-8) were defined according to the MTS tensile machine load capability.

Table 3-8 Specimen information (Grade, diameter and amount of pre-strain)

Specimen	Grade	Diameter [mm]	Pre-strain [mm/mm]
1	300E	12	0.05
2	300E	12	0.10
3	300E	16	0.05
4	300E	16	0.10
5	500E	12	0.05
6	500E	12	0.10

The six steel specimens were cut into 180 mm lengths and plastically strained up to 0.05 mm/mm and 0.10 mm/mm (see Table 3-8). The unsupported length between the MTS V-grips was approximately 50 mm. After pre-straining, the bars were prepared for hardness testing. The plastically deformed region was cut from the rest of the specimen, two parallel surfaces were machined, ground and polished. Hardness measurements were carried out over a 30 mm length of the rebars, following approximately a 2 mm square grid pattern. Five hardness indentation rows were made on D12 specimens, and six rows were made on the D16 samples (see Fig. 3-48, Fig.

3-50, Fig. 3-52, Fig. 3-54, Fig. 3-56, and Fig. 3-58). The top and bottom rows are approximately 1 mm to 2 mm from the edges, and as a consequence, the second and the second last rows are 3 mm to 4 mm from the edges. In the following pages, results from the experimental test are presented. A pictures of each sample is shown with a table summarising the hardness measurements (from Table 3-9 to Table 3-14). Finally a plot presents the hardness indentations per row at each longitudinal location (Fig. 3-49, Fig. 3-51, Fig. 3-53, Fig. 3-55, Fig. 3-57 and Fig. 3-59).

Fig. 3-48 Specimen 1

Table 3-9 Hardness readings, Specimen 1

Row	Average HV	Standard deviation HV
1	156	4.4
2	156	1.5
3	155	2.7
4	157	2.3
5	156	4.4

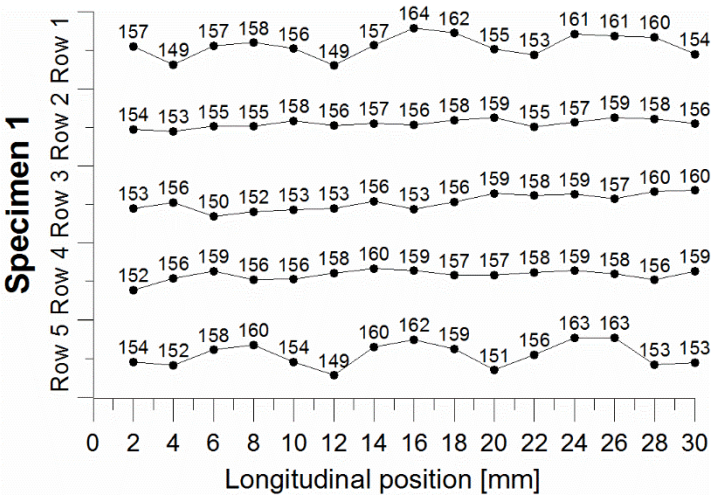

Fig. 3-49 Vickers hardness profile of Specimen 1

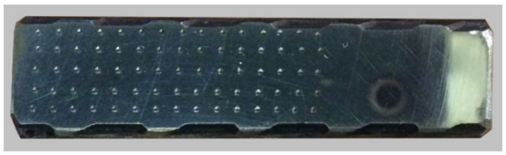

Table 3-10 Hardness readings Specimen 2

Fig. 3-50 Specimen 2

Row	Average HV	Standard deviation HV
1	167	6.2
2	168	3.6
3	168	2.3
4	168	2.6
5	167	5.4

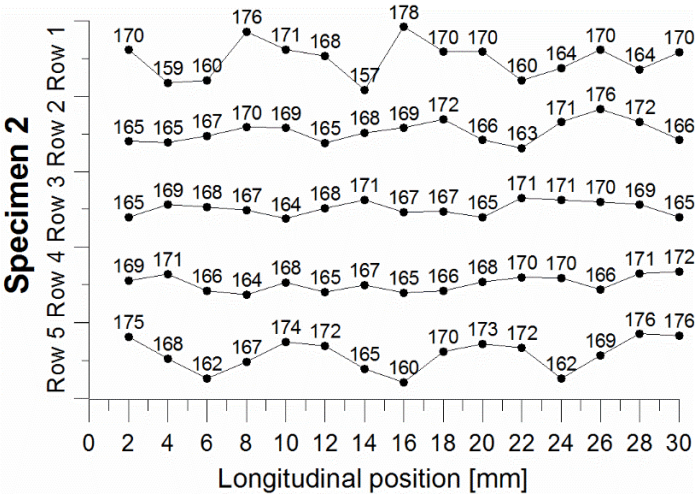

Fig. 3-51 Vickers hardness profile of Specimen 2

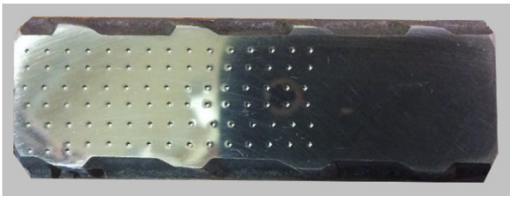

Table 3-11 Hardness readings Specimen 3

Fig. 3-52 Specimen 3

Row	Average HV	Standard deviation HV
1	179	3.9
2	178	2.3
3	178	1.9
4	177	2.2
5	177	1.8
6	177	6.9

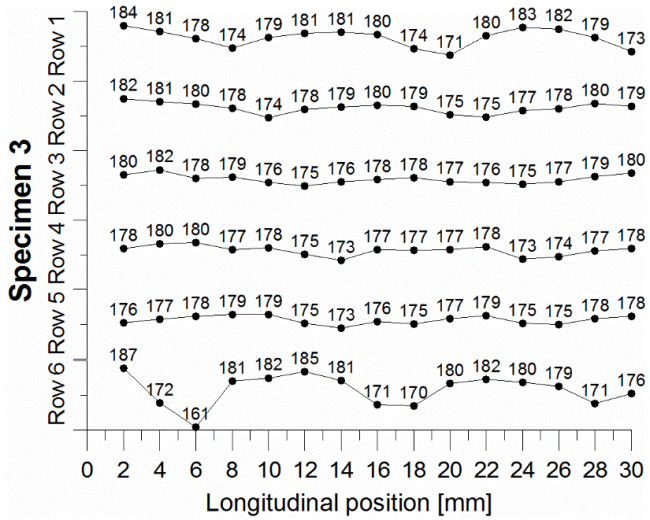

Fig. 3-53 Vickers hardness profile of Specimen 3

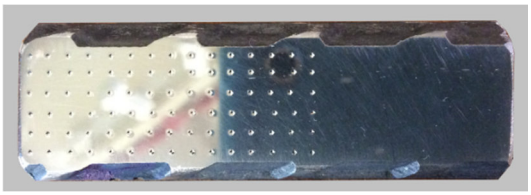

Table 3-12 Hardness readings Specimen 4

Fig. 3-54 Specimen 4

Row	Average HV	Standard deviation HV
1	200	8.0
2	203	3.5
3	204	3.1
4	205	2.8
5	205	3.8
6	205	7.1

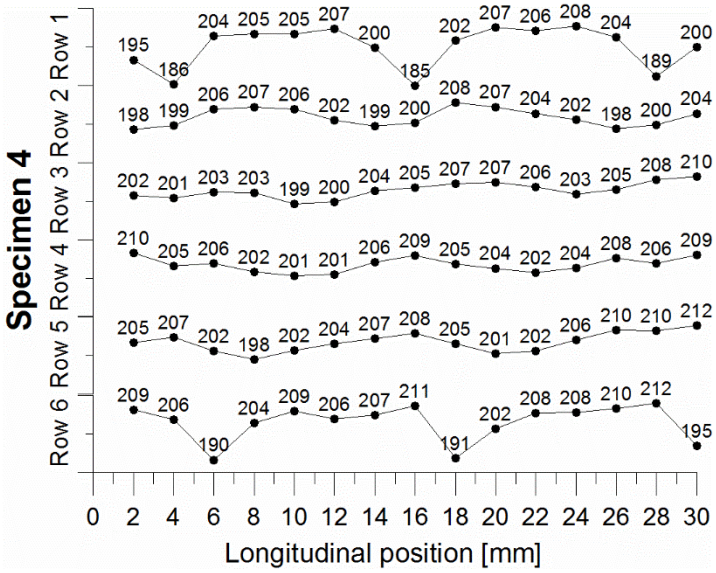

Fig. 3-55 Vickers hardness profile of Specimen 4

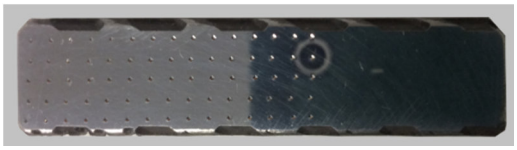

Table 3-13 Hardness readings Specimen 5

Fig. 3-56 Specimen 5

Row	Average HV	Standard deviation HV
1	244	3.4
2	246	2.3
3	247	1.5
4	246	1.8
5	242	3.1

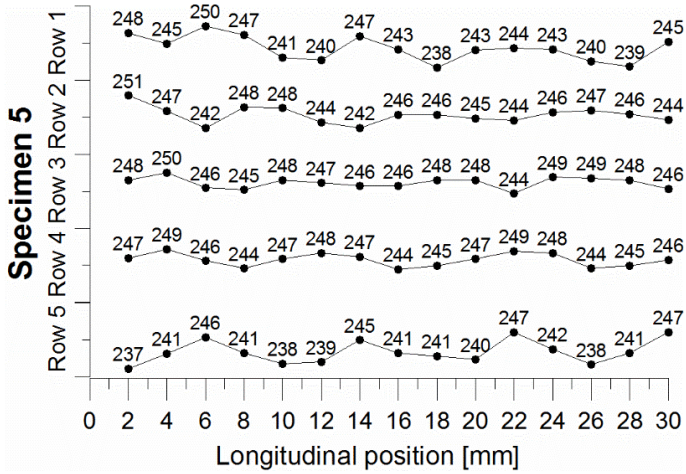

Fig. 3-57 Vickers hardness profile of Specimen 5

Fig. 3-58 Specimen 6

Table 3-14 Hardness readings Specimen 6

Row	Average HV	Standard deviation HV
1	258	5.7
2	258	3.5
3	258	2.6
4	257	3.3
5	254	3.7

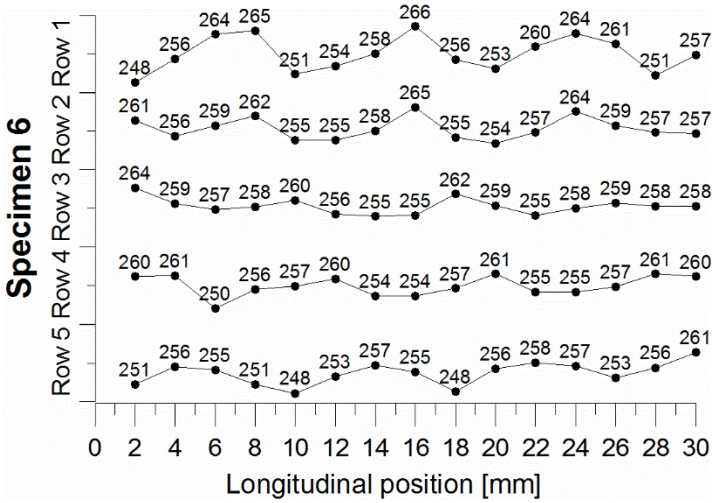

Fig. 3-59 Vickers hardness profile of Specimen 6

Similarly to the other experiments, hardness increases with the amount of pre-strain. Looking at the plots, for each specimen, the hardness longitudinal profile of the central rows, from row 2 to 4 (for D12 specimens) or to 5 (for D16 specimens), was relatively constant compared with the hardness at the top and bottom row where "peaks" and "valleys" were more evident. The fluctuation in longitudinal hardness was measured using its standard deviation. For example, in Specimen 1, the standard deviation in the central rows ranged from 1.5 to 2.7; meanwhile in the top and bottom rows, standard deviation doubled to 4.4. Similar results were observed in the other specimens, where the increase in standard deviation varied from 50% to over 100% in the outermost rows. These numbers demonstrated that a higher fluctuation exists in the rows closer to the top and bottom edges of the sample. Notwithstanding this fluctuation, the average hardness of the top and bottom rows was the same as the central rows.

The second step consisted of determining the exact locations of the peak and valley hardness measurements. Comparing the indentations in the specimens' pictures and the plots, it can be observed that the valley occurs below the ribs. This is consistent with (Erasmus & Pussegoda, 1978). Below the ribs, no Lüders bands (the dark region) are present; that means no plastic strain has occurred. In the valley location the hardness reading is approximately 4.9% lower than the average value. On the other hand, hardness increases at the root of the ribs and between the ribs. This is the location where the Lüders bands start to form, and plastic strain is expected to concentrate. The hardness in the peak locations is approximately 3.9% higher than the average. It is then suggested that the tranverse hardness measurements for D12 and D16 rebars should be conducted at least 4 to 5 mm away from the edges. For larger rebars, it is recommended that the hardness indentations be performed no closer than 25% of the bar diameter from the edge.

3.5 CONCLUSIONS

The Vickers hardness method developed in this thesis relies on the hypothesis that hardness increases with plastic deformation, and a robust relationship between hardness and plastic strain can be developed for any steel grade and diameter. A standardised methodology to determine the calibration curves—Vickers hardness (HV_{30}) versus pre-strain (ε_{PRE}), and residual strain capacity (ε_{UTS}) versus HV_{30}—was developed. The experiments conducted provided the following suggestions:

- The flat "dog-bone" shape specimen geometry was the most convenient for hardness and tensile testing. Compared to cylindrical "dog-bone" specimens, the flat-shape geometry facilitated the hardness testing since two flat and parallel surfaces are required. The flat geometry also allowed the re-testing of the same samples in tension in order to obtain the residual strain capacity after ageing.
- The Vickers hardness method and scale were adopted. Vickers, Rockwell and Leeb hardness methodologies were compared. The Rockwell scale resolution showed limited sensitivity to develop the calibration curve for the strain range investigated. The Leeb hardness measurements were affected by larger standard deviations when compared with the Vickers hardness testing. In addition, the Leeb hardness curves were unable to resolve small variation in pre-strain, because of the close-to-zero exponent in the power-law calibration curve. Furthermore, Leeb hardness measurements were also dependent on the sample's support material (steel, concrete and wood) used during the testing.
- The surface finish was determined as a compromise between the time required to obtain the desired finish level and the legibility of the diamond indentation, determined by the contrast between the hardness indentation and surrounding material when observed in a

microscope. Sequentially grinding the sample surface from 180, 240, 320, 400 to 600 grit using silicon carbide paper, and then finally polishing to a 9-micron finish is recommended.

- The strain ranges of interest from 0% to 10% for the calibration curves are recommended. It might be impractical to consider a pre-strain greater than 10%, since the resultant will have a residual strain capacity well below the limits set by the current standard for reinforcing steel (Standards, Australia and New Zealand, 2001).
- The amount of steel required for the development of the calibration curves is a function of the strain range of interest, pre-strain intervals and the number of samples required for determining the baseline mechanical properties and for pre-straining. In total, at least 21 samples are required. Depending on the steel sample's length, which is approximately 150 to 180 mm, at least 4 m of steel rebars are required (this includes a few samples used as backup).
- In order to provide statistical validity to the test and contemporaneously conduct the experiment in a reasonable amount of time, three samples need to be strained to each specific limit and 10 hardness measurements need to be carried out on each sample. Average values and standard deviations need to be specified.
- The strain-ageing effects were produced using the accelerated method. It is recommended to age steel samples in boiling water (100°C) for four hours. This simulates the strain-ageing effects that would occur at 15°C for a year. Further investigation of this phenomenon is discussed in Chapter 6.

- The standard methodology to obtain a calibration curve is summarised in the following points:

  Step 1: Tensile specimen preparation (machining, grinding and polishing);

  Step 2: Tensile pre-straining testing;

  Step 3: Hardness testing before ageing;

  Step 4: "Accelerated" ageing for 4 hours at 100°C;

  Step 5: Hardness testing after ageing;

  Step 6: Tensile testing to failure;

  Step 7: Data analysis and development of calibration curves.

- Calibration curves allow a user, knowing the Vickers hardness of the steel bar(s) under investigation, to estimate the plastic deformation experienced during a seismic event and predict the residual strain capacity (and ductility) of the bar(s) at the location of the damaged.
- Calibration curves are not universal, and due to the variability of the chemical composition of the steel, the steel-making process and the heat treatment during the rolling phase, a universal relationship could not be developed. It is recommended that specific calibration curves for each combination of diameter and steel grade are derived. It is also suggested that the damaged and undamaged steel for the calibration curve be recovered from the same RC member, whenever possible.
- Steel ribs are stress concentrations points that cause localised plastic strain and peak hardness. It is recommended that hardness tests are restricted to the centreline of a reinforcement bar. Hardness indentation must be carried out at least 25% of the bar diameter away from the bar surface.

3.6 REFERENCES

Allington, C. (2011). *Materials testing in buildings of interest. Gallery Apartments, Westpac centre, IRD building*. (Report 107267-1 (v1.1) prepared for royal commission). Retrieved from HolmesSolution, Christchurch:

ASTM. (2011a). E8/E8M - 11 *Standard Test Method for Tension Testing of Metallic Materials*. West Conshohocken, PA, United States.

ASTM. (2011b). E384 - 11$^{\varepsilon 1}$ *Standard Test Method for Knoop and Vickers Hardness of Materials*. West Conshohocken, PA, United States.

ASTM. (2012a). A956 - 12 *Standard test method for Leeb hardness testing of steel products*. West Conshohocken, PA, United States.

ASTM. (2012b). E18-12 *Standard test methods for Rockwell hardness of metallic materials*. West Conshohocken, PA, United States.

Cahoon, J., Broughton, W., & Kutzak, A. (1971). The determination of yield strength from hardness measurements. *Metallurgical Transactions, 2*(7), 1979-1983.

Dieter, G. E. (1976). *Mechanical metallurgy* (Vol. 3): McGraw-Hill New York.

Dowling, N. E. (2013). *Mechanical behavior of materials: engineering methods for deformation, fracture, and fatigue* (Fourth Edition ed.): Pearson.

Erasmus. (1964). Effect of small additions of Vanadium on the austenitic grain size, forgeability. and impact properties of steel'. *J. Iron Steel Inst, 202*, 128.

Erasmus, & Pussegoda. (1980). The strain aging characteristics of reinforcing steel with a range of vanadium contents. *Metallurgical Transactions A, 11*(2), 231-237.

Erasmus, & Pussegoda, N. (1978). Safe bend radii for deformed reinforcing bar to avoid failure by strain age embrittlement. *New Zealand Engineering, 33*(8), 170.

Frank, S., & Technologies, G. I. (2005). Mobile Hardness Testing. Application Guide for Hardness Testers *GE Inspection Technologies*.

Hundy, B. B. (1954). Accelerated Strain Ageing of Mild Steel. *Journal of The Iron and Steel Institute, 178*.

Loporcaro, G., Pampanin, S., & Kral, M. V. (2014). *Investigating the relationship between hardness and plastic strain in reinforcing steel bars*. Paper presented at the NZSEE conference, Auckland.

Loporcaro, G., Pampanin, S., & Kral, M. V. (2016). *Comparison between accelerated and natural strain ageing effects on New Zealand manufactured Grade 300E steel reinforcing bars*. Paper presented at the NZSEE, Christchurch.

O'Neill, H. (1967). *Hardness measurement of metals and alloys* (Second edition ed.): Chapman and Hall.

Proceq. (2007). Equotip 3 Portable hardness tester. Operating instructions.

Standards, Australia and New Zealand (2001). AS/NZS 4671:2001 *4671:2001 Steel reinforcing materials*. Wellington, New Zealand.

Surajit Kumar, P., Pritam Kumar, R., Debdulal, D., Sanjay, C., & Saurabh, K. (2014). High and low cycle fatigue performance comparison between micro-alloyed and TMT rebar. *Construction and Building Materials, 54*, 170-179.

Tabor, D. (1951). *The hardness of metals*: Oxford university press.

Vander Voort, G. F. (1999). *Metallography: principles and practices*: ASM International.

4 EFFECTS OF CYCLIC STRAIN ON STEEL HARDNESS

The calibration curves presented in Chapter 3 were developed by carrying out monotonic tensile tests only. In this chapter, the calibration curves will be extended to specimens subjected to more complex stress–strain histories, i.e., fatigue testing. Experimental tests were conducted to investigate whether the number of fatigue cycles affects the relationship between Vickers hardness and monotonic plastic strain.

Because of the load capacity (100 kN) of the MTS 810 tensile testing machine available in the Mechanical Engineering lab, only 12 mm diameter (D12) Grade 300E unmachined steel reinforcing bars could be tested beyond the material's elastic limit.

4.1 PRETESTING PHASE

4.1.1 Stress-relief annealing heat treatment

The D12 rebars received from the supplier are produced in coils, then re-straightened and aged for an hour in boiling water (100°C) prior to delivery (Roberts, 2016). The re-straightening process could have caused residual stresses in the rebars. The hardness might not be uniform across the cross section. In order to verify this hypothesis, three 1-cm lengths of D12 rebar were mounted in a Buehler Epomet mounting compound in order to facilitate hardness testing through the specimen's thickness. The specimens were prepared using standard metallographic methods as explained in Chapter 3. Hardness indentations were applied on a 2 by 2 mm grid (see Fig. 4-1). Average and standard deviations were calculated. Results are provided in Table 4-1.

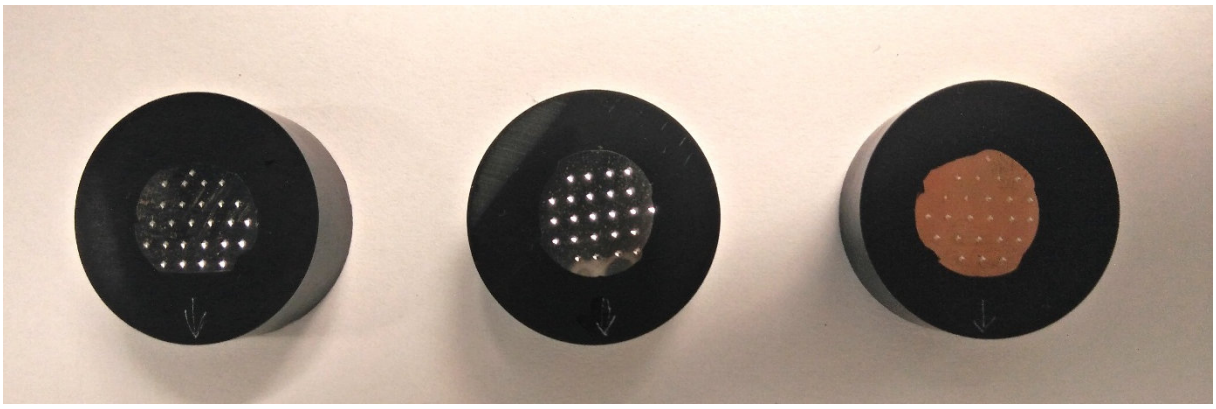

Fig. 4-1 Specimens used for cross-sectional Vickers hardness baseline

Table 4-1 Cross-sectional Vickers hardness measurements for the pretreated steel specimens.

Specimen number	**Number of readings**	**Average Vickers hardness [HV_{30}]**	**HV standard deviation [HV_{30}]**
Specimen 1	22	143	7.9
Specimen 2	23	144	7.5
Specimen 3	21	142	6.9

The results showed that the Vickers hardness readings were not constant across the section of the specimens; the standard deviation ranged from 6.9 to 7.9 HV_{30}. In general, the hardness in the cross-section's outer region was higher than the hardness in the inner region, as can be appreciated from Fig. 4-2.

Previous work showed that internal stresses in cold-worked bars were relieved, without hardness decrease, when heated at 500°C for an hour (Adeyemi, Stark, & Modlen, 1980; Krauss, 2005). Therefore, to relieve the residual stress caused by the re-straightening process, three samples collected from the same rebar were uniformly heated in a furnace at 500°C for an hour and then slowly air cooled. Cross-sectional Vickers hardness was measured following a similar 2 by 2 grid pattern. Results are summarized in Table 4-2

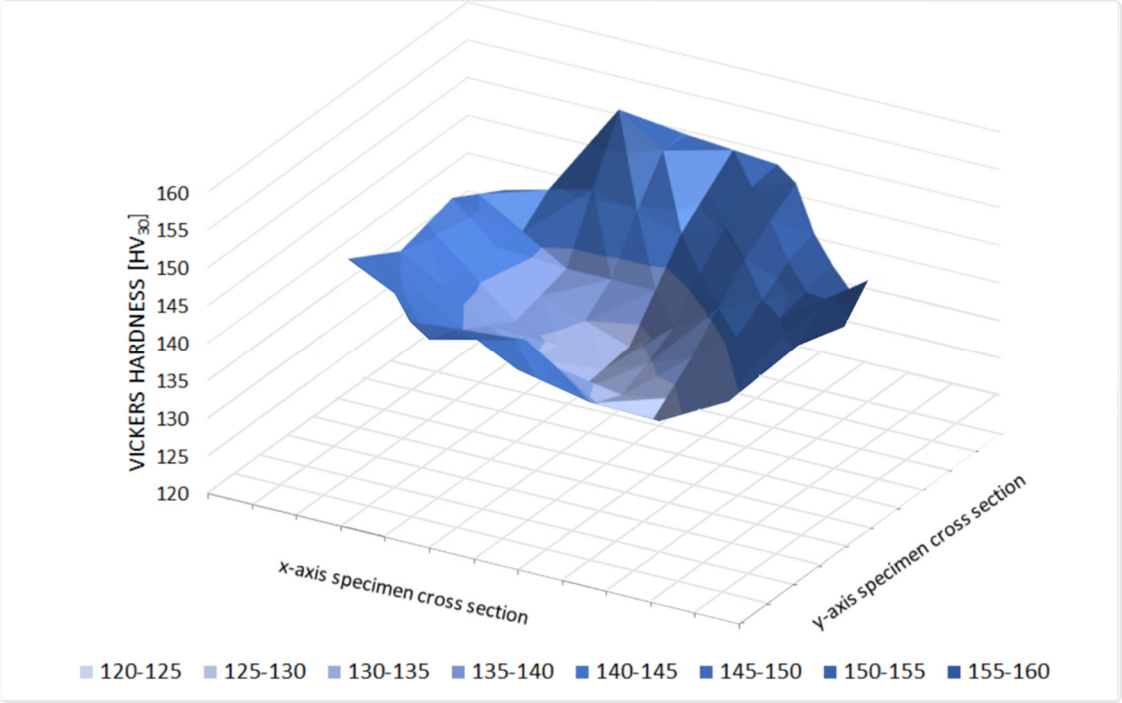

Fig. 4-2 Three-dimensional plot of the HV distribution on the cross-sectional area of an as-received bar.

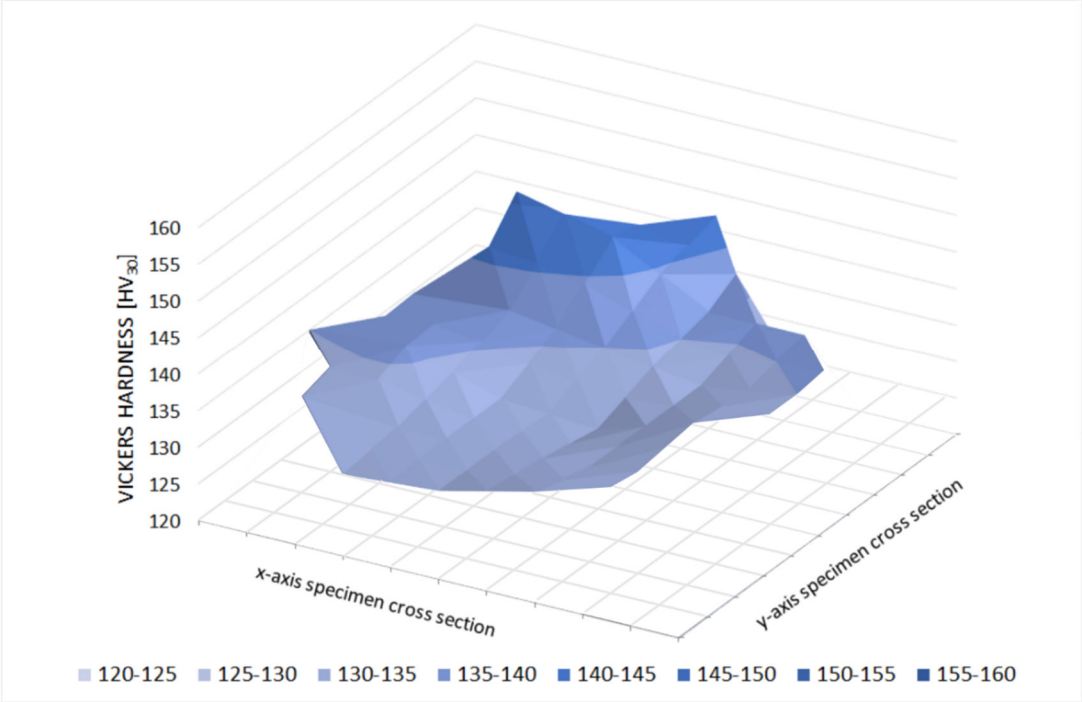

Fig. 4-3 Three-dimensional plot of the HV distribution on the cross-sectional area of stress relieved bar.

Table 4-2 Cross-sectional Vickers hardness measurements for the treated steel specimens.

Specimen number	Number of readings	Average Vickers hardness [HV_{30}]	HV standard deviation [HV_{30}]
Specimen 4	23	135	3.8
Specimen 5	20	134	4.1
Specimen 6	23	135	3.6

In this case, the hardness readings were more uniform, as shown by the reduced HV standard deviation and comparing Fig. 4-3 with Fig. 4-2. In addition, the average hardness reduced from approximately 143 to 135, probably due to softening during the heat treatment. Furthermore, the stress–strain curve of an as-received sample (Fig. 4-4) exhibited no discontinuous yielding point. The stress-relief process caused the reappearance of the Lüders strain (see Fig. 4-5). In conclusion, all the specimens tested during this experiment were subjected to the stress-relief treatment in the furnace for one hour at 500°C.

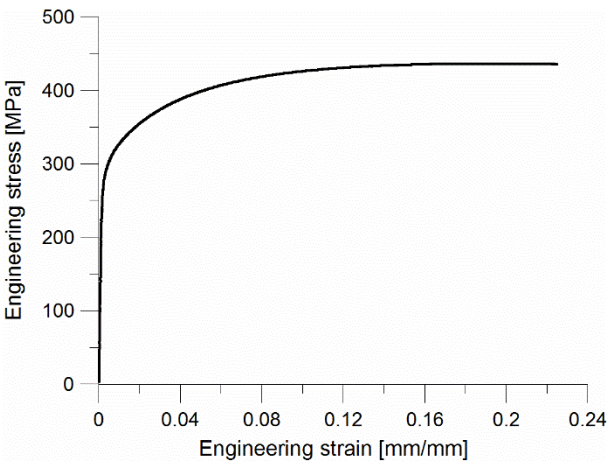

Fig. 4-4 Stress–strain curve of an as-received D12 Grade 300E reinforcing bar.

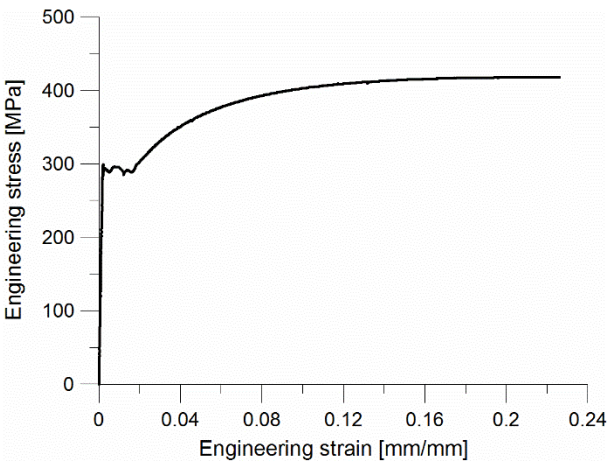

Fig. 4-5 Stress–strain curve of a stress-relieved D12 Grade 300E reinforcing bar.

4.2 CONSTANT-STRAIN AMPLITUDE EXPERIMENTAL TEST

Three separate calibration curves were developed: a monotonic calibration curve used as a benchmark, and two "cyclic" calibration curves – the first applying 5 zero-to-tension constant amplitude cycles, and a second applying 10 cycles. The experimental test was divided into several phases, following the standardised method defined in Chapter 3:

- Phase 1: Specimen pre-straining (monotonic and cyclic);
- Phase 2: Accelerated strain ageing;
- Phase 3: Specimen preparation for hardness testing;
- Phase 4: Hardness testing;
- Phase 5: Specimen machining for tensile testing;
- Phase 6: Tensile testing to failure;
- Phase 7: Data analysis.

4.2.1 Procedure

As a preliminary phase, three steel coupons were selected to obtain the main mechanical properties: lower yield strength, ultimate tensile strength (UTS) and strain at UTS (ε_{UTS}) (see Table 4-3).

Table 4-3 Mechanical properties of D12 Grade 300E rebars after the stress-relief treatment.

	Lower yield stress [MPa]	**UTS [MPa]**	**ε_{UTS} [mm/mm]**
Specimen 1	284	418	0.209
Specimen 2	288	419	0.213
Specimen 3	285	418	0.212
Average	**286**	**418**	**0.212**

During Phase 1, unmachined steel specimens were tested. The D12 reinforcing bars were cut into 140 mm lengths, which enabled an unsupported length between the MTS V-grips of 24 mm (twice the longitudinal diameter) for testing, and approximately 60 mm for gripping (see Fig. 4-6 and Fig. 4-7). The 24-mm clear length was selected to avoid bar buckling (upper unsupported length limit) and to allow enough clear space to position the extensometer on the specimen (lower unsupported length limit) (see Fig. 4-7). An unsupported length longer than 24 mm would have caused buckling in the specimen during the compression phase, while a shorter length would have not allowed enough room for the extensometer to be placed. Bar buckling was not in the scope of this experimental testing. The majority of the suspected damaged reinforcing bars received in the laboratory from earthquake-damaged buildings (details in Chapter 5) were not buckled and did not show any evident signs of damage. However, plastic deformation was detected through hardness and tensile testing. On site, concrete cracks extended over minimal width that caused no bar buckling; however, it was sufficiently large to deform the steel reinforcement. This test aimed to replicate similar circumstances: reinforcing bars with no apparent damage that have potentially plastically strained during a seismic event.

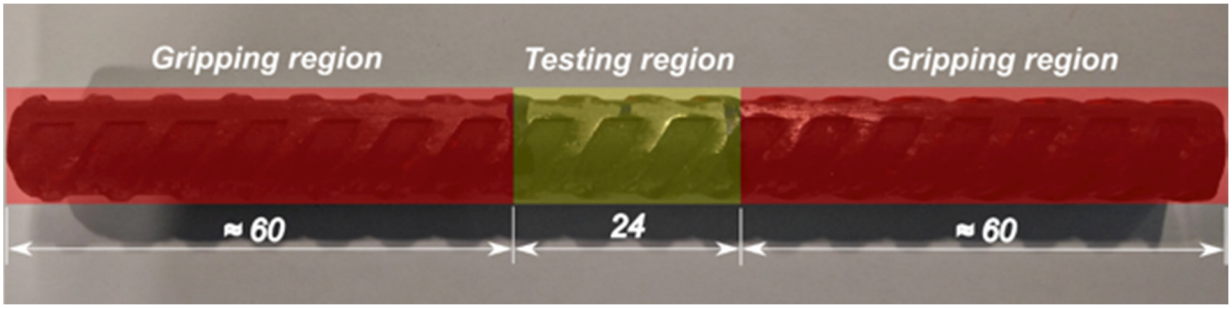

Fig. 4-6 Reinforcing bar specimen used for the experimental testing described in Section 4-2. Gripping and testing region are specified (dimensions are in mm).

The test set-up is shown in Fig. 4-7. An 8-mm gauge length MTS extensometer with 8% travel in tension and 2% in compression was attached to the steel specimen in order to record the strain every 0.25 s. The strain capability of the extensometer also defined the maximum strain limit

allowable (0.08 mm/mm). The strain limits selected were: 0.02, 0.04, 0.06 and 0.08 mm/mm (the same as in the experiment described in Section 3.3.1).

Fig. 4-7 Test set-up for the pre-straining, Phase 1

Cyclic tests were run in displacement control. When the strain limit selected was reached, the direction of the actuator displacement was manually reversed. For example, for the case of 0.02 mm/mm pre-strain and 5 cycles (Tests 13, 14 and 15, see Table 4-4), the actuator was programmed to apply a positive strain to the specimen up to 0.02 mm/mm (± 0.0005). Once the limit was reached the actuator was reversed in the opposite direction until the strain in the specimen reached 0.02 mm/mm (± 0.0005). Again, the actuator was instructed to move into the positive direction. After the upper 0.02 mm/mm strain limit was reached 5 times, the test was stopped and the load was removed. A residual plastic strain of 0.02 mm/mm (minus the elastic recovery, in the order of 0.0018 mm/mm) was achieved.

The same process was repeated for the strain limits 0.04, 0.06 and 0.08 mm/mm, subjecting the samples to 5 and 10 cycles for each strain limit. Three steel specimens were used for each combination of test type (monotonic, 5 cycles or 10 cycles) and pre-strain limit. The testing plan

is shown in Table 4-4. Examples of the strain histories and hysteresis loops are plotted in Fig. 4-8 to Fig. 4-11.

Table 4-4 Phase 1: testing plan.

		TEST TYPE		
		Monotonic	**5 cycles**	**10 cycles**
STRAIN LIMITS	**0 to 0.02 mm/mm**	Test 1	Test 13	Test 25
		Test 2	Test 14	Test 26
		Test 3	Test 15	Test 27
	0 to 0.04 mm/mm	Test 4	Test 16	Test 28
		Test 5	Test 17	Test 29
		Test 6	Test 18	Test 30
	0 to 0.06 mm/mm	Test 7	Test 19	Test 31
		Test 8	Test 20	Test 32
		Test 9	Test 21	Test 33
	0 to 0.08 mm/mm	Test 10	Test 22	Test 34
		Test 11	Test 23	Test 35
		Test 12	Test 24	Test 36

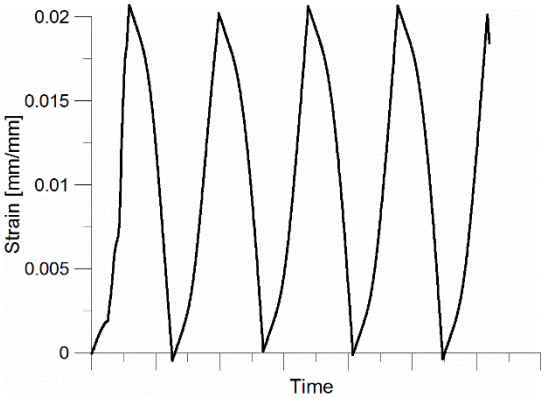

Fig. 4-8 Typical strain history for Tests 13, 14 and 15 (Pre-strain 0.02 mm/mm and 5 cycles).

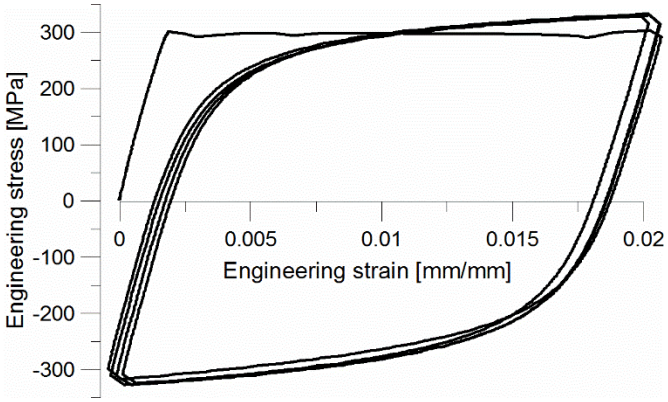

Fig. 4-9 Typical hysteresis loop for tests 13, 14 and 15 (Pre-strain 0.02 mm/mm and 5 cycles).

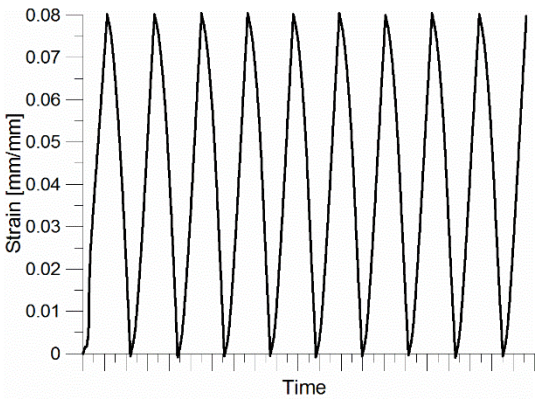

Fig. 4-10 Typical strain history for Tests 34, 35 and 36 (Pre-strain 0.08 mm/mm and 10 cycles).

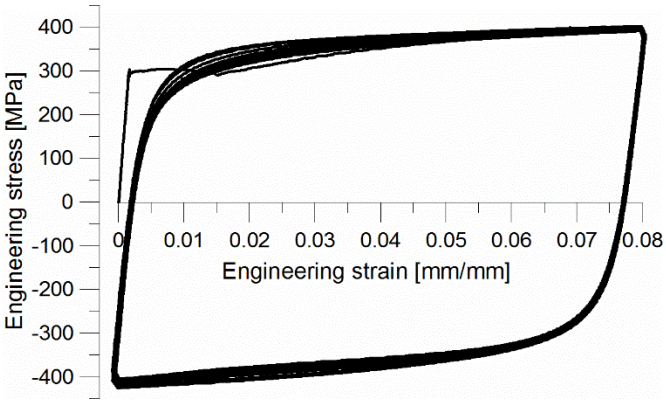

Fig. 4-11 Typical hysteresis loop for Tests 34, 35 and 36 (Pre-strain 0.08 mm/mm and 10 cycles).

After the pre-straining phase, the specimens were strain-aged at 100°C for four hours and then prepared for hardness testing by milling two parallel flat surfaces on opposite faces. One of the two faces was then ground and polished. Vickers hardness indentations were carried out every 2 mm within the 24-mm unsupported length plastically deformed during Phase 1. After hardness testing, the samples were machined into flat "dog-bone" shape tensile coupons for tensile testing to failure. The reduced area of the tensile coupon contained only the region of bar that was previously pre-strained (the 24-mm central length).

4.2.2 Results

Three Vickers hardness versus pre-strain (Fig. 4-12) calibration curves, and three residual strain capacity versus Vickers hardness calibration curves were developed (Fig. 4-13). Consistent with the previous experiment, hardness increased with plastic strain, while residual strain capacity decreased; however, the new variable, the number of cycles, allowed us to make a further observation. Vickers hardness only slightly increased when 5 cycles were applied; this increase was approximately 2 to 3 HV_{30} at each strain interruption. An even smaller, further increase in hardness was observed, in the order of 1 to 2 HV_{30}, when 10 cycles were applied. This increase

was probably due to the cyclic hardening occurring after the first cycle (see Fig. 4-9). The residual strain capacity versus hardness followed the same trend (Fig. 4-13).

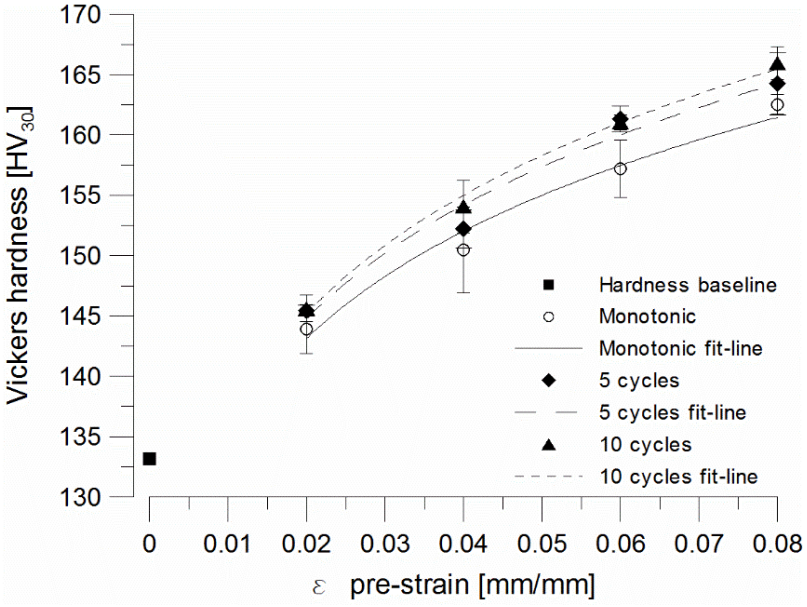

Fig. 4-12 Vickers hardness versus pre-strain calibration curves for monotonic, 5-cycle and 10-cycle testing.

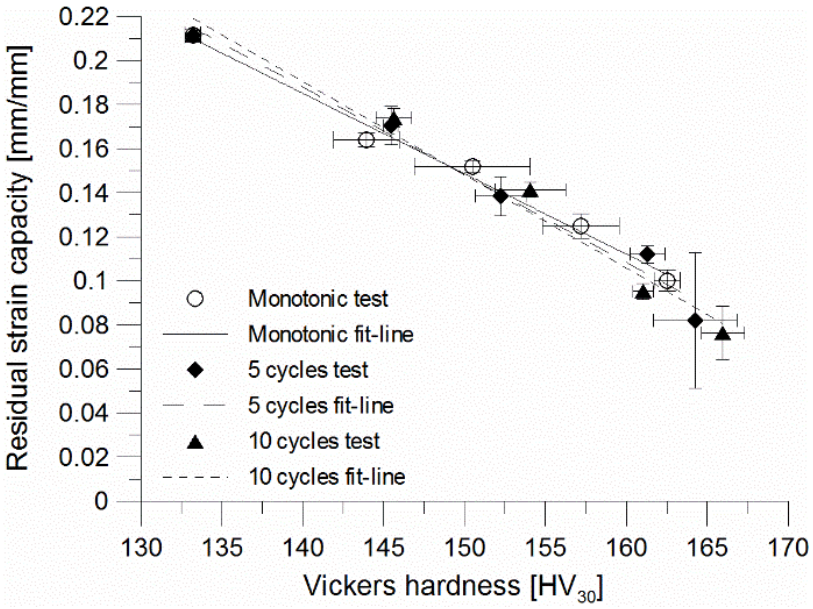

Fig. 4-13 Residual strain capacity versus Vickers hardness calibration curves for monotonic, 5-cycle and 10-cycle testing.

Table 4-5 Calibration curve equations.

	HV_{30} vs. ε	Residual strain capacity (ε_{UTS}) vs. HV_{30}
Monotonic test	$HV_{30} = 201.1\ \varepsilon^{0.087}$	$\varepsilon_{UTS} = -0.0036\ HV_{30} + 0.70$
5-cycle test	$HV_{30} = 206.8\ \varepsilon^{0.091}$	$\varepsilon_{UTS} = -0.0040\ HV_{30} + 0.74$
10-cycles test	$HV_{30} = 210.0\ \varepsilon^{0.094}$	$\varepsilon_{UTS} = -0.0042\ HV_{30} + 0.78$

Table 4-5 compares the calibration curve equations derived from the three tests. If, for example, the Vickers hardness of a rebar is 150, using the monotonic equation the estimated strain would be 0.035 mm/mm, using the 5-cycles equation the strain would be 0.029, while using the 10-cycle equation the strain would be 0.028. Comparing the two extreme results, the difference is 0.007 mm/mm, that is a 20% of the "monotonic" estimation. If the same calculation is repeated for the residual strain capacity, the prediction using the monotonic equation is 0.16 mm/mm, 0.14 mm/mm using the 5-cycle equation, and 0.15 mm/mm using the 10-cycle equation. In this case, the difference between the most and least conservative prediction is 0.02 mm/mm, which is a 12.5% uncertainty. This statistical variation is often observed during the mechanical testing of virgin rebars, as shown by the certificate of testing provided by Pacific Steel (Appendix B).

In conclusion, these results showed that the relationships between hardness, strain and residual strain capacity are not affected by the number of cycles considered (5 and 10) since the three regression lines follows the same trend. This implies that it is not possible to discern from the plastic strain the number of cycles a rebar has experienced during a seismic event. This conclusion is limited to steel samples tested up to 10 cycles and to 8% strain.

4.3 VARIABLE-STRAIN-AMPLITUDE EXPERIMENTAL TEST

A second part of the experimental testing consisted of applying a variable strain history on 8 samples (designated as V1, V2, V3, V4, V5, V6, V7, and V8) obtained from the same heat-treated steel. The strain histories were selected by considering 0.02, 0.04, 0.06 and 0.08 mm/mm as strain limits.

4.3.1 Procedure

The criteria adopted to define the variable-strain histories were:

- At least three strain amplitudes needed to be included;
- In the case of the variable history with 10 cycles, three consecutive cycles are at the same strain limit amplitude.

Strain histories and hysteresis loops for the 8 specimens are presented in Fig. 4-14 to Fig. 4-29.

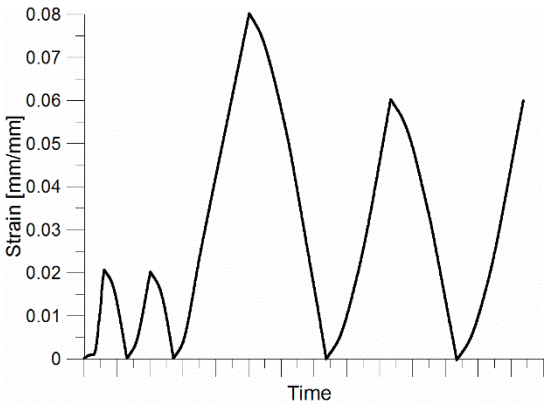

Fig. 4-14 Strain history applied on Specimen V1.

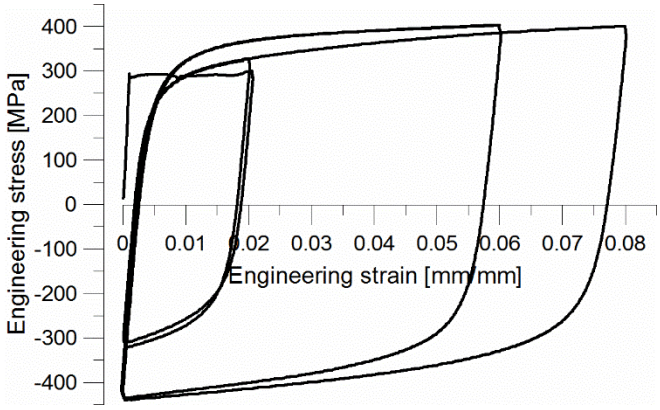

Fig. 4-15 Hysteresis loop obtained from Specimen V1.

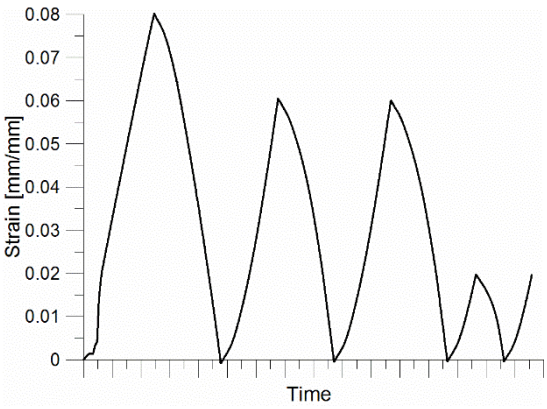

Fig. 4-16 Strain history applied on Specimen V2.

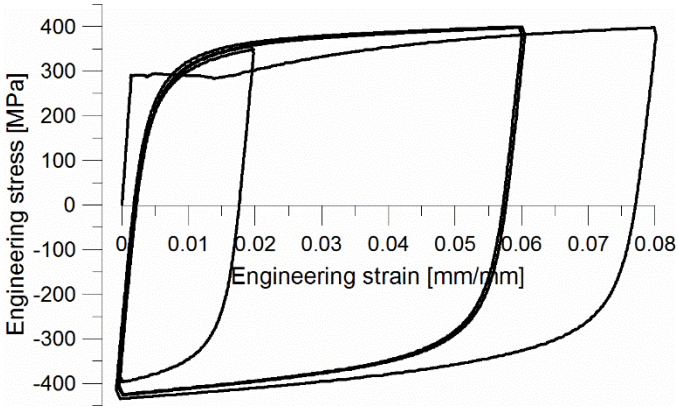

Fig. 4-17 Hysteresis loop obtained from Specimen V2.

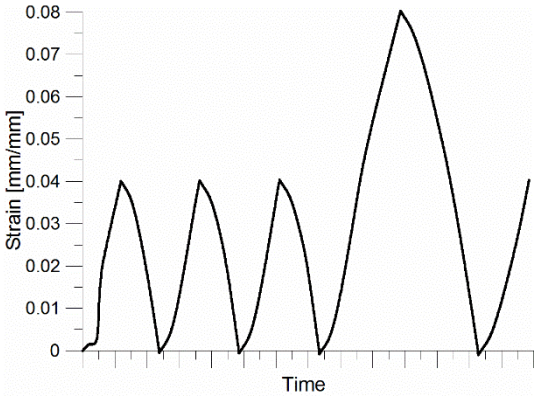

Fig. 4-18 Strain history applied on Specimen V3.

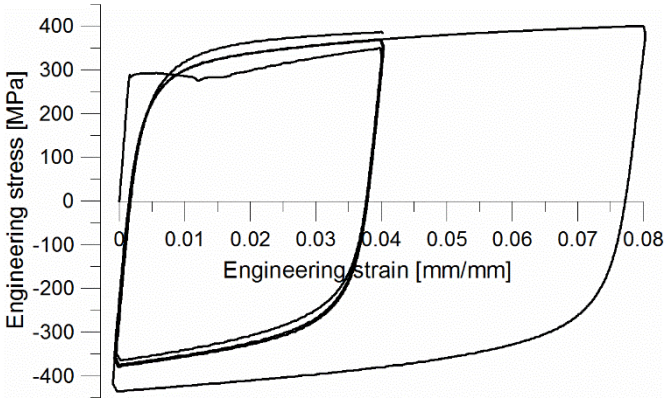

Fig. 4-19 Hysteresis loop obtained from Specimen V3.

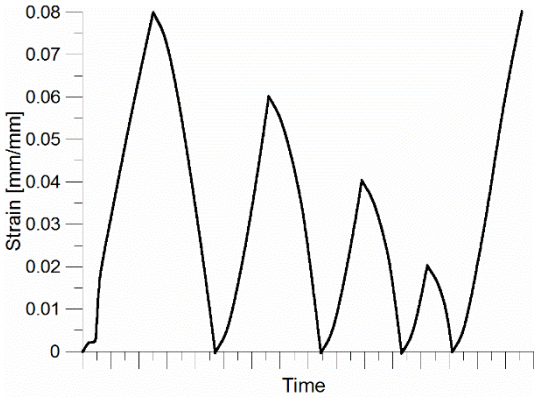

Fig. 4-20 Strain history applied on Specimen V4.

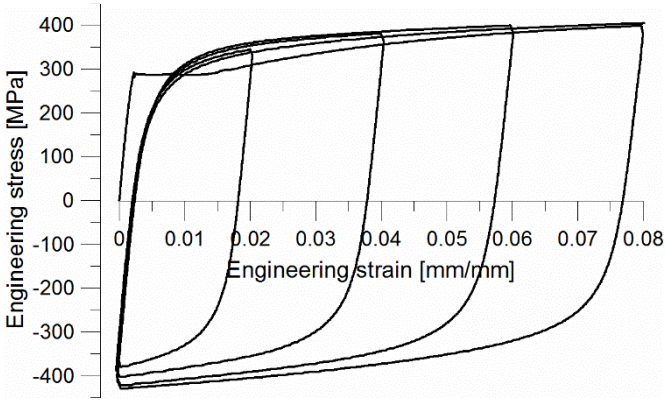

Fig. 4-21 Hysteresis loop obtained from Specimen V4.

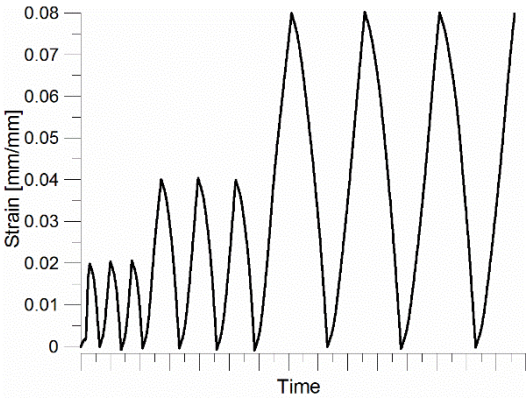

Fig. 4-22 Strain history applied on Specimen V5.

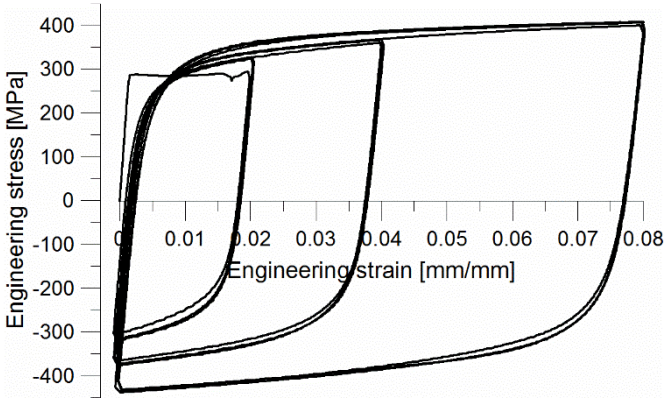

Fig. 4-23 Hysteresis loop obtained from Specimen V5.

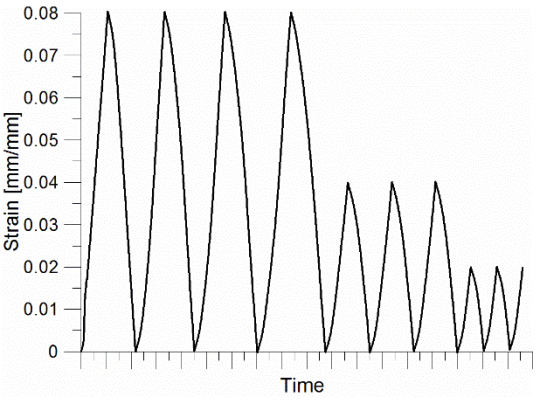

Fig. 4-24 Strain history applied on Specimen V6.

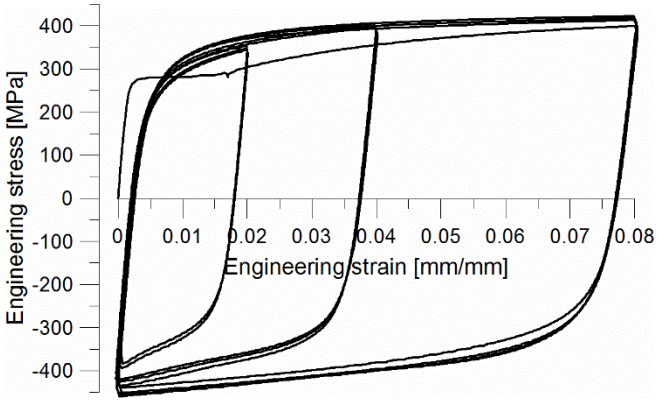

Fig. 4-25 Hysteresis loop obtained from Specimen V6.

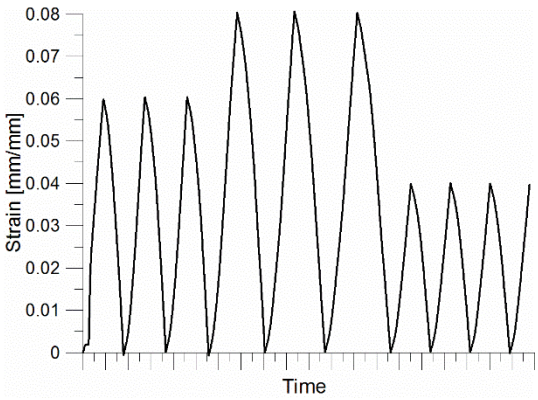

Fig. 4-26 Strain history applied on Specimen V7.

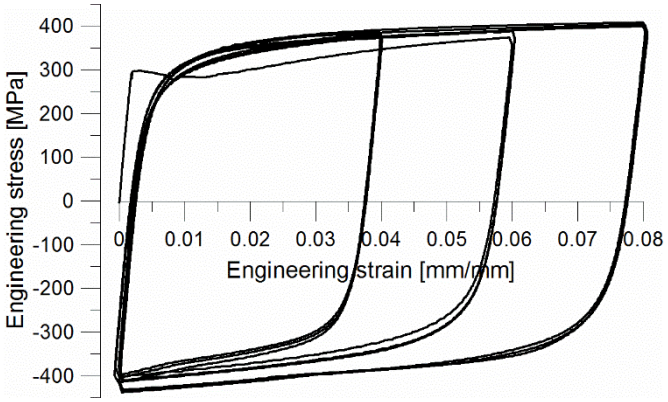

Fig. 4-27 Hysteresis loop obtained from Specimen V7.

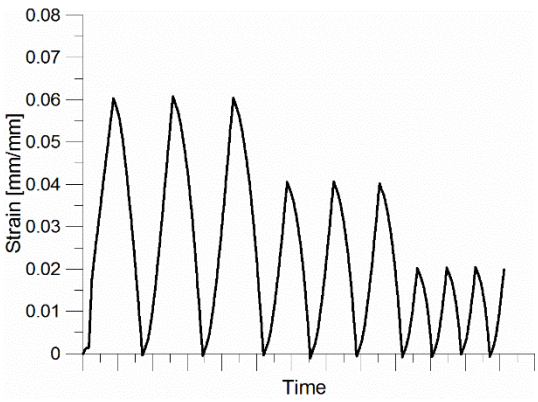

Fig. 4-28 Strain history applied on Specimen V8.

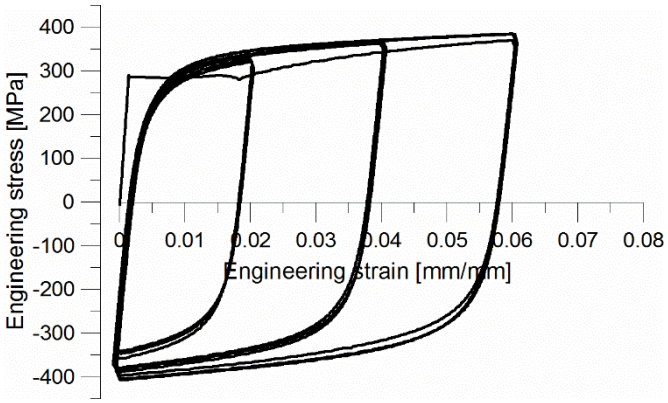

Fig. 4-29 Hysteresis loop obtained from Specimen V8.

4.3.2 Results

Vickers hardness and residual strain capacity values obtained from tests on Specimens V1 to V8 are presented in Table 4-5. Estimated pre-strain and estimated residual strain capacity from the calibration curves are also shown in the same table. Two values of the estimated pre-strain were obtained: the first was determined using the monotonic calibration curve as in Fig. 4-12; the second estimate used the average of two "cyclic" calibration curves. The predicted residual strain capacity was derived using the average of three calibration curves (monotonic, 5- and 10-cycles) of Fig. 4-13.

Fig. 4-30 shows a comparison of the experimental (actual) pre-strain and the estimated pre-strain based on the monotonic calibration curve. The y-axis is the ratio between the estimated pre-strain, (using the monotonic calibration curve [relationship $HV_{30} = 201.1\ \varepsilon_{PRE}^{0.087}$, where ε_{PRE} is the unknown]) and the actual pre-strain, (obtained from the pre-straining experimental test). On the x-axis, the Vickers hardness is plotted. An estimation of the pre-strain with no error would correspond to a value of 1; the further the ratio of estimated/actual is from 1, the less accurate is the estimation. The dashed lines represent a limit corresponding to a 50% error. Three out of five specimens are approximately within the 50% error bands. A better estimation of pre-strain is obtained using the "cyclic" calibration curve, see Fig. 4-31. In this case, six specimens are within

the 25% of the estimation error band delimited by the two dashed lines. The major outlier is Specimen V6.

Table 4-5 Experimental, estimated and predicted results from the specimens subjected to a variable-strain history

Specimen	**Observed Vickers hardness [HV]**	**Pre-strain[1] (ε_{PRE}) [mm/mm]**	**ε_{PRE} estimated[2] [mm/mm]**	**ε_{PRE} estimated[3] [mm/mm]**	**Observed residual strain capacity[4] (ε_{UTS}) [mm/mm]**	**ε_{UTS} predicted[5] [mm/mm]**
V1	159	0.06	0.066	0.052	0.098	0.113
V2	154	0.02	0.045	0.037	0.163	0.130
V3	158	0.04	0.064	0.050	0.118	0.114
V4	165	0.08	0.102	0.077	0.079	0.091
V5	164	0.08	0.095	0.073	0.075	0.094
V6	161	0.02	0.075	0.058	0.119	0.106
V7	158	0.04	0.064	0.050	0.087	0.114
V8	148	0.02	0.029	0.024	0.165	0.151

[1] Pre-strain obtained from test. This corresponds to the strain when the test was stopped.

[2] Estimated from Vickers hardness using the monotonic calibration curve in Fig. 4-12.

[3] Estimated from Vickers hardness using the cyclic calibration curve in Fig. 4-12.

[4] Residual strain capacity obtained from test. It corresponds to the strain at UTS.

[5] Predicted from Vickers hardness using the calibration curve in Fig. 4-13.

Fig. 4-32 shows a comparison of the predicted and the experimental residual strain capacity (y-axis) for the different specimens. The prediction is accurate for the majority of the specimens: two of the eight samples are included in the central band of the plot, which corresponds to a 10% error prediction; four predictions are within the 10 to 20 % error band. Finally, the error in the prediction of the residual strain capacity of Specimens V5 and V7 is within 30%.

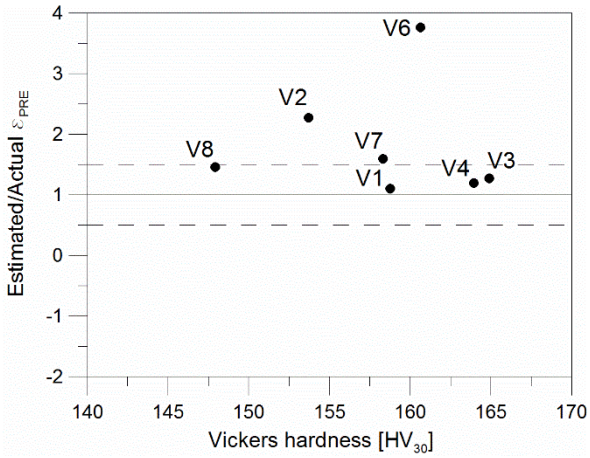

Fig. 4-30 Comparison of the estimated and experimental ε_{PRE} (pre-strain) using the monotonic calibration curve.

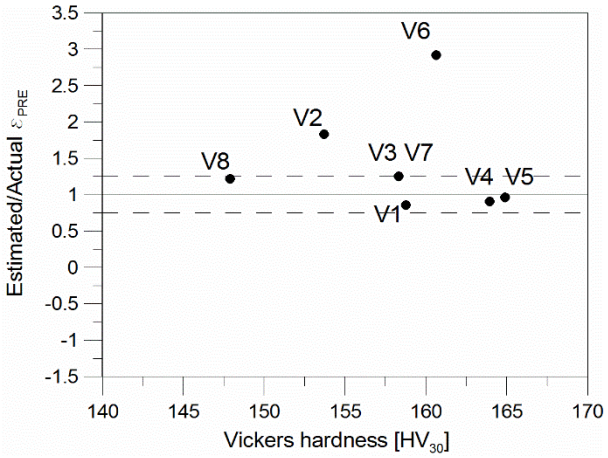

Fig. 4-31 Comparison of the estimated and experimental ε_{PRE} (pre-strain) using the cyclic calibration curves.

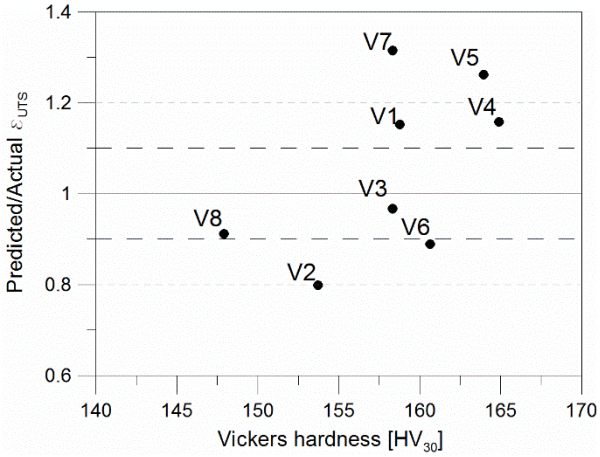

Fig. 4-32 Comparison of the predicted and experimental ε_{UTS} (residual strain capacity) using residual strain capacity vs. hardness calibration monotonic curve plotted in Fig. 4-13.

4.4 CONCLUSIONS

The experiment described in this chapter was designed to study the effects of cyclic strain on hardness and other mechanical properties, and to compare with monotonic straining. The as-received D12 steel reinforcing bars were affected by residual stresses that caused nonuniform hardness over the bar cross section. This limitation could affect the hardness methodology, which is based on the assumption that virgin bars have uniform baseline hardness. A stress-relief heat treatment at 500°C for an hour was undertaken to remove these stresses and to obtain uniform cross-sectional hardness.

Unmachined bar samples were tested and the 24-mm testing length (twice the longitudinal diameter) was selected in order to avoid buckling and to accommodate the 8-mm gauge length extensometer. The test protocol included constant-strain amplitude (monotonic, 5- and 10-cycle) pre-strain tests for developing the calibration curves. Variable-strain-amplitude cyclic tests were undertaken to verify the reliability of the methodology.

For the range from 0 to 10 cycles, this experiment showed that the number of cycles did not affect the residual strain capacity compared with that obtained with monotonic strain. The calibration curves of 5- and 10-cycle pre-straining testing followed the same trend as the monotonic curves. Hardness only increased by a maximum of 2.5% (4 HV_{30}) as the number of cycles increased, which "shifted" the calibration curve up, probably due to cyclic hardening.

However, as in this context the residual strain capacity is the relevant parameter required to assess the residual capacity (ductility) of a reinforced concrete member, it can be confirmed that developing only a monotonic calibration curve is a good approximation. The variable-strain-amplitude test showed that the predicted residual strain capacity error varied from approximately 5% to 35%. In general, the majority of the samples tested (6 out of 8) fell within the 20% error

band from the exact value. However, this conclusion is only limited to the load protocol applied (completely reversed cycles tests up to 10 cycles, maximum strain amplitude equal to 0.08 mm/mm). If the number of cycles in the plastic strain range increases as well as the strain amplitude and the mean strain, the monotonic response of the damaged rebars will be possibly compromised. In this case, it is unknown whether or not the hardness is affected. Further experiments are required to monitor the effects of large number of cycles on the hardness of rebars and monotonic strain capacity.

The result obtained implied that the monotonic strain curve could be used to estimate the plastic deformation experienced by steel rebars. Based on the variable-strain-amplitude test, an average improvement of 30% would be obtained using the cyclic straining curve at a cost of further time-consuming tests. On the other hand, no improvement can be obtained using the cyclic straining results compared with the monotonic one when the residual strain capacity is predicted. Therefore, the additional tests required to develop the cyclic straining curve are unnecessary. In addition, the results obtained confirmed that, knowing only the hardness of material compared with the baseline, it is not possible to discern whether a steel specimen was previously monotonically or cyclically strained; neither is it possible to estimate the number of cycles experienced.

4.5 REFERENCES

Adeyemi, M. B., Stark, R. A., & Modlen, G. F. (1980). Isothermal stress relief of cold-extruded mild steel rods. *Studies in Surface Science and Catalysis*, 122-125.

Krauss, G. (2005). *Steels: heat treatment and processing principles*. Ohio: ASM International.

Roberts, B. (2016). [Personal communication].

5 THE HARDNESS METHOD TO ASSESS EARTHQUAKE DAMAGE IN STEEL REINFORCEMENT

5.1 STATE OF ART

In Chapters 3 and 4, the correlation between hardness and strain was discussed. Experiments proved that plastic deformation in steel samples can be detected if an increase in Vickers hardness is observed. Although techniques to estimate the plastic strain in earthquake-damaged steel reinforcing bars are not fully developed in the literature, very few applications exist that use hardness as a parameter.

For example, a methodology to estimate the amount of plastic strain generated in steel structural elements during earthquakes, based on the relationship between hardness and plastic strain, was investigated by Matsumoto (2009). A series of tensile tests and hardness tests was conducted on Japanese SN490 structural steel members in order to investigate the correlation between hardness and tensile properties. The tests showed that tensile strength increased in proportion to the hardness, and uniform elongation decreased as hardness increased. Thus, hardness is an intrinsic property, and a key parameter to estimate the residual plastic strain capacity of plastically strained steel members.

The reliability and accuracy of a hardness testing device is a fundamental issue. A team from the Hitachi-GE Nuclear Energy Ltd, the Keio University and the Aoyama Gakuin University in Japan, analyzed three different types of portable hardness testers: a portable Vickers hardness tester, a UCI (Ultrasonic Contact Impedance) hardness tester and a rebound (Leeb) hardness tester (Nakane et al., 2010). Specimens obtained from austenitic stainless steel and ferrite steel were pre-strained up to 8–10%; hardness was subsequently measured with the three portable hardness

devices and a conventional Vickers hardness tester. Results were compared: the portable Vickers hardness tester provided the most reliable results when compared with those obtained from the conventional Vickers hardness machine. The ultrasonic device requires a calibration depending on the elastic modulus of the metals tested. In addition, results showed dependency on the sample thickness.

Fig. 5-1 Portable hardness testing machines: on the left, the Vickers hardness tester; in the centre, the ultrasonic hardness tester; on the right, the rebound Leeb hardness tester (Nakane et al., 2010).

Extensive studies and practical applications were conducted soon after the Christchurch earthquakes in New Zealand (2010 to 2011). A proposed method of testing on-site with minimal damage (referred to henceforth as the "in situ hardness method") is based on measuring hardness with a portable hardness testing device and then correlating the measured hardness to plastic strain determined from laboratory tensile tests on the same or similar material (Allington, 2011; Nashid et al., 2014). Leeb hardness and Rockwell B hardness tests respectively were used on-site and in the laboratory, on the eccentrically braced frames (EBF) of the Pacific Tower in Christchurch (Nashid et al., 2014). Hardness measurements showed an increase compared with the virgin material in Leeb and Rockwell B hardness in the web section of the active link beam of damaged EBFs. This increase in hardness was an indication of plastic deformation of the structural element.

Leeb hardness tests, based on rebound hardness, were conducted on-site on the steel reinforcing bars that crossed concrete cracks in earthquake-damaged buildings (Allington, 2011).

Near to crack locations, the bars were exposed by removing the covering concrete. The exposed surface was ground and surface-finished to approximately 120 grit to facilitate the hardness measurement operations. Leeb hardness readings were obtained at regularly spaced intervals along a significant length of the bar, to detect any systematic increase in hardness near cracks, which could demonstrate that the elastic limit of the bar had been exceeded. In order to quantify the amount of plastic deformation, a correlation between Leeb hardness and steel plastic strain was determined through laboratory-based hardness and tensile tests.

5.2 THE HARDNESS METHOD

Having established Vickers hardness and tensile test protocols based on the results of the experiments presented in Chapters 3 and 4, the following overall method was applied to several Christchurch buildings and structures identified as having been damaged in the 2010/2011 earthquakes.

5.2.1 Procedure

A total of 49 samples were tested. The method took place over four distinct phases:

I. Suspected damaged reinforcement was removed from the building.

II. Vickers hardness tests were performed to precisely identify the location and extent of damage on the reinforcement.

III. If damage was detected, a calibration of that specific grade and diameter of steel was performed and used to quantify damage and residual plastic deformation capacity.

IV. Tensile tests of the damaged location were performed and compared to tensile tests of undamaged steel from the same bar.

In Phase I, structural engineers identified locations in each building as having evidence of damage, i.e., cracks in reinforced concrete structural members, structural assessment and analysis,

in situ physical testing of reinforcement, such as in situ Leeb testing. The location of a specific reinforcing bar crossing a crack was determined using electromagnetic methods. These bars were suspected to have been damaged during the seismic events. The cover concrete was then removed to expose the steel bar, using mechanical or hydraulic equipment, taking care to prevent further damage to the steel. The steel was typically exposed over a length of approximately 400–700 mm and then removed for damage assessment in the laboratory, with the intention of recovering at least 100 mm either side of the crack location, and also recovering a 200-mm section of the same bar from the concrete with no sign of damage.

Phase II consisted of Vickers hardness testing and damage assessment. The removed bars were cut to 150–200 mm lengths, centred on the crack location. The portion of the bar identified as having been removed from undamaged concrete was set aside for future tensile testing. Two opposing sides of each bar section were surface-ground flat and parallel using a water-cooled grinder, then sequentially ground by hand from 180, 240, 320, 400 to 600 grit using silicon carbide papers, and then finally polished to a 9-micron finish. Vickers hardness measurements were initially collected along the longitudinal section of the steel bar at 4-mm spacings (see Fig. 5-2). When a rise in hardness was detected, the spacings were reduced to 2 mm. The Vickers hardness profile along the length of the specimen was recorded.

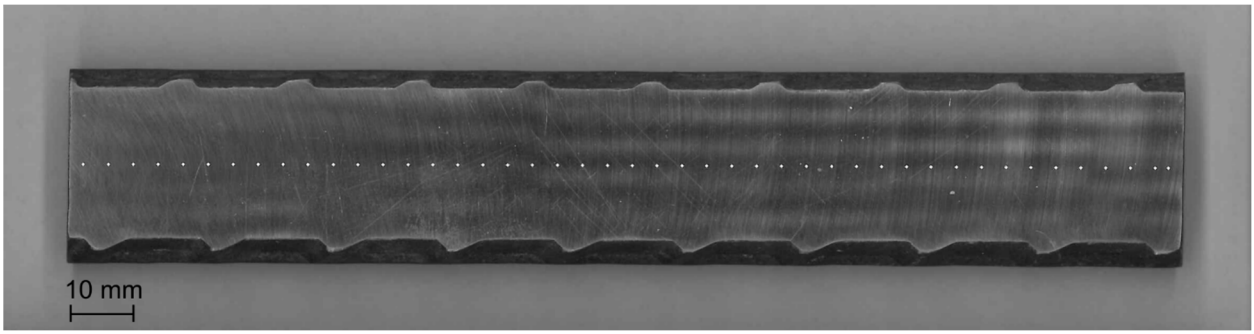

Fig. 5-2 Vickers hardness indents shown on a typical polished surface.

Phase III was performed, as described in Section 3.3 to obtain a calibration between hardness and strain and residual capacity, accounting for strain ageing. This required the on-site removal of enough material of each diameter and grade to produce 21 tensile test specimens, enough material to make three bars for each pre-strain value of 0, 0.01, 0.02, 0.03, 0.04, 0.05 and 0.10 mm/mm. Since approximately 200mm was required for each specimen, 4.2 metres of material of each grade and diameter of material of interest needed to be extracted from the building. A comparison between the hardness profile and the calibration data enabled an estimate of the maximum strain and minimum residual plastic strain capacity.

In Phase IV, tensile specimens were machined so that the gauge length corresponded to the length of specimen with elevated hardness, or, if no elevated hardness was detected, the gauge length was centred upon the location of the crack in the covering concrete. Tensile specimens from undamaged sections of the same bar were also machined with the same dimensions. This enabled a direct comparison of damaged steel with its original state, as well as a comparison with the hardness test results.

5.2.2 Results

To illustrate the application of the method, four damaged reinforcing bars, extracted from a reinforced concrete structure, constructed in various stages from 1990 to 2010, have been selected as examples. The basic mechanical properties of these four example bars (named D1, D2, D3 and D4) are presented in Table 5-1. Note that the grade determination was based on the mechanical properties obtained from laboratory testing, existing drawings, construction date, bar mark indicating grade and the applicable steel reinforcing material standard.

This case study was conducted approximately four years after the Canterbury 2010/2011 earthquake sequence concluded. Therefore, it is reasonable to assume that natural strain ageing

occurred in the ensuing period of time. However, since buildings were not generally accessible to the authors between the most significant earthquakes (4 September 2010, 22 February 2011, 13 June 2011 and 23 December 2011), it was not practical or possible to monitor the evolving crack pattern, steel damage and de-bonding that may have occurred after each event.

Table 5-1 Basic mechanical properties of the selected reinforcing bars (away from the damaged region).

Bar sample	Diameter [mm]	Grade	Lower Yield strength [MPa]	Ultimate tensile strength (UTS) [MPa]	Strain at UTS [%]
D1	25	300	316	501	19.8
D2	25	300	316	501	19.8
D3	16	430	467	629	15.6
D4	16	430	467	629	15.6

Hardness transverses (lengthwise profiles) of the four examples bars are shown from Fig. 5-3 to Fig. 5-6. The hardness testing data are summarised in Table 5-2. As the bar samples are cut centred on the crack location, hardness peaks often occurred in the central regions, then the hardness decreased to the baseline value at the edges. However, in some cases (see Fig. 5-4 and Fig. 5-5), the elevated hardness extended over to the sample edges. This behaviour might be attributed to two causes: 1) the plastic deformation occurred over a length larger than the sample bar, or 2) the bar was overheated during the cutting process and metallurgical properties were altered. Further investigation of the material microstructure could allow a more detailed answer.

Table 5-2 Summary of the hardness test data.

Bar sample	Vickers hardness baseline [HV_{30}]	Average maximum Vickers hardness [HV_{30}]	Increase in Vickers hardness [HV_{30}]
D1	146	165	19
D2	146	172	26
D3	189	211	22
D4	189	197	8

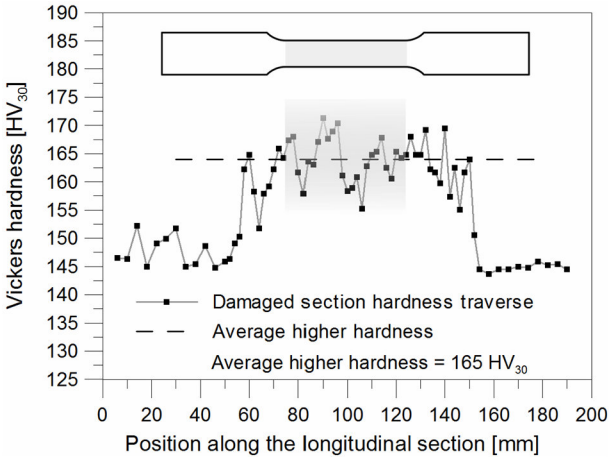

Fig. 5-3. Vickers hardness transverse profile of the D1 damaged bar.

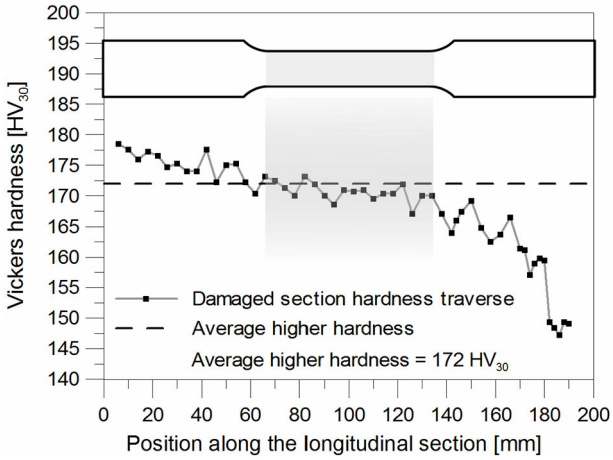

Fig. 5-4. Vickers hardness transverse profile of the D2 damaged bar.

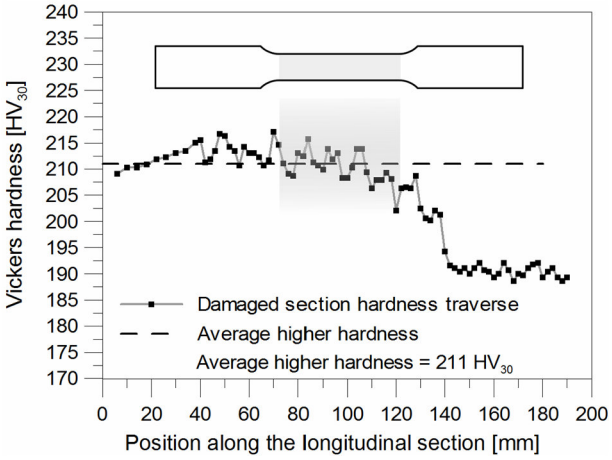

Fig. 5-5. Vickers hardness transverse profile of the D3 damaged bar.

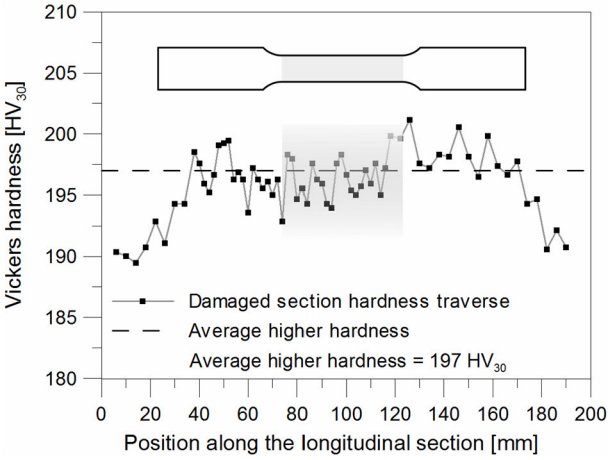

Fig. 5-6. Vickers hardness transverse profile of the D4 damaged bar.

Due to the variable baseline, differences in the pre-exponential constant and work-hardening exponent of the various grades, and even between heats and diameters of the same grade of steel, each reinforcing steel material has a unique calibration curve. Therefore, calibration curves were developed for each combination of bar diameter, grade and baseline hardness. Two sets of calibration curves were developed: a) the hardness versus plastic strain calibration curve (Fig. 5-7 and Fig. 5-9), and b) the residual strain capacity versus hardness calibration curve (Fig. 5-8 and Fig. 5-10). The "before ageing" calibration curve is never used but shown for comparison. Strain

ageing effects were accounted for using the accelerated ageing process. The strain at UTS for the strain-aged samples was considered to be the residual strain capacity.

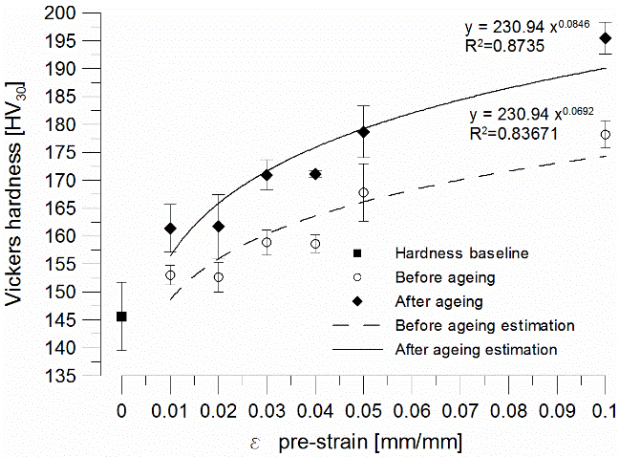

Fig. 5-7. Hardness versus pre-strain calibration curve for 25-mm diameter Grade 300.

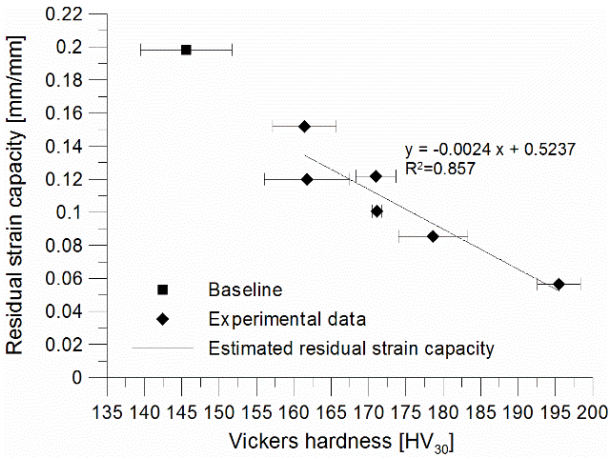

Fig. 5-8. Residual strain capacity versus Vickers hardness calibration curve for 25-mm diameter Grade 300.

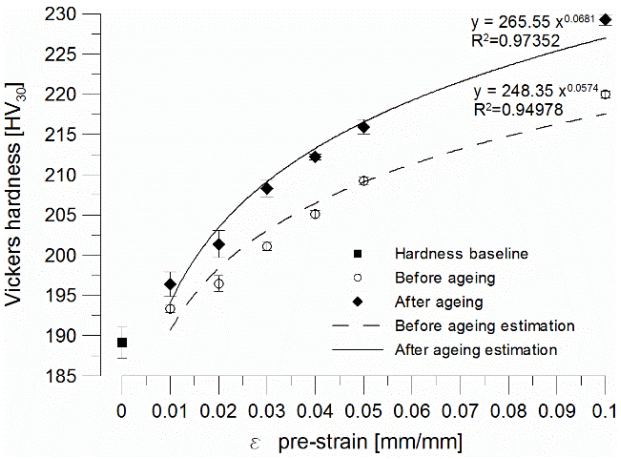

Fig. 5-9 Hardness versus pre-strain calibration curve for 16-mm diameter Grade 430.

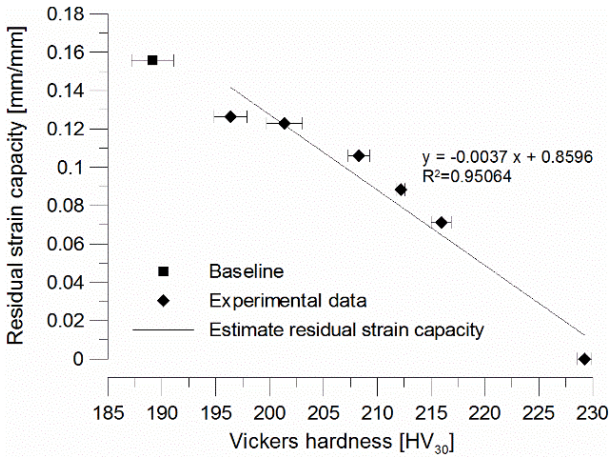

Fig. 5-10 Residual strain capacity versus Vickers hardness calibration curve for 16-mm diameter Grade 430.

Based on the average maximum hardness and calibration results, bar D1 is estimated to have undergone approximately 0.02–0.03 mm/mm plastic strain; its residual strain capacity is expected to be 0.125 mm/mm, which is about the 60% of the original capacity (~0.20 mm/mm strain at UTS). Bar D2 was suspected to have deformed about 0.03 mm/mm and the predicted residual strain capacity was 0.11 mm/mm. The estimated plastic deformation for bar D3 was around 0.035–0.04 mm/mm and the predicted remaining strain was 0.085 mm/mm. Bar D4 had probably experienced approximately 0.015 mm/mm plastic strain; the expected residual deformation capacity was approximately 0.13 mm/mm. These results are summarised in Table 5-4.

Finally, the damaged bars were machined for tensile testing, ensuring that the reduced area of the testing sample contained only the damaged material (see the grey region in Fig. 5-3 as an example). The extensometer was located within the damaged area (identified by the Vickers hardness transverse). Stress–strain curves of the damaged samples, superimposed on the undamaged ones, are plotted in Fig. 5-11 to Fig. 5-14. The comparison with the monotonic benchmark tests revealed a shortened Lüders strain, increased upper yield strength, increased UTS and decreased strain at UTS as summarised in Table 5-3. As expected, the mechanical properties of the steel changed due to the plastic deformation that occurred during the seismic event.

Table 5-3 Mechanical properties of the damaged reinforcing bars.

Bar name	Lower yield strength [MPa]	Lüders extension [mm/mm]	Ultimate tensile strength (UTS) [MPa]	Strain at UTS [mm/mm]
D1	393	0.006	527	0.122
D1 Undamaged	329	0.016	511	0.185
D2	373	0.001	536	0.136
D2 Undamaged	323	0.016	514	0.192
D3	640	0.015	669	0.082
D3 Undamaged	449	0.019	628	0.149
D4	545	0.000	625	0.104
D4 Undamaged	448	0.017	600	0.163

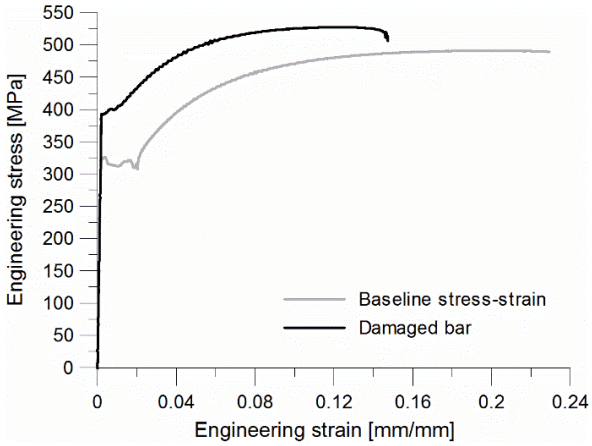

Fig. 5-11. Stress–strain curve of the D1 damaged bar and a virgin bar of same grade and diameter.

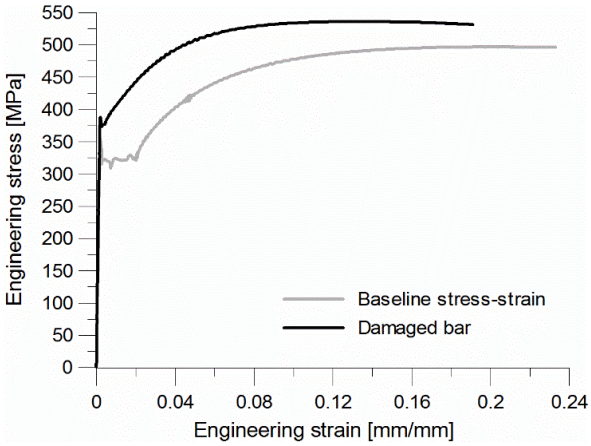

Fig. 5-12. Stress–strain curve of the D2 damaged bar and a virgin bar of same grade and diameter.

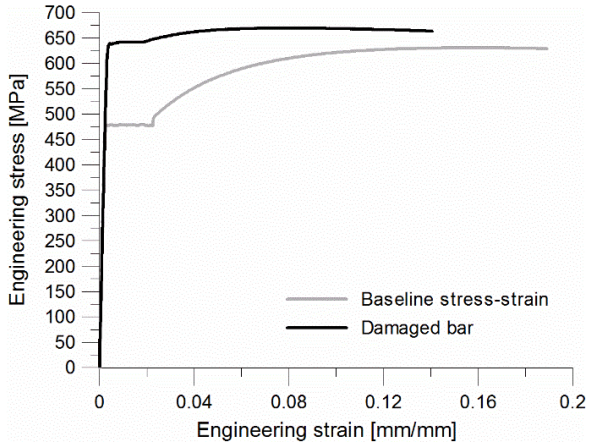

Fig. 5-13. Stress–strain curve of the D3 damaged bar and a virgin bar of same grade and diameter.

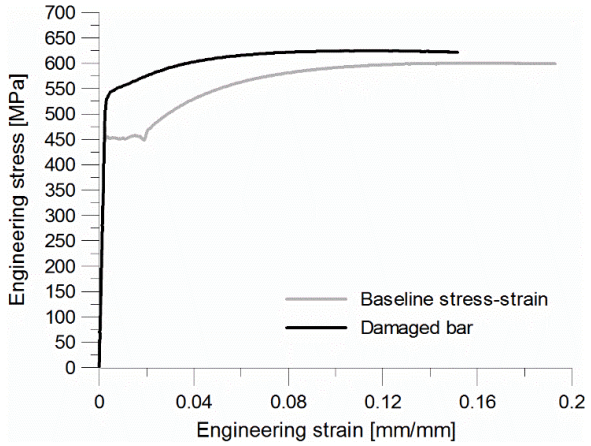

Fig. 5-14 Stress–strain curve of the D4 damaged bar and a virgin bar of same grade and diameter.

The comparison between predicted and actual residual strain capacity is presented in Table 5-4. In the case of samples D1 and D3 the hardness method predicted the residual strain capacity within a 5% error. Meanwhile, in the case of D3 and D4 the error was higher, around 20–25 %, which means a difference from the actual residual strain of approximately 0.026 mm/mm. As can be observed in the testing certificate in Appendix B, the standard deviation for the uniform elongation is about 0.017 mm/mm, while the difference between the highest and the lowest values is 0.033. Therefore, if errors below 5% are negligible, an error of 0.026 mm/mm, as obtained in this experiment, can still be considered acceptable.

Table 5-4 Comparison between predicted and actual residual strain capacity.

Bar name	**Average maximum Vickers hardness [HV_{30}]**	**Predicted residual strain capacity [mm/mm]**	**Actual residual strain capacity [mm/mm]**	**Error [%]**
D1	165	0.125	0.122	2.5 %
D2	172	0.110	0.136	19.1%
D3	211	0.085	0.082	3.7 %
D4	197	0.131	0.104	25.9%

5.2.3 Code compliance

As described in Section 5.2, the “damaged” rebars showed an increase in yield stress and reduction in strain capacity. In this section, the mechanical properties of the damaged samples are compared with the minimum requirements by code. The origin of reinforcing bars could not be traced; however, the information available on the undamaged bars (building construction date, yield and ultimate tensile strength, etc.) allowed their grade to be determined. Therefore, the mechanical properties obtained from the lab testing were compared against those prescribed by standards.

Samples D1 and D2 were removed from a structure constructed between 2009 and 2010; the current available standard in that period was AS/NZS 4671 (Standards, Australia and New Zealand, 2001). The yield strength obtained by testing an undamaged sample of the same steel was approximately 315 MPa, a value suggesting that the steel was Grade 300E. The comparison between the mechanical properties of the damaged bars D1 and D2 against the code requirements is shown in Table 5-5. The yield stress of both samples is larger than the upper characteristic values. In both cases, the uniform elongation (the elongation at maximum force) was lower than the minimum of 15% specified by code. Thus, Samples D1 and D2 did not meet the standard requirements.

Table 5-5 Comparison of the mechanical properties of samples D1 and D2 against the relative standard.

Property	**300E (AS/NZS 4671:2001)**	**D1**	**D2**
Yield stress (MPa) $R_{eK,L}$	≥ 300	393	387
$R_{eK,U}$	≤ 380	(Not complying)	(Not complying)
Ratio tensile strength/yield stress	≥ 1.15	1.46	1.31
	≤ 1.50	(Complying)	(Complying)
Uniform elongation (%)	≥ 15.0	12.2	13.6
		(Not complying)	(Not complying)

$R_{eK,L}$: Lower characteristic value of the yield strength obtained from series of tensile tests
$R_{eK,U}$: Upper characteristic value of the yield strength obtained from series of tensile tests

Samples D3 and D4 were recovered from a structure constructed after 1989 but before 2001, when the corresponding standard was the NZS 3402 (Standards, New Zealand, 1989). The yield strength of the undamaged portions of the same bars varied from 440 MPa to 465 MPa, which is consistent with Grade 430 steel available between 1989 and 2001. The mechanical properties obtained from the tensile tests are compared in Table 5-6. The yield stresses of Samples D3 and D4 were higher than the maximum prescribed. In contrast with AS/NZS 4671:2001, NZS 34025:1989 specified that the elongation at fracture for a 5-diameter gauge length specimen must

be larger than 15%. The elongation experimentally determined in this work corresponded to the uniform elongation and cannot be directly compared with that prescribed by the standard. In the current code, Grade 430 was superseded by Grade 500E. Therefore, for practicality the uniform elongation was compared to the 10% limit prescribed for Grade 500E. Based on the tests conducted, both samples did not meet the minimum by standard (see Table 5-6).

Table 5-6 Comparison of the mechanical properties of samples D3 and D4 against the relative standard.

Property	**430 (NZS 3402:1989)**	**D3**	**D4**
Yield stress (MPa) Min	≥ 410	639	545
Max	≤ 520	(Not complying)	(Not complying)
Ratio tensile strength/yield stress	≥ 1.15	1.05	1.15
	≤ 1.40	(Not complying)	(Complying)
Elongation (%)*	≥ 10.0	7.7	10.4
		(Not complying)	(Complying)

*NZS 3402:1989 specifies that elongation should be measured at fracture determined on a gauge length of 5 diameters.

5.3 SIMPLIFIED HARDNESS METHOD

Within the 49 bars tested during this experimental testing campaign, seven more rebars were found to have their ductility reduced. In all the cases, this reduction in ductility was predicted by an increase in hardness. Following the established protocol, the "suspected" damaged rebars were hardness tested along the longitudinal length in order to detect and locate the "damaged" area. Results are shown in Fig. 5-15, Fig. 5-17, Fig. 5-19, Fig. 5-21, Fig. 5-23, Fig. 5-25, and Fig. 5-27.

In this case, Phase III (calibration) was bypassed and samples were tensile tested after hardness testing. Tensile specimens were machined from the damaged and undamaged bars in order to compare the mechanical properties and stress–strain curves. Results are summarised in Table 5-7 and Table 5-8. Stress–strain curves of the damaged and undamaged specimens are presented in Fig. 5-18, Fig. 5-20, Fig. 5-22, Fig. 5-24, Fig. 5-26 and Fig. 5-28. Evidence of damage can be observed by comparing the stress–strain curves. In addition to the reduced ductility, the damaged rebars present either an increase in yield strength (Samples D6, D7 and D8) or reduced yield discontinuous point (D5, D8, D9, D10 and D11). It is important to note that the mechanical properties of the steel samples changed throughout the longitudinal section; in particular the yield strength, proportional to the hardness, varied according to the hardness profile.

Table 5-7 Mechanical properties in the undamaged region of Samples D6 to D11.

Bar name	**Diameter [mm]**	**Grade**	**Average hardness in the undamaged region [HV_{30}]**	**Lower yield strength (LYS) in the undamaged area [MPa]**	**Strain at UTS [mm/mm]**
D5	16	430	181	439	0.157
D6	12	500	224	515	0.113
D7	16	500	225	520	0.120
D8	12	430	190	465	0.152
D9	12	430	203	488	0.145
D10	16	430	185	450	0.159
D11	16	430	194	473	0.146

In order to standardise the machining process of the samples and the testing protocol, the reduced testing area of the tensile samples was kept constant for each sample (32 mm). Depending on the extent and the level of the damage, the mechanical properties of the tested samples were not uniform. As an example, Fig. 5-27 shows that the hardness in the reduced testing area (in grey in the figure) is variable; a single peak is observed and the hardness decreases substantially in the vicinity of the peak. As a consequence, the mechanical properties of the test coupon are different at each point. The stress–strain curve obtained is most likely relative to the softer portion of steel, which is the region where the lowest hardness is recorded. Since hardness is proportional to the yield strength, during a tensile test the yield strength of the entire specimen, that is not uniform, is governed by the lowest yield strength, which will start to plastically deform first. Then, if the ultimate strength of the softer region is lower than the yield strength of the harder one, this will remain elastic because necking will occur before its elastic limit is reached.

Because the prediction of the residual strain capacity of the rebars is based on the average hardness in the damaged area, if the hardness varies significantly, the residual strain prediction might be affected by an error. In order to have an accurate prediction of the residual strain capacity,

the hardness in the reduced area of the testing sample should be approximately constant, and a calibration curve for the same steel grade and diameter must be used.

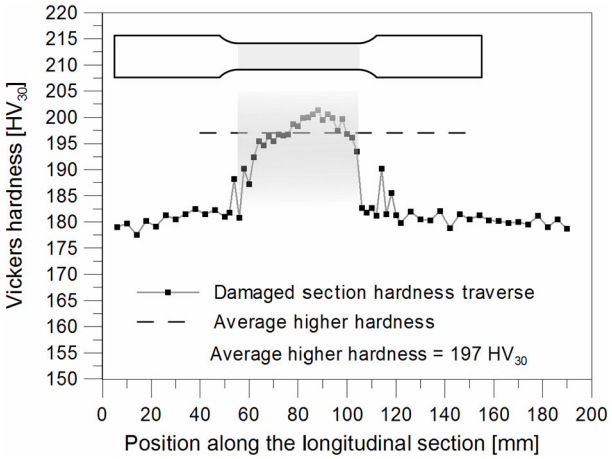

Fig. 5-15 Vickers hardness transverse profile of the D5 damaged bar.

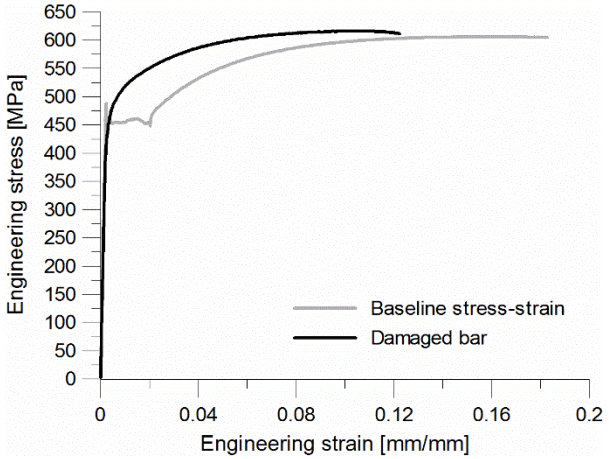

Fig. 5-16 Stress–strain curve of the D5 damaged bar and an undamaged sample of the same bar.

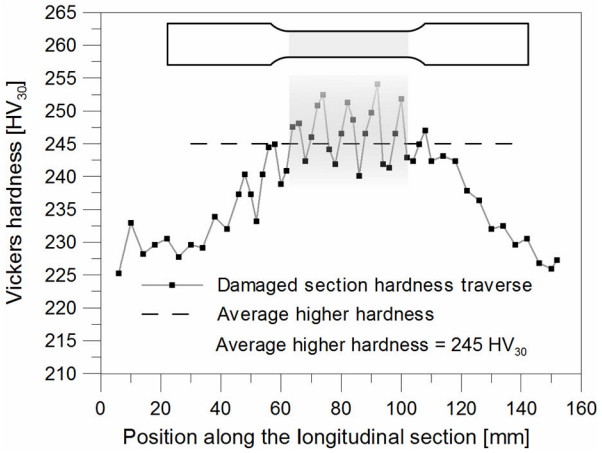

Fig. 5-17. Vickers hardness transverse profile of the D6 damaged bar.

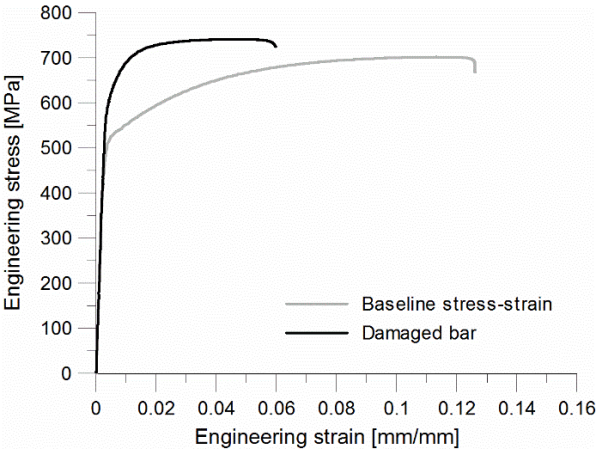

Fig. 5-18. Stress–strain curve of the D6 damaged bar and an undamaged sample of the same bar.

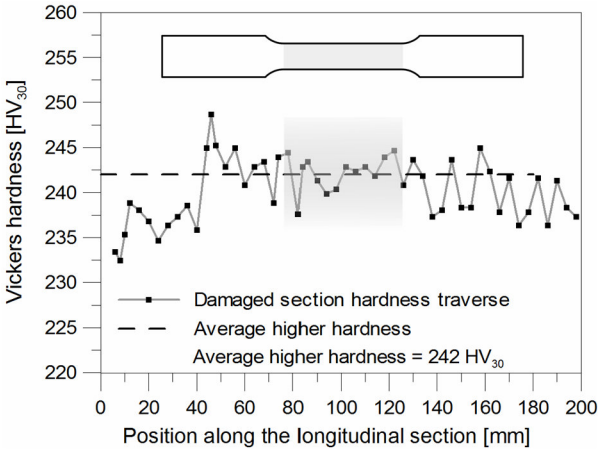

Fig. 5-19. Vickers hardness transverse profile of the D7 damaged bar.

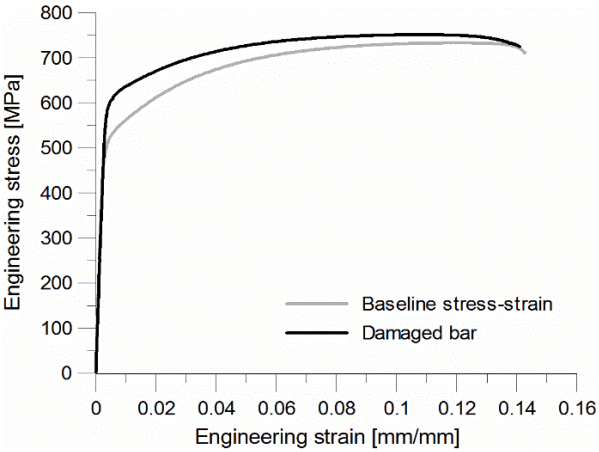

Fig. 5-20. Stress–strain curve of the D7 damaged bar and an undamaged sample of the same bar.

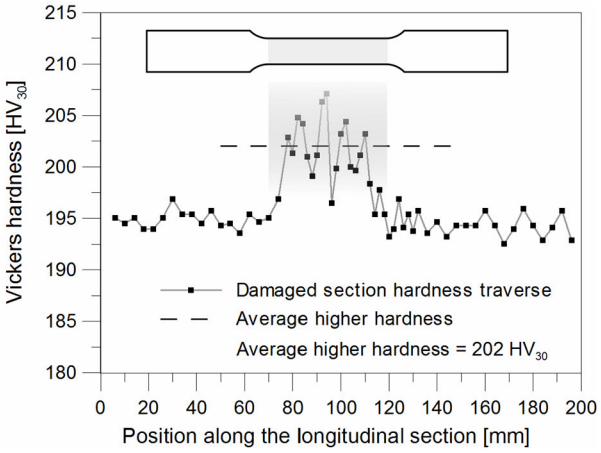

Fig. 5-21. Vickers hardness transverse profile of the D8 damaged bar.

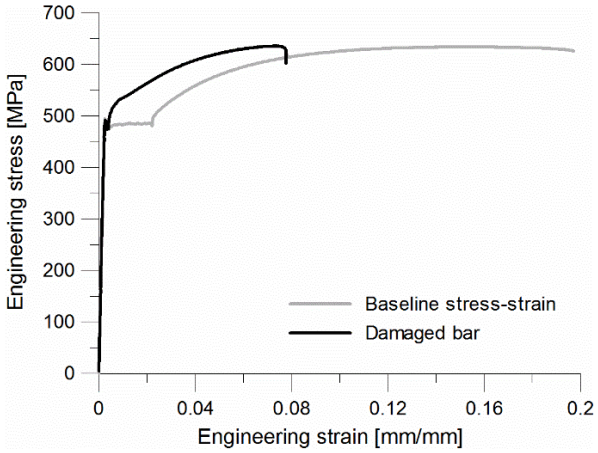

Fig. 5-22. Stress–strain curve of the D8 damaged bar and an undamaged sample of the same bar.

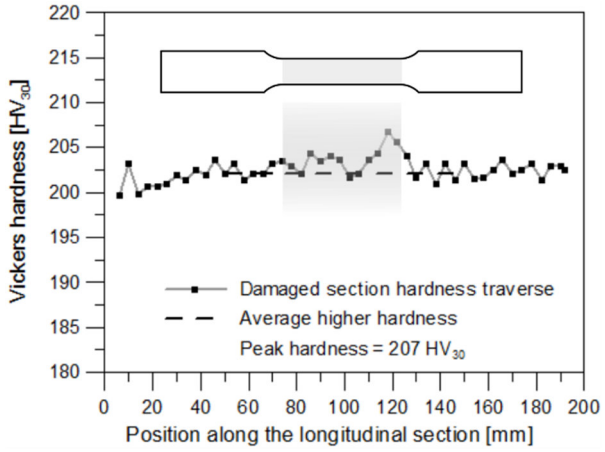

Fig. 5-23. Vickers hardness transverse profile of the D9 damaged bar.

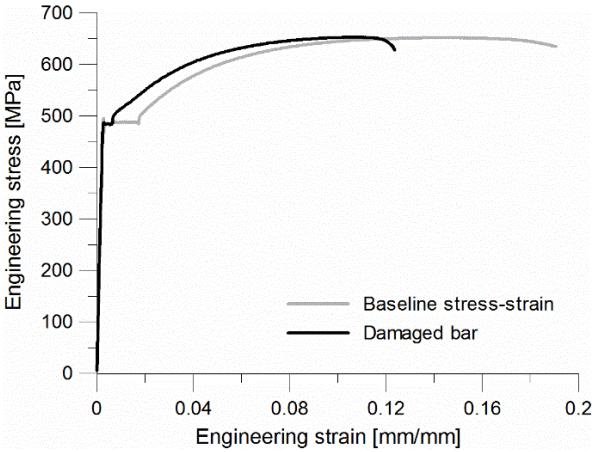

Fig. 5-24. Stress–strain curve of the D9 damaged bar and an undamaged sample of the same bar.

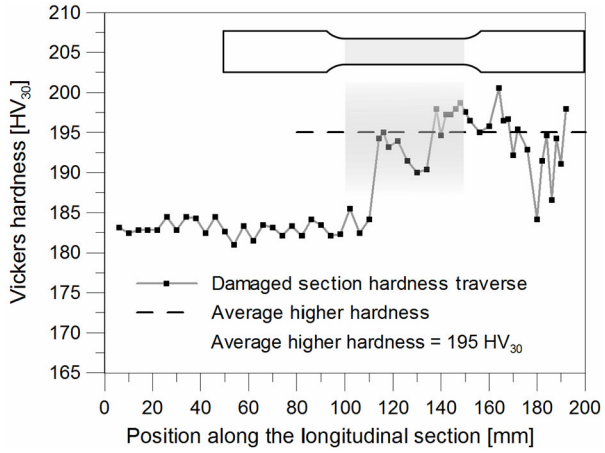

Fig. 5-25. Vickers hardness transverse profile of the D10 damaged bar.

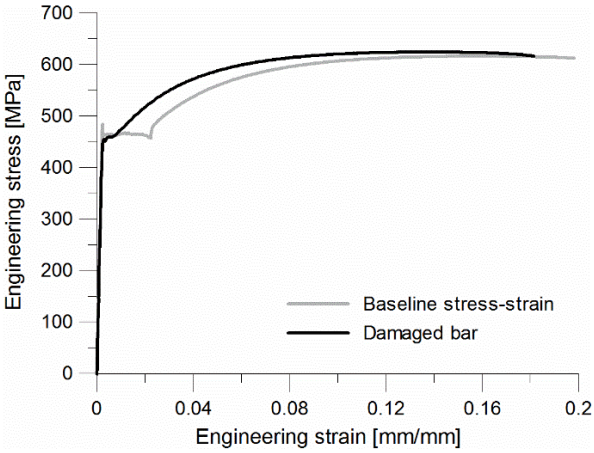

Fig. 5-26. Stress–strain curve of the D10 damaged bar and an undamaged sample of the same bar.

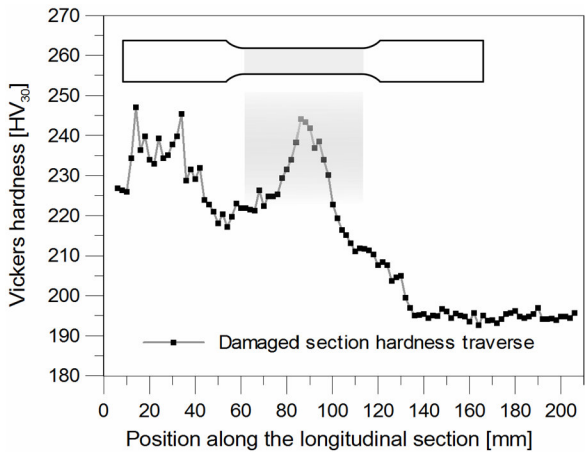

Fig. 5-27. Vickers hardness transverse profile of the D11 damaged bar.

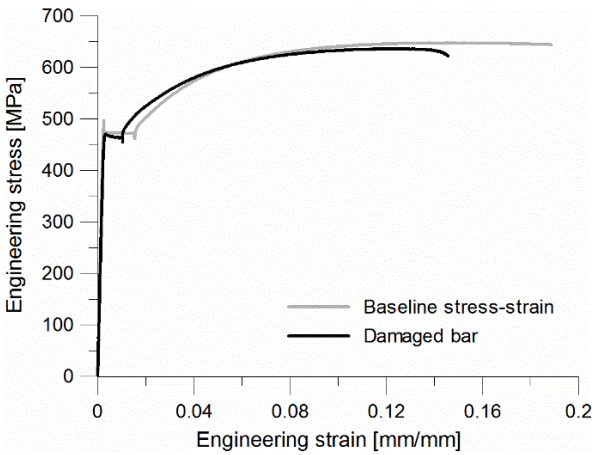

Fig. 5-28. Stress–strain curve of the D11 damaged bar and an undamaged sample of the same bar.

Table 5-8 Mechanical properties in the damaged region of Samples D5 to D11.

Bar name	**Average hardness in the damaged region [HV_{30}]**	**Increase in hardness from baseline [HV_{30}]**	**LYS in the damaged area [MPa]**	**Strain at UTS [mm/mm]**	**Residual strain capacity loss [%]**
D5	197	16	470	0.101	36
D6	245	21	515	0.046	59
D7	242	17	520	0.109	9
D8	202	12	465	0.073	52
D9	207**	4	488	0.106	27
D10	195	10	450	0.137	14
D11*	245**	51	473	0.122	16

* Sample was found cracked and buckled.

**Peak hardness.

The mechanical properties of the damaged samples are summarised in Table 5-8. The loss in residual strain capacity varied from a minimum of 9% to a maximum of almost 60%. The simplified Vickers hardness method identified as damaged 7 bars out of a total 59 tested. The increase in hardness above the baseline was always an indication of a change in mechanical properties from a virgin material. Rebars that did not show any increase in hardness were never found damaged. The simplified Vickers hardness has the advantage of reducing the time and costs of testing since the calibration curve development (Phase III) is bypassed.

5.4 FINAL DISCUSSION AND METHODOLOGY LIMITATIONS

5.4.1 Discussion

The Vickers hardness test results obtained in Section 5.2 were consistent with the tensile test results and enabled an accurate determination of the damage and residual strain capacity at each damaged location. The simplified method provided more practical, cost- and time-effective results.

Other evidence that could potentially provide insight to steel damage that can be quantified is the residual crack width. Static residual crack widths were provided as part of the data set. Fig. 5-29 plots the measured crack width versus the measured plastic strain capacity. The detailed data shows that only 11% of cracks with width below approximately 0.5 mm showed detectable damage. Only 17% of cracks below 1 mm width showed damage. However, 100% of cracks above 1 mm width showed damage that was detected via the hardness method. This suggests that larger crack widths tend to correlate with detectable damage to the underlying steel. However, the residual crack width does not reveal the maximum crack width because closure can, and probably does, occur.

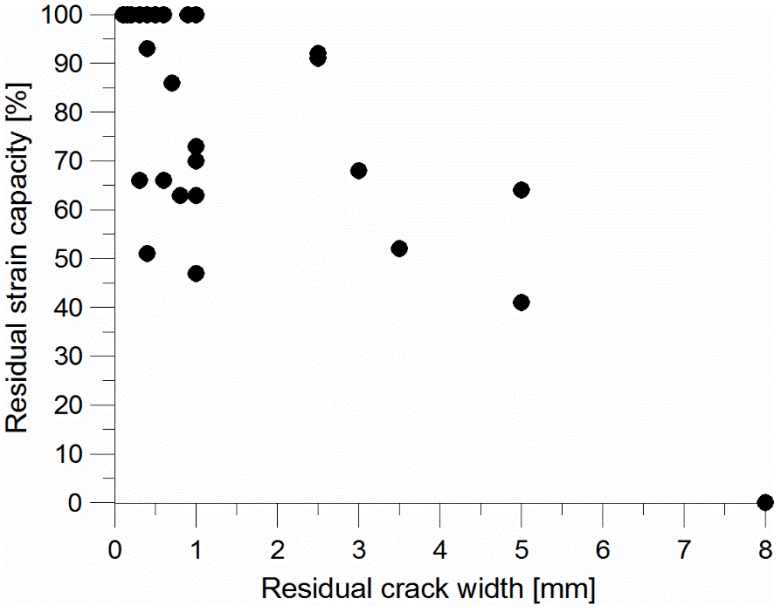

Fig. 5-29 Reinforcing bar residual strain capacity versus static residual crack width.

It is also important to note that, while the material has lost ductility only over the length containing the damage, if further plastic capacity is not made available by further de-bonding from the concrete, then further plastic elongation will be limited. On the other hand, if the material on either side of the damaged region is allowed to strain, then the damaged region will most likely remain elastic under future demand, and any plastic deformation will occur away from the damaged region. It is not yet clear which scenario would occur in service. In this regard, experiments conducted in the laboratory on reinforced concrete members repaired with epoxy resin, a relatively common repairing technique in Christchurch, could provide some insight. Tasai et al. (1988) showed that, after epoxy repairing, cracking first reoccurred at the same critical locations, but subsequent cracking occurred elsewhere and strain distribution concentrated near these new cracks. Strain hardening and strain ageing of the previously damaged reinforcing steel are likely responsible for the strain relocation. In addition, when the bond was recovered through the epoxy injection, strain hardening caused as much as 20% greater increase in flexural resistance

of the repaired members compared to the virgin material. However, an increase in flexural strength could potentially cause a change in the hierarchy of strength and encourage less desirable brittle failure mechanisms (Momtahan et al., 2009; Restrepo-Posada et al., 1994).

5.4.2 Limitations

It would be most desirable to develop a noninvasive method to detect and quantify damage to steel reinforcement bars. The Vickers hardness method described here is invasive, since damaged reinforcing bars need to be removed from the building and tested under laboratory conditions, and undamaged bar lengths need to be extracted from the building for calibration.

In addition, because of the variability of the chemical composition and thermomechanical history of the different steels, a "universal" calibration curve has not been determined yet. Therefore, calibration curves need to be developed for each specific steel of interest (e.g., grade, diameter and heat). Obtaining these calibration curves is time-consuming and expensive. Moreover, the method is based on the assumption that the hardness baseline of the as-received samples is constant throughout the bar cross-section, this might not be true in the case of quenched and tempered and thermo mechanical treatment (TMT) rebars (Surajit Kumar et al., 2014). Finally, the hardness method can provide no insight into the number of fatigue cycles experienced or remaining.

5.5 CONCLUSIONS

The Vickers method presented in this chapter was successfully applied on a real case study. Forty-nine "suspected" damaged rebar samples were removed from a Christchurch building damaged during the 2010/2011 events. A total of eleven samples were found damaged: the mechanical properties had been altered; in particular the ductility had decreased. The Vickers hardness test predictions were consistent with the tensile test results and enabled an accurate determination of the damage and residual strain capacity at each damaged location.

A simplified hardness method, which bypasses Phase III, was also proposed. This method provided information about the extent of the plastic deformation; however, the ductility prediction phase was not conducted. When the increase in hardness was detected in a steel rebar, a tensile testing sample was machined, ensuring that damaged material was contained in the reduced area of the sample. In all cases, the elevated hardness from the baseline was the indication of damage.

5.6 REFERENCES

Allington, C. (2011). *Materials testing in buildings of interest. Gallery Apartments, Westpac centre, IRD building*. (Report 107267-1 (v1.1) prepared for royal commission). Retrieved from HolmesSolution, Christchurch:

Matsumoto, Y. (2009). Study on the residual deformation capacity of plastically strained steel *Behaviour of Steel Structures in Seismic Areas*: CRC Press.

Momtahan, A., Dhakal, R., & Rieder, A. (2009). Effects of strain-ageing on New Zealand reinforcing steel bars. *Bulletin of the New Zealand Society for Earthquake Engineering, 42*(2).

Nakane, M., Kanno, S., Kurosake, Y., Takagi, Y., Komotori, J., & Ogawa, T. (2010). Accuracy of Plastic Strain Estimated by Hardness to Assess Remaining Fatigue Lives. *Material Properties Measurement*.

Nashid, H., Ferguson, W. G., Clifton, C., Hodgson, M., Battley, M., Seal, C., & Choi, J. H. (2014). Non-destructive method to investigate the hardness-plastic strain relationship in cyclically deformed steel structural steel elements. *Bulletin of the New Zealand Society for Earthquake Engineering, 47*(3), 181-189.

Restrepo-Posada, J., Dodd, L., Park, R., & Cooke, N. (1994). Variables Affecting Cyclic Behavior of Reinforcing Steel. *Journal of Structural Engineering, 120*(11), 3178-3196.

Standards, Australia and New Zealand (2001). AS/NZS 4671:2001 *4671:2001 Steel reinforcing materials*. Wellington, New Zealand.

Standards, New Zealand (1989). NZS 3402:1989 *Steel bars for the reinforcement of concrete*. Wellington New Zealand.

Tasai, A., Otani, S., & Aoyama, H. (1988). Resistance of reinforced concrete component repaired with epoxy resin. *Journal of the faculty of engineering, the University of Tokyo (B), XXXIX*(3), 345-359.

6 EFFECTS OF STRAIN AGEING ON NEW ZEALAND-MANUFACTURED STEEL REINFORCEMENT

Strain ageing is a time- and temperature-dependent phenomenon that affects low-carbon steels previously subjected to cold work (Baird, 1963, 1971; Cottrell & Bilby, 1949; Erasmus & Pussegoda, 1977). Previous studies on this topic were discussed in Section 2.4. The major effect of this phenomenon is a change in mechanical properties such as an increase in yield strength and reduction in ductility.

Strain ageing is caused by a locking effect of the mobile dislocations caused by interstitial solute atoms of nitrogen and carbon. However, at temperatures below 100°C to 150°C, nitrogen is the more significant cause of strain ageing. Carbon plays an important role when steel is aged at temperatures above 150°C (Leslie, 1981). At "ambient" temperatures (around 15°C to 25°C), strain ageing is slow. Its effects, such as an increase in yield and ultimate strength, and a decrease in ductility, take place over a number of days, or even weeks. However, this phenomenon is accelerated when ageing occurs at higher temperatures. Hundy (1954) found a correlation between strain-ageing effects at different temperatures, Table 6-1 summarises his results. The relationship found by Hundy shows that the strain-ageing effects that take place during a year at 15°C can be accelerated by ageing in boiling water (100°C) for four hours.

Table 6-1 Equivalent ageing times at room temperature and at elevated temperatures (Hundy, 1954)

Temperature	**15°C**	**21°C**	**100°C**	**120°C**	**150°C**
Ageing time	1 year	6 months	4 hours	1 hour	10 min.
	6 months	3 months	2 hours	30 min.	5 min.
	3 months	6 weeks	1 hour	15 min.	2.5 min.
	1 month	2 weeks	20 min.	5 min.	
	1 week	4 days	5 min.		
	3 days	36 hours	2 min.		

Strain ageing might impact the seismic performance of buildings that are severely damaged during a significant earthquake. Extensive cracking is expected to form at the plastic hinges' location, and the steel reinforcing bars might plastically deform. If the steel is prone to this phenomenon, the rebars will strain age over the following months, and their mechanical properties could be altered. These changes could potentially compromise the ductility of plastic hinges and their capacity to dissipate energy in subsequent earthquakes. In addition, the flexural strength of the plastic hinges could increase and modify the hierarchy of strength, if low overstrength factors are used (Momtahan et al., 2009).

Although numerous studies exist in the literature, more investigation is required. The majority of the studies conducted on NZ-manufactured steel rebars is dated before the introduction of the current steel reinforcement standard AS/NZS 4671:2001 (Standards, Australia and New Zealand, 2001). Existing literature refers to superseded steel grades such as Grades 275, 380 and 430 or custom-made steel grade manufactured with the addition of vanadium or titanium (Erasmus & Pussegoda, 1980; 1978; Lim, 1991; Pussegoda & Erasmus, 1977; Restrepo-Posada et al., 1994). More recent works on the strain-ageing effects on Grade 300 steel were conducted on the NZS 3402:1989 version of the current Grade 300E (Earthquake ductility) steel reinforcement (Standards, New Zealand, 1989; Allington, 2012). Momtahan et al. (2009) quantified the increase in yield strength due to natural ageing on the current Grade 300E steel with up to 50 days of ageing time. However, since the strain-ageing phenomenon takes place over several months (if not years), long-term experiments are recommended. In this chapter, long-term ageing effects on Grade 300E, aged up to one year, are presented and discussed.

The hardness method assumes that Grade 300E is prone to strain ageing at any temperature, while Grade 500E only above 150°C. This implies that steel rebars suspected to have been

damaged during an earthquake might have hardness and ductility altered over the months after the seismic event, due to this phenomenon. Hardness measurements obtained from "suspected" earthquake-damaged steel samples are generally compared against "aged" calibration curves in order to take into account the ageing effects developed in the period between the seismic event and the assessment tests. Experiments were conducted and results are presented here to demonstrate the detrimental effects of long-term strain ageing on the material ductility, and to evaluate the increase in the other mechanical properties for Grade 300E and Grade 500E at 15°C, 100°C and 200°C. Furthermore, it is expected that strain-ageing effects increase with ageing time (Hundy, 1954); experiments were designed to verify whether or not an accelerated strain-ageing method (at 100°C) can reliably simulate the effects of long-term natural strain ageing (at 15°C).

6.1 ACCELERATED STRAIN-AGEING EFFECTS ON GRADE 300E AND GRADE 500E STEEL REINFORCEMENT

Experimental tests conducted on accelerated strain-aged steel samples of certified seismic Grade 300E and seismic Grade 500E MA are described in this section. Rebars 25 mm in diameter were obtained from Pacific Steel Ltd and machined into 16 cylindrical "dog-bone" tensile coupons (eight of Grade 300E and eight of Grade 500E), of diameter 13 mm (see Fig. 6-1). Steel chemical composition is listed in Table 6-2. It must be noted that the amount of vanadium in Grade 500E is approximately 30 times larger than in Grade 300E. For each steel grade, three samples were used to obtain the basic mechanical properties: lower yield strength, ultimate tensile strength (UTS) and uniform elongation (the strain at UTS) (see Table 6-3). Tests were conducted using a SATEC system tensile machine with an MTS 25-mm gauge length extensometer, capable of 50% travel in tension; data points were recorded every 0.25 s.

Table 6-2 Chemical composition data (wt %) from Mill Certification Sheet

Material	C	Mn	Si	S	P	Ni	Cr	Mo	Cu	Sn	V	C_{eq}
300E	0.18	0.78	0.22	0.024	0.013	0.09	0.09	0.017	0.28	0.018	0.003	0.36
500E	0.18	1.27	0.35	0.032	0.017	0.07	0.11	0.013	0.26	0.017	0.085	0.46

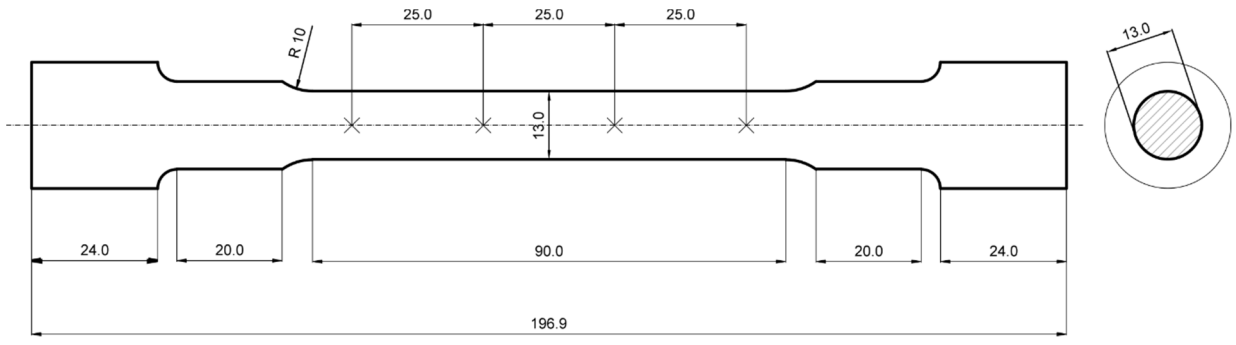

Fig. 6-1 Cylindrical "dog-bone" steel specimen samples, dimensions in mm.

Table 6-3 Average Tensile properties of reinforcing steel

Material	Lower yield strength (MPa)	Ultimate tensile strength (MPa)	Uniform elongation (%)
300E	323	503	19.3
500E	524	671	14.4

6.1.1 Experimental testing on Grade 300E

Procedure

The remaining five Grade 300E specimens were pre-strained up to five pre-strain values: 0.015, 0.03, 0.06, 0.12 and 0.18 mm/mm. The amounts were selected in order to cover a homogenous range of the stress–strain curve before necking. The samples were (if required) stored below 0°C, then aged in boiling water for four hours in order to simulate the effects of natural ageing at 15°C for a year. Finally, the samples were tensile-tested until failure.

Results and discussion

Stress–strain curves of the aged samples are superimposed on the baseline stress–strain curve in Fig. 6-2 to Fig. 6-6. From these curves, some qualitative observations can be made:

- the yield strength increased (Δy) in all specimens
- when observed, the ultimate tensile strength increased (Δu) in three out of four specimens
- the ductility (or strain at ultimate tensile strength) reduced in all specimens ($\Delta \varepsilon$)
- the sample pre-strained up to 0.18 mm/mm, showed only an elastic behaviour after ageing. Once the material reached the elastic limit it started to neck. Note that in Fig. 6-6, only the elastic branch of the stress–strain curve is shown because the sample necked outside the extensometer gauge length, and no strain measurements could be monitored.

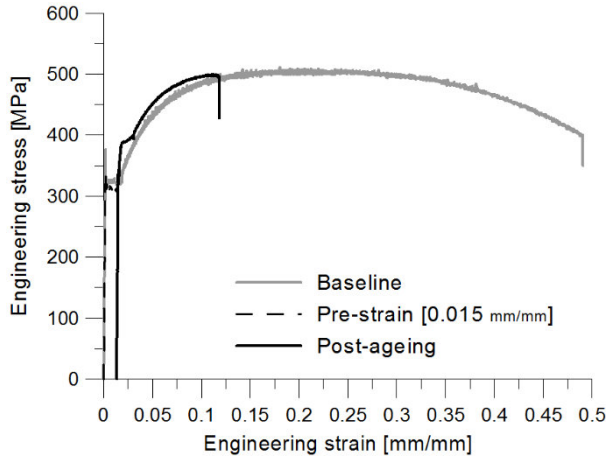

Fig. 6-2 Stress–strain curve of a Grade 300E sample pre-strained to 0.015 mm/mm and aged for 4 hours at 100°C.

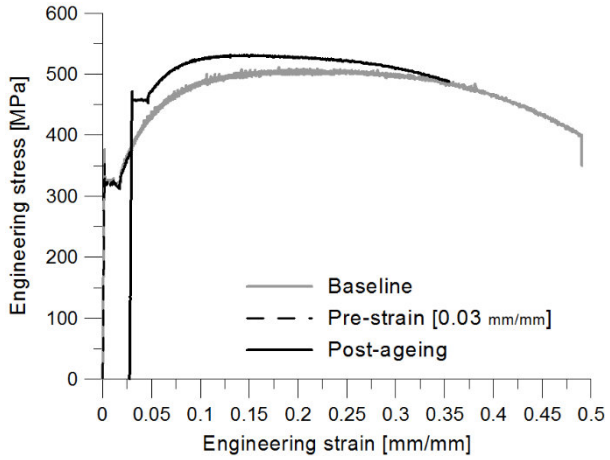

Fig. 6-3 Stress–strain curve of a Grade 300E sample pre-strained to 0.03 mm/mm and aged for 4 hours at 100°C.

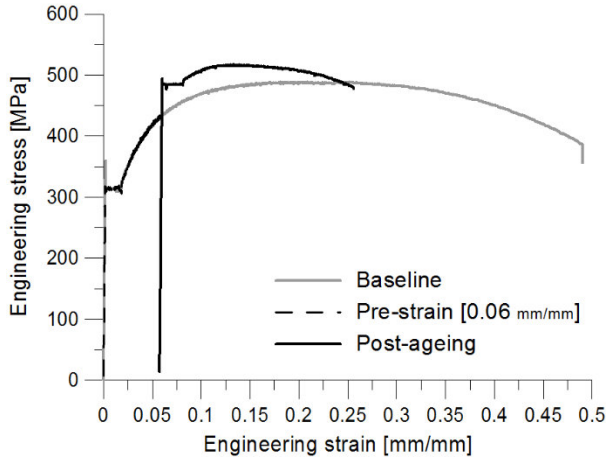

Fig. 6-4 Stress–strain curve of a Grade 300E sample pre-strained to 0.06 mm/mm and aged for 4 hours at 100°C.

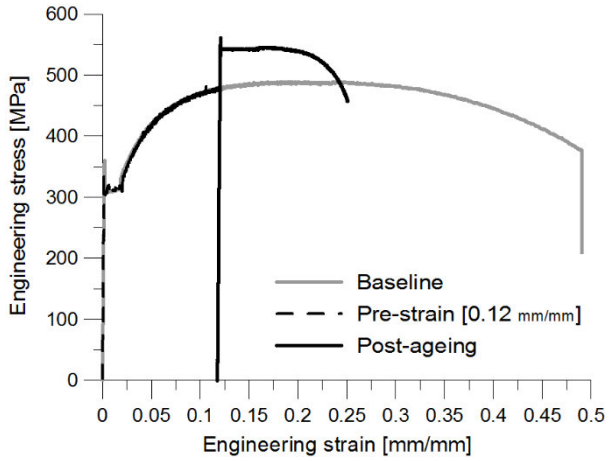

Fig. 6-5 Stress–strain curve of a Grade 300E sample pre-strained to 0.12 mm/mm and aged for 4 hours at 100°C.

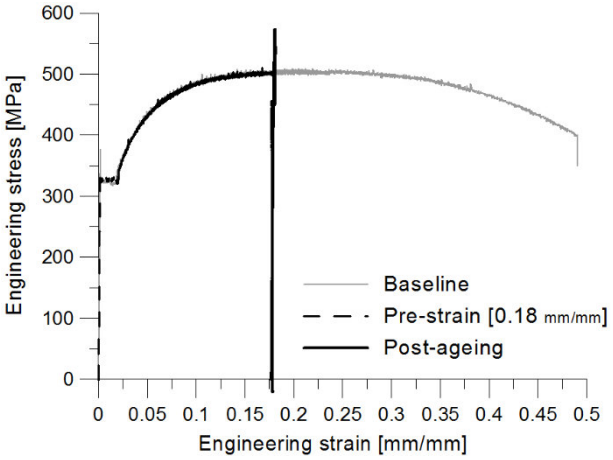

Fig. 6-6 Stress–strain curve of a Grade 300E sample pre-strained to 0.18 mm/mm and aged for 4 hours at 100°C.

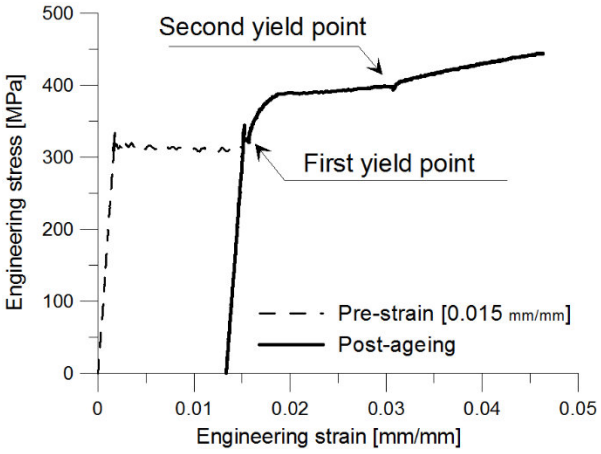

Fig. 6-7 Double yield point observed on the 0.015 mm/mm pre-strained and aged sample.

The changes in mechanical properties are summarised in Table 6-4. In the case of the specimen pre-strained to 0.01 mm/mm, two yield points can be observed in Fig. 6-7: a first discontinuous point at a stress just above 300MPa, and a second one at a stress of approximately 400 MPa. This double yielding point can be explained because during the pre-straining phase the sample was not uniformly plastically deformed over its entire gauge length. Lüders bands, which correspond to the regions of plastic deformation in steel (or where dislocation motion occurred), did not form everywhere in the sample. As a consequence, some regions of the sample were strained only elastically. During the subsequent tensile loading, the regions of the samples that were only elastically deformed yielded first, since they had a lower elastic limit; this explains the appearance of the first discontinuous point at a stress of approximately 320 MPa. The regions of the sample where the Lüders bands formed originally yielded at a higher stress, due to hardening and ageing, explaining the second discontinuous yielding point.

Table 6-4 Change in lower yield strength (LYS) due to strain ageing for certified Grade 300E.

	Lower yield strength		
Sample	**Unaged [MPa]**	**Aged [MPa]**	**Difference (Δy) [MPa]**
Pre-strained to 0.015 mm/mm	307	388[1]	81
Pre-strained to 0.03 mm/mm	379	453	74
Pre-strained to 0.06 mm/mm	432	476	44
Pre-strained to 0.12 mm/mm	475	527	52
Pre-strained to 0.18 mm/mm	500	574	74

[1]Stress at the second yield point

Table 6-5 Change in ultimate tensile strength due to strain ageing for certified Grade 300E.

	Ultimate tensile strength (UTS)		
Sample	**Unaged [MPa]**	**Aged [MPa]**	**Difference (Δu) [MPa]**
Pre-strained to 0.015 mm/mm	492[1]	499	7
Pre-strained to 0.03 mm/mm	497[1]	531	34
Pre-strained to 0.06 mm/mm	489[1]	518	29
Pre-strained to 0.12 mm/mm	489[1]	546	57
Pre-strained to 0.18 mm/mm	503[1]	574	71

[1] This value is obtained by calibrating the stress–strain curve of the benchmark specimens with respect to the lower yield strength of the pre-strained sample.

Table 6-6 Change in the expected ultimate strain due to strain ageing for certified Grade 300E.

	Uniform elongation		
Sample	**Expected unaged [mm/mm]**	**Actual aged [mm/mm]**	**Difference (Δε) [%]**
Pre-strained to 0.015 mm/mm	0.200 – 0.015 = 0.180	0.098	-45.6
Pre-strained to 0.03 mm/mm	0.170	0.103	-39.4
Pre-strained to 0.06 mm/mm	0.140	0.075	-46.4
Pre-strained to 0.12 mm/mm	0.080	0.051	-36.3
Pre-strained to 0.18 mm/mm	0.020	0.001	-95.0

The change in lower yield strength (Δy), as defined in Fig. 2-34, is plotted against the amount of pre-strain for the certified Grade 300E steel in Fig. 6-8. The data point relative to the sample pre-strained to 0.015 mm/mm corresponds to the stress at the second yield point. However, if the first yield point were plotted, no increase in yield strength would have been observed. The experimental data demonstrated that the increase in yield strength is independent of the amount of pre-strain; this is agreement with a study by Pussegoda and Erasmus (1977) on Grade 275 and an earlier study by Wilson and Russell (1960). This confirms that the increase in yield strength is insensitive to the dislocation density but depends on the number of solute atoms per dislocation, known as atmosphere density (Wilson & Russell, 1960). A similar trend was also observed on Grade 300E samples extracted after the 2011 earthquake from a Christchurch building constructed from 2008–2010, the results of which are plotted in Fig. 6-9.

On average, the increase in yield strength was approximately 60 MPa for the Certified Grade 300E and 41 MPa for the Grade 300E steel recovered from the Christchurch building. These average values do not include the data points relative to pre-strain values below 2%. This is because specimens pre-strained within the range of the discontinuous point will have two yield points, but in a subsequent tensile test/axial load, they will perform elastically only up to the first yield point. The increase in yield strength observed by Restrepo-Posada et al. (1994) for Grade 300 was approximately 45 MPa for samples pre-strained to 0.02 mm/mm and aged for 37 and 147 days. An increase of approximately 60–70 MPa was observed by Momtahan et al. (2009) for Grade 300E samples pre-strained to $15\varepsilon_y$ (this is equal to 0.025 mm/mm, assuming σ_y = 300 MPa and E = 200 GPa) and aged naturally for 30 and 50 days. The results obtained, compared with those obtained from previous works, suggest that an increase in yield strength (due only to strain ageing)

in the range of 40–70 MPa must be expected for plastic strained and aged Grade 300(E) reinforcing bars.

Ultimate tensile strength (UTS) increased proportionally to the amount of pre-straining, as shown in Table 6-5, Fig. 6-10 and Fig. 6-11. The UTS values of the pre-strained and aged samples were compared with the average UTS obtained from the benchmark tensile tests normalised with respect to the lower yield strength of the pre-strained specimen. The trends observed for both certified and "recovered" Grade 300E were similar; the increase in UTS was approximated with a linear regression line, and the coefficients of determination obtained were 0.86 and 0.78. Again, the trend observed is in accordance with the work conducted by Pussegoda and Erasmus (1977) and Wilson and Russell (1960). It must be noted that the upper yield strength of the sample pre-strained to 0.12 mm/mm was higher that the UTS (Fig. 6-5); in fact, after yielding, it was subjected only to a very small amount of strain hardening before necking started (see Fig. 6-5). The sample pre-strained to 0.18 mm/mm showed only elastic behaviour; therefore the UTS was assumed to correspond to the upper yield strength (Fig. 6-6).

The last property compared was the uniform elongation (or strain at UTS or ultimate strain) which represents a measure of the ductility of the material (Table 6-6). In this case, the actual strain at UTS measured from the aged samples was compared with the expected strain at UTS if the specimens were not prone to strain-ageing effects. For example, in the case of the specimen pre-strained to 0.015 mm/mm, the expected unaged uniform elongation is equal to the uniform elongation of the benchmark sample (0.20 mm/mm) minus the amount of pre-strain (0.015 mm/mm). A linear correlation is proposed for both certified and noncertified Grade 300E (see Fig. 6-12 and Fig. 6-13). The results obtained proved the hypothesis of the detrimental effects on the residual strain capacity of strain ageing. Supposing the case of a suspected damaged Grade 300E

rebar that is estimated to be plastically deformed to 0.03 mm/mm, the actual residual strain capacity is approximately 60% (0.10 mm/mm) of that expected (0.17 mm/mm). Therefore, the experimental results recommend incorporating a strain-ageing phase in the hardness method to predict the residual ductility of damaged steel rebars.

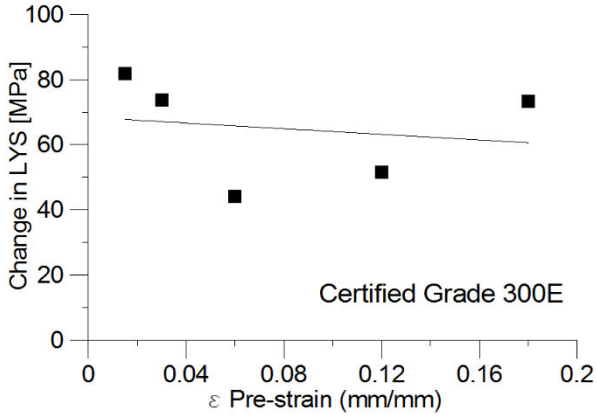

Fig. 6-8 Change in LYS versus the amount of pre-strain for certified Grade 300E.

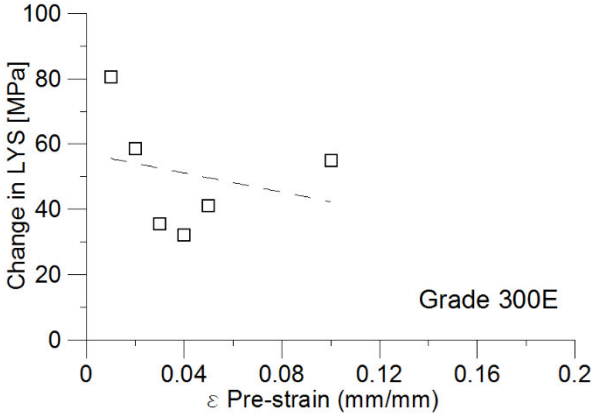

Fig. 6-9 Change in LYS versus the amount of pre-strain for Grade 300E.

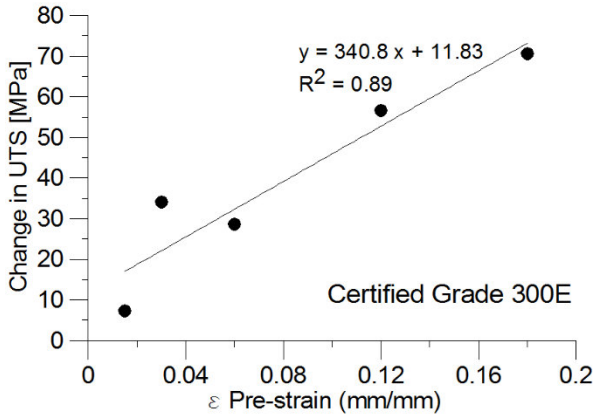

Fig. 6-10 Change in UTS versus the amount of pre-strain for certified Grade 300E.

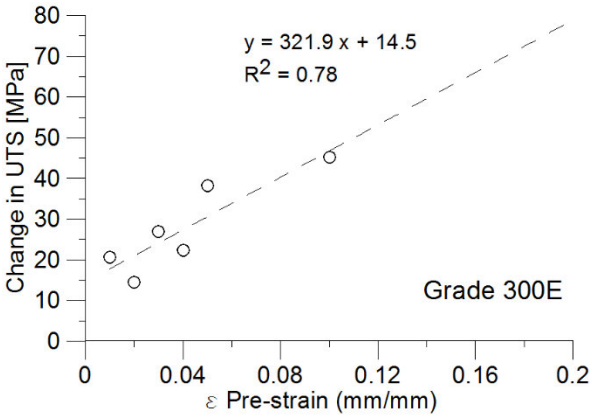

Fig. 6-11 Change in UTS versus the amount of pre-strain for Grade 300E.

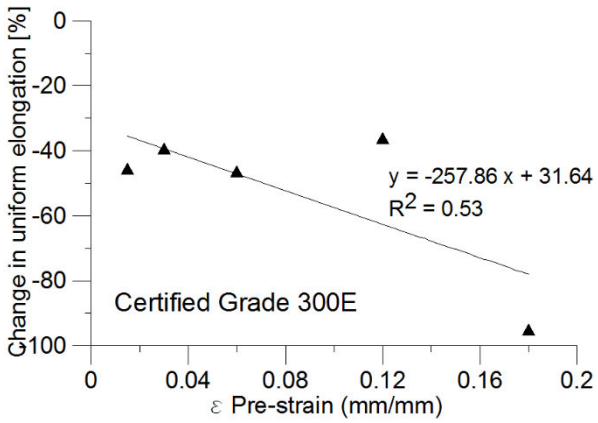

Fig. 6-12 Change in uniform elongation versus the amount of pre-strain for certified Grade 300E.

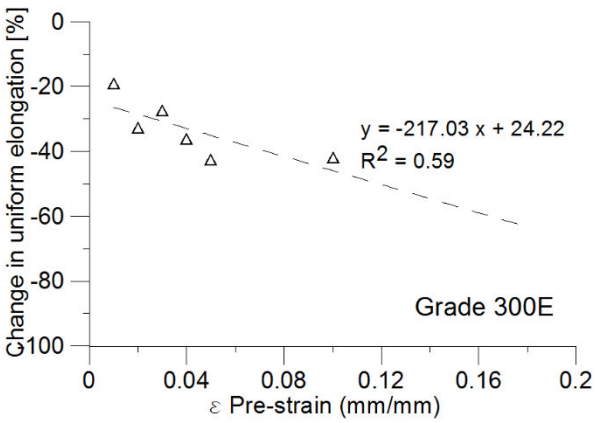

Fig. 6-13 Change in uniform elongation versus the amount of pre-strain for Grade 300E.

6.1.2 Experimental testing on Grade 500E micro alloy (MA)

While Erasmus and Pussegoda (1978) and Restrepo-Posada et al. (1994) conducted experimental testing on strain-aged high-steel Grades 380 and 430, no studies have been published on the effects of strain ageing on the tensile properties of current Grade 500E. New Zealand Grade 500E MA is manufactured with the addition of 0.08% to 0.10% by mass of vanadium. This element has two major functions: first, it enhances the tensile strength of the steel; and second, it forms an insoluble nitride that eliminates the effects of strain ageing at temperatures below 150°C. Erasmus and Pussegoda (1980) demonstrated that 0.06% vanadium completely removes the effects of strain ageing, and any other increase in vanadium content produces only insignificant effects on the strain-ageing trend. The experiment presented in this section aims to prove that Grade 500E is not prone to strain-ageing effects at temperatures up to 100°C.

Procedure

Following the same protocol used for Grade 300E, three steel specimens out of eight were tensile-tested to obtain the benchmark mechanical properties (see Table 6-3), the remaining five specimens were pre-strained up to the following five strain limits: 0.015, 0.03, 0.06, 0.10 and

0.14 mm/mm. Subsequently the specimens were aged in boiling water (at 100°C) for four hours and then tensile-tested until failure.

Results and discussion

The stress–strain curves of all the samples, superimposed on the benchmark stress–strain curve, are presented in Fig. 6-14 to Fig. 6-18, while a summary of the mechanical properties is shown in Table 6-7, Table 6-8, and Table 6-9. In this case, no reappearance of the discontinuous yield point was observed. During the reloading phase, the stress–strain curve followed the same unloading linear-elastic line up to the stress at interruption and then the material flowed plastically as the test was not previously interrupted.

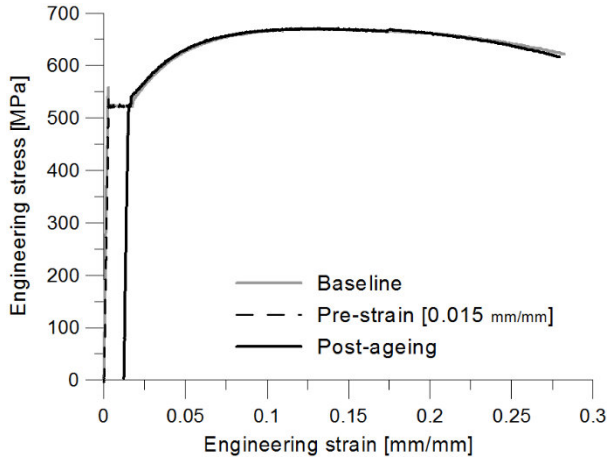

Fig. 6-14 Stress–strain curve of a Grade 500E sample pre-strained to 0.015 mm/mm and aged for 4 hours at 100°C.

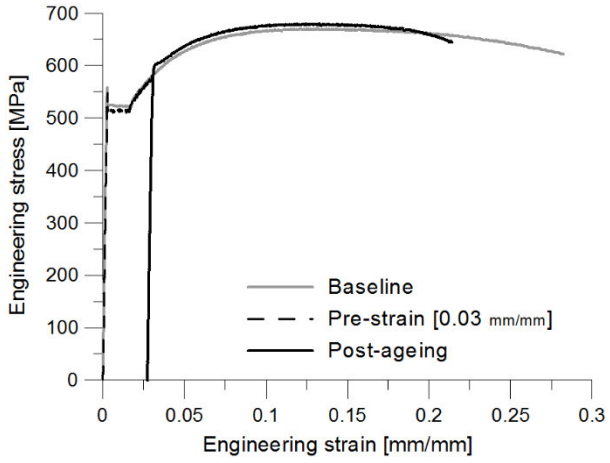

Fig. 6-15 Stress–strain curve of a Grade 500E sample pre-strained to 0.03 mm/mm and aged for 4 hours at 100°C.

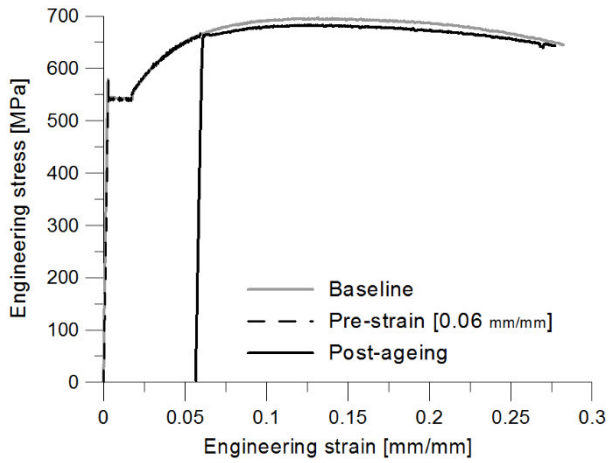

Fig. 6-16 Stress–strain curve of a Grade 500E sample pre-strained to 0.06 mm/mm and aged for 4 hours at 100°C.

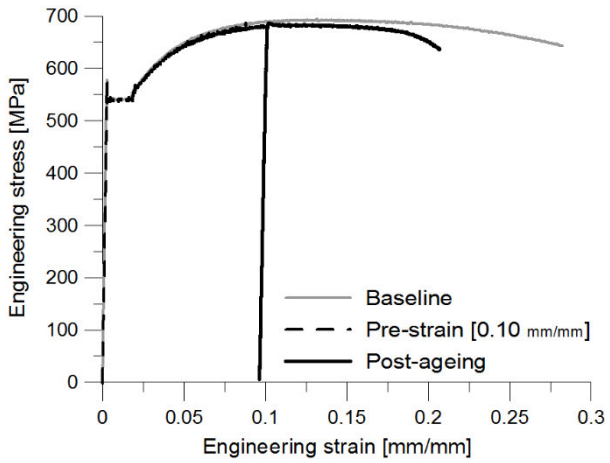

Fig. 6-17 Stress–strain curve of a Grade 500E sample pre-strained to 0.10 mm/mm and aged for 4 hours at 100°C.

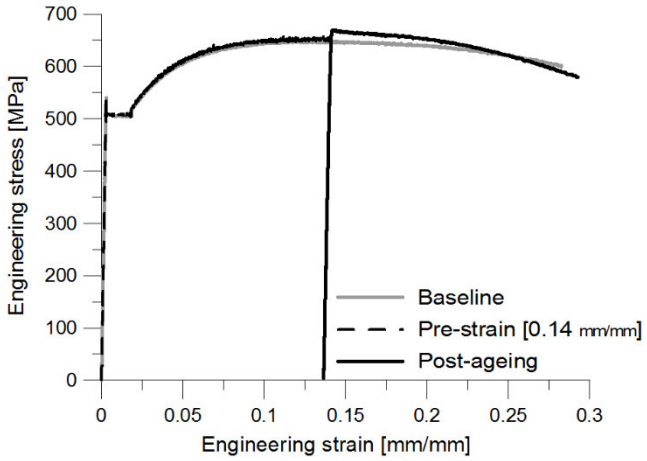

Fig. 6-18 Stress–strain curve of a Grade 500E sample pre-strained to 0.14 mm/mm and aged for 4 hours at 100°C.

Table 6-7 Change in lower yield strength (LYS) due to strain ageing for certified Grade 500E.

	Lower yield strength		
Sample	**Unaged [MPa]**	**Aged [MPa]**	**Difference (Δy) [MPa]**
Pre-strained to 0.015 mm/mm	523	523	0
Pre-strained to 0.03 mm/mm	579	600	21
Pre-strained to 0.06 mm/mm	662	662	0
Pre-strained to 0.10 mm/mm	679	687	8
Pre-strained to 0.14 mm/mm	651	669	18

Table 6-8 Change in ultimate tensile strength due to strain ageing for certified Grade 500E.

	Ultimate tensile strength (UTS)		
Sample	**Unaged [MPa]**	**Aged [MPa]**	**Difference (Δu) [MPa]**
Pre-strained to 0.015 mm/mm	671[1]	671	0
Pre-strained to 0.03 mm/mm	671[1]	679	8
Pre-strained to 0.06 mm/mm	696[1]	683	–13
Pre-strained to 0.10 mm/mm	694[1]	687	–7
Pre-strained to 0.14 mm/mm	649[1]	669	20

[1] This value is obtained by calibrating the stress–strain curve of the benchmark specimens with respect to the lower yield strength of the aged sample.

Table 6-9 Change in the expected ultimate strain due to strain ageing for certified Grade 500E.

	Uniform elongation		
Sample	**Expected unaged [mm/mm]**	**Actual aged [mm/mm]**	**Difference (Δε) [%]**
Pre-strained to 0.015 mm/mm	0.131 – 0.015 = 0.116	0.132	13.8
Pre-strained to 0.03 mm/mm	0.101	0.098	–3.0
Pre-strained to 0.06 mm/mm	0.071	0.078	9.9
Pre-strained to 0.10 mm/mm	0.031	0.005	–83.9
Pre-strained to 0.14 mm/mm	0.000	0.000	0

The experiment confirmed that no significant increase in yield strength occurred: the average increase measured was approximately 8 MPa, less than 2% of the steel's yield strength (Fig. 6-19). Similarly, the increase in ultimate tensile strength was near to 0 MPa (Fig. 6-20). Finally, also the decrease in the expected uniform elongation was not affected. The outlier in Fig. 6-21 was produced because the uniform elongation was measured at the maximum stress observed in the stress–strain curve of the aged material (Fig. 6-17). In this case, the small increase in yield strength due to strain ageing (7.8 MPa) was such that the yield strength was also the maximum stress; therefore the uniform elongation considered was only elastic. In conclusion, the effect of strain ageing did not provide a significant change in the steel's mechanical properties. The strain-ageing effects might be ignored when the hardness method is employed, in order to reduce the experimental time. The residual strain capacity can be calculated as the difference between the ultimate strain obtained from the benchmark tests and the strain loss due to the pre-strain.

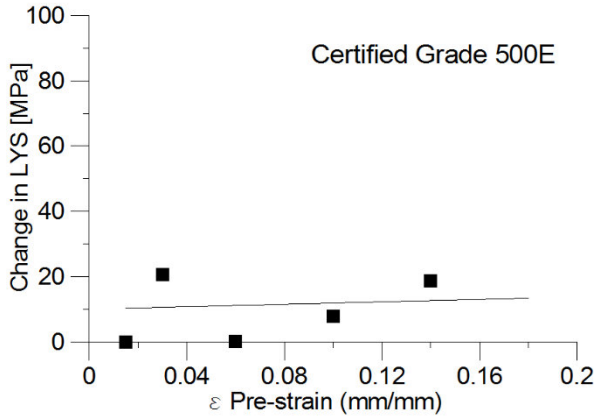

Fig. 6-19 Change in LYS versus the amount of pre-strain for certified Grade 500E.

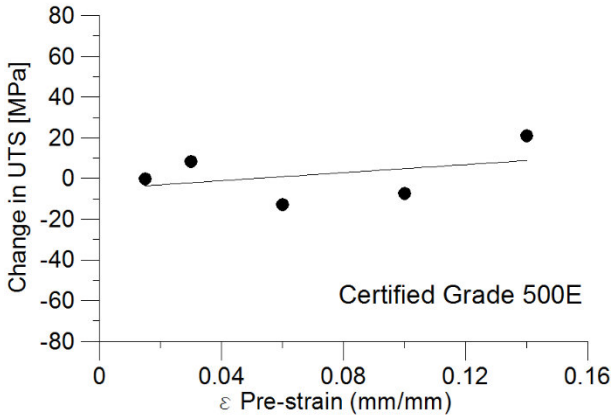

Fig. 6-20 Change in UTS versus the amount of pre-strain for certified Grade 500E.

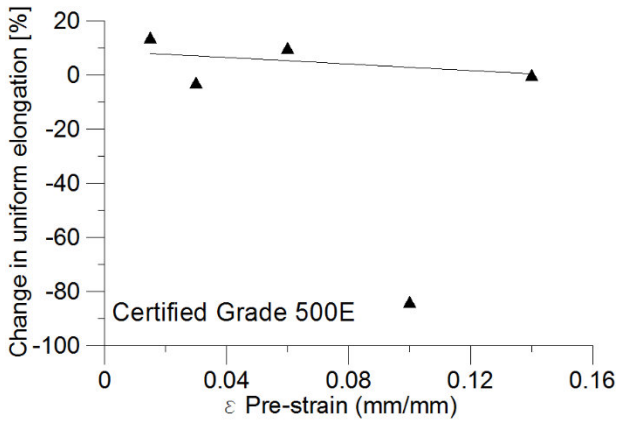

Fig. 6-21 Change in uniform elongation versus the amount of pre-strain for Grade 300E.

6.2 NATURAL AND ACCELERATED STRAIN AGEING COMPARISON

Strain-ageing effects are enhanced when ageing occurs at high temperature, as observed by Hundy (1954). The scope of the experimental test described in this section is to determine if, using an "accelerated method" based on Hundy's relationship, it is possible to accurately simulate "ambient" temperature strain-ageing effects on steel rebars. In long-term ageing, 365 days at 15°C and 4 hours at 100°C, the changes in mechanical properties of Grade 300E steel specimens pre-strained by the same amount are expected to be similar. As seen in Chapters 5, the accelerated method consists of ageing the steel samples in boiling water. Using boiling water to enhance strain-ageing effects was also suggested by the superseded steel reinforcing material standard (New Zealand Standards, 1989) for the reverse bend test on deformed bar. In fact, the immersion of the steel samples for at least 30 minutes in boiling water before re-straightening the bar was prescribed. This test was introduced after a series of brittle fractures, attributed to strain-ageing embrittlement, were observed on-site due to re-straightening of previously bent reinforcing bars (L. A. Erasmus, 1981).

6.2.1 Procedure

Eighteen metres of rebar of 25 mm diameter were received from Pacific Steel and machined for tensile testing according to the ASTM E8/E8M (ASTM, 2011a) (see Fig. 6-22). The chemical composition of the steel is provided in Table 6-2. A total of 33 samples were machined for this test: three for the benchmark test, 15 for the accelerated strain-ageing test and 15 for the natural strain ageing. The pre-strain amounts selected were 0.01 (1%), 0.03 (3%) and 0.05 (5%) mm/mm. After the pre-straining phase, the samples allocated for the natural ageing test were left to age at a constant temperature of 15ºC for 7, 30, 90, 183 and 365 days. According to Hundy's relationship,

steel samples had to be aged at 100 ºC for 5 minutes, 20 minutes, and 1, 2 and 4 hours to obtain the same strain-ageing effects. These time values were used.

The mechanical properties under investigation were: lower yield strength (LYS), ultimate tensile strength (UTS), uniform strain (ε_U) (or strain at UTS) and Vickers hardness (HV_{30}). The results obtained were expressed in terms of changes in mechanical properties (Δy, Δu, $\Delta \varepsilon$ and ΔHV_{30}, see Fig. 2-34). The benchmark mechanical properties of the steel tested are provided in Table 6-10.

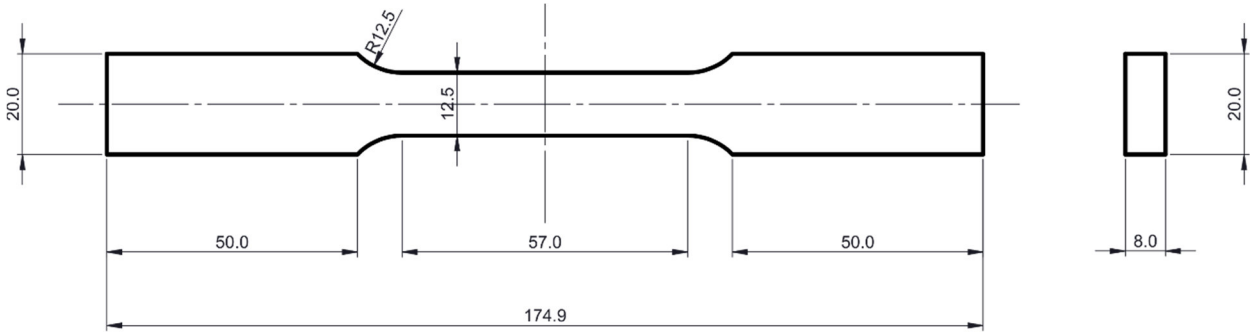

Fig. 6-22 Flat "dog-bone" steel specimen samples, dimensions in mm.

Table 6-10 Benchmark mechanical properties of the steel reinforcing bars.

Sample	Lower Yield strength [MPa]	Ultimate tensile strength [MPa]	Uniform strain [mm/mm]	Vickers hardness [HV_{30}]
1	321	498	0.205	149
2	321	505	0.202	150
3	336	519	0.203	150

Natural strain-ageing experiments

The natural strain-ageing tests were conducted from June 2014 to June 2015. The 15 samples were divided into five ageing groups (see Table 6-11) made of three samples. The groups were pre-strained to 0.01, 0.03 and 0.05 mm/mm. All the samples were pre-strained on the same day.

On the testing days (after 7, 30, 90, 183 and 365 days), 10 hardness measurements were first carried out along the longitudinal section before the samples were tensile-tested to failure.

Table 6-11 Sample groups for natural ageing experiment

Group	Ageing time	Pre-strain limits		
		0.01 mm/mm	0.03 mm/mm	0.05 mm/mm
Group 1	7 days	P01NA007	P03NA007	P05NA007
Group 2	30 days	P01NA030	P03NA030	P05NA030
Group 3	90 days	P01NA090	P03NA090	P05NA090
Group 4	183 days	P01NA183	P03NA183	P05NA183
Group 5	365 days	P01NA365	P03NA365	P05NA365

Accelerated strain-ageing experiment

For the accelerated ageing experiments, the 15 samples used for the accelerated strain-ageing test were divided into the same five ageing groups (see Table 6-12) made of three samples and pre-strained to 0.01, 0.03 and 0.05 mm/mm. After pre-straining, the steel samples were aged in boiling water for different periods of time (see Table 6-12). After ageing, ten hardness indentations were performed on each sample and then the tensile tests to failure were performed.

Table 6-12 Sample groups and data for accelerated ageing experiment

Group	Ageing time	Pre-strain amount		
		0.01 mm/mm	0.03 mm/mm	0.05 mm/mm
Group 1	5 minutes (7 e.d.*)	P01AA007	P03AA007	P05AA007
Group 2	20 minutes (30 e.d*)	P01AA030	P03AA030	P05AA030
Group 3	1 hour (90 e.d.*)	P01AA090	P03AA090	P05AA090
Group 4	2 hours (183 e.d*)	P01AA183	P03AA183	P05AA183
Group 5	4 hours (365 e.d*)	P01AA365	P03AA365	P05AA365

e.d.* = equivalent days at 15°C

6.2.2 Results

Stress–strain curves for the natural and accelerated experiments are plotted in Fig. 6-24 and Fig. 6-25, respectively. Samples pre-strained to 0.01 mm/mm did not show any apparent increase in yield strength. However, similarly to the strain-ageing experiment presented in Section 6.1.1, a second discontinuous point at about 0.03 mm/mm strain was observed (Fig. 6-23). For pre-strain amounts of 0.03 and 0.05 mm/mm, the reappearance of the upper yielding point at higher stress is already appreciable after 7 days at 15°C or 5 minutes in boiling water, and is accompanied by a noticeable Lüders strain (discontinuous yielding point) that increases with ageing time. A major difference that is apparent when comparing Fig. 6-24 and Fig. 6-25 is the reappearance of the upper yield strength point in the samples pre-strained to 0.01 and aged for 5, 20 and 60 minutes. A new upper yield point does not exist for the samples aged to the equivalent ageing times (7, 30 and 90 days) at 15°C. The reappearance of the upper yield point, in the natural ageing experiment, only occurred after 183 days.

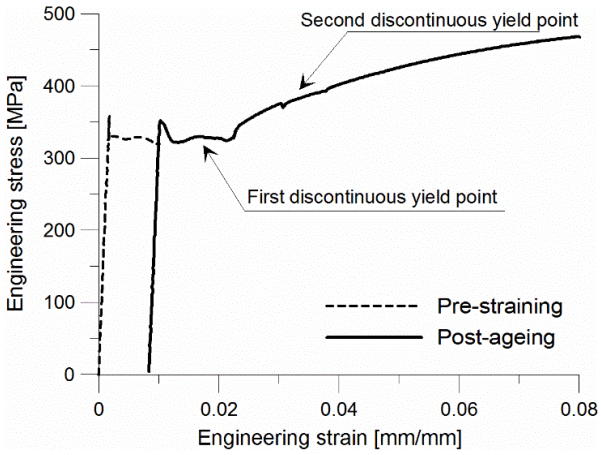

Fig. 6-23 Stress–strain curve of the 1% pre-strain sample naturally aged for 365 days.

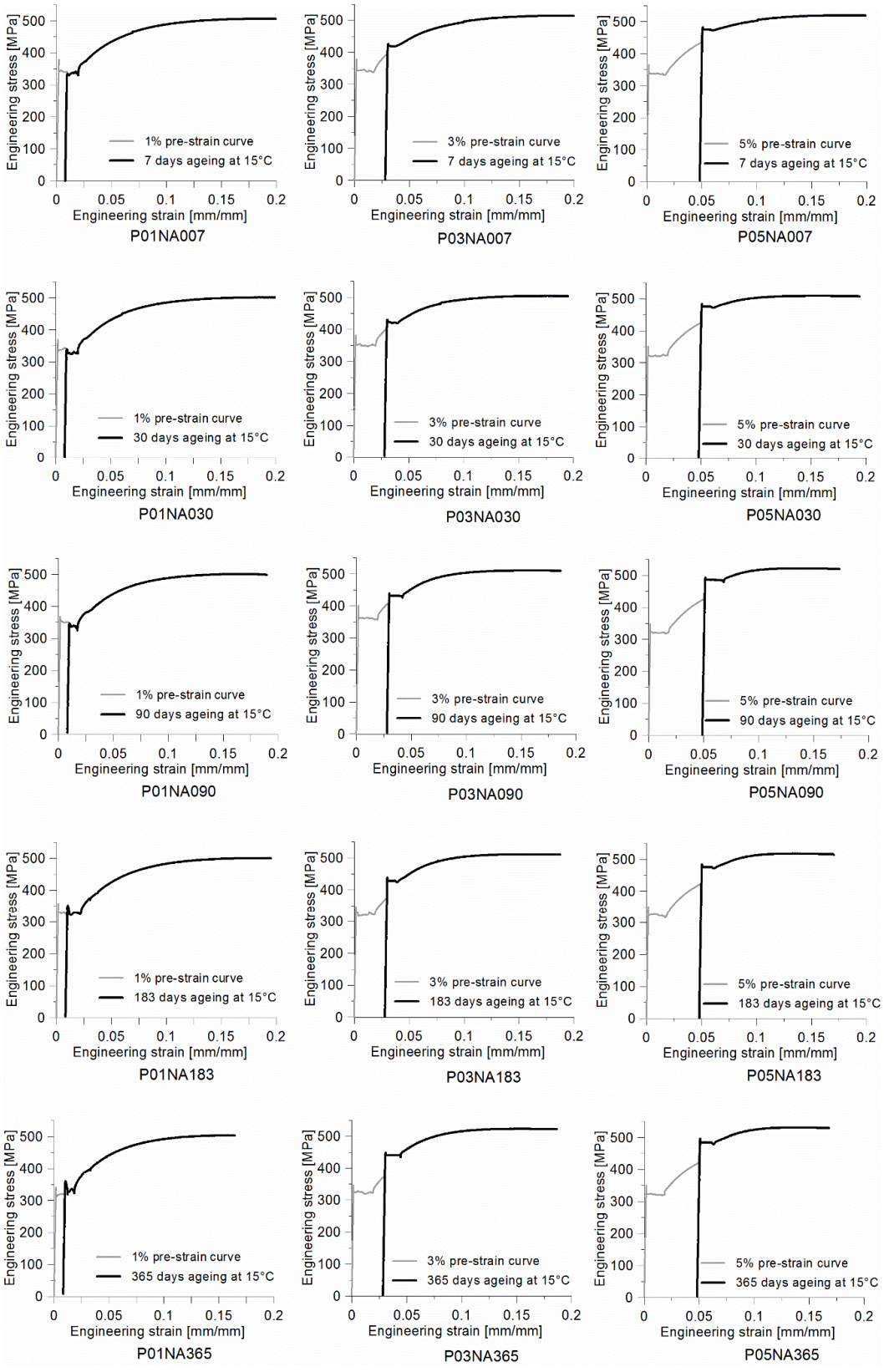

Fig. 6-24 Stress–strain curves for natural aged samples.

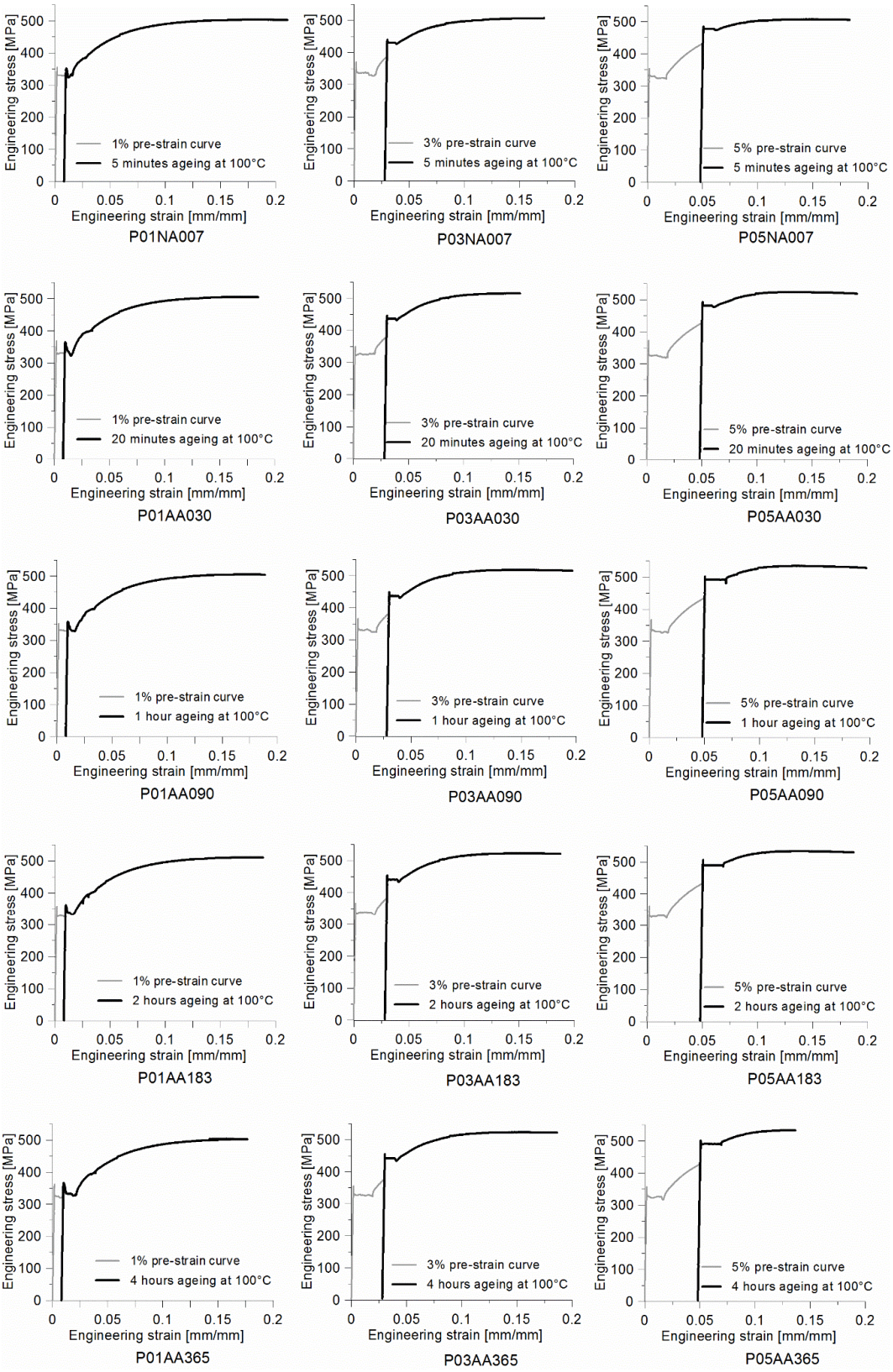

Fig. 6-25 Stress–strain curves for accelerated aged samples.

6.2.3 Discussion

The increases in yield strength caused by natural and accelerated long-term ageing, 365 days and 4 hours respectively, are shown in Table 6-13. The normalised error was calculated as the difference between the values obtained from both tests normalised with respect to the lower yield strength of the naturally aged sample. Since it was the scope of the experiment to determine the effects of strain ageing on the steel's mechanical properties, the values in the table for the samples pre-strained to 1% refer to the second yield strength, even though, in reality, the aged specimens performed approximately elastically up to a stress value similar to that of the undeformed specimens (approximately 300 MPa). In the case of the specimens pre-strained to 3% and 5%, the results obtained were similar to those obtained in Section 6.1.1; the average increase in yield strength was about 55 to 60 MPa. Natural and accelerated strain ageing produced similar increases in ultimate tensile strength (see Table 6-14); the difference between the quantities obtained from both examples was insignificant (approximately 1 to 2 MPa).

In Table 6-15, the change in uniform strain for each sample was calculated as the difference between the expected and the actual values, as in Section 6.1.1. The loss in ductility for natural and artificial aged specimens was comparable. For example, in the case of the specimen pre-strained to 1%, the uniform strain for the natural aged specimen was 0.156 mm/mm; meanwhile for the accelerated aged specimens it was 0.169. Therefore, the difference, 0.013 mm/mm, corresponded to an error of 8.3%, or 1 standard deviation calculated from the uniform elongation values provided by the steel manufacturer in the "certificate of test" (see Appendix 2, Fig. B-1). The increases in Vickers hardness for both natural and accelerated strain ageing, shown Table 6-16 were comparable.

Table 6-13 Comparison of Δy [MPa] for natural versus accelerated long-term ageing

Pre-strain	Natural strain ageing (at 15°C for 365 days)	Accelerated strain ageing (at 100°C for 4 hours)	Difference	Normalised error
1% pre-strain	81[1] MPa	72[1] MPa	–9 MPa	2.3 %
3% pre-strain	58 MPa	56 MPa	–2 MPa	0.5 %
5% pre-strain	57 MPa	60 MPa	3 MPa	0.6 %

[1]The second yield strength is compared

Table 6-14 Comparison of Δu [MPa] for natural versus accelerated long-term ageing

Pre-strain	Natural strain ageing (at 15°C for 365 days)	Accelerated strain ageing (at 100°C for 4 hours)	Difference	Normalised error
1% pre-strain	–3 MPa	–5 MPa	–2 MPa	0.4 %
3% pre-strain	16 MPa	15 MPa	–1 MPa	0.2 %
5% pre-strain	24 MPa	26 MPa	2 MPa	0.4 %

Table 6-15 Comparison of Δε [%] for natural versus accelerated long-term ageing

Pre-strain	Natural strain ageing (at 15°C for 365 days)	Accelerated strain ageing (at 100°C for 4 hours)	Difference
1% pre-strain (0.192[1] mm/mm)	–19 % (0.156[2] mm/mm)	–12 % (0.169[2] mm/mm)	7 % (0.013 mm/mm)
3% pre-strain (0.172[1] mm/mm)	–28 % (0.123[2] mm/mm)	–29 % (0.122[2] mm/mm)	1 % (0.001 mm/mm)
5% pre-strain (0.152[1] mm/mm)	–39 % (0.093[2] mm/mm)	–42 % (0.088[2] mm/mm)	3 % (0.005 mm/mm)

[1] Expected uniform strain if the steel were not prone to strain-ageing effects.

[2] Actual uniform strain measured during the test.

Table 6-16 Comparison of $\Delta HV_{30\,for}$ natural versus accelerated long-term ageing

Pre-strain	Natural strain ageing (at 15°C for 365 days)	Accelerated strain ageing (at 100°C for 4 hours)	Difference
1% pre-strain	3 [HV_{30}]	4 [HV_{30}]	+1 [HV_{30}]
3% pre-strain	13 [HV_{30}]	10 [HV_{30}]	–3 [HV_{30}]
5% pre-strain	14 [HV_{30}]	17 [HV_{30}]	+3 [HV_{30}]

The changes in yield strength, uniform strain and Vickers hardness with respect to ageing time are compared in Fig. 6-26 to Fig. 6-31. As observed in previous studies (Baird, 1971; Hundy, 1954; Wilson & Russell, 1960), the general trends show that strain-ageing effects become more pronounced as the ageing time increases. This is because more time is allowed for the nitrogen (and carbon) atoms to migrate to the new dislocation sites created during pre-straining, and to lock them as before. Moreover, the strain-ageing phenomenon can be assumed to be concluded after one year. For example, in Fig. 6-29 where the change in uniform strain is plotted, after a steep reduction in ductility, the value tends to stabilise after 90 days (or 60 minutes at 100°C) and then remains constant. Natural and accelerated ageing methods provided a similar reduction in ductility. The only anomaly occurs in short-term ageing where the accelerated method amplifies the ductility loss of approximately 18% (or 0.024 mm/mm).

A similar amplification of the accelerated strain-ageing effects can be observed in the rise in the lower yield strength for the specimens pre-strained to 3% (see Fig. 6-26). While there is an agreement between the accelerated and natural ageing in the long-term ageing and for the 5% pre-strained specimen (Fig. 6-27), the increase in yield strength is higher in the 3% pre-strained sample aged at 100°C for less than two hours. Similarly, the Vickers hardness increase at short-ageing times for the accelerated samples are more pronounced. However, as the ageing time increases, the hardness difference decreases and both values converged for long-term ageing. It appears that the accelerated strain effects on Vickers hardness occurred at higher temperature faster than expected and the phenomenon is then completed within 20 minutes. By contrast, the increase in Vickers hardness during the natural strain-ageing process followed trend of the expected steady increase.

In conclusion, it can be confirmed that long-term strain-ageing effects at ambient temperatures can be simulated using the accelerated method in boiling water. Moreover, these effects can be assumed to be concluded after one year at 15°C or four hours at 100°C, or in this last case, even earlier. Because of the limited number of samples used, this experiment is not intended to provide a statistical proof of Hundy's relationship; more experiments are required to investigate the different trends, in particular for short-term ageing.

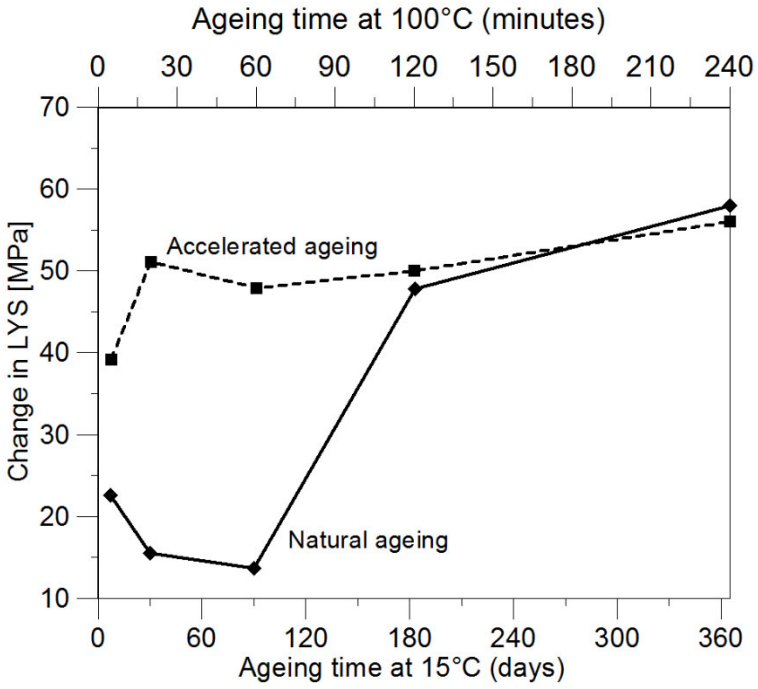

Fig. 6-26 Natural vs. accelerated ageing comparison for the increase in lower yield strength occurring in the 3% pre-strained specimens.

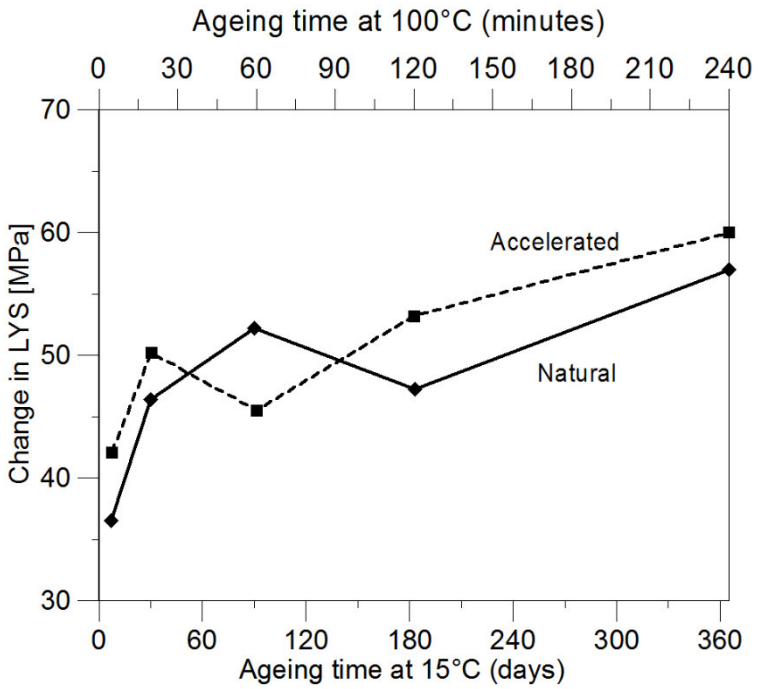

Fig. 6-27 Natural vs. accelerated ageing comparison for the increase in lower yield strength occurring in the 5% pre-strained specimens.

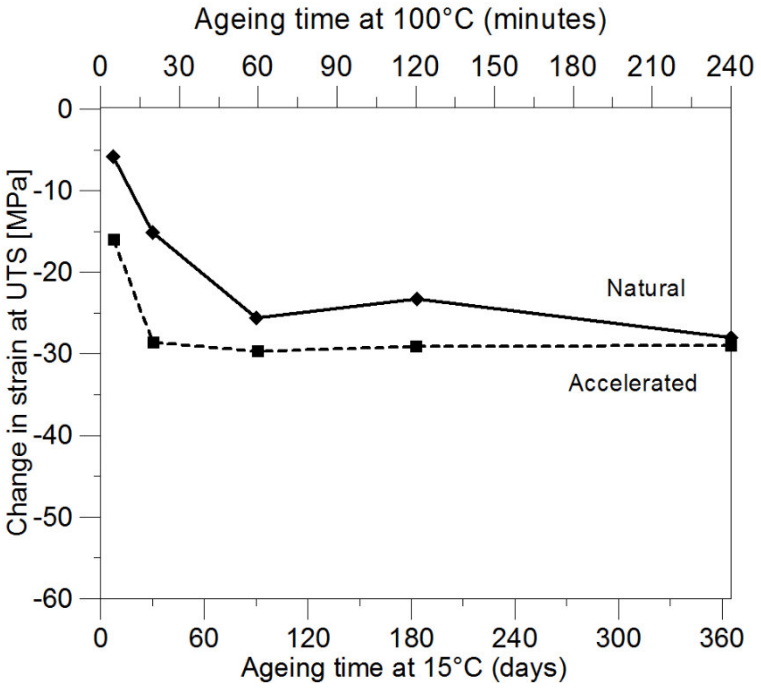

Fig. 6-28 Natural vs. accelerated ageing comparison for the reduction in ductility occurring in the 3% pre-strained specimens.

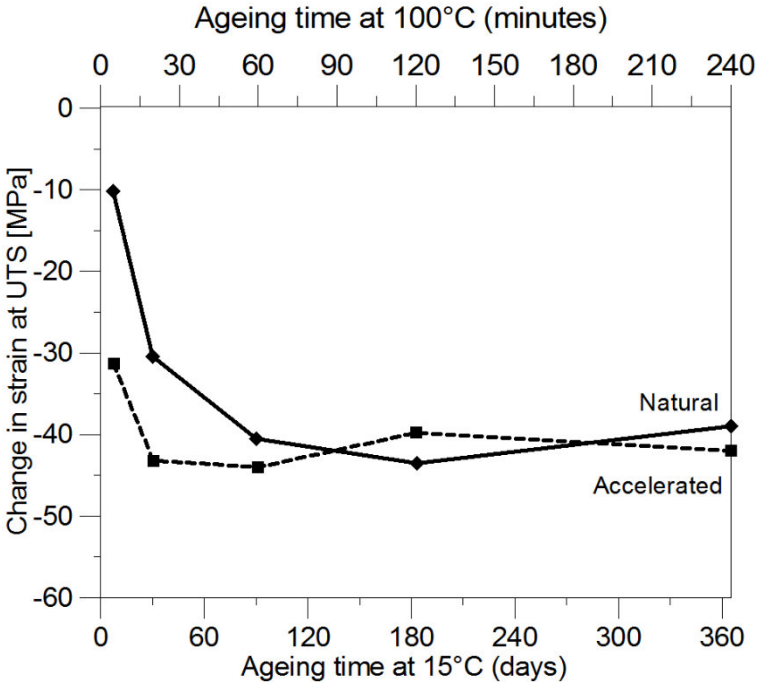

Fig. 6-29 Natural vs. accelerated ageing comparison for the reduction in ductility occurring in the 5% pre-strained specimens.

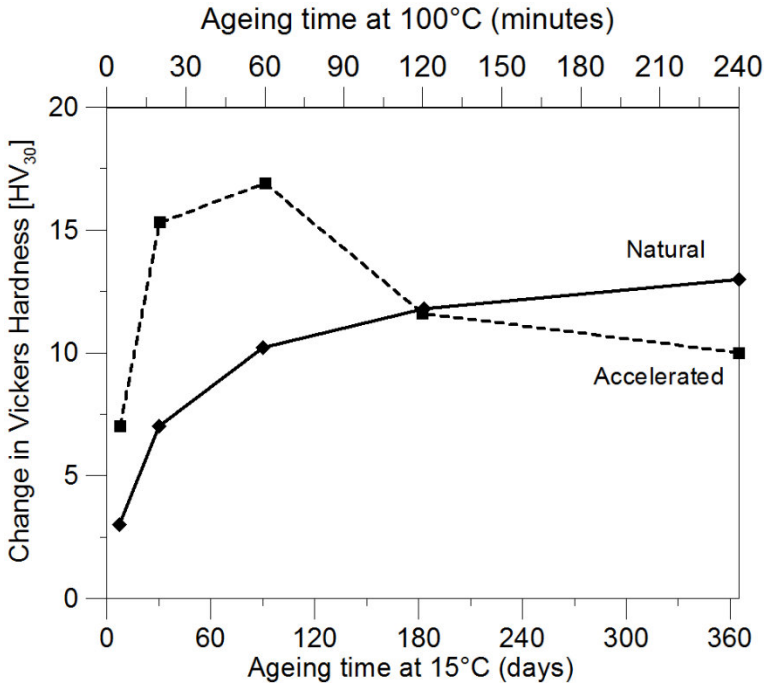

Fig. 6-30 Natural vs. accelerated ageing comparison for the increase in Vickers hardness occurring in the 3% pre-strained specimens.

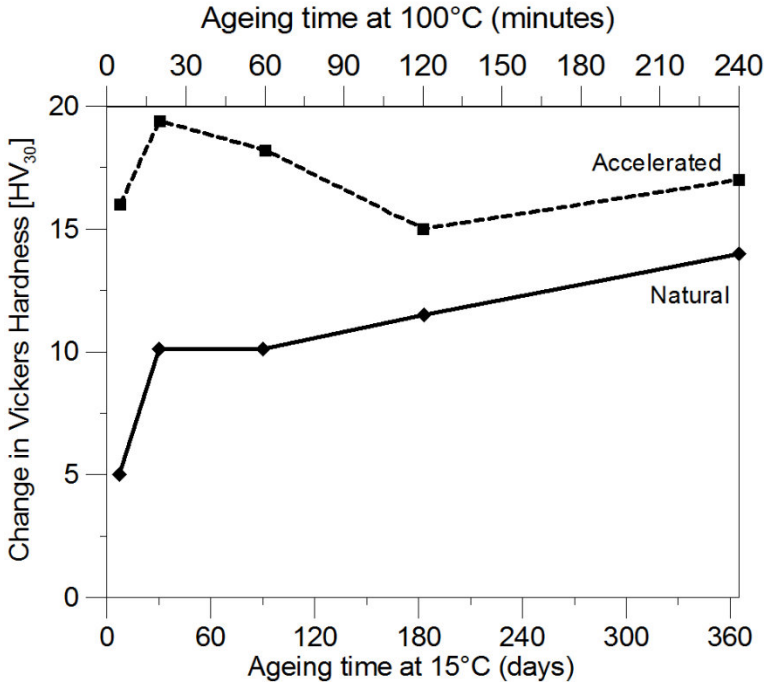

Fig. 6-31 Natural vs. accelerated ageing comparison for the increase in Vickers hardness occurring in the 5% pre-strained specimens.

6.3 STRAIN-AGEING EFFECTS AT TEMPERATURES ABOVE 150°C

In Sections 6.1 and 6.2, the effects of strain ageing on Grade 300E and Grade 500E steel, aged at room temperature and 100°C, and established through a series of experiments, were discussed. Since Grade 500E steel is obtained by the addition of vanadium, which forms an insoluble nitride, no significant changes in mechanical properties were observed. However, at ageing temperatures above 150°C, carbon is expected to diffuse within the steel crystal structure, locking the mobile dislocations and causing a change in mechanical properties. This is also expected on steel not prone to strain ageing below 150°C (Baird, 1971). The experiment presented here was designed to verify whether this hypothesis is true for the NZ-manufactured Grade 500E. The effects of strain ageing caused by the diffusion of carbon were investigated for both steel grades.

Table 6-17 Chemical composition data (wt %) from Mill Certification Sheet

Material	C	Mn	Si	S	P	Ni	Cr	Mo	Cu	Sn	V	C_{eq}
300E	0.18	0.85	0.24	0.030	0.016	0.08	0.10	0.013	0.24	0.018	0.003	0.37
500E	0.18	1.32	0.32	0.024	0.013	0.06	0.07	0.009	0.18	0.023	0.107	0.45

6.3.1 Procedure

Five cylindrical “dog-bone” steel tensile coupons (see Fig. 6-1) were machined from 25 mm Grade 300E and Grade 500E. One specimen of each grade was used to obtain the baseline mechanical properties (lower yield strength, ultimate tensile strength, and strain at UTS). The tensile coupons had a reduced testing area of length 90 mm and diameter 13 mm. The other four samples were pre-strained up to 0.05 mm/mm (5%) and aged at 200°C in a furnace for 15, 30, 45 and 60 minutes; according to Hundy’s equation (6-1) and using an average value of 4200 for the constant *H*, this corresponds to approximately 16, 32, 49 and 65 years at 15°C.

$$\log_{10}\frac{t_r}{t} = H\left(\frac{1}{T_r} - \frac{1}{T}\right) - \log_{10}\frac{T}{T_r} \quad (6\text{-}1)$$

After ageing, the samples were tensile-tested to failure. The samples were tested using the 1000 kN load-cell SATEC system machine; the strain was measured using a 50-mm gauge length MTS extensometer. The gauge length dimension of the extensometer allowed the monitoring of strain until fracture, as necking occurred within its gauge length. The test set-up is shown in Fig. 6-32. The changes in mechanical properties were monitored at the ageing time intervals mentioned above (15, 30, 45 and 60 minutes).

Fig. 6-32 Tensile test set-up.

6.3.2 Results and discussion

The stress–strain curves of the pre-strained and aged Grade 300E bars superimposed on the baseline stress–strain curve are presented in Fig. 6-33 to Fig. 6-36. The changes in properties occurred almost immediately with the reappearance of a new (and higher) discontinuous yield point, higher ultimate tensile strength, and reduction of ultimate strain. By contrast, the stress–strain curves for Grade 500E in Fig. 6-37 to Fig. 6-40, show a gradual reappearance of the upper and discontinuous yield point as the ageing time increases.

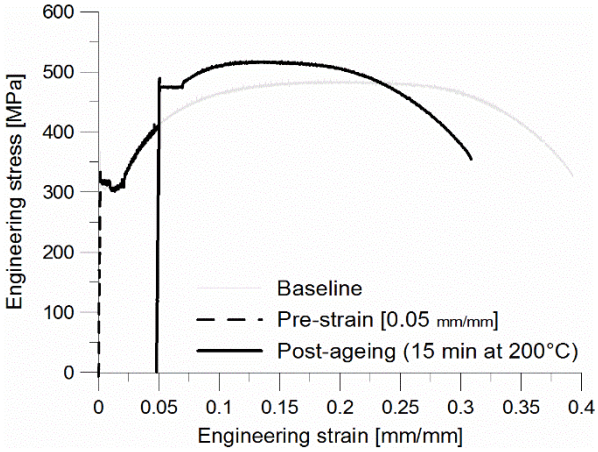

Fig. 6-33 Stress–strain curve of a Grade 300E sample pre-strained to 0.05 mm/mm and aged at 200°C for 15 minutes.

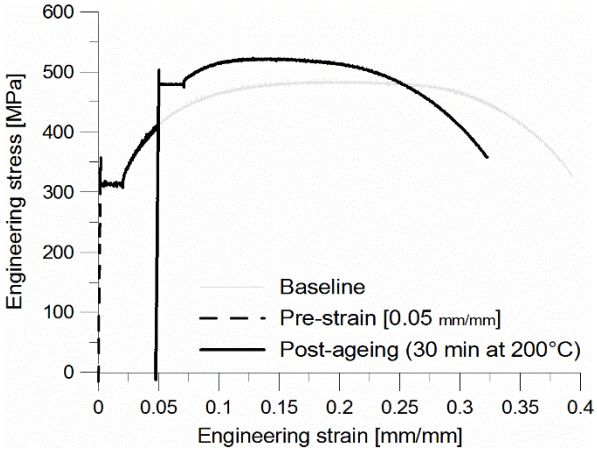

Fig. 6-34 Stress–strain curve of a Grade 300E sample pre-strained to 0.05 mm/mm and aged at 200°C for 30 minutes.

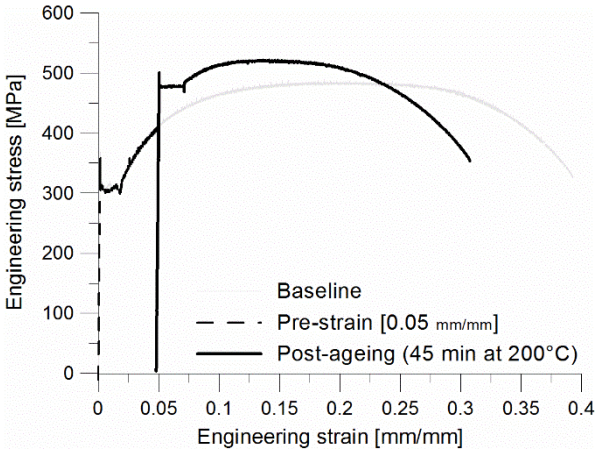

Fig. 6-35 Stress–strain curve of a Grade 300E sample pre-strained to 0.05 mm/mm and aged at 200°C for 45 minutes.

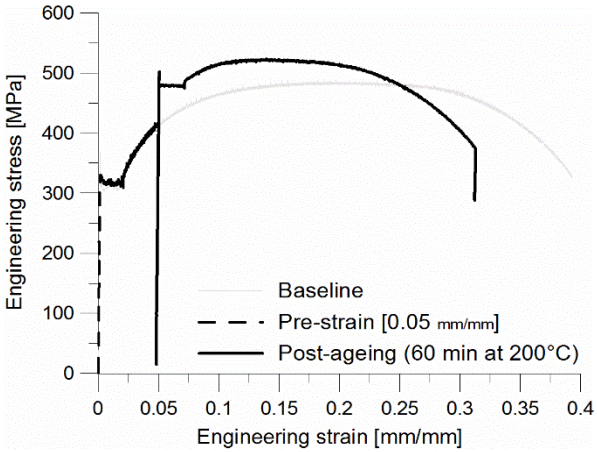

Fig. 6-36 Stress–strain curve of a Grade 300E sample pre-strained to 0.05 mm/mm and aged at 200°C for 60 minutes.

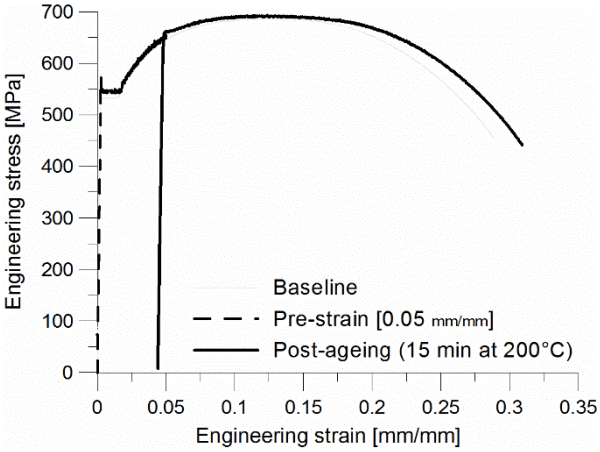

Fig. 6-37 Stress–strain curve of a Grade 500E sample pre-strained to 0.05 mm/mm and aged at 200°C for 15 minutes.

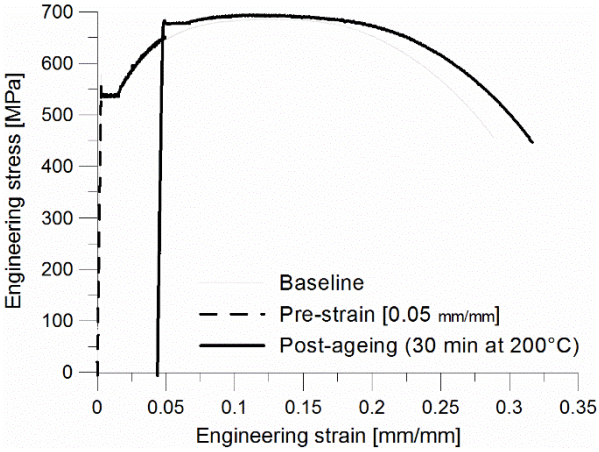

Fig. 6-38 Stress–strain curve of a Grade 500E sample pre-strained to 0.05 mm/mm and aged at 200°C for 30 minutes.

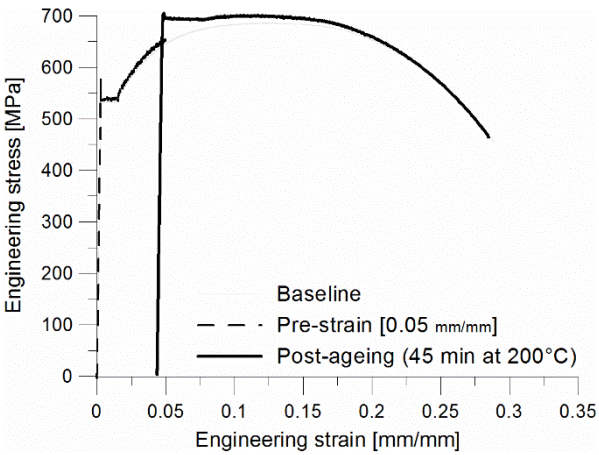

Fig. 6-39 Stress–strain curve of a Grade 500E sample pre-strained to 0.05 mm/mm and aged at 200°C for 45 minutes.

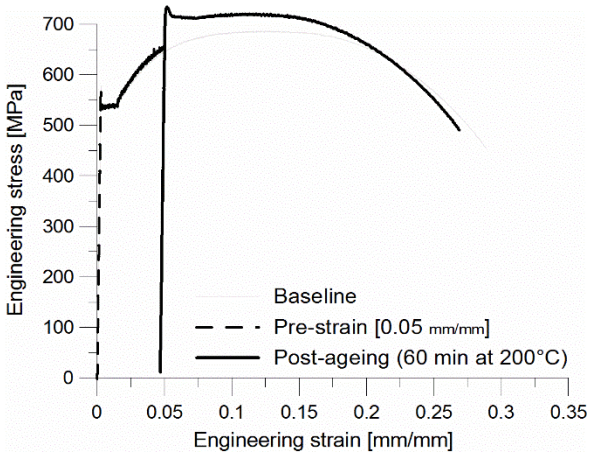

Fig. 6-40 Stress–strain curve of a Grade 500E sample pre-strained to 0.05 mm/mm and aged at 200°C for 60 minutes.

Looking at the Grade 300E results more in detail (Table 6-18), it can be deduced that the strain-ageing phenomenon at 200°C can be considered complete after only 15 minutes of ageing. Fig. 6-41 shows that the change in properties is independent of the ageing time since no further changes were detected after 15 minutes of ageing. In Table 6-19 the long-term strain-ageing effects at 15°C, 100°C, and 200°C are compared. The results showed that the ageing at 200°C did not cause an increase in yield strength, nor a decrease in ductility; the 36% increase (from 25 MPa to 36 MPa) in ultimate strength observed is probably caused entirely by carbon atoms. Baird (1971) stated that, while the discontinuous yield point in Stage I of strain ageing reappears at a higher stress, due to the formation of dislocation atmospheres, during Stage II and III only, an increase in ultimate tensile strength is observed. This is probably caused by precipitate formation, occurring at higher temperatures, that locks the dislocations and causes strain-age-hardening (Pussegoda & Erasmus, 1977).

Table 6-18 Changes in mechanical properties of Grade 300E aged at 200°C.

5% pre-strain	**15 min**	**30 min**	**45 min**	**60 min**
Change in lower yield stress (Δy) [MPa]	63.0	60.5	59.8	58.1
Change in UTS (Δu) [MPa]	28.9	34.2	32.9	34.4
Change in strain at UTS (Δε) [%]	–32.7	–31.2	–31.2	–30.2

Table 6-19 Changes in properties due to strain ageing at different temperatures for Grade 300E.

Ageing temperature (and time)	**Δy [MPa]**	**Δu [MPa]**	**$\Delta\varepsilon_{expected}$ [%]**
15°C (for 365 days)	57	24	–38
100°C (for 4 hours)	60	26	–41
200°C (for 1 hour)	58	34	–39

Table 6-20 and Fig. 6-42 show the changes in properties as the ageing time increases for the 5% pre-strained Grade 500E bar samples. While no significant increase in yield strength occurred after 15 minutes of ageing at 200°C, higher values were observed at ageing times of 30, 45 and 60 minutes. The increase in yield strength appeared to be approximately linear. No previous data exists on similar steels aged at 200°C. Hundy (1954) observed a similar trend on mild steel samples aged at 240°C in an oil bath for a time varying from a few seconds up to 1 to 2 minutes; that is equivalent to 5 to 9 minutes at 200°C. Hundy (1954) also observed that ageing was completed within 2 minutes. This is in contrast with what was observed during the test conducted in this research, where the increase in yield strength was observed after 15 minutes and continued until 60 minutes. This inconsistency is probably due to the amount of carbon, in addition to the active nitrogen, in the steel used in Hundy's study, which was three times that used in this research.

The increase in ultimate tensile strength followed a slightly different trend but consistent with the previous studies. As mentioned earlier, strain-age-hardening does occur later, approximately between Stage II and III (Baird, 1971; Wilson & Russell, 1960). This explained the near-zero increase in UTS in the ageing-time range of 0 to 30 minutes and the subsequent increase to 14.5

MPa at 45 minutes and then to 37.5 MPa at 60 minutes. Like the increase in UTS, the reduction in uniform elongation (or strain at UTS) is expected to occur later in Stage II and then reach the highest value in Stage III, as observed by Wilson and Russell (1960) on a low-carbon rimmed aged at 60°C. In this case, the results showed a steady reduction in ductility up to 45 minutes ageing time; no further reduction was observed at 60 minutes. It is worth remembering that no experimental tests have previously been conducted on Grade 500E; the comparison with previous experiments on low-carbon steels are only indicative, since the strain-ageing effects are highly dependent on the amount of active nitrogen and carbon.

Table 6-20 Change in mechanical properties of Grade 500E aged at 200°C.

5% pre-strain	**15 min [%]**	**30 min [%]**	**45 min [%]**	**60 min [%]**
Change in lower yield stress (Δy) [MPa]	8.4	24.2	39.7	55.6
Change in UTS (Δu) [MPa]	6.6	7.6	14.5	37.5
Change in strain at UTS (Δε) [%]	–4.0	–7.9	–11.9	–11.1

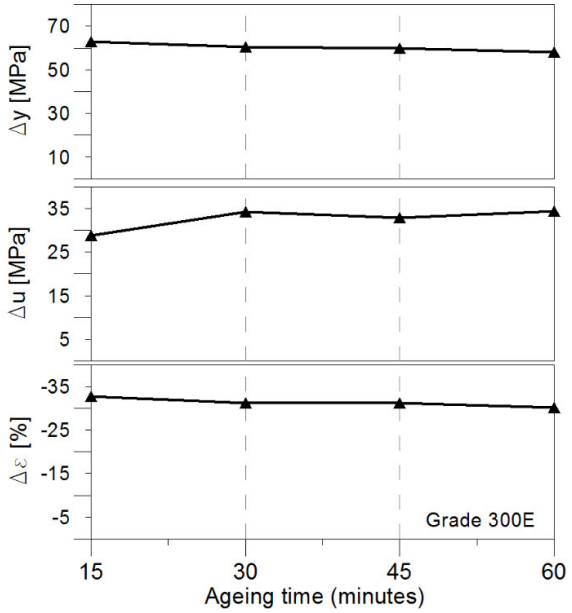

Fig. 6-41 Change in lower yield strength (Δy), ultimate tensile strength (Δu), and uniform elongation (Δε) of Grade 300E 5% pre-strained specimens, aged at 200°C.

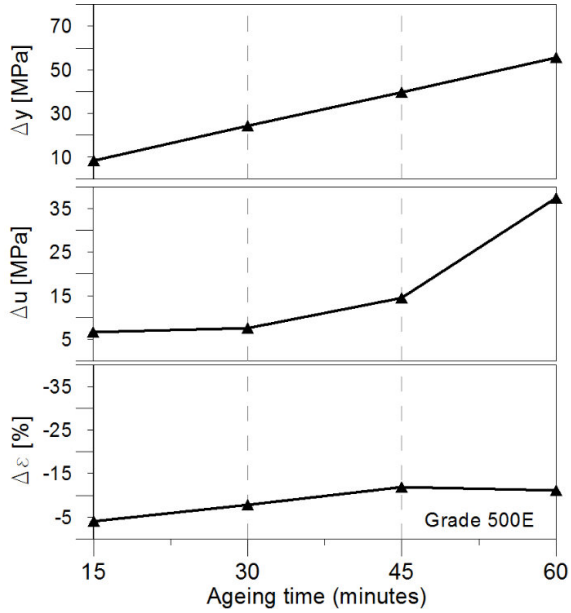

Fig. 6-42 Change in lower yield strength (Δy), ultimate tensile strength (Δu) and uniform elongation (Δε) of Grade 500E 5% pre-strained specimens, aged at 200°C.

In conclusion, the results obtained showed that long-term ageing at 200°C did not cause substantial changes in the mechanical properties of Grade 300E steel when compared with long-term ageing at 15°C and 100°C; only a 35 % increase in ultimate tensile strength was observed. Moreover, the strain-ageing effects were completed after 15 minutes. Results from Grade 500E steel confirmed the hypothesis that the diffusion of carbon atoms is activated when steel is aged at temperatures around 200°C, consequently causing changes in the mechanical properties usually observed in Grade 300E steel at room temperature. Although the long-term increases in yield strength and ultimate tensile strength are comparable to those observed in Grade 300E, the reduction in ductility is significant lower (approximately one third). Strain ageing at 200°C might occur in very rare events in the service life of a reinforced concrete building since it requires that a bar is plastically deformed and then aged at very high temperatures, for example, during a fire. However, the results demonstrated that further effects observed on Grade 300E can be ignored.

6.4 CONCLUSIONS

In this chapter the long-term effects of strain ageing on local manufactured steel Grade 300E and Grade 500E were investigated. The following conclusions can be drawn:

- At temperatures up to 100°C, only Grade 300E steel is affected by changes in mechanical properties caused by strain ageing. Because of the vanadium addition, negligible changes occurred in Grade 500E samples.
- Long-term strain-ageing tests demonstrated that the increase in lower yield and ultimate tensile strength, and reduction in ductility depend on the ageing time. The changes in mechanical properties in Grade 300E can be assumed to be concluded only at 365 days.
- Although in short-term ageing, the accelerated method overestimates the changes in mechanical properties, at long-term (one year), the method can reasonably simulate the ambient temperature strain-ageing effects. Four hours at 100°C (for example, in boiling water) are recommended to simulate one year of ageing at 15°C. However, if testing-time is limited, the four hours can be reduced to two.
- The calibration curves required in Phase III of the "hardness method" must be developed after ageing using the accelerated method only for Grade 300E samples, or the superseded steels prone to strain ageing, such as Grade 275 and Grade 300.
- The increase in lower yield strength is not dependent on the amount of pre-strain. Results from Grade 300E suggested that an increase of approximately 60 MPa needs to be accounted for when the new yield strength of damaged and aged Grade 300E bars is estimated. This amount must be added to the increase in yield strength caused by strain hardening. For example, Grade 300E samples pre-strained to 5% and aged for a year at ambient temperature can have a yield strength as high as 480 MPa.

- Strain ageing, combined with strain hardening, could potentially cause an increase in the flexural strength of the RC member. Further research can be focused on determining the overstrength factors that include the effects of strain hardening and strain ageing for New Zealand manufactured Grade 300E steel.
- Additional tests were conducted at 200°C to determine the effects of strain ageing caused by interstitial carbon atoms. For Grade 300E, the phenomenon was completed after only 15 minutes. The changes in mechanical properties were similar to those observed during the long-term ageing tests at 15°C and 100°C. Therefore, for Grade 300E the accelerated method testing-time can be reduced to 15 minutes at 200°C.
- Strain-ageing effects on Grade 500E were observed in samples aged at 200°C. The increase in yield and ultimate tensile strength, and the reduction in ultimate strain became more pronounced as ageing time increased. It must be noted that similar conditions can occur only in very rare events during the life of a building.

6.5 REFERENCES

ASTM. (2011). E8/E8M - 11 *Standard Test Method for Tension Testing of Metallic Materials*. West Conshohocken, PA, United States.

Baird, J. (1963). Strain-ageing of steel - A critical review. *Iron and Steel, 36*, 186,326,368,400,450.

Baird, J. (1971). The effects of strain-ageing due to interstitial solutes on the mechanical properties of metals. *Metallurgical Reviews, 16*(1), 1-18.

Cottrell, A. H., & Bilby, B. A. (1949). Dislocation theory of yielding and strain ageing in iron. *Proceedings of the Physical Society. Section A, 62*(1).

Erasmus, & Pussegoda. (1977). Strain age embrittlement of reinforcing steels. *New Zealand Engineering, 32*(8).

Erasmus, & Pussegoda. (1980). The strain aging characteristics of reinforcing steel with a range of vanadium contents. *Metallurgical Transactions A, 11*(2), 231-237.

Erasmus, & Pussegoda, N. (1978). Safe bend radii for deformed reinforcing bar to avoid failure by strain age embrittlement. *New Zealand Engineering, 33*(8), 170.

Erasmus, L. A. (1981). Cold straightening of partially embedded reinforcing bars - A different view. *Concrete International*.

Hundy, B. B. (1954). Accelerated Strain Ageing of Mild Steel. *Journal of The Iron and Steel Institute, 178*.

Leslie, W. C. (1981). *The physical metallurgy of steels* (M.-H. B. Company Ed.). Washington.

Lim, W. T. (1991). *Statistical analysis of reinforcing steel properties.* (Master of engineering), University of Canterbury, Christchurch.

Momtahan, A., Dhakal, R., & Rieder, A. (2009). Effects of strain-ageing on New Zealand reinforcing steel bars. *Bulletin of the New Zealand Society for Earthquake Engineering, 42*(2).

Pussegoda, & Erasmus. (1977). *The effect of titanium on the strain ageing characteristics of a carbon manganese structural steel*. Paper presented at the 6th Australas Conf on the Mech of Struct and Mater, Christchurch.

Restrepo-Posada, J. I. (1992). *Seismic behaviour of connections between precast concrete elements: a thesis submitted in partial fulfilment of the requirements for the degree of Doctor of Philosophy in Civil Engineering at the University of Canterbury.* (Dissertation/Thesis).

Restrepo-Posada, J., Dodd, L., Park, R., & Cooke, N. (1994). Variables Affecting Cyclic Behavior of Reinforcing Steel. *Journal of Structural Engineering, 120*(11), 3178-3196.

Standards, A. a. N. Z. (2001). AS/NZS 4671:2001 *4671:2001 Steel reinforcing materials*. Wellington, New Zealand.

Standards, N. Z. (1989). NZS 3402:1989 *Steel bars for the reinforcement of concrete*. Wellington New Zealand.

Wilson, D. V., & Russell, B. (1960). The contribution of precipitation to strain ageing in low carbon steels. *Acta Metallurgica, 8*(7), 468-479.

7 THE LEAST INVASIVE METHOD

7.1 INTRODUCTION

In Chapter 5, a method to assess the plastic deformation of the steel reinforcement and predict its residual strain capacity was proposed. The method was based on empirically tested hardness versus strain (calibration) curves developed for each combination of steel grade and diameter. Although the method provided reliable predictions, the biggest limitation was the test invasiveness, and the time and cost required to perform the calibration tests. In order to overcome these limitations, an improvement of the method is proposed. It was conceived with the objective of deriving a reasonably accurate residual-strain capacity prediction of the damaged rebars based on minimal information: hardness baseline, hardness in the damage location and strain at ultimate tensile strength. Ideally, to obtain this information, only two 150-mm lengths of steel rebar are required: one must be obtained from the suspected damage location, and another from an undamaged location. The latter will be used to determine the baseline stress–strain curve and the baseline Vickers hardness. It is essential to recover the two samples from the same rebar; for example, if damage is suspected to have occurred at the base of a wall, it is recommended, if possible, to extract the 150-mm undamaged length from the top end of the same bar. An application of the method, only on Grade 300 steels, is presented in this chapter.

7.2 APPLICATION OF THE METHOD

7.2.1 Procedure

The method is based on the hypothesis that a universal calibration curve (Vickers hardness versus strain) can be developed for steels of the same grade. The universal calibration curve was determined by averaging the calibration curves obtained for Grade 300 steels in Section 3.3.2 (Steels 01 to 05 of Table 3-6). The increase in hardness from the baseline was measured at each strain increment (see Table 7-1) and an average increase was determined from the values obtained. As discussed in Chapter 3, this hardness increase is the sum of two contributions: pre-strain and strain ageing; both in fact are responsible for the increase in the material's yield strength. In Table 7-1, only the total increase is reported.

Table 7-1 Increase in Vickers hardness from the baseline for the Grade 300 steels selected.

Pre-strain	Steel 01	Steel 02	Steel 03	Steel 04	Steel 05	Average
0.01	9.1	11.4	13.6	9.2	15.8	11.8
0.02	50.4	19.5	17.4	15.8	16.2	17.8
0.03	28.2	26.2	22.2	21.7	25.4	24.7
0.04	31.8	31.1	27.3	27.2	25.5	28.6
0.05	37.0	35.0	30.9	33.1	33.1	33.8
0.10	54.0	N/A	N/A	47.7	49.9	50.5

The average increase in Vickers hardness is then plotted against the pre-strain in Fig. 7-1; the curve obtained represents the universal calibration curve. Knowing the peak Vickers hardness, at the damage location, and the baseline Vickers hardness, this curve allows the estimation of the deformation experienced by the damaged bar under investigation. The strain amount obtained also represents the loss in ductility due to pre-strain. However, because Grade 300 is prone to strain ageing, to determine the residual strain capacity it is essential to estimate the loss in ductility due to this phenomenon. In Chapter 6, for Grade 300E, it was shown that this ductility loss increased

with the amount of pre-strain; however the relationship found between loss and pre-strain was not robust, as indicated by the R^2 value being below 0.6. Moreover, the ductility loss was not strongly dependent upon pre-strain, as shown in Fig. 7-2 . Therefore, for practicality, the ductility loss due to strain ageing was assumed to be a constant value, obtained as the average loss found, which was 0.055 mm/mm with standard deviation of 0.011.

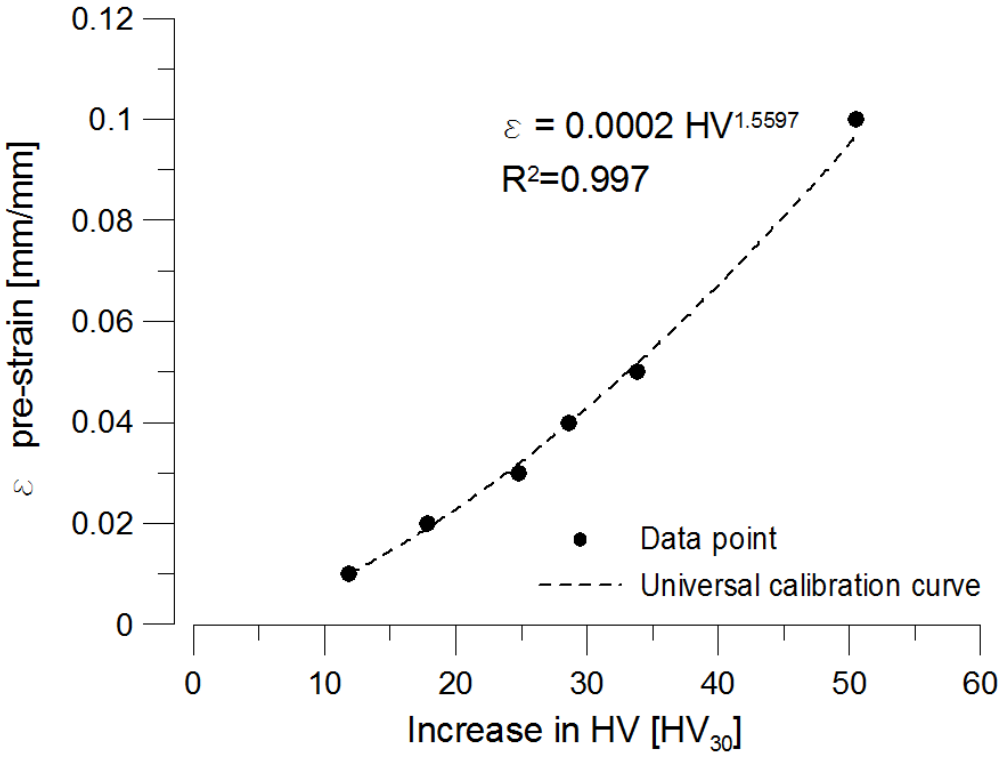

Fig. 7-1 Universal calibration curve for Grade 300 steels.

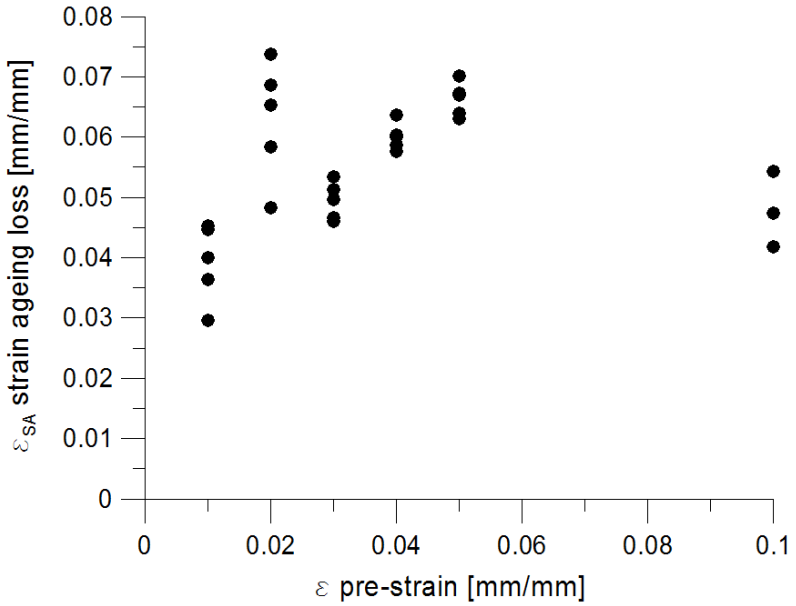

Fig. 7-2 Strain ageing loss as function of pre-strain.

Based on the measured baseline strain at UTS (ε_{BL}) (obtained from the tensile test), the estimated pre-strain (ε_{PR}) (obtained from the calibration curve) and the assumed loss in strain due to strain ageing (ε_{SA}), it was possible to predict the residual strain capacity of the damaged rebars (ε_{UTS}), using the following equation:

$$\varepsilon_{UTS} = \varepsilon_{BL} - \varepsilon_{PR} - \varepsilon_{SA} \quad (7\text{-}1)$$

7.2.2 Results

In order to verify the estimations and the predictions using the universal calibration curve and equation (7-1), the method was applied to the Grade 300E samples used in Section 3.3.1. In that case, the rebar specimens were pre-strained up to 0.02, 0.04, 0.06 and 0.08 mm/mm and the hardness was measured after ageing. The only information required from testing is the Vickers baseline (150 HV_{30}), the Vickers hardness of the samples after pre-straining and ageing (see Table 7-2), and the baseline strain at UTS (ε_{BL} = 0.203 mm/mm). Following the procedure described in Section 7.2.1, the estimated ε_{PR} and the predicted ε_{PR} were calculated. A demonstration of the

procedure is shown here for the sample pre-strained to 0.08 mm/mm. The peak Vickers hardness measured was 198 HV_{30}, which corresponds to an increase from the baseline of 48 HV_{30}, and using the curve in Fig. 7-1, a pre-strain of 0.084 mm/mm (ε_{PR}). The residual strain capacity is obtained using equation (7-1) and the strain amounts obtained, assuming ε_{SA} = 0.055:

$$\varepsilon_{UTS} = 0.203 - 0.084 - 0.055 = 0.064\, mm/mm \quad (7\text{-}2)$$

Table 7-3 shows a comparison between the measured and predicted values, and shows a maximum error of 7.1 %.

Table 7-2 Vickers hardness measurements for the Grade 300E samples.

Pre-strain [mm/mm]	**Vickers hardness [HV_{30}]**	**Increase in HV [HV_{30}]**
0.02	168	18
0.04	180	30
0.06	191	41
0.08	198	48

Table 7-3 Comparison between the measured and predicted estimation of ε_{PR} and ε_{UTS}

Measured ε_{PR} [mm/mm]	**Estimated ε_{PR} [mm/mm]**	**Error [%]**	**Measured ε_{UTS} [mm/mm]**	**Predicted ε_{UTS} [mm/mm]**	**Error [%]**
0.02	0.018	1.4	0.140	0.130	7.1
0.04	0.040	0.0	0.102	0.108	5.9
0.06	0.066	7.4	0.081	0.083	2.5
0.08	0.084	5.9	0.067	0.064	4.5

The method was also applied to each of fifteen Grade 300 steel rebars that were found damaged after the Canterbury and Kaikoura (New Zealand) earthquakes. The increase in hardness was calculated as the difference between an average peak hardness measured at the damaged location and the hardness baseline. This is only an approximation, since the Vickers hardness profile in

damaged samples is not constant, but varies, depending (not only) on the amount of plastic deformation experienced by the bars during the earthquake (see Chapter 5). The baseline strain at UTS was determined from tensile tests conducted on undamaged rebars. The baseline and average peak hardness was obtained from the hardness measurements conducted on the rebars when received in the laboratories. The predicted residual strain capacity is compared to the measured capacity in Table 7-4. Note that D1 and D2 are the same samples presented in Chapter 5.

Table 7-4 Summary of the least invasive method results from 15 earthquake-damaged rebars.

	Information required			**Prediction and check**		
Sample	**HV baseline [HV_{30}]**	**HV peak avg. [HV_{30}]**	**ε_{BL} [mm/mm]**	**Measured ε_{UTS} [mm/mm]**	**Predicted ε_{UTS} [mm/mm]**	**Error [%]**
D1	146	165	0.185	0.122	0.111	9.0
D2	146	172	0.192	0.136	0.105	22.8
S3	145	170	0.200	0.142	0.115	19.0
S4	146	177	0.198	0.140	0.101	27.9
S5	151	188	0.168	0.049	0.057	16.3
S6	151	185	0.168	0.086	0.064	25.6
S7	153	175	0.168	0.046	0.088	91.3
S8	153	175	0.168	0.060	0.088	46.7
S9	145	174	0.207	0.124	0.114	8.1
S10	153	204	0.200	0.056	0.053	5.4
S11	153	208	0.200	0.038	0.042	10.5
S12	130	147	0.193	0.150	0.122	18.7
S13	139	166	0.196	0.085	0.107	25.9
S14	129	159	0.217	0.070	0.121	72.9
S15	133	141	0.203	0.114	0.143	25.4

7.2.3 Further improvements

The predicted and measured residual strain capacity comparison is summarised in Fig. 7-3; all the samples falling within the dashed and the solid (1:1) lines are affected by an error below 30%. Only 3 out of the 15 (20%) samples are affected by an error larger than 30%. There is no tendency to observe more or less conservative predictions; the data points are approximately evenly distributed. The residual strain capacity predictions obtained from the (more invasive) method employed in Chapter 5, and the least invasive method for D1 and D2 is shown in Table 7-5. In both cases, the least invasive method provided less accurate results.

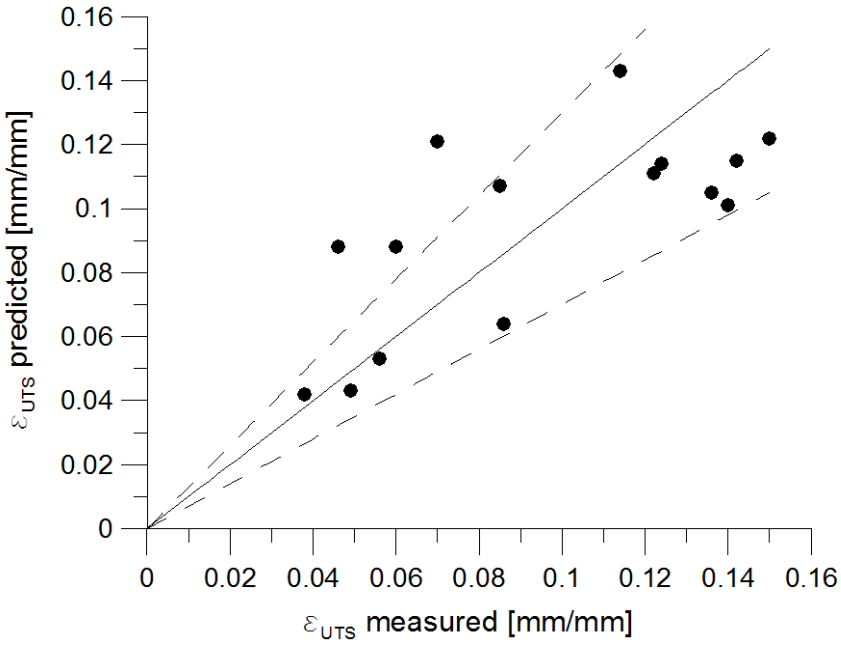

Fig. 7-3 Predicted vs. measured residual strain capacity for the 15 damaged samples. The solid line represents the no-error prediction line, whereas the dashed lines represent the 30% error prediction.

Table 7-5 Comparison between the error in the prediction from the standard and the least invasive method

Specimen	Measured ε_{UTS}	Predicted ε_{UTS} with invasive method	Predicted ε_{UTS} with least invasive method
D1	0.122	0.125	0.111
(Error %)		(2.5)	(9.0)
D2	0.136	0.110	0.105
(Error %)		(19.1)	(22.8)

In order to improve the prediction, instead of using the average hardness calculated over the damaged location, the residual strain capacity is measured at each 5-mm spacing (where the hardness was measured) and summed over the entire gauge length used during the tensile testing. An example of the refined calculation is described here for the sample D1. Prior to tensile testing, hardness measurements were carried out every 5 mm along the reduced area of the tensile specimen at the location where the extensometer gauge length (25 mm) was placed during the tensile testing. The hardness increase obtained at each point was used to calculate the predicted ε_{UTS}: this value was multiplied by 5 mm to determine the elongation over this distance, and finally each elongation was summed and the total elongation over the entire 25-mm gauge length was determined. The refined-predicted residual strain capacity $(\varepsilon_{UTS\ refined})$ was calculated as the ratio between the calculated elongation and the 25-mm gauge length. Calculation details are reported in Table 7-6. The same refined calculation was performed for the steel samples D1 to S8, and the results are shown in Table 7-7. The refined calculation has improved the prediction by a further 2% approximately.

Table 7-6 Calculation of the refined-predicted residual strain capacity for sample D1.

Hardness	**Predicted ε_{UTS} [mm/mm]**	**Elongation over 5 mm [mm]**
163	0.114	0.570
163	0.114	0.570
165	0.111	0.555
163	0.114	0.570
166	0.109	0.545
	Elongation (ΔL)	2.810
	Gauge length (L)	25.000
	Predicted $\varepsilon_{UTS\ refined}$ (ΔL/L)	**0.112**

Table 7-7 Comparison between the measured, and the predicted approximated and refined residual strain capacity.

	Approximated method			**Refined method**	
Sample	**Measured ε_{UTS} [mm/mm]**	**Predicted ε_{UTS} [mm/mm]**	**Error [%]**	**Predicted $\varepsilon_{UTS\ refined}$ [mm/mm]**	**Error [%]**
D1	0.122	0.111	9.0	0.112	8.2
D2	0.136	0.105	22.8	0.106	22.1
S3	0.142	0.115	19.0	0.117	17.6
S4	0.140	0.101	27.9	0.103	26.4
S5	0.049	0.057	16.3	0.056	14.3
S6	0.086	0.075	12.8	0.077	10.5
S7	0.046	0.088	91.3	0.086	87.0
S8	0.060	0.088	46.7	0.087	45.0

7.3 ADDITIONAL CORRELATIONS

7.3.1 Correlation between hardness and other mechanical properties

As previously discussed, plastic deformation and strain ageing cause an increase in yield strength that could potentially cause changes in the failure mechanism of structures. Therefore, while it is important to determine the residual strain capacity, it is also important to determine the new yield strength. Correlations between Vickers hardness and yield strength, and ultimate tensile strength and strain at UTS were derived from testing 342 steel rebar samples. The steel used in the experimental tests were machined from reinforcing bar obtained from two sources: the local steel manufacturer Pacific Steel and steel removed from local reinforced concrete buildings. The dataset includes steel tested as received as well as steel previously cold worked (plastically deformed in tension); in this case, Vickers hardness was measured after the pre-strain phase and correlated with the mechanical properties of the cold-worked and aged material for consistency. The yield strength ranged from 284 MPa to 765 MPa. Results are shown in Fig. 7-4 to Fig. 7-6.

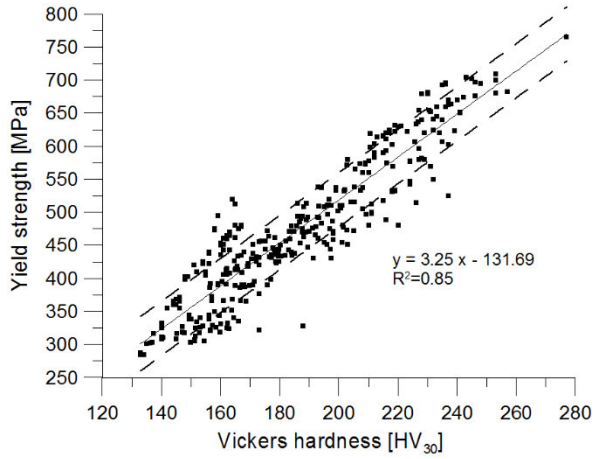

Fig. 7-4 Yield strength versus Vickers hardness from the test conducted on 342 steel specimens. Dashed lines represent the ± 1 standard error of the regression line.

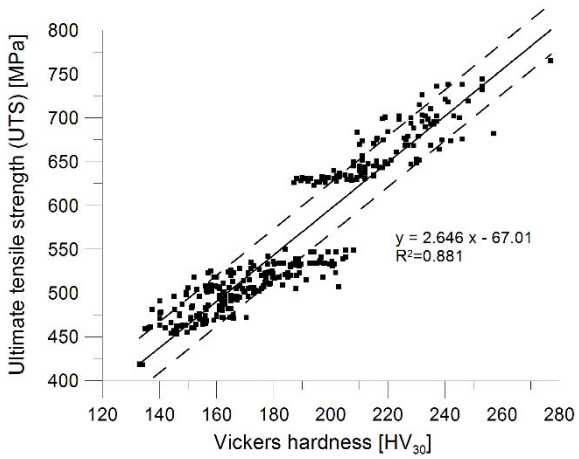

Fig. 7-5 Ultimate tensile strength (UTS) versus Vickers hardness from the test conducted on 342 steel specimens. Dashed lines represent the ± 1 standard error of the regression line.

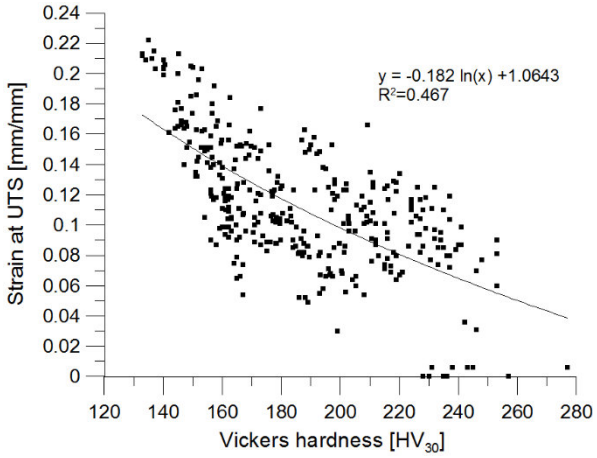

Fig. 7-6 Strain at UTS versus Vickers hardness from the test conducted on 342 steel specimens.

Consistent with previous research (see section 2.3.2), Vickers hardness (HV_{30}) increased with yield strength (YS) and ultimate tensile strength (UTS) (see Fig. 7-4 and Fig. 7-5). Experimental data were well approximated with linear regression lines represented by the equations:

$$YS = -131.69 + 3.25\, HV_{30} \tag{7-3}$$

$$UTS = -67.01 + 2.65\, HV_{30} \tag{7-4}$$

For equation (7-3), R^2 was 0.85 and standard error was 41 MPa, whereas for equation (7-4), R^2 was 0.88, while the standard error was 29 MPa.

In contrast, experimental data show a higher dispersion when Vickers hardness was correlated to strain at UTS (ε_{UTS}). A logarithmic equation fitted all the data. However, R^2 in this case was only 0.467.

$$\varepsilon_{UTS} = 1.0643 - 0.182 \ln(HV_{30}) \tag{7-5}$$

The method presented in Section 7.2 combined with the empirical relationships (7-3) and (7-4) can provide insights into the mechanical properties of the damaged materials: yield and ultimate tensile strengths, and the residual strain capacity can be estimated and provided to structural engineers for the assessment phase of reinforced concrete structures and members.

7.4 FINAL DISCUSSION

The application of the least invasive method on steel rebars damaged during the Christchurch and Kaikoura earthquakes has demonstrated that it is possible to estimate the plastic deformation and residual ductility. The level of invasiveness is minimised, only 300 to 400 mm of the steel rebars needs to be removed from the building and tested in the laboratory. The method provides a prediction of the residual strain capacity within an error below 30%, in 80% of the cases. A refined calculation improved the predictions by a further 2% in each case, approximately. In this section, answers to the following questions are discussed: "What is the purpose of the method?" and "What are the implications?"

The main purpose of the method is to provide practitioner engineers, building owners, territorial authorities, and insurance companies with a supporting tool in order to make informed decisions on the demolition or repair of damaged RC buildings. Although over the previous year the method has been used to prove evidence of damage of the steel rebars during insurance controversies, it does not aim to provide an absolute answer to the question: "Will the building survive another earthquake of similar intensity?" However, it contributes to reducing the uncertainties during the assessment stage.

Results have demonstrated that the method can certainly answer the question: "Does the damaged steel meet the current steel reinforcement standards AS/NZS 4671:2001?" For example, first the predictions, and then the actual measurements demonstrated that none of the fifteen samples listed in Table 7-4 met the ductility requirements (uniform elongation larger than 15%) (Standards Australia and New Zealand, 2001). However, it might be argued that the material does not meet the requirement only within a small region of the material that is at the crack location. One might ask then: "Is this information sufficient to decide whether a building must be demolished or not?"

Certainly not. The residual capacity of a building to survive another earthquake of similar or larger intensity depends on the overall behaviour of a structure, which is a function of several aspects such as the structural systems, structure redundancy, structural configuration, members' geometry, and material properties.

In the assessment stage of any structure, information regarding the material properties is essential to determine the local behaviour of structural members that contributes to understanding the overall behaviour of the entire structure. The example of an earthquake-damaged bridge pier might explain the importance of the proposed method. Bridge piers are usually modelled as fixed-base cantilever columns loaded at the free-top end. They are designed for a specific displacement ductility factor (μ) and are expected to plastically deform at the base over an assumed plastic hinge length (NZTA, 2016). The displacement ductility is a function of the assumed plastic hinge length and curvature ductility, which is determined from moment-curvature analysis based also on the steel properties of yield strength and strain ductility (Priestley, Calvi, & Kowalsky, 2007). During the recent Kaikoura earthquake (14 November 2016), plastic hinging occurred at the pier base in many bridges. Concrete was expulsed and the steel rebars were exposed (Palermo et al., 2017), see Fig. 7-7. To determine the pier's residual ductility, in the assessment phase, it is important to identify the extent and amount of plastic deformation of the rebars so that it is possible to reasonably assume the plastic hinge length and the residual strain capacity. The hardness method allows better informed assumptions about the plastic hinge length and residual strain capacity of the rebars to be made.

The level of accuracy required from the prediction might depend on the approximation set by the designer during the assessment. The reinforcing material standard requires that the minimum elongation at maximum force (strain at UTS) for Grade 300E rebars during tensile tests is 15%. In

the tests conducted during this research, values larger than 18% have been often observed. For moment curvature-analysis, Priestley et al. (2007) suggest reducing the steel's ultimate strain limit to 60% of the strain at UTS obtained from a tensile test, because this value is reduced by the peak compressive strain experienced by a previous load reversal, by buckling and the slip between concrete and the rebars. For example, for NZ Grade 300E, the ultimate strain from tensile tests can be assumed conservatively at 0.15 mm/mm, so the 60% corresponds to 0.09 mm/mm. Based on these considerations, the designer can adopt appropriate approximations when the analysis is conducted, allowing for the numerous uncertainties in the material. The number of cases provided in this chapter might not be sufficiently large to derive reliable safety factors to apply to the predicted residual strain capacity values. It is recommended that the number of cases be enlarged up to 100, for example.

The plastic hinge length and the residual strain capacity are not the only parameters required during the assessment. It has been demonstrated that plastic strain and strain ageing increase yield strength; in the assessment of the residual capacity of a structure, the new yield strength of the steel reinforcement is also essential. If the plastic deformation is assumed to occur over the entire plastic hinge length, the flexural capacity of the damaged member has increased accordingly and the hierarchy of strength might change. Equation (7-3) can provide an estimation of the new yield strength at the damage locations and determine the new flexural capacity of a member. It must be noted, however, that this is based on the assumption that a uniform crack pattern has occurred at the plastic hinge location, and the plastic deformation of the rebars is spread uniformly. This assumption might not be true in the case of single-cracked concrete members, but it might be possible in bridge piers whose bars have been exposed over a few tens of centimetres (see Fig. 7-7).

Fig. 7-7 Plastic hinging formed at the base of bridge piers subsequent to the Kaikoura 2016 earthquake.

Finally, it could be argued that the method is still invasive: rebars must be removed from the building and then, when tested in the laboratory, it might be found that damage is not detected. This is a risk that at this stage must be taken; further studies using portable hardness testers based on the Vickers methodology are recommended. By contrast, if damage is detected, it could be possible to extend the results obtained from the single rebar to other rebars of the same structural element, according to the level of stress or strain determined from the structural analysis.

7.5 CONCLUSIONS

In this chapter, a least invasive method for damage assessment of Grade 300E steel rebars was proposed, based on a universal calibration curve (hardness versus strain). The method was applied to fifteen bars removed from RC buildings that were damaged during the Canterbury and Kaikoura earthquakes. The method demonstrated that is possible to quantify the residual strain capacity of damaged rebars using the following three parameters: Vickers hardness baseline, average peak Vickers hardness (of the damaged bar), and strain at UTS (of an undamaged sample of the same bar under investigation). Additional correlations between Vickers hardness and lower yield strength and ultimate tensile strength can be employed to determine the mechanical properties of the steel rebars at the damage locations. Because the strain hardening exponents and the ratio between ultimate and yield tensile strength vary significantly in other steel grades (430 and 500E), the universal calibration curve developed here is only applicable to Grade 300 steels.

7.6 REFERENCE

NZTA. (2016). Bridge manual (SP/M/022).

Palermo, A., Liu, R., Rais, A., McHaffie, B., Andisheh, K., Pampanin, S., Gentile, R., Nuzzo, I., Granerio, M., Loporcaro, G., McGann, C. . Wotherspoon, L. (2017). Performance of road bridges during the 14 November 2016 Kaikoura earthquake. *Bulletin of the New Zealand Society for Earthquake Engineering (under printing)*.

Priestley, M. J. N., Calvi, G. M., & Kowalsky, M. J. (2007). *Displacement-based seismic design of structures*. Pavia, Italy: IUSS Press.

Standards Australia and New Zealand. (2001). AS/NZS 4671:2001 *4671:2001 Steel reinforcing materials*. Wellington, New Zealand.

8 LOW-CYCLE FATIGUE (LCF) BEHAVIOUR OF NZ STEEL REINFORCEMENT

The last stage of the thesis consists of the investigation of the low-cycle fatigue (LCF) behaviour of Grade 300E steel reinforcement with a particular focus on the strain-ageing effects. Uniaxial tension/compression tests were conducted on unmachined steel reinforcing bars in order to derive strain versus life curves.

During earthquakes, steel reinforcing bars embedded in reinforced concrete columns, beams or walls could be subjected to large inelastic deformation in tension and compression as high as 6% strain, eventually leading the rebars to fracture due to low-cycle fatigue (Mander et al., 1994). This mode of failure was observed in laboratory testing and post-earthquake damage inspections. For example, fatigue fractures of longitudinal rebars were observed on circular bridge columns laboratory tested to constant and variable amplitude displacement histories, including selected ground motions (El-Bahy et al., 1999b; El-Bahy, Kunnath, Stone, & Taylor, 1999a).

LCF fracture of rebars was also observed in bridge piers during the recent Mw 7.8 Kaikoura earthquake in New Zealand (NZ). Although no fracture surface analysis was conducted, Fig. 8-1 and Fig. 8-2 showed that no necking occurred in the fractured rebars. The fatigue life was probably significantly affected by the severe buckling.

The current NZ standard for steel reinforcing materials AS/NZ 4671:2001 (Standards Australia and New Zealand, 2001) does not provide specific requirements for the fatigue strength of reinforcing bars. It only suggests that, if fatigue tests are required, an agreement between the parties should be reached. No other information can be found. Furthermore, the existing standard for the design of concrete structures NZ 3101:2006 (New Zealand Standards, 2006) does not include any specific section for low-cycle fatigue issues. However, numerous studies exist on the

LCF behaviour of reinforcing bars, including studies by Mander et al. (1994), Restrepo-Posada et al. (1994) Dodd and Restrepo-Posada (1995), Brown and Kunnath (2004), and Hawileh (2010a, 2010b, 2016).

Fig. 8-1 Fractured longitudinal reinforcing bars in a bridge pier close to the Mw 7.8 Kaikoura earthquake epicentre.

Fig. 8-2 Detail of a fractured longitudinal steel rebar.

Earthquakes are usually preceded and/or followed by other events of larger or smaller intensity; longitudinal steel failures might not occur during a first event, but in a subsequent one due to the cumulative damage. Seismic events can also occur several months apart and during this period, if the steel has experienced any post-yielding deformation during the first event, strain ageing takes place, modifying the mechanical properties of the material. Although, the LCF behaviour of rebars has been extensively studied, no previous research exists on the effects of strain ageing on the fatigue life of steel rebars. In this chapter, fatigue lives for unaged and aged 12-mm diameter reinforcing bars are compared. The strain amplitude versus fatigue-life curve of unaged Grade 300E steel is first determined. Then, specimens of the same grade, diameter and steel heat are subjected to a number of (pre-) cycles, aged and cyclically retested to failure. The objective is to determine to what degree the fatigue life of the aged samples changes.

The analysis of the experimental results is performed using the strain-based approach method. The method considers the plastic deformation occurring at locations such as stress raisers where fatigue cracks start. This is typical in ductile materials subjected to large inelastic strain and short lives (Dowling, 2013). During this research, fatigue crack initiation was observed to occur at the base of the steel ribs, which is consistent with what was observed by Brown and Kunnath (2004).

8.1 LCF TESTS ON CURRENT NZ STEEL GRADE 300E

8.1.1 Monotonic benchmark test

The 12-mm diameter steel reinforcing bars received from Pacific Steel (www.pacificsteel.co.nz) were tested monotonically to obtain the basic mechanical properties and are shown in Table 8-1.

The stress–strain curve (see Fig. 8-3) showed that the 12-mm diameter rebars do not exhibit the discontinuous yielding point, thus the yield stress was determined as the 0.2% proof stress. The results obtained confirmed that the material's mechanical properties complied with the standard requirements (Standards, Australia and New Zealand, 2001) .

Table 8-1 Basic mechanical properties

Specimen code	Yield strength [MPa]	Ultimate tensile strength [MPa]	Ultimate tensile strain [mm/mm]
Monotonic Sample 1	330	446	0.186
Monotonic Sample 2	307	442	0.200
Monotonic Sample 3	305	452	0.192

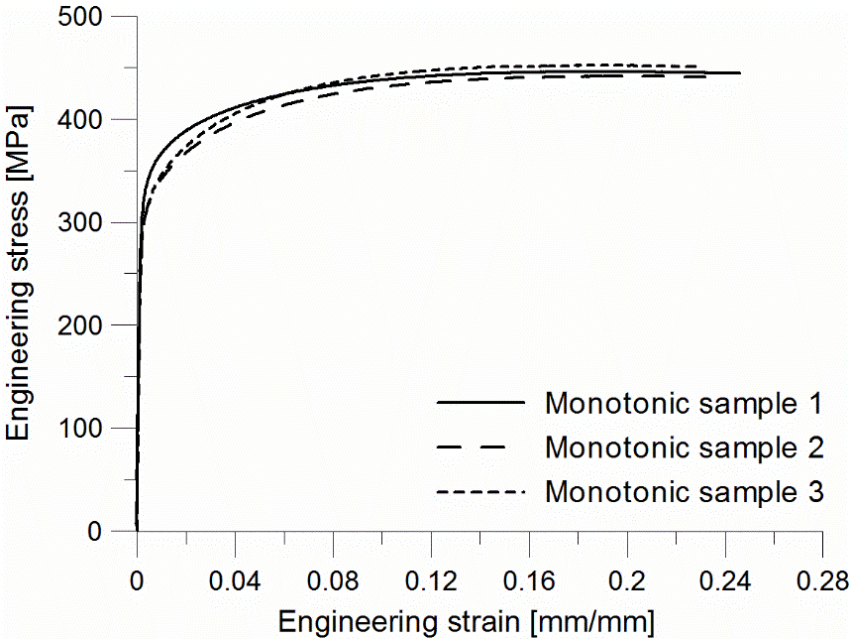

Fig. 8-3 Stress–strain curves of the benchmark samples.

8.1.2 Experimental tests

The strain-life curve for steel Grade 300E reinforcing bars of 12-mm diameter was first derived. Steel specimens were subjected to completely reversed cyclic loading (R = −1) between constant-strain limits (see Fig. 8-4). In order to subject the samples to a constant-strain amplitude, tests were required to be conducted in strain control. Fatigue-life curves were obtained by applying a number of strain amplitude cyclic histories, maintaining the mean strain equal to zero. The fatigue life is determined for each strain limit and plotted in a strain-life diagram on log–log coordinates (see Fig. 2-37) (Dowling, 2013).

The test set-up was designed with consideration of the laboratory constraints such as the 100 kN load capability of the MTS 810 machine, the geometry of the vee-wedge devices for gripping the steel samples, the extensometer dimensions and the travel lengths. The most suitable bar diameter size was 12 mm.

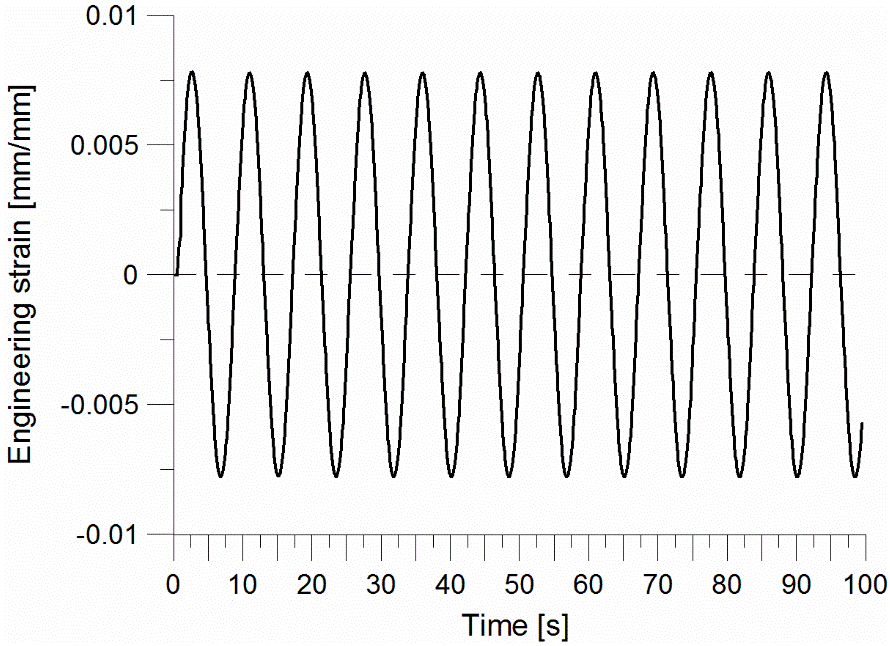

Fig. 8-4 Example of a typical cyclic strain history applied to the steel specimens.

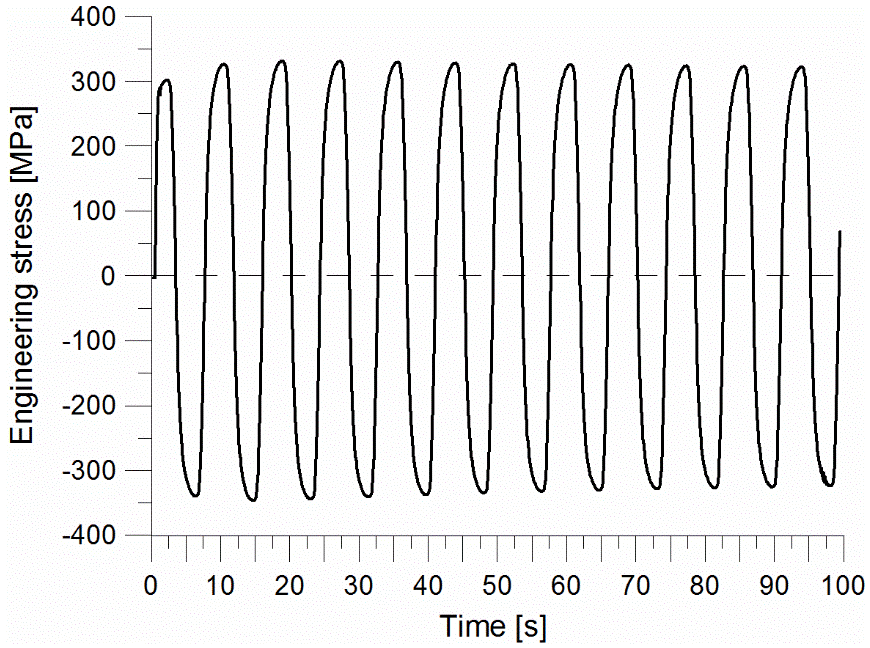

Fig. 8-5 Example of a stress history obtained from one fatigue test.

Strain-controlled tests are routine practice in material testing in the case of machined specimens that are designed to avoid buckling. In such experiments, specimens are machined to either a smooth cylinder (uniform-gauge specimen) or an hour-glass shape (ASTM, 2012c) and the surface finish is often polished. The specimen geometry and the surface finish allow the strain device to be attached to the specimen, usually an extensometer, to measure the strain and control the actuator motion with a very small risk of slippage. The ratio between specimen gauge length and cross sectional area is sufficiently small to avoid buckling (Dowling, 2013). However, since the objective of the test was to determine the low-cycle fatigue behaviour of reinforcing bars used in concrete members, the original geometry of the rebars was maintained and buckling was not prevented. Strain-controlled cyclic tests conducted on unmachined rebars prone to buckling could potentially cause machine instability when the extensometer controlling the tensile machine is directly attached to the testing specimen.

Fig. 8-6 Example of steel reinforcing bar specimen used during the test. The white marks define the unsupported length.

Preliminary tests were conducted on 180-mm long unmachined rebar samples (see Fig. 8-6). The unsupported length s of the specimen was 72 mm, which is six times the bar diameter d_b. White marks were placed on each specimen 72 mm apart to identify the unsupported length. This value was suggested by Mander et al. (1994) and confirmed by Brown and Kunnath (2004). They compared the cyclic behaviour of specimens with ratios s/d_b of 6, 8 and 9. It was observed that for samples with a ratio s/d_b of 6, the tension and compression stress–strain curves were similar; the only exception was that the ultimate stress in the compression range was observed at a lower strain. Samples with ratios s/d_b larger than 6 experienced a decrease in the ultimate compressive stress and strain due to the significant buckling.

The preliminary tests confirmed the stability problems of the MTS machine caused by the buckling of the rebars when the 25-mm gauge length extensometer used to control the actuator motion was attached to the specimen. In addition, accurate strain measurements could not be obtained when the bars buckled, especially during the compression half-cycle. In order to avoid these issues, Mander et al. (1994) used a custom-made extensometer. It was mounted over the central three-bar-diameter gauge length whose extremes corresponded to the expected inflection points of the buckled specimens.

Since controlling the tensile machine with the extensometer attached to the steel specimen was not viable, an alternative method to conduct strain-controlled fatigue tests was proposed. Henceforth, this method will be referred as the “indirect method”. A steel device was rigidly mounted to the top and bottom head of the tensile machine. As can be seen in Fig. 8-7, the device was made by two L-shaped steel elements welded to two smooth steel rods. The extensometer responsible for controlling the machine was attached to the top and bottom rods. Initially, a 50-mm gauge length extensometer was used; however, the extensometer showed some issues. The

electrical output signal was not stable and provided fluctuations in the strain reading. This issue caused an irregular strain history pattern and unusable results. Therefore, an adjustable gauge length extensometer was used instead, in which the gauge length was set to 25 mm. This extensometer was selected as it provided the lowest signal error (10^{-5} mm/mm strain).

Fig. 8-7 Initial test set-up employed in order to perform the low-cycle fatigue tests.

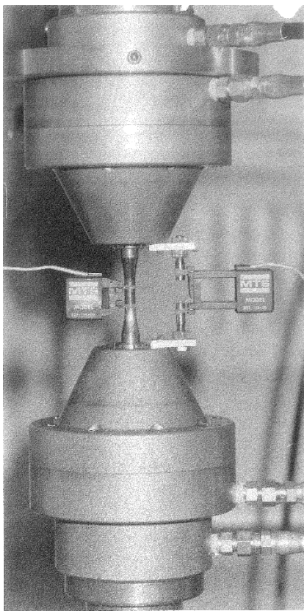

Fig. 8-8 Test set-up proposed by Dowling (courtesy of Norman Dowling).

The indirect method required an initial calibration (Dowling, 1977). For this purpose, two extensometers were used: one was attached directly to the steel specimen and another ("external extensometer") was placed on the external steel device. Three monotonic tensile tests, with both extensometers, were conducted in order to calibrate the relationship between the "real" strain in the material (ε), and the strain measured by the external extensometer (v).

The calibration was performed using the following procedure:

- the elastic modulus of the material (E) was measured from the actual stress–strain curve (σ–ε); an elastic constant (K) was also obtained using the stress–"displacement" curve (σ–v) derived using the external extensometer;
- the plastic strain $\varepsilon_p = \varepsilon - \frac{\sigma}{E}$ and the "plastic displacement" $v_p = v - \frac{\sigma}{K}$ were calculated;
- ε_p and v_p were plotted on log–log coordinates (Fig. 8-9) and a power equation relationship was obtained:

$$\varepsilon_p = 0.3395\ v_p^{1.0885}\ ; \tag{8-1}$$

- the strain limits (ε) that will be used in the test were selected; the equation above was used to determine v, the "displacement" limits to apply to the external extensometer.

The calibration process was applied on a monotonic tensile test to verify the method. Fig. 8-10 compares the actual stress–strain curve with the "calibrated" stress–strain curve obtained using the relationship derived. Fig. 8-10 demonstrates that the calibrated curve approximates the actual one reasonably well.

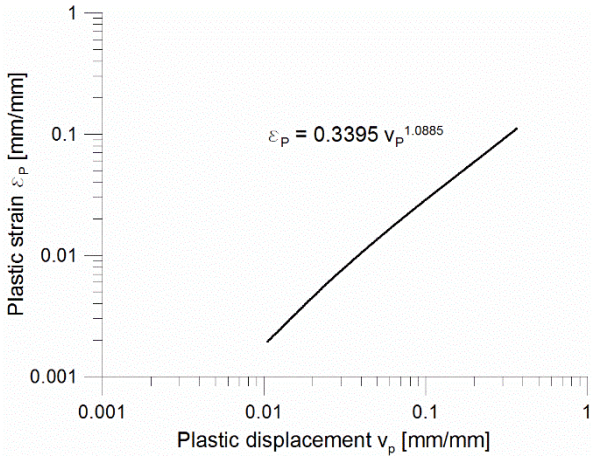

Fig. 8-9 Plastic strain ε_p versus plastic displacement v_p curve on log–log coordinates.

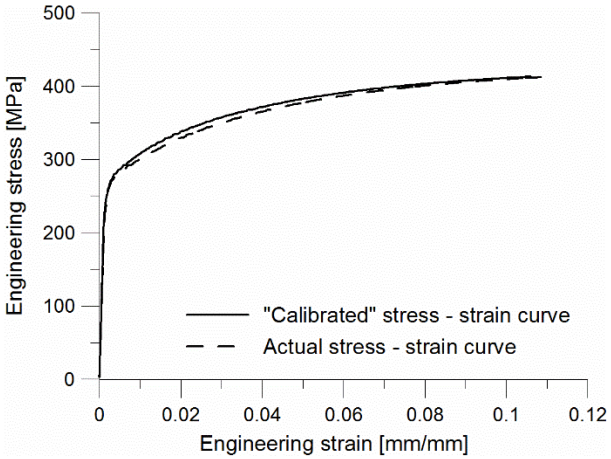

Fig. 8-10 "Calibrated" versus actual stress–strain curves.

The reliability of the calibration relationship having been verified, the constant-strain limits (amplitude) were selected. Due to limitations of the extensometer travel lengths in compression, the maximum strain amplitude allowable was 0.03 mm/mm. The wave type selected was sinusoidal. The frequency was determined based on an empirical relationship derived by Professor Norman Dowling (2016):

$$f = \frac{0.0008}{\varepsilon_{pa}} \tag{8-2}$$

where f is the test frequency and ε_{pa} is the plastic strain amplitude. This relationship gives a constant average strain rate for sinusoidal loading that is low enough to avoid heating of the sample due to dissipation of plastic strain energy. The sample rate was approximately 200 measurements per cycle. Sample codes, strain limits, and frequencies selected are presented in Table 8-2.

Table 8-2 Low-cycle fatigue tests initial parameters and results

Sample code	Strain amplitude (Strain limits)	Plastic strain amplitude	Frequency [Hz]	No. cycles to failure
01	0.0078	0.0061	0.12	125
02	0.0078	0.0062	0.12	130
03	0.0083	0.0067	0.12	98
04	0.0107	0.0089	0.11	61
05	0.0140	0.0121	0.09	34
06	0.0140	0.0121	0.09	32
07	0.0178	0.0156	0.06	14
08	0.0179	0.0160	0.06	16
09	0.0179	0.0160	0.06	13
10	0.0271	0.0250	0.04	6
11	0.0272	0.0252	0.04	6
12	0.0275	0.0254	0.04	7

8.1.3 Results

Examples of the stress–strain curves obtained during the tests are presented in Fig. 8-11, Fig. 8-13, Fig. 8-15. The curves show that, for the strain levels investigated, Grade 300E exhibited cycle-dependent hardening, where stress increases with the number of cycles until it reaches a stable hysteresis loop. In this case, as can be seen from Fig. 8-5, the stress increase occurred only after the first cycle, then the stress remained approximately constant until cracking started. This behaviour can also be observed in Fig. 8-12, where the normalised stress at reversal (f_i/f_0) is plotted against the number of cycles, where f_i is the stress at the reversal point during the i^{th} generic cycle, while f_0 is the stress at the first reversal. The stress at reversal differs in tension and compression. The graph shows how the normalised stress increased after the first cycle and then remained constant before dropping significantly before failure. The normalised stress at reversal vs. cycle number curves were also be used for determining the specimen's strain life. As observed by previous studies, an inflection point ("cusp formation") exists in the compressive region of the cyclic stress–strain curve at high strains (see for example Fig. 8-11) (Brown & Kunnath, 2004; Hawileh, Abdalla, et al., 2010; Mander et al., 1994). This phenomenon occurred approximately toward the end of the specimen fatigue life, when cracking initiated.

In order to determine the number of cycles to failure, the available literature was consulted. Lefebvre and Ellyin (1984) defined as fatigue failure the instant where the hysteresis loop started to distort and the maximum stress decreased. This corresponded to macrocracking formation and propagation. Mander et al. (1994) identified the fatigue life when the ratio f_i/f_0 drops significantly, for large-fatigue lives; and, visually for short-fatigue lives. Hawileh, Abdalla, et al. (2010) defined the LCF failure when the stress in the bar during the last cycle was half of the maximum stress in

the first cycle. In a subsequent test, they defined as failure the moment when the maximum stress dropped to 80% of the maximum stress obtained in the first cycle (Hawileh et al., 2016).

In this research two methods were used depending on the amount of strain amplitude applied to the specimen. In the case of those specimens subjected to a strain amplitude above 0.02 mm/mm, the life to failure was determined by counting the cycles when the first crack was visually observed. Cracking started at the base of the steel deformation on the bar surface, as these locations represented stress concentration points (see Fig. 8-17 and Fig. 8-18). When the strain amplitude was below 0.02 mm/mm, the normalised stress at reversal (f_i/f_0) versus number of cycles curves were used. Failure was determined when the ratio f_i/f_0, (tension) after the cycle-dependent hardening effect reached 1. The fatigue life of the tested specimen is presented in Table 8-2.

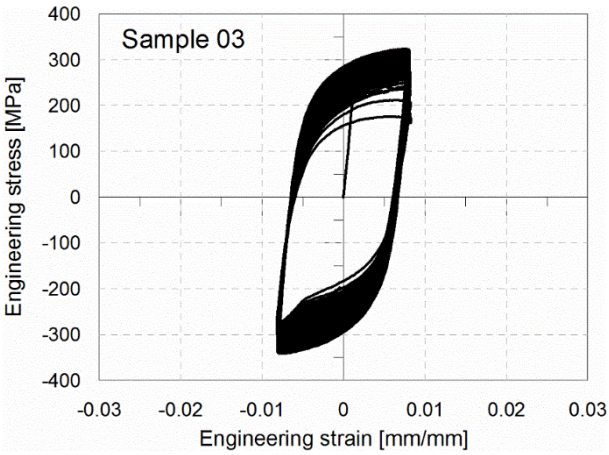

Fig. 8-11 Cyclic stress–strain curve for Sample 03.

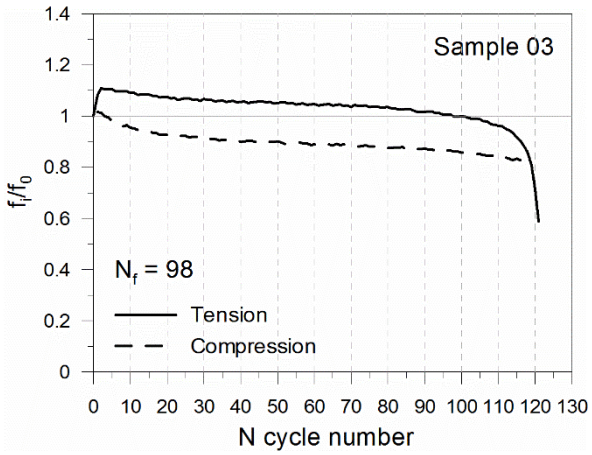

Fig. 8-12 Normalised stress at reversal versus number of cycles for Sample 03.

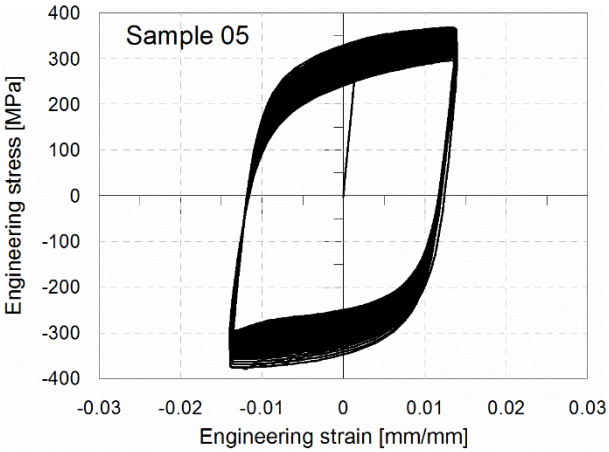

Fig. 8-13 Cyclic stress–strain curve for Sample 05.

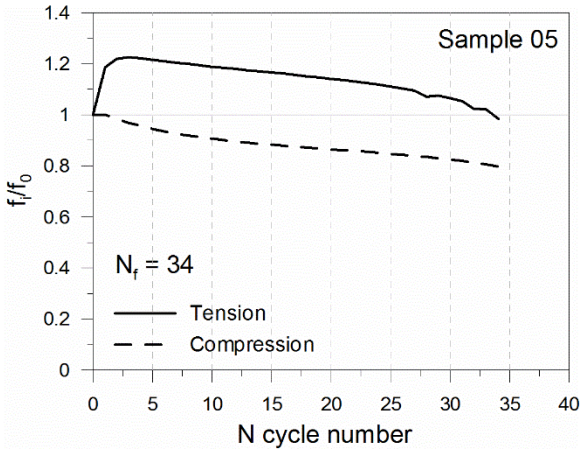

Fig. 8-14 Normalised stress at reversal versus number of cycles for Sample 05.

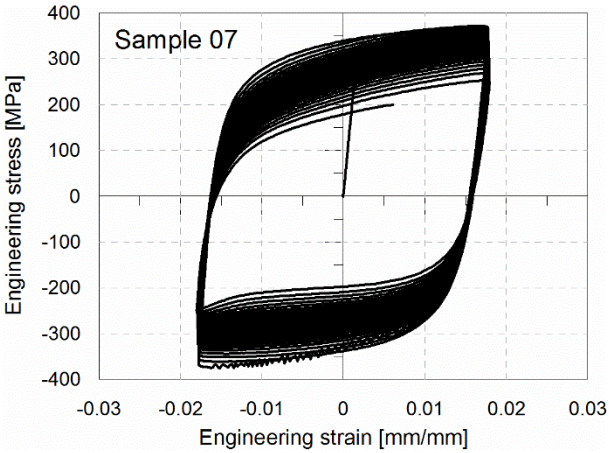

Fig. 8-15 Cyclic stress–strain curve for Sample 07.

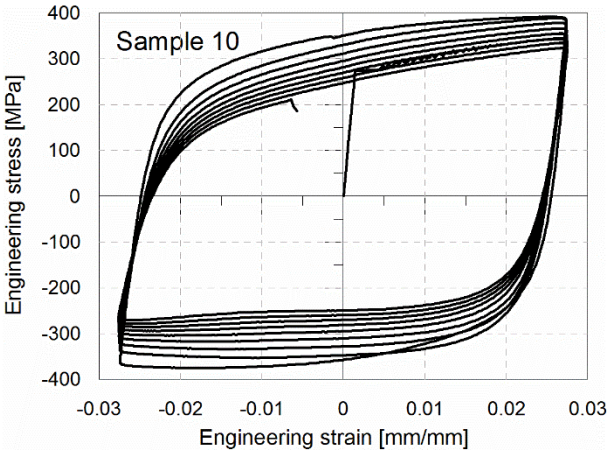

Fig. 8-16 Cyclic stress–strain curve for Sample 10.

Fig. 8-17 Example 1 of cracking initiating at the base of the steel ribs.

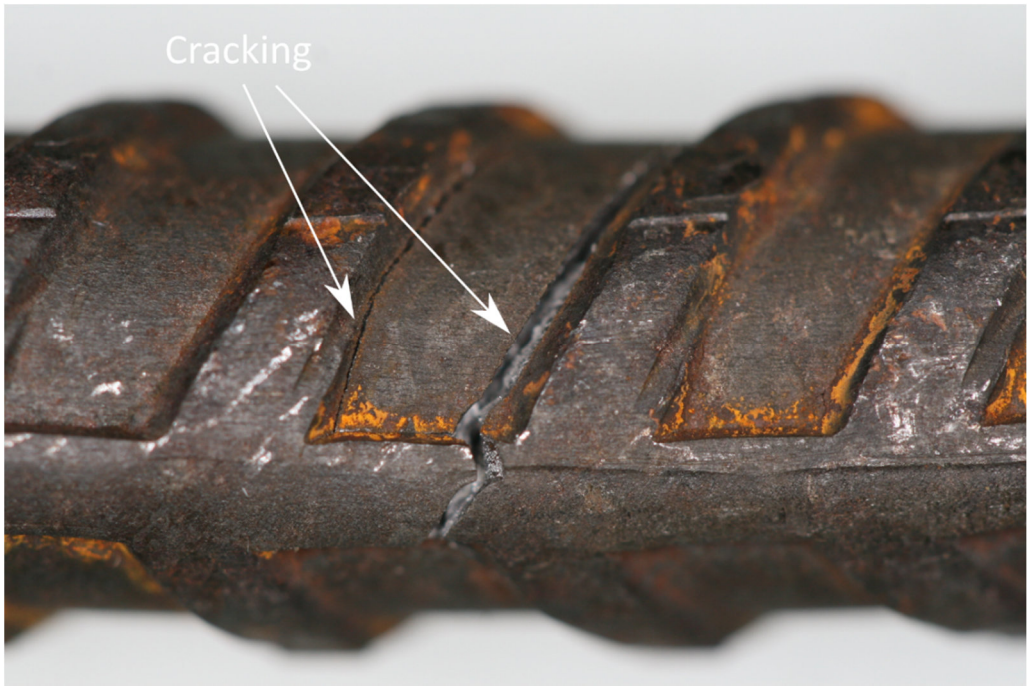

Fig. 8-18 Example 2 of cracking initiating at the base of the steel ribs.

8.1.4 Application of the fatigue models

Several strain-life fatigue models exist in literature. These models correlate the strain amplitude to the number of cycles to failure. The most common predictive strain–fatigue model is the Coffin–Manson, developed separately in the 1950s by Coffin (1954) and Manson (1953) (Dowling, 2013). This model requires the measurements of the total strain ε_a, the plastic strain ε_{pa}, and the stress σ_a amplitudes. Ideally, these quantities need to be measured during the stable hysteresis loop which occurs at approximately half of the specimen fatigue life. The Coffin–Manson relationship represents the total strain amplitude ε_a as the sum of the elastic strain amplitude ε_{ea}, the first term in the right-hand side of Equation (8-3), and the plastic strain amplitude $\varepsilon_{pa,}$ the second term in Equation (8-3):

$$\varepsilon_a = \frac{\sigma'_f}{E}\left(2N_f\right)^b + \varepsilon'_f\left(2N_f\right)^c \tag{8-3}$$

The coefficients σ_f, b, ε_f, and c are material dependent. They are determined by performing a linear regression analysis.

Based on the experimental data, the coefficients were calculated and Equation (8-3) became:

$$\varepsilon_a = 0.0025\left(2N_f\right)^{-0.076} + 0.080\left(2N_f\right)^{-0.464} \tag{8-4}$$

In Fig. 8-19 and Fig. 8-20, the elastic and the plastic strain amplitudes versus fatigue life are plotted separately. In Fig. 8-21, the fatigue life curve is plotted in terms of the total strain amplitude. The fitting curve described by Equation (8-4) is plotted for the life range $N_f = 6$ to 130. Then in Fig. 8-22, the Coffin–Manson relationship is projected to $N_f = 10^5$. The elastic and plastic strain curves are superimposed on the total strain curve. Since LCF failures are governed by large plastic deformation, the total strain amplitude versus fatigue-life curve is very well approximated

by the plastic strain curve at large strain amplitudes. The relationship obtained by considering only the plastic contribution is:

$$\varepsilon_{pa} = 0.080\left(2N_f\right)^{-0.464} \tag{8-5}$$

The R^2 value was 0.989. This is consistent with the results obtained by Mander et al. (1994) for ASTM A615 (1987) Grade 40 deformed billet-steel reinforcing bars:

$$\varepsilon_{pa} = 0.08\left(2N_f\right)^{-0.5} \tag{8-6}$$

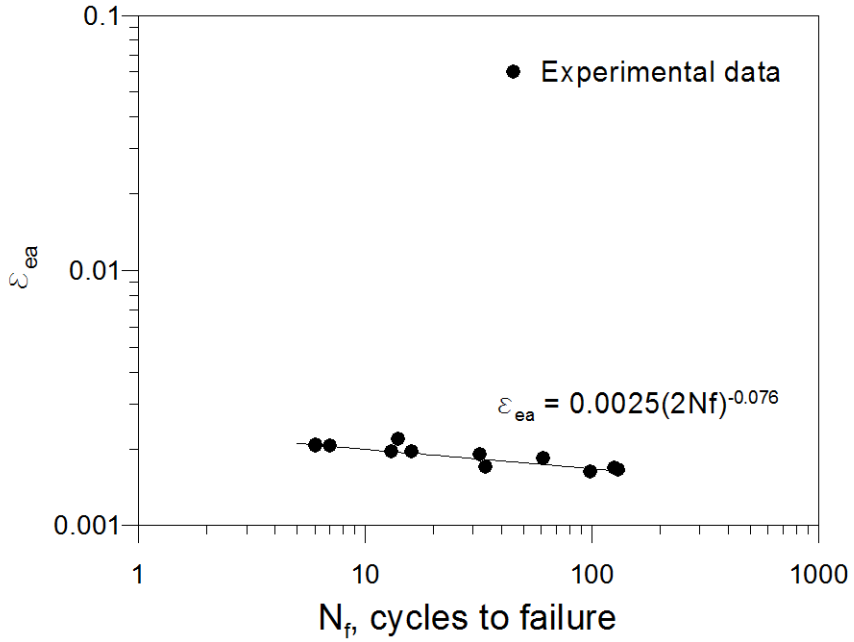

Fig. 8-19 Elastic strain amplitude versus fatigue life.

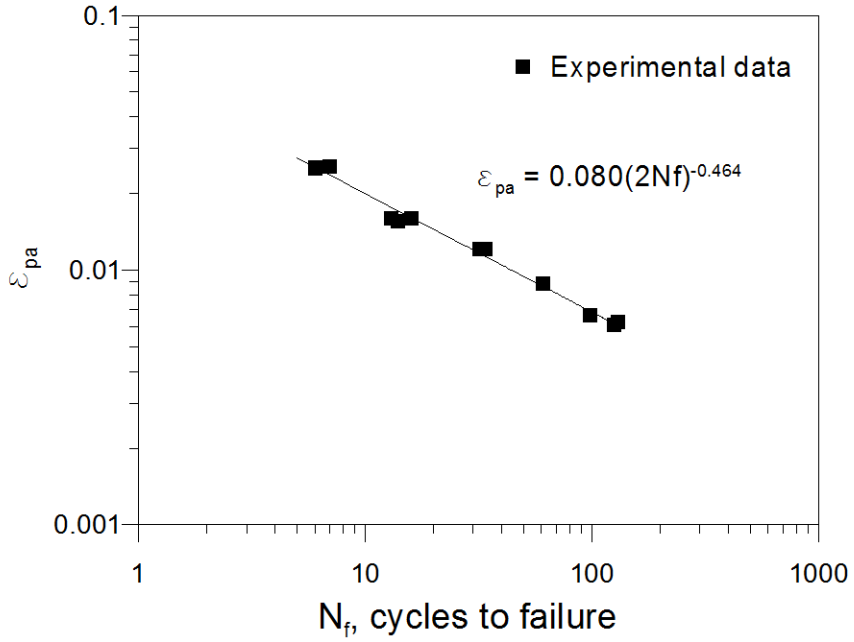

Fig. 8-20 Plastic strain amplitude versus fatigue life.

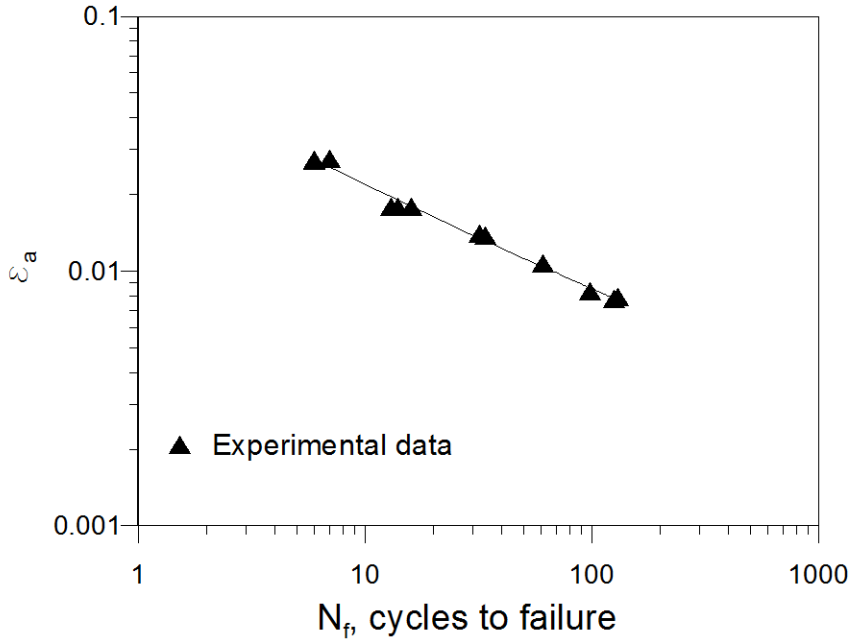

Fig. 8-21 Total strain amplitude versus fatigue life fitted with the Coffin–Manson model.

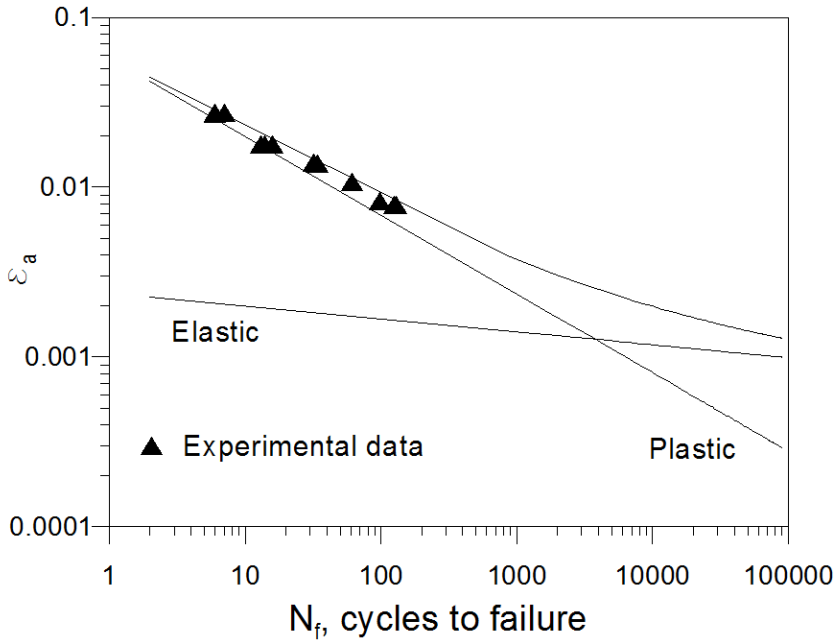

Fig. 8-22 Total, elastic and plastic strain amplitude versus fatigue-life curves.

Koh and Stephens (1991) provided an alternative model to the Coffin–Manson model. They observed that the Coffin–Mason model did not provide conservative predictions for shorter lives (below 50 cycles). The alternative model relates the fatigue life N_f, to the total strain amplitude ε_a, and is described by the equation (Stephens & Koh, 1988):

$$\varepsilon_a = M\left(2N_f\right)^m \tag{8-7}$$

The coefficient M = 0.0755 and exponent m = –0.412 were derived by performing a linear regression analysis. The calculated R^2 value was 0.990. Substituting the coefficient obtained in Equation (8-7), the Koh–Stephens equation for NZ-manufactured Grade 300E 12-mm diameter steel reinforcing bar became:

$$\varepsilon_a = 0.0755\left(2N_f\right)^{-0.412} \tag{8-8}$$

The curve is plotted in Fig. 8-23.

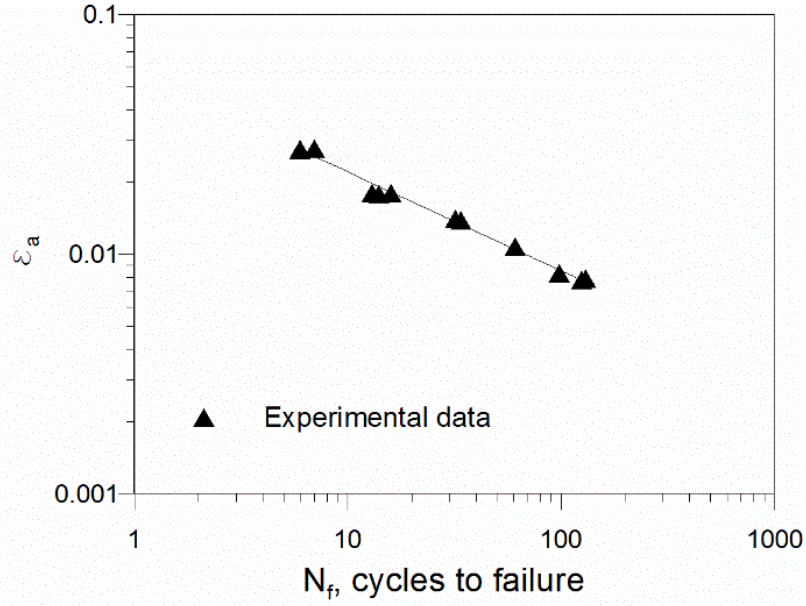

Fig. 8-23 Total strain amplitude versus fatigue life fitted with the Koh–Stephens model.

Coffin–Manson (only plastic strain) and Koh–Stephens models provided similar results. The high coefficient of determination R^2 suggested an extremely good correlation between the experimental results and the fatigue-life predictions. Therefore, both models provided a good approximation of the fatigue life. This first part of the experimental testing campaign was conducted to provide the benchmark low-cycle fatigue life of Grade 300E steel reinforcing bars. In the next section, the results obtained are used as a benchmark to quantify the change in the fatigue life caused by strain ageing.

8.2 STRAIN-AGEING EFFECTS ON THE FATIGUE LIFE

In this chapter the effects of strain ageing on the fatigue life of steel rebars are investigated. The material tested is obtained from the same source and heat as in the experiment described in Section 8.1. Reinforcing bar samples were cyclically tested between the same constant-strain limits selected in the previous experiment. The adopted protocol required that the specimens are first precycled, then aged at 100°C and finally cyclically loaded again (at the same strain amplitudes) until failure. Two experimental series were performed. In the first experiment, the bar specimens were first cyclically loaded up to 33% of the fatigue life previously obtained before ageing. In the second experiment, the number of precycles was equal to the 66% of the original fatigue life. Results and details of both experiments are presented in the following sections.

8.2.1 Effects of strain ageing on LCF life: Experimental test 1

For practical reasons, six specimens were tested in Experiment 1. The strain amplitudes selected are shown in Table 8-3. They are the same as in the experiment conducted on the unaged samples. Based on the original fatigue life, the number of precycles to which each specimen was subjected was calculated. This corresponded to 33% of the original fatigue life. Details are in Table 8-3.

After the precyclic loading phase, the six specimens were "artificially" aged at 100°C for four hours in boiling water, following the same protocol described in the previous chapters. After ageing, the samples were remounted on the tensile testing machine, maintaining the same unsupported length defined by the white marks on the specimen (Fig. 8-6). The specimens were then cyclically loaded again until failure; the strain amplitudes applied did not change. The cycles to failure determined after ageing were summed to the number of precycles, and the total fatigue life of the aged specimens was obtained.

A comparison between the fatigue life of the unaged and aged specimens is showed in Table 8-3. A reduction in fatigue life is evident. For the sample subjected to the smallest strain amplitude (sample 1.33), the reduction in fatigue life was approximately 15%, whereas in the other cases, the life reduction was higher and ranged from 26% to 50%. This outcome might be explained by the fact that large plastic deformation governs the LCF behaviour of materials, and strain ageing reduces the capacity of the material to plastically deform.

Table 8-3 LCF fatigue "aged" tests: initial parameter and results (Experiment 1).

Sample code	**Strain amplitude**	**Original fatigue life**	**Precycles applied**	**Cycles to failure after precycling**	**Total number of cycles to failure**	**Change in total fatigue life [%]**
1.33	0.0078	125	42	66	108	–14
3.33	0.0083	98	32	37	69	–30
4.33	0.0107	61	20	25	45	–26
6.33	0.0140	32	11	12	23	–28
8.33	0.0179	16	5	3	8	–50
12.33	0.0275	7	2	3	5	–29

A further observation can be made by comparing the expected remaining life (calculated as the difference between the original fatigue life and the precycles applied) with the actual remaining life. A drastic reduction in fatigue life can be observed in the results presented in Table 8-4. The remaining fatigue-life loss varied from 20% to 70%. However, on average the loss was approximately 43%.

Table 8-4 Remaining fatigue-life loss due to strain ageing (Experiment 1).

Sample code	Strain amplitude	Expected remaining life with no strain ageing	Actual remaining life with strain ageing.	Loss due to strain ageing [%]
1.33	0.0078	83	66	20.5
3.33	0.0083	66	37	43.9
4.33	0.0107	41	25	39.0
6.33	0.0140	21	12	42.9
8.33	0.0179	11	3	72.7
12.33	0.0275	5	3	40.0

The Coffin–Manson and Koh–Stephens models were used to fit the experimental data. Regression analyses were performed to determine the coefficients σ_f, b, ε_f, c for the first model, and M and m for the second. Equations (8-9) and (8-10) were obtained using the Coffin–Manson model:

$$\varepsilon_a = 0.0025\left(2N_f\right)^{-0.076} + 0.067\left(2N_f\right)^{-0.456} \quad (8\text{-}9)$$

$$\varepsilon_{pa} = 0.067\left(2N_f\right)^{-0.456} \quad (8\text{-}10)$$

The coefficient of determination for equation (8-10) was 0.971.

The Koh–Stephens equation derived was:

$$\varepsilon_a = 0.064\left(2N_f\right)^{-0.404} \quad (8\text{-}11)$$

The coefficient of determination was $R^2 = 0.967$.

Equation (8-10) is plotted in Fig. 8-24, superimposed on the unaged strain–fatigue-life curve. Both curves are approximately parallel but shifted because the fatigue life of the aged samples is shorter. Similar results can be observed when the total strain amplitude is plotted versus the fatigue life using both the Coffin–Manson (see Fig. 8-25), and the Koh–Stephens (Fig. 8-26) equations.

In summary, both models provided a very good approximation of the experimental results: the coefficients of determination was close to 1. Most importantly, the fatigue life of the specimens was reduced due to strain ageing. The magnitude of this reduction varied depending on the strain amplitude.

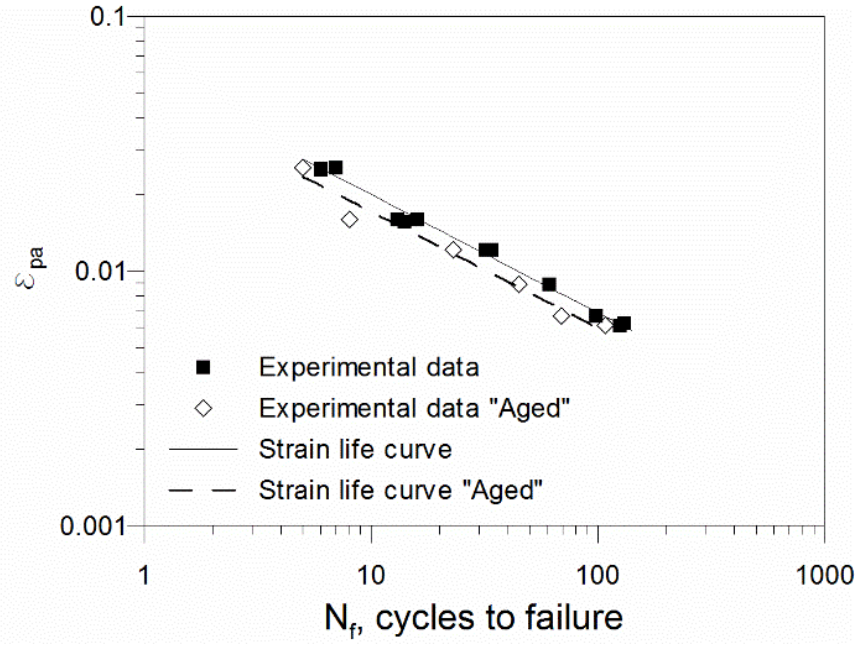

Fig. 8-24 Comparison between unaged and aged samples (33% precycled). Coffin–Manson model using plastic strain.

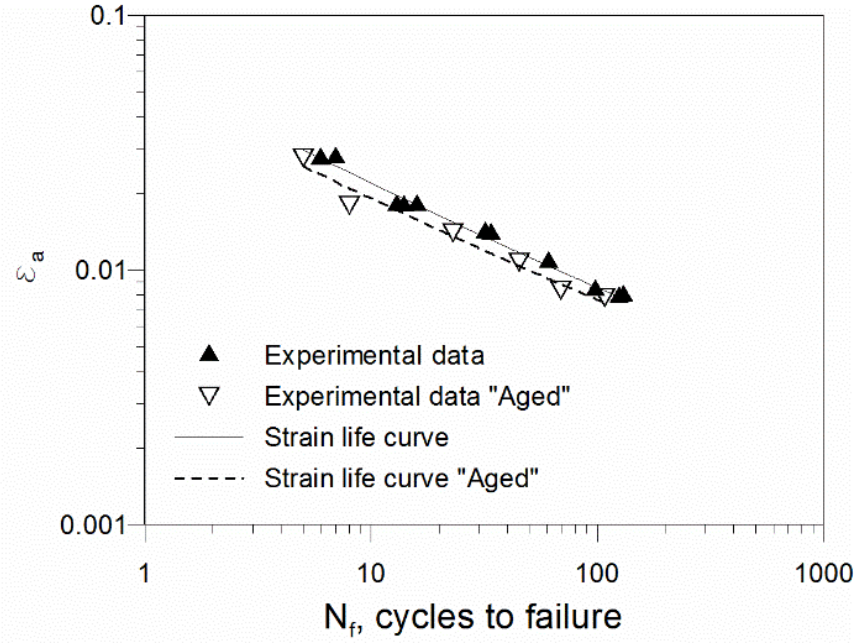

Fig. 8-25 Comparison between unaged and aged samples (33% precycled). Coffin–Manson model using total strain.

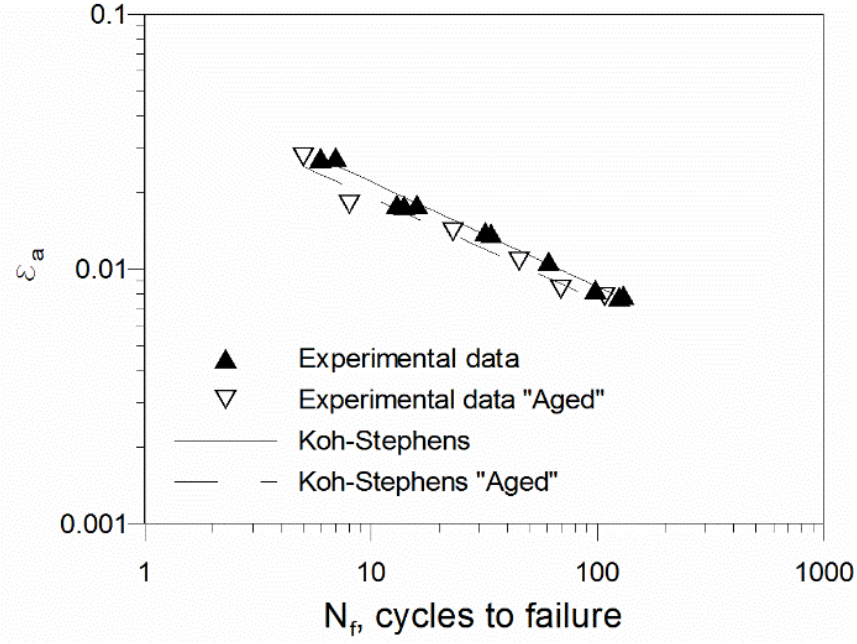

Fig. 8-26 Comparison between unaged and aged samples (33% precycled). Koh–Stephens model.

8.2.2 Effects of strain ageing on LCF life: Experimental test 2

The second experiment consisted of applying 66% of the original fatigue life to each specimen before ageing. The test protocol adopted was the same as in Section 8.2.1. Initial inputs and fatigue-life results are shown in Table 8-5. A reduction in fatigue life due to strain ageing was observed also in Experiment 2. This reduction varied by between 14% and 24%.

Table 8-5 LCF fatigue "aged" tests initial parameter and results (Experiment 2)

Sample code	Strain amplitude	Original fatigue life	Precycles applied	Cycles to failure after precycling	Total number of cycles to failure	Change in total fatigue life [%]
1.66	0.0078	125	84	18	102	–18
3.66	0.0083	98	65	9	74	–24
4.66	0.0107	61	40	8	48	–21
6.66	0.0140	32	21	6	27	–16
8.66	0.0179	16	10	3	13	–19
12.66	0.0275	7	4	2	6	–14

The same comparison made in Section 8.2.1 between the expected and actual remaining life is proposed also for Experiment 2 (see Table 8-6). In this case, the reduction in the remaining fatigue life was more dramatic. It ranged from 33% to 73%, with an average loss of about 53%. Therefore, given the same amount of ageing time, the larger the amount of precycling, the more significant is the remaining fatigue-life loss.

Table 8-6 Remaining fatigue-life loss due to strain ageing (Experiment 2).

Sample code	Strain amplitude	Expected remaining life with no strain ageing	Actual remaining life with strain ageing.	Loss due to strain ageing [%]
1.66	0.0078	41	18	56.1
3.66	0.0083	33	9	72.7
4.66	0.0107	21	8	61.9
6.66	0.0140	11	6	45.5
8.66	0.0179	6	3	50.0
12.66	0.0275	3	2	33.3

The Coffin–Manson and Koh–Stephens fatigue models were used again to fit the experimental results. The Coffin–Manson relationship for total strain amplitude obtained was:

$$\varepsilon_a = 0.0025\left(2N_f\right)^{-0.076} + 0.088\left(2N_f\right)^{-0.507} \quad (8\text{-}12)$$

If considering only the plastic strain, (8-12) becomes:

$$\varepsilon_{pa} = 0.088\left(2N_f\right)^{-0.507} \quad (8\text{-}13)$$

In this case the scatter is negligible as demonstrated by the $R^2 = 0.994$, very close to 1.

Similarly, the Koh–Stephens model provided the following result:

$$\varepsilon_a = 0.082\left(2N_f\right)^{-0.449} \quad (8\text{-}14)$$

The $R^2 = 0.993$ was also very close to 1.

In Fig. 8-27, Fig. 8-28 and Fig. 8-29 the fatigue models developed for the aged samples are compared with the unaged. The two curves are not parallel: at shorter fatigue lives the curves almost coincide, while at larger fatigue lives, the effect of strain ageing becomes more significant. This is easily explained because at short lives, in the order of 6 to 7 cycles, the number of precycles (66% of the original fatigue life) is approximately 4 to 5, which is close to the fatigue life. Only 1 or 2 cycles are sufficient to reach the original fatigue life. In other words, for strain amplitudes

above 2%, the effects of strain ageing could be neglected if the number of cycles experienced is approximately two-thirds of the fatigue life.

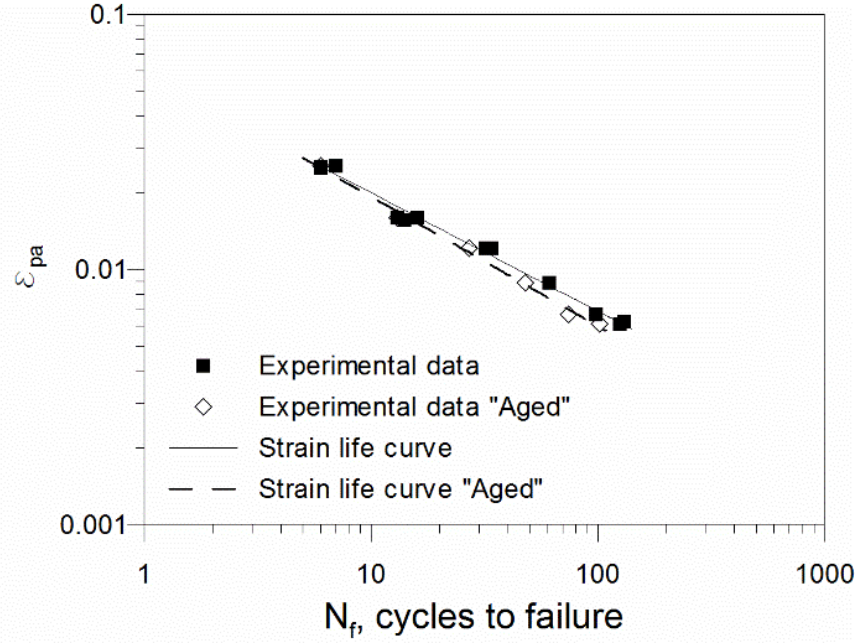

Fig. 8-27 Comparison between unaged and aged samples (66% precycled). Coffin–Manson model using plastic strain.

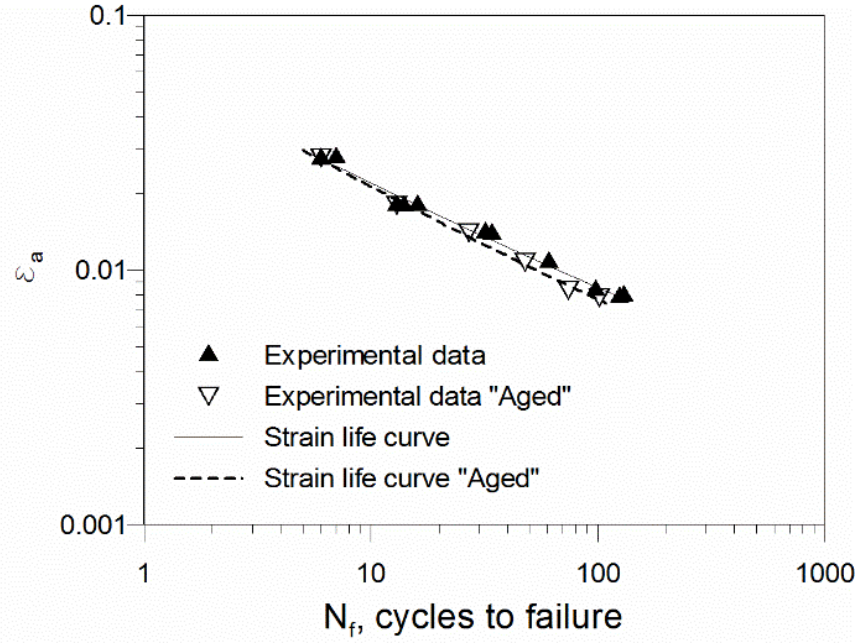

Fig. 8-28 Comparison between unaged and aged samples (33% precycled). Coffin–Manson model using total strain.

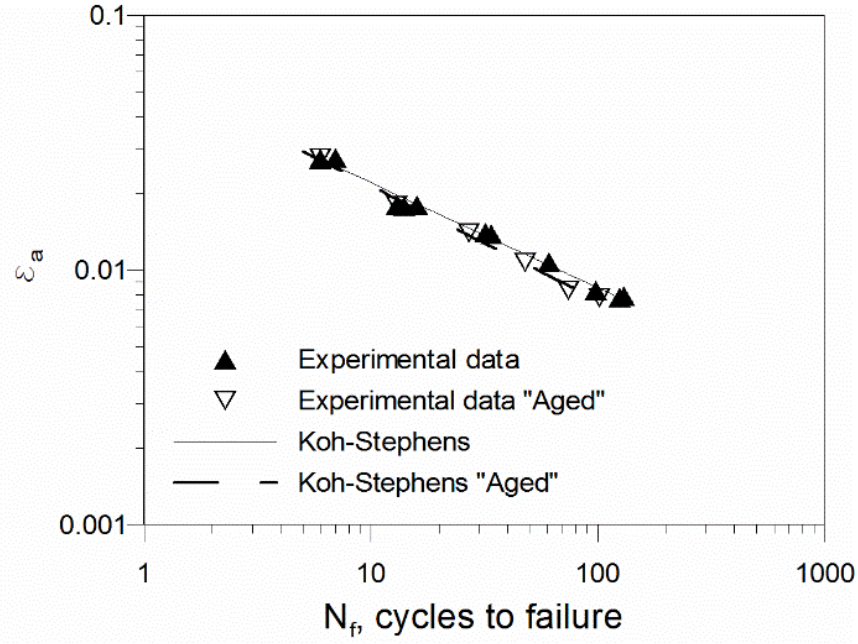

Fig. 8-29 Comparison between unaged and aged samples (33% precycled). Koh–Stephens model.

8.3 CONCLUSIONS

In this chapter the reduction in the LCF life of local manufactured Grade 300E steel 12 mm diameter reinforcing bars was determined. An indirect method, which required a calibration, was used to control the MTS 810 tensile machine. Strain-life fatigue curves were obtained from constant-strain-amplitude cyclic-loading tests. The experimental results were fitted using the Coffin–Manson and Koh–Stephens fatigue models. The experimental results obtained from the unaged specimens were used as a benchmark to calculate the fatigue-life loss due to strain ageing.

The following conclusions were drawn:

- The strain–fatigue-life equation determined as a benchmark was consistent with previous works conducted by Mander et al. (1994), and Brown and Kunnath (2004).
- Experiments demonstrated that strain ageing reduced the expected fatigue life of 12-mm Grade 300E steel rebars. The expected fatigue life for precycled samples was dramatically reduced. For example, the expected remaining life of rebars precycled at 1% constant-strain amplitude up to 66% of the original fatigue life was reduced by 62%, from 21 to 8 cycles.
- Strain–fatigue-life models were successfully applied on the aged Grade 300E samples. The coefficient of determinations were between 0.97 and 0.99. The modified fatigue-life relationship derived might be used to determine the LCF fatigue effects on structures subjected to earthquake sequences (Mander & Rodgers, 2015).

8.4 REFERENCES

ASTM. (2012). E606/E606M *Standard Test Method for Strain-controlled Fatigue Testing*. West Conshohocken, PA, United States.

Brown, J., & Kunnath, S. K. (2004). Low-cycle fatigue failure of reinforcing steel bars. *ACI materials journal, 101*(6).

Coffin, J. (1954). A Study of the Effects of Cyclic Thermal Stresses on a Ductile Metal. *Trans. of the American Society of Mechanical Engineers, 76*.

Dodd, L., & Restrepo-Posada, J. (1995). Model for Predicting Cyclic Behavior of Reinforcing Steel. *Journal of Structural Engineering, 121*(3), 433-445.

Dowling, N. E. (1977). Crack growth during low cycle fatigue of smooth axial specimens. *Stress strain and plastic deformation aspects of fatigue crack growth, ASTM STP 637*, 97-121.

Dowling, N. E. (2013). *Mechanical behavior of materials: engineering methods for deformation, fracture, and fatigue* (Fourth Edition ed.): Pearson.

Dowling, N. E. (2016). [Personal Communication].

El-Bahy, A., Kunnath, S., Stone, W., & Taylor, A. (1999b). Cumulative seismic damage of circular bridge columns: Variable amplitude tests. *ACI Structural Journal, 96*(5).

El-Bahy, A., Kunnath, S. K., Stone, W. C., & Taylor, A. W. (1999a). Cumulative seismic damage of circular bridge columns: Benchmark and low-cycle fatigue tests. *ACI Structural Journal, 96*(4).

Hawileh, Abdalla, J., Oudah, F., & Abdelrahman, K. (2010). Low-cycle fatigue life behaviour of BS 460B and BS B500B steel reinforcing bars. *Fatigue & Fracture of Engineering Materials & Structures, 33*(7), 397-407.

Hawileh, Rahman, A., & Tabatabai, H. (2010). Evaluation of the Low-Cycle Fatigue Life in ASTM A706 and A615 Grade 60 Steel Reinforcing Bars. *Journal of Materials in Civil Engineering, 22*(1), 65-76.

Hawileh, Tabatabai, H., Abu-Obeidah, A., Balloni, J., & Rahman, A. (2016). Evaluation of the Low-Cycle Fatigue Life in Seven Steel Bar Types. *Journal of Materials in Civil Engineering, 28*(5).

Koh, S., & Stephens, R. (1991). Mean stress effects on low cycle fatigue for a high strength steel. *Fatigue & Fracture of Engineering Materials & Structures, 14*(4), 413-428.

Lefebvre, D., & Ellyin, F. (1984). Cyclic response and inelastic strain energy in low cycle fatigue. *International Journal of Fatigue, 6*(1), 9-15.

Mander, J., Panthaki, F., & Kasalanati, A. (1994). Low-cycle fatigue behavior of reinforcing steel. *Journal of Materials in Civil Engineering, 6*(4), 453-468.

New Zealand Standards. (2006). NZS 3101:2006 *Concrete structures standard*. Wellington.

Restrepo-Posada, J., Dodd, L., Park, R., & Cooke, N. (1994). Variables Affecting Cyclic Behavior of Reinforcing Steel. *Journal of Structural Engineering, 120*(11), 3178-3196.

Standards, A. a. N. Z. (2001). AS/NZS 4671:2001 *4671:2001 Steel reinforcing materials*. Wellington, New Zealand.

Stephens, R. I., & Koh, S. K. (1988). Improvements in empirical representation of A356-T6 cast aluminum alloy round-robin low cycle fatigue data. *SAE SP-760*, 29-38. doi:10.4271/881702

9 SUMMARY, CONCLUSIONS AND RECOMMENDATIONS FOR FUTURE STUDIES

The scope of this research was to develop a reliable, useful and least-invasive methodology to quantify the plastic deformation and estimate the residual strain capacity (ductility) of steel reinforcing bars embedded in reinforced concrete (RC) structures damaged during earthquakes. Over the research period, the author had the unique opportunity to apply and to validate the methodology developed on real case studies: RC buildings damaged during the 2010 and 2011 Christchurch earthquake events. At the time of writing, the "simplified methodology", presented in Chapters 5 and 7, is being successfully applied on Wellington (New Zealand) RC buildings damaged during the M_w7.8 Kaikoura earthquake on 14 November 2016.

In Section 9.1, the major findings obtained during the entire research are summarised with reference to the topics discussed in Chapters 3 to 8. In Section 9.2, the final conclusions and recommendations are provided. Finally, suggestions and recommendations for future studies are given in Section 9.3.

9.1 SUMMARY

9.1.1 The relationship between hardness and strain

The method is based on the main hypothesis that hardness increases with plastic strain and a robust relationship between them can be found. Hardness was selected as the key parameter because hardness testing is a practical, easily accessible, and an inexpensive method to obtain information about metals' properties such as strength and heat treatment (Dieter, 1976). More importantly, in materials subjected to work hardening, such as steel, plastic deformation increases yield strength, and yield strength is proportional to hardness (Tabor, 1951b); therefore hardness

and plastic strain could be correlated. Equations linking hardness and strain for steel reinforcing bars do not exist in the open literature, nor do standardised procedures exist to develop such relationships. In addition, correlations between residual ductility and hardness have never been attempted.

The hardness versus strain, and residual strain capacity versus hardness power-law curves developed verified the main hypothesis. If the Vickers hardness of the bars under investigation is known, the calibration curves allow the estimation of the plastic deformation, experienced – for example, during a seismic event – and predict the residual ductility at the location of damage. Prior to determining the above-mentioned relationships, it was necessary to identify:

- the most suitable hardness testing technique
- the surface-preparation procedure for the hardness testing
- the strain range of interest.

Suitable hardness testing technique

Hardness testing machines (Vickers, Rockwell and Leeb), available at the University of Canterbury, were used. Vickers and Rockwell workbench machines are based on the static indentation method, whereas the Leeb hardness machine, which is a portable device, is based on the dynamic (rebound) method. The Leeb hardness device has the big advantage that it can be used on site, and consequently the testing invasiveness is reduced. By contrast, the Vickers and Rockwell methods require the rebars to be brought into the laboratory for testing.

Grade 300E steel rebars were pre-strained in tension up to different strain limits and ten hardness measurements were carried out on the samples' surfaces. Vickers, Leeb and Rockwell hardness readings versus pre-strain results were fitted with power-law curves. The near-zero

exponents for the Rockwell (n = 0.064) and the Leeb (n = 0.007) hardness power-law curves showed the limited ability of these hardness method to detect 0.02 mm/mm differences in pre-strain, compared to Vickers (n > 0.1). Furthermore, the coefficient of determination (R^2) for the Leeb hardness curve was only 0.18, compared with $R^2 = 0.99$ obtained from the Vickers hardness results. For the strain range of interest (2% to 10% pre-strain), the Vickers hardness testing technique provided the most accurate hardness measurements, and was selected as the hardness testing methodology.

Surface-preparation procedure

The surface preparation for the hardness-testing procedure was based on the methodology selected. Vickers testing can be accurately conducted only on samples of metals with a flat-surface. Moreover, to avoid tilting problems during testing, two parallel surfaces needed to be machined. This is a limitation of the method that, at this stage, cannot be overcome. The geometry of the steel rebars must be altered irreversibly.

A comparison was conducted between smooth-ground and polished-surface finishes. The smooth-ground finish was achieved by grinding the metal's surface sequentially with silicon carbide grinding paper from 180 to 600 grit. An extra step, using 9-micron diamond paste was performed to achieve the polished finish. Vickers hardness readings were obtained by optically measuring, with the aid of a microscope, the diagonal length of the pyramidal indentation impression. The indentation vertices could be more easily identified in the polished specimen than in the smooth-ground. It is therefore recommended to perform the extra polishing step to accurately measure the indentation diagonals during the Vickers testing.

Vickers hardness tests, conducted on a 2-mm by 2-mm grid arrangement along the longitudinal section of pre-strained bars, showed that localised strain at the ribs' roots affects the hardness

measurements. A non-constant strain profile was observed; hardness increased from the average hardness by 4% between the ribs and decreased by 5% below them. It is therefore suggested that hardness indentations are performed at a distance from the rebars' surface of approximately 25% of the bar diameter. The amount of material to remove, during the machining phase, can be easily determined. For example, for a rebar 28 mm in diameter, at least 7 mm of surface material must be removed in addition to the steel ribs. It is also recommended that the longitudinal hardness measurements be conducted along the rebar centreline.

Strain range of interest

The strain range of interest was selected by considering the following:

- The Vickers hardness of the as-received steel material must always be included as a benchmark (hardness baseline).
- In the elastic range, no increase in hardness can be observed, because atomic bonds are only elastically deformed and no dislocation motion (plastic deformation) occurs; therefore, any hardness measurement conducted on specimens pre-strained only elastically is not relevant.
- In the discontinuous yield-strain range (approx. 0.015 mm/mm to 0.020 mm/mm for Grade 300E), plastic strain does not occur uniformly over the entire gauge length of the sample. Plastic deformation concentrates at discrete locations known as Lüders bands (dislocation lines). In these regions, hardness is higher than in those that remained elastic; therefore, although pre-strain limits within this range cause plastic deformation, this is localised. As a consequence, because hardness measurements in the deformed regions will be higher than in the undeformed regions, the hardness standard deviation (SD) of specimens pre-

strained below ~0.020 mm/mm is generally twice as high as the SD of specimens pre-strained above ~0.020 mm/mm.

- The residual strain capacity of specimens machined from Grade 300E and 500E and pre-strained up to 0.10 mm/mm is below 0.05 mm/mm (and in some cases, for historical steel grade, near 0 mm/mm); that is well below the limits set by the current steel reinforcing standards AS/NZS 4671:2001. Therefore, it might not be relevant to correlate the hardness to pre-strain limits higher than 0.10 mm/mm.

In conclusion, to develop the hardness versus pre-strain and residual strain calibration curves, it is recommended that a 0.02 mm/mm to 0.10 mm/mm strain range of interest be considered. The hardness baseline must always be included as a benchmark. The strain limits adopted can be either: 0.02, 0.03, 0.04, 0.05, and 0.10 mm/mm, or 0.02, 0.04, 0.06, 0.08, and 0.10 mm/mm.

Based on the considerations provided above, the standard method to derive the calibration curves was established and applied to a number of steel grades obtained from a local manufacturer, or to rebars extracted from Christchurch buildings. The curves are obtained by measuring the Vickers hardness on samples pre-strained (and aged) to the limits mentioned above. The Vickers hardness is also correlated to the strain at ultimate tensile strength of the pre-strained (and aged samples). For each combination of steel grade and diameter tested, two sets of calibration curves were obtained. For the number of cases studies (12 different steels), the R^2 coefficient was always above 0.85, and in 80% of the cases was higher than 0.90. This confirmed the main hypothesis that a robust correlation between hardness and plastic strain can be developed, with some limitations, however. A unique calibration curve for every steel grade was not derived. Even when the curves were normalised with respect to the hardness baseline, the hardening behaviour, different for each steel, did not allow the determination of a generic calibration curve. A unique calibration curve

applicable to any steel grade and diameter would allow a significant reduction in the amount of material needing to be removed, hence reducing the cost and testing-time. This variability is explained because hardness varies, not only as function of cold work, but also depending on the chemical composition and the steel microstructure. Therefore, if hardness is employed as a parameter to estimate the plastic deformation and predict the residual ductility of a rebar, it is essential to develop calibration curves for that specific combination of steel grade and diameter. It is recommended that the material used to develop such curves is recovered from a location in the building, near to the rebar(s) under investigation as it could be assumed that the same steel was used.

9.1.2 The effects of the number of cycles on the steel calibration curves

The calibration curves described in Section 9.1.1 are derived from monotonic tests. During earthquakes, reinforcing bars are subjected to cyclic-strain reversal; therefore it is more appropriate to develop calibration curves derived from cyclic tests, or to determine the effects of a pre-identified number of cycles on the curves.

Unmachined steel rebars of 12-mm diameter were used to derive three sets of curves for hardness versus strain, and residual strain capacity versus hardness. The rebars were subjected to three testing load protocols: monotonic, up to 5 cyclic zero-to-tension, and up to 10 zero-to-tension cycles. Limited to the number of cycles applied and the strain amplitude adopted (up to 8%), the results demonstrated that the hardness versus strain calibration was “shifted” up to higher hardness values by only 4 HV_{30}, which corresponds to 2.5% of the original hardness. This increase was probably caused by the cyclic hardening that occurred after the first cycle. By contrast, no effects were observed on the calibration curve for residual strain capacity versus hardness.

The "cyclic" calibration curves were used to estimate the plastic deformation of rebars subjected to pre-identified variable cyclic-strain histories. A 30% improvement was observed in the plastic-strain estimation when the cyclic curve was used instead of the monotonic, whereas no significant improvement in the prediction of the residual ductility was obtained by using the cyclic curve. In conclusion, the additional tests required to obtain the cyclic curves might not be justified if the residual ductility is required.

9.1.3 Effects of strain ageing on steel reinforcement and its implications on the hardness method

Strain ageing causes changes in mechanical properties in steels prone to this phenomenon that have been plastically strained (for example, during a seismic event) and then left to age for a period of time. The most important implications of the method are an increase in hardness and a reduction in ductility. Previous studies conducted on determining the relationship between hardness and strain for structural steel did not take into account the strain-ageing effects (Allington, 2011; Nashid et al., 2014). Experimental tests conducted within this research on strain-ageing-prone steels (for example, NZ-manufactured Grade 300E) confirmed that strain ageing caused an increase in hardness up to 10%, and a 40% reduction approximately in the expected ductility, when compared with the unaged state. The calibration curves for a steel in the aged state differed from those for the unaged state. This implies that if calibration curves for unaged steel are employed to estimate the plastic deformation and predict the residual ductility of aged rebars, the results obtained are not accurate.

Natural and accelerated strain ageing

The changes in mechanical properties caused by strain ageing take place over several months at ambient temperatures. Due to the limited time available to perform the experimental testing, an

"accelerated" method to simulate the long-term strain-ageing effects was required. The method proposed was based on Hundy's relationship (Hundy, 1954): pre-strained specimens must be aged at 100°C, for example in boiling water, for four hours to obtain the same changes of mechanical properties that are expected in a year at 15°C. A one-year-long experiment was conducted on Grade 300E steel to verify this hypothesis. Results showed that the change in mechanical properties can be assumed to be concluded after one year of ageing at 15°C. Furthermore, while for short-term ageing periods the accelerated method overestimates the change in mechanical properties, for long-term ageing periods the effects were similar. Therefore, the accelerated method can (and must) be fully employed in the Vickers hardness method to derive the after-ageing calibration curves for steels prone to strain-ageing.

Experimental tests on NZ-manufactured Grade 500E specimens aged at 100°C demonstrated that this steel grade is not prone to strain ageing: the changes in mechanical properties were negligible (the increase in yield and ultimate tensile strength was below 3%, reduction in ductility was null) due to the presence of 0.107% by mass of vanadium (see Appendix B) in the steel. The calibration curves for unaged and aged states are the same, and consequently the accelerated strain-ageing step might be bypassed.

Strain ageing at temperatures above 200°C

While carbon atoms did not cause any strain-ageing effects at temperatures below 150°C, as demonstrated by the experimental tests conducted on Grade 500E, at higher temperatures, tests on the same steel grade demonstrated that carbon is responsible for the changes in mechanical properties. Tests on Grade 500E samples, aged at 200°C for up to 60 minutes, showed an increase in yield and ultimate tensile strength, and a reduction in ductility. The changes in mechanical properties were proportional to the ageing time. During the life of a building (approx. 50 years),

strain ageing at temperatures above 200°C can occur in very rare events; for example, it can be caused by high temperatures obtained during a fire that follows a severe seismic event.

By contrast, experimental tests on Grade 300E pre-strained rebars aged at 200°C demonstrated that the changes in mechanical properties were concluded after only 15 minutes. Compared with the ageing at 100°C and 15°C, there was no increase in yield strength nor a reduction in ductility; only a limited increase in ultimate strength (below 4%) was observed. Therefore, if testing time is limited, strain-ageing effects can be accelerated even further.

Beside the implications of the hardness method, the strain-ageing phenomenon could potentially modify the hierarchy of strength of a RC structure, because the increase in yield due the combined effects of strain ageing and strain hardening might increase the flexural strength, assuming that proper overstrength factors were not used during the design. Long-term, natural (up to a year) and accelerated (up to 4 hours) strain-ageing tests demonstrated that the increase in yield strength due only to strain ageing is on average approximately 60 MPa and did not depend on the amount of pre-strain. This quantity (60 MPa) must be added to the increase in yield strength due to strain hardening that depends on the amount of pre-strain. In conclusion, further research can be focused on determining the overstrength factors that account for both strain ageing and strain hardening.

9.1.4 Application of the "hardness method" to RC buildings damaged during the 2010 and 2011 Canterbury earthquakes

The "Vickers hardness method" was fully developed and applied to a number of cases. It takes place through four different phases:

I. Reinforcing bars that are suspected to be damaged are extracted from the building.

II. Vickers hardness tests are performed throughout the bars' longitudinal length to precisely identify the location and extent of damage to the reinforcement (where hardness is higher than the baseline).

III. If damage is detected, calibration curves of that specific grade and diameter of steel are performed and used to quantify damage and the residual plastic deformation capacity.

IV. Tensile tests of the damaged location are performed and compared with tensile tests of undamaged steel from the same bar.

The Christchurch seismic events showed that, in some cases, only a few large cracks formed in plastic hinges, instead of the expected, uniformly-distributed cracking pattern (Bull, 2013). The hardness method confirmed that plastic deformation and ductility loss occurred only at the crack locations and spread only in the crack neighbourhood. The yield strength at the crack location is increased; however, the ductility is reduced due to strain hardening and strain ageing. If, during the repair stage, the bond between concrete and steel is recovered (for example, with epoxy injection), it is not yet clear if the plastic deformation will concentrate at the same crack location, in a subsequent earthquake, or somewhere else. If the former occurs, then the available ductility will be significant lower than the original. By contrast, if the latter takes place, the overall ductility of the global member might not be affected. Further studies in this topic are required.

The hardness method was developed further: a universal calibration curve was obtained for Grade 300 steels. The universal curve allowed to estimate plastic deformation and residual strain capacity from only three parameters: Vickers hardness baseline, average peak hardness at the damaged location, and ultimate strain of an undamaged region of the same bar. This improvement reduced the test invasiveness, time and costs without compromising the method reliability. Morevoer, a correlation between lower yield strength and Vickers hardness was developed from

342 steel rebars samples locally sourced. This correlation can be used to determine the steel's yield strength at the damaged location.

9.1.5 Low-cycle fatigue behaviour of Grade 300E strain-aged steel reinforcing bars

Earthquakes cause severe tension and compression strain reversals in steel rebars that might lead to low-cycle fatigue (LCF) fracture. The LCF behaviour has been investigated by many researchers and strain–fatigue life equations and curves have been developed (Brown & Kunnath, 2004; Mander et al., 1994). Furthermore, cumulative damage models based on these equations have also been derived to determine the LCF effects of multiple earthquakes on structures (Mander & Rodgers, 2015). Often, multiple seismic events occur several months apart, and strain ageing takes place. In this research, through experimental testing, the reduction of the expected remaining fatigue life was quantified, and fatigue-life equations of strain-aged rebars were proposed. Initially, a benchmark strain versus fatigue-life curve was derived for 12-mm diameter Grade 300E rebars, using "indirect" strain-controlled cyclic tests. Coffin-Manson and Koh-Steven models were used to fit the experimental tests. Further experiments were conducted on precycled (33% and 66% of the original fatigue life) and aged rebars. Fatigue-life comparisons demonstrated that the expected remaining fatigue life is reduced dramatically (on average by approximately 40%). For example, the expected remaining life of rebars precycled at 1% constant-strain amplitude up to 33% of the original fatigue life was reduced from 41 to 25 cycles.

9.2 CONCLUDING REMARKS

The primary objective of this thesis was achieved: a least-invasive method was developed and applied to earthquake-damaged buildings to determine the damage and residual ductility of steel reinforcing bars. Mechanical properties vary in steels, depending on manufacturing methods and chemical composition, even when obtained from a single supplier; therefore, in order to relate hardness to plastic strain and ductility, calibration curves for each combination of steel grade and diameter of the rebars under investigation were developed. For Grade 300 steels, a universal calibration curve was developed. This curve allowed to estimate the plastic deformation experienced by damage rebars and predict their residual strain capacity, based only on the hardness baseline, the hardness at the damage location and the ultimate strain of similar undamaged the rebar. The method can be employed as a support tool for practitioner engineers, owners, and territorial authorities in taking informed decisions on the demolition or repair of damaged RC buildings. This research answered the the community questions: “Have the steel bars been damaged in places corresponding to the concrete cracks?”, “How much plastic deformation have the steel bars undergone?”, and “What is the residual strain capacity of the damaged bars?”

9.2.1 Key findings

- Vickers hardness can provide information about the pre-strain and monotonic residual strain capacity of damaged rebars with the limitations defined in Chapters 3 and 4.
- Static indentation hardness methods, and in particular the Vickers hardness method, are superior to dynamics methods (Leeb hardness) for determining the change in hardness in small-mass metal objects such as rebars.

- Unless it is proved that the steel under investigation is not prone to strain ageing, its effects must be always accounted for to determine the residual ductility of damaged rebars. The strain-ageing accelerated method described in this thesis is recommended.
- Hardness versus strain calibration curves are dependent on the material chemical composition and heat treatment. The universal calibration curve developed for grade 300E provided good predictions. However, whenever it is possible, it is recommended to derive calibration curves for the specific steel grade and diameter under investigation. This will also allow to increase the data base developed in this thesis.
- Due to the limited number of samples collected, universal calibration curves were not obtained for Grade 430 and Grade 500E. Therefore, specific calibration curves should be developed for these steels grades in the case of damage assessment.
- The low-cycle fatigue of rebars is reduced not only due to the number of cycles previously experienced (for example, during an earthquake), but also due to the strain-ageing phenomenon. Therefore, the reduction in fatigue life due to strain ageing of the rebars is recommended in the assessment of the LCF cumulative damage of structures subjected to earthquake sequences. Fatigue-life equations are proposed for pre-cycled and strain-aged Grade 300E steel rebars.
- Cyclic tests demonstrated that the hardness method cannot provide information regarding the fatigue life of damaged rebars; the number of cycles do not significantly affect the steel hardness. It is therefore impossible to discern the exact number of cycles experienced during an earthquake using hardness as a parameter.

9.3 RECOMMENDATIONS FOR FUTURE STUDIES

As demonstrated by the 2010 and 2011 Canterbury earthquakes, and confirmed by the recent Kaikoura earthquake, the residual-capacity assessment of RC buildings damaged during seismic events still remains a priority for New Zealand and other earthquake-prone countries. For example, by 2014, the Canterbury Earthquake Recovery Authority (CERA) completed the demolition of 1,544 Christchurch CBD buildings, at a cost of NZ$117 million. This corresponds to 40% of the total demolitions in the area. The costs were then transferred to building owners and insurance companies, causing a significant economic loss for the local and national community (OAG, 2017). This research has advanced the knowledge regarding techniques to assess the level of damage in the steel reinforcement material; more studies are required, however, to improve the methodology and understand the effects of the steel damaged at a global level, reducing further the uncertainties over the decision between building repair or demolition. For future developments, the residual capacity project should aim to provide engineers, tools and guidelines for assessing the performance of buildings in terms of their initial capacity, for example, comparing displacement, strength, and energy dissipation capacity. These tools should be easily accessible, reliable and low invasive. Moreover, this research has looked only at the damage of steel reinforcement using hardness as the key parameter, alternative techniques (e.g. ultrasonic testing, acoustic emission testing, etc.) should be explored. A final recommendation for long-term future research is to enlarge the scope. Diagnostics technologies and non-destructive testing should be developed or adapted from other fields for testing materials and structures, in the context of earthquake damage.

This chapter is organised in three different sections. In the first section (9.3.1), recommendations are provided to further develop the Vickers hardness method in order to

overcome the limitations highlighted in this thesis and propose suggestions for alternative techniques. In Section **Error! Reference source not found.**, suggestions for the future work at the material level are proposed. In Section 9.3.3, recommendations are provided for future research at the member scale.

9.3.1 Improvements to the Vickers hardness method and alternative techniques

The Vickers hardness method is currently the least invasive, but is still invasive. Future research must be focused on reducing the testing invasiveness; this might be achieved, for example, in the following ways:

- Hardness testing on site is highly desirable, since it will reduce the amount of steel removed from a building. The Leeb hardness portable device available during this research proved to be insufficiently accurate when used on steel reinforcement for several reasons: lack of sensitivity in the hardness range of interest, poor spatial resolution, variable support of the bars, and the surface finish. By contrast, the Vickers hardness method provided reliable results in the laboratory. New research questions that might be asked: “Will the Vickers hardness method be reliable on site?”, “Are the portable Vickers hardness testers available in the industry suitable for testing rebars on site?”, “What is the test protocol for testing on site?” This includes (but is not limited to) defining a procedure to expose the rebars, prepare the bar surface for testing (grinding and polishing), attach the portable device to the concrete element and perform the test. For example, one of portable Vickers hardness tester commercially available is the Through Indenter Viewing (TIV) portable Vickers hardness by General Electric (GE) (https://www.gemeasurement.com/). However, at the time of writing the author has been informed that this device is now out of production and only few of them are still available for purchasing. An alternative option is designing and

manufacturing a custom-made device, however this device must comply with the recognised international standard agencies (e.g. ASTM). Assuming that a suitable portable hardness device is found, another question that can be raised is "Are the hardness readings obtained with the workbench Vickers hardness tester consistent with those obtained with the portable Vickers hardness device?"

Moreover, the universal calibration curve was developed only for low grade steel (i.e. Grade 300). In New Zealand, the high-grade steels used over the years are Grade 380, 430 and 500. As a consequence the following questions require an answer: "Is it possible to derive a universal calibration curve for all the high-grade steels? Or, must a universal curve be developed for each grade?" Calibration curves should be derived also for overseas steel grades and comparisons should be conducted for steels of the similar grades.

- The method proposed in this thesis has looked only to the damage of steel reinforcement. Future works should be oriented to develop diagnostics technologies for detecting damage in other types of structural systems and materials (including steel reinforcement). It is first recommended to conduct an exhaustive literature review of the current state of art of non-destructive techniques (NDT) used in other fields such as aerospace structures and explore the possibility to extend to earthquake-damaged structures. Collaborations with different experts on different disciplines is required. The main questions that future research should answer are: "Is it possible, with the minimal damage, to gather all the information required to assess and repair earthquake-damaged buildings? What are the techniques available? What is the most appropriate for our purposes? What is the level of confidence we have in the information obtained?"

9.3.2 Experimental tests at material level

- In Chapter 4, the effects of the number of cycles was limited to samples subjected to completely reversed cycles tests up to 10 cycles, maximum strain amplitude equal to 0.08 mm/mm). If the loading pattern varies (for example, number of cycles, amplitude and mean strain changes), the monotonic behaviour of the damaged rebars could potentially change. Further experiments are suggested to monitor the effects of large number of cycles on the hardness of rebars and monotonic strain capacity.
- Brown and Kunnath (2004) showed that the LCF life of the rebars depends also on the bar diameter. Due to the load-capability limitation of the tensile machine, the effects of strain ageing on the LCF life were determined only on 12-mm diameter rebars. Therefore, it might be questionable to extend the findings obtained from this research to different steel diameters and grades (historical grades included). Further experimental testing on different steel bar diameters is required.
- In structures such as bridges and offshore constructions, the high-cycle fatigue (HCF) of rebars might be a problem (Surajit Kumar et al., 2014; Tilly, 1979). In these structures, previous earthquakes might have caused inelastic deformation and (later) strain ageing of the steel rebars. The level of stress in members subjected to HCF is sufficiently low that yielding does not occur. Moreover, the yielding strength has increased due to the combination of strain hardening and ageing. Therefore, whereas the strain–ageing phenomenon causes an LCF fatigue-life loss, its effects on the HCF life is unknown and might be different. Further experimental studies must be conducted to determine if this phenomenon also has detrimental effects on the HCF life of rebars.

9.3.3 Experimental studies at member level

Future studies must also be conducted at member levels. Suggested work includes:

- Vickers hardness tests on earthquake-damaged rebars showed that hardness increased over a specific length, defined as "damage length". Systematic experimental tests on RC specimens (beams, columns, wall) are recommended in order to correlate the damage length to the residual crack width, and, if possible, to the de-bonding length.
- Applications of the Vickers hardness method demonstrated that the loss in ductility and increase in yield strength occurred only in localised steel regions, and were most likely at the crack location. Repair techniques might recover the bond between steel and concrete, but the steel damage scenario expected in subsequent earthquakes is still unknown: "Will the crack re-open at the same location?", "Will the steel strain localise in the same region?" or, "Because strain hardening and strain-ageing effects increase the yield strength, is a new cracking pattern expected and will strain localise somewhere else?" Future experimental studies must focus on answering these questions. For example, a sufficient number of RC beams must be tested to provide statistical evidence. The beams will initially be subjected to a cyclic loading protocol (static or dynamic) that causes plastic deformation at the crack locations; then the beams are left to age before repairing the cracks with epoxy injection. The beams are then cyclically retested. Cracking patterns and the strain profile must be monitored during the tests.

9.4 REFERENCES

Allington, C. (2011). *Materials testing in buildings of interest. Gallery Apartments, Westpac centre, IRD building.* (Report 107267-1 (v1.1) prepared for royal commission). Retrieved from HolmesSolution, Christchurch:

Brown, J., & Kunnath, S. K. (2004). Low-cycle fatigue failure of reinforcing steel bars. *ACI materials journal, 101*(6).

Bull, D. K. (2013). Earthquakes and the effects on structures: Some of the lessons learnt. *Australian Journal of Structural Engineering, 14*(2), 145-165.

Dieter, G. E. (1976). *Mechanical metallurgy* (Vol. 3): McGraw-Hill New York.

Hundy, B. B. (1954). Accelerated Strain Ageing of Mild Steel. *Journal of The Iron and Steel Institute, 178.*

Mander, J., Panthaki, F., & Kasalanati, A. (1994). Low-cycle fatigue behavior of reinforcing steel. *Journal of Materials in Civil Engineering, 6*(4), 453-468.

Mander, J., & Rodgers, G. (2015). *Analysis of low cycle fatigue effects on structures due to the 2010-2011 Canterbury Earthquake Sequence.* Paper presented at the Tenth Pacific Conference on Earthquake Engineering, Sydney, Australia.

Nashid, H., Ferguson, W. G., Clifton, C., Hodgson, M., Battley, M., Seal, C., & Choi, J. H. (2014). Non-destructive method to investigate the hardness-plastic strain relationship in cyclically deformed steel structural steel elements. *Bulletin of the New Zealand Society for Earthquake Engineering, 47*(3), 181-189.

Office of the Auditor General. (2017). *Canterbury Earthquake Recovery Authority: Assessing its effectiveness and efficiency*. Retrieved from http://www.oag.govt.nz/2017/cera/docs/cera.pdf

Standards Australia and New Zealand. (2001). AS/NZS 4671:2001 *4671:2001 Steel reinforcing materials.* Wellington, New Zealand.

Surajit Kumar, P., Pritam Kumar, R., Debdulal, D., Sanjay, C., & Saurabh, K. (2014). High and low cycle fatigue performance comparison between micro-alloyed and TMT rebar. *Construction and Building Materials, 54*, 170-179.

Tabor, D. (1951). *The hardness of metals*: Oxford University Press.

Tilly, G. P. (1979). Fatigue of steel reinforcement bars in concrete: a review *Fatigue & Fracture of Engineering Materials & Structures, 2*(3), 251-268.

A APPENDIX: TABLES FROM HISTORICAL STEEL REINFORCEMENT MATERIAL STANDARDS

In this section, a summary of mechanical properties and bar sizes prescribed by the historical New Zealand steel reinforcement codes is presented. It is intended to be used as a reference when the assessment of existing reinforced concrete building is required.

The list of tables is reported below:

Table A-1 Mechanical properties of steel reinforcement bars– pre-1960s

Code / Steel Property	NZS 197 – 1949 (BS 785 – 1938)			
Type of steel	Plain round bar *Mild steel (MS)* *Medium tensile (MT)* *High tensile (HT)*			
Yielding Stress	*Bar size (diameter)*	*MS*	*MT*	*HT*
	Up to 1 inch	Not Specified	19.5 tsi (≈270 MPa)	23.0 tsi (≈317 MPa)
	Over 1 to 1½ inch		18.5 tsi (≈255 MPa)	22.0 tsi (≈303 MPa)
	Over 1½ to 2 inch		17.5 tsi (≈241 MPa)	21.0 tsi (≈290 MPa)
	Over 2 to 2½ inch		16.5 tsi (≈227 MPa)	20.0 tsi (≈275 MPa)
	Over 2½ to 3 inch		16.5 tsi (≈227 MPa)	19.0 tsi (≈262 MPa)
Tensile Strength		≥ 28 tsi (≈ 386 MPa)	≥ 33 tsi (≈ 455 MPa)	≥ 37 tsi (≈ 510 MPa)
		≤ 33 tsi (≈ 455 MPa)	≤ 38 tsi (≈ 524 MPa)	≤ 43 tsi (≈ 593 MPa)
Elongation at fracture (%)	Up to 1 inch	≥ 20(1)	≥ 18(1)	≥ 18(1)
	Over 1 to 1½ inch	≥ 16(1)	≥ 14(1)	≥ 14(1)
	Under ⅜ inch	≥ 24(2)	≥ 22(2)	≥ 22(2)

Note:

psi pounds per square inch

tsi tons per square inch

(1) measured on a minimum 8 diameters gauge length

(2) measured on a minimum 4 diameters gauge length

Table A-2 Mechanical properties of steel reinforcement bars between 1960s and mid-1970s

Steel / Code / Parameters	NZSS 1693:1962	NZSS 1879:1964	NZ 3423P:1972
Type of steel	Deformed steel bar	HY60 Deformed	Plain round bar
Yielding Stress	33000 psi (≈ 227 MPa)	60000 psi (≈ 415 MPa)	40000 psi (≈ 275 MPa)
Tensile Strength	≥ 55000 psi (≈ 380 MPa) ≤ 75000 psi (≈ 517 MPa)	1.2 yield stress but not less than 90000 psi (≈ 620 MPa)	≥ 55000 psi (≈ 380 MPa) ≤ 75000 psi (≈ 517 MPa)
Elongation at fracture (%)	≥ 20(1)	≥ 12(1)	≥ 20(1)
Note: (1) Measured on a 5 diameters gauge length			

Table A-3 Mechanical properties of steel reinforcement bars – from 1973 to 2001

Steel / Code / Parameters	NZ 3402P:1973		NZS 3402:1989	
Type of steel	Grade 275	Grade 380	Grade 300	Grade 430
Yielding Stress (MPa) **Lower** **Upper**	275	380	 ≥ 275(min) (300(k)) ≤ 380(max) (355(k))	 ≥ 410(min) (430(k)) ≤ 520(max) (500(k))
Tensile Strength (MPa)	≥ 380 ≤ 520	≥ 570*	Not specified	
Ratio R_m/R_e (TS/YS)	Not specified		$1.15 \leq \frac{TS}{YS} \leq 1.50$	$1.15 \leq \frac{TS}{YS} \leq 1.40$
Elongation at maximum force A_{gt} (%)	Not specified		Not specified	
Elongation at fracture (%)	≥ 20(1)	≥ 12(1)	≥ 20(1)	≥ 12(1)
Note: * But not less than 1.2 times the actual yield stress (1) measured on a minimum 4 diameters gauge length (k) characteristic value *TS* Tensile strength *YS* Yield stress R_m value of maximum tensile strength (determined from a single tensile test in accordance with AS 1391) R_e value of the yield stress or 0.2% proof stress (determined from a single tensile test in accordance with AS 1391)				

Table A-4 Mechanical properties of steel reinforcement bars – from 2001

Steel / Code / Parameters	AS/NZS 4671:2001	
Type of steel	Grade 300	Grade 500
Yielding Stress (MPa)		
Lower	$\geq$ 300(k)	$\geq$ 500(k)
Upper	$\leq$ 380(k)	$\leq$ 600(k)
Tensile Strength (MPa)	Not specified	
Ratio Rm/Re (TS/YS)	$1.15 \leq \frac{R_m}{R_e} \leq 1.50$	$1.15 \leq \frac{R_m}{R_e} \leq 1.40$
Elongation at maximum force Agt (%)	$\geq$ 15	$\geq$ 10
Elongation at fracture (%)	Not specified	

Note:

(k) characteristic value

R_m value of maximum tensile strength (determined from a single tensile test in accordance with AS 1391)

R_e value of the yield stress or 0.2% proof stress (determined from a single tensile test in accordance with AS 1391)

Table A-5 Diameters of steel reinforcement bars – before the mid-1970s.

NZS 1693:1962		NZS 1879:1964		NZS 3423P:1972	
Bar designation	**d inch (mm)**	**Bar designation**	**d inch (mm)**	**Bar designation**	**d inch (mm)**
3	3/8 (9.525)	3	3/8 (9.525)		3/8 (9.525)
4	1/2 (12.7)	4	1/2 (12.7)		1/2 (12.7)
5	5/8 (15.875)	5	5/8 (15.875)		5/8 (15.875)
6	3/4 (19.05)	6	3/4 (19.05)		3/4 (19.05)
7	7/8 (22.225)	7	7/8 (22.225)		7/8 (22.225)
8	1.000 (25.4)	8	1.000 (25.4)		1.000 (25.4)
9	1 1/8 (28.575)	9	1 1/8 (28.575)		1 1/8 (28.575)
10	1 1/4 (31. 75)	10	1 1/4 (31. 75)		1 1/4 (31. 75)
11	1 3/8 (34.925)	11	1 3/8 (34.925)		1 3/8 (34.925)
12*	1 1/2*(38.1)	12*	1 1/2*(38.1)		1 1/2(38.1)
					2 (50.80)

* Introduced in 1970

Table A-6 Diameters of steel reinforcement bars - from mid-1970s onward

NZ 3402P:1973 (Stage 1)				NZ 3402P:1973 (Stage 2)			NZS 3402:1989			AS/NZS 4671:2001		
Bar designation		**d (inch)**	**d (mm)**	**Bar designation**		**d (mm)**	**Bar designation**		**d (mm)**	**Bar designation**		**d (mm)**
R10	D10		10	R10	D10	10	R6	D6	6	R6	D6	6
R13	D13	½	12.7	R12	D12	12	R8	D8	8	R10	D10	10
R16	D16		16	R16	D16	16	R10	D10	10	R12	D12	12
R20	D20		20	R20	D20	20	R12	D12	12	R16	D16	16
R22	D22	7/8	22.23	R24	D24	24	R16	D16	16	R20	D20	20
R25	D25		25.4	R28	D28	28	R20	D20	20	R25	D25	25
R28	D28		28	R32	D32	32	R24	D24	24	R32	D32	32
R32	D32		32	R40	D40	40	R28	D28	28	R40	D40	40
R38	D38	1 ½	38.1				R32	D32	32			
							R40	D40	40			

B APPENDIX: STEEL CERTIFICATE OF TEST

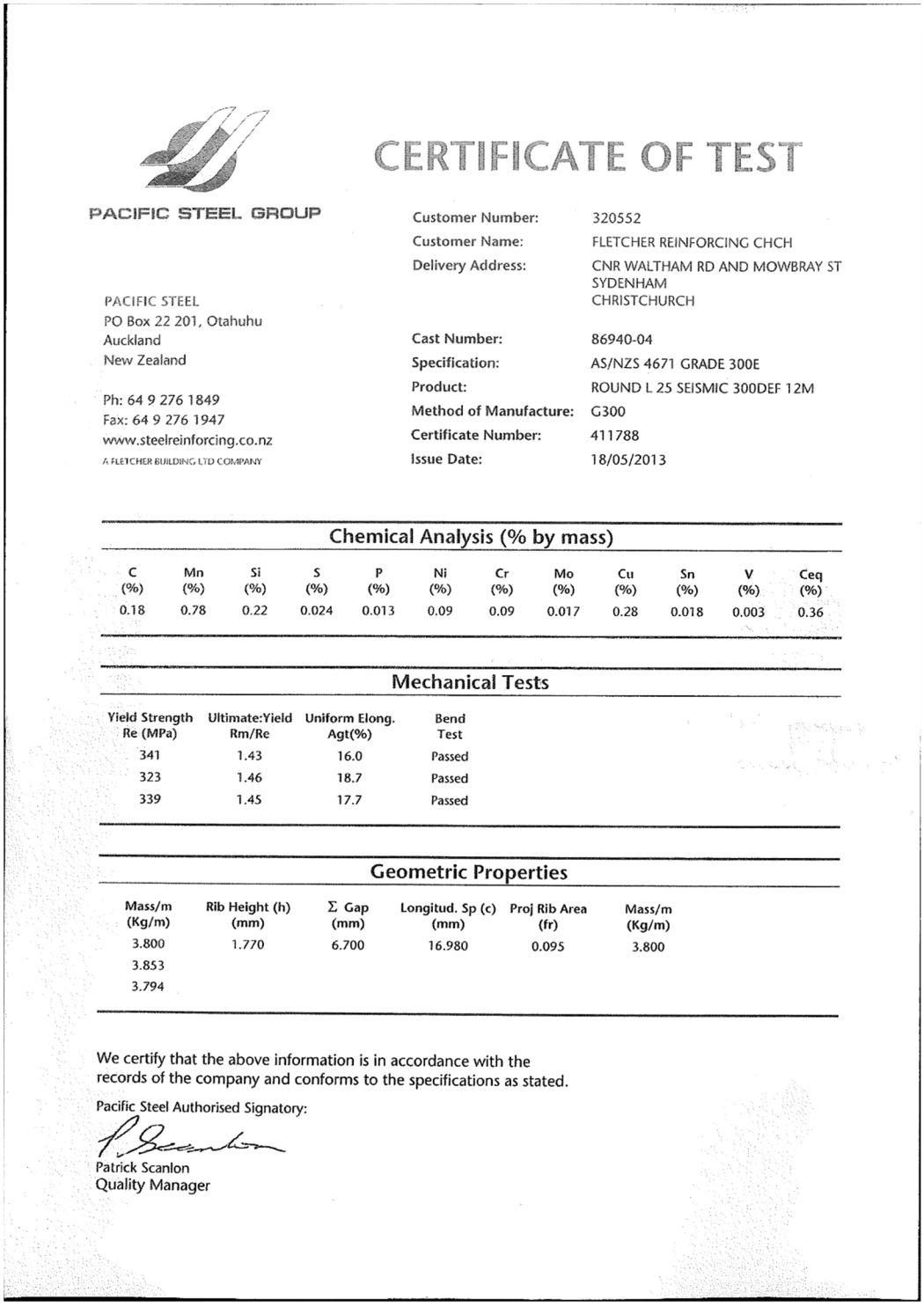

PACIFIC STEEL GROUP

CERTIFICATE OF TEST

PACIFIC STEEL
PO Box 22 201, Otahuhu
Auckland
New Zealand

Ph: 64 9 276 1849
Fax: 64 9 276 1947
www.steelreinforcing.co.nz
A FLETCHER BUILDING LTD COMPANY

Customer Number:	320552
Customer Name:	FLETCHER REINFORCING CHCH
Delivery Address:	CNR WALTHAM RD AND MOWBRAY ST SYDENHAM CHRISTCHURCH
Cast Number:	86940-04
Specification:	AS/NZS 4671 GRADE 300E
Product:	ROUND L 25 SEISMIC 300DEF 12M
Method of Manufacture:	G300
Certificate Number:	411788
Issue Date:	18/05/2013

Chemical Analysis (% by mass)

C (%)	Mn (%)	Si (%)	S (%)	P (%)	Ni (%)	Cr (%)	Mo (%)	Cu (%)	Sn (%)	V (%)	Ceq (%)
0.18	0.78	0.22	0.024	0.013	0.09	0.09	0.017	0.28	0.018	0.003	0.36

Mechanical Tests

Yield Strength Re (MPa)	Ultimate:Yield Rm/Re	Uniform Elong. Agt(%)	Bend Test
341	1.43	16.0	Passed
323	1.46	18.7	Passed
339	1.45	17.7	Passed

Geometric Properties

Mass/m (Kg/m)	Rib Height (h) (mm)	Σ Gap (mm)	Longitud. Sp (c) (mm)	Proj Rib Area (fr)	Mass/m (Kg/m)
3.800	1.770	6.700	16.980	0.095	3.800
3.853					
3.794					

We certify that the above information is in accordance with the records of the company and conforms to the specifications as stated.

Pacific Steel Authorised Signatory:

Patrick Scanlon
Quality Manager

Fig. B-1 Certificate of origin of diameter 25 mm Grade 300E steel reinforcing bars.

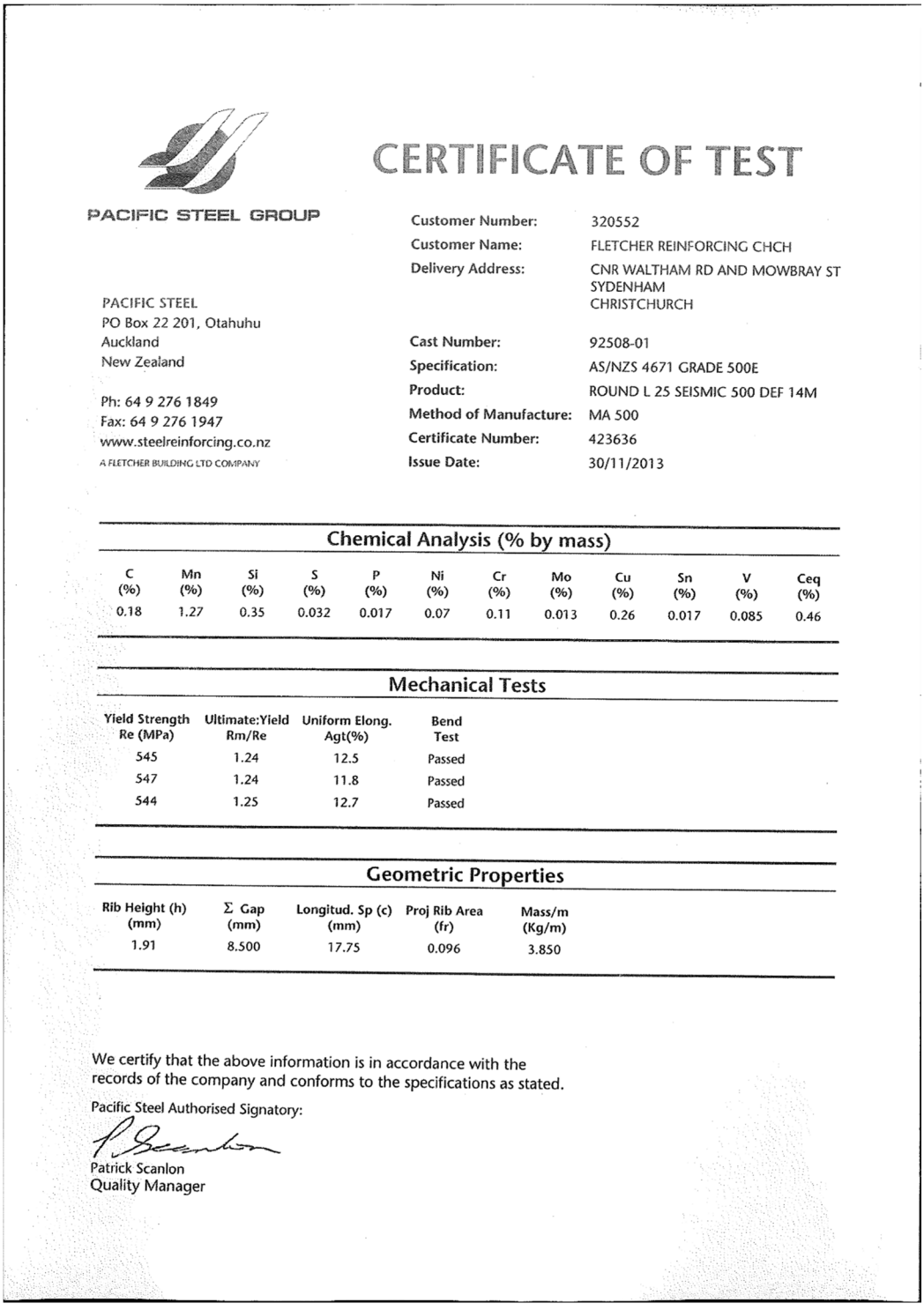

PACIFIC STEEL GROUP

CERTIFICATE OF TEST

PACIFIC STEEL
PO Box 22 201, Otahuhu
Auckland
New Zealand

Ph: 64 9 276 1849
Fax: 64 9 276 1947
www.steelreinforcing.co.nz
A FLETCHER BUILDING LTD COMPANY

Customer Number:	320552
Customer Name:	FLETCHER REINFORCING CHCH
Delivery Address:	CNR WALTHAM RD AND MOWBRAY ST SYDENHAM CHRISTCHURCH
Cast Number:	92508-01
Specification:	AS/NZS 4671 GRADE 500E
Product:	ROUND L 25 SEISMIC 500 DEF 14M
Method of Manufacture:	MA 500
Certificate Number:	423636
Issue Date:	30/11/2013

Chemical Analysis (% by mass)

C (%)	Mn (%)	Si (%)	S (%)	P (%)	Ni (%)	Cr (%)	Mo (%)	Cu (%)	Sn (%)	V (%)	Ceq (%)
0.18	1.27	0.35	0.032	0.017	0.07	0.11	0.013	0.26	0.017	0.085	0.46

Mechanical Tests

Yield Strength Re (MPa)	Ultimate:Yield Rm/Re	Uniform Elong. Agt(%)	Bend Test
545	1.24	12.5	Passed
547	1.24	11.8	Passed
544	1.25	12.7	Passed

Geometric Properties

Rib Height (h) (mm)	Σ Gap (mm)	Longitud. Sp (c) (mm)	Proj Rib Area (fr)	Mass/m (Kg/m)
1.91	8.500	17.75	0.096	3.850

We certify that the above information is in accordance with the records of the company and conforms to the specifications as stated.

Pacific Steel Authorised Signatory:

Patrick Scanlon
Quality Manager

Fig. B-2 Certificate of origin of diameter 25 mm Grade 500E steel reinforcing bars.

PACIFIC STEEL
CERTAIN STRENGTH

259 James Fletcher Drive.
PO Box 22 201, Otahuhu
Auckland 1640, New Zealand

T. +64 9 276 1849
F. +64 9 270 4282
www.pacificsteel.co.nz

CERTIFICATE OF TEST

Cast Number:	937152-02
Specification:	AS/NZS 4671 D300E
Product:	ROUND S 12 MM
Certificate Number:	937152-02
Test Date:	01/03/2016
Mass of Test Unit:	00000000000028t

Chemical Analysis (%by mass):

C (%)	Mn (%)	Si (%)	S (%)	P (%)	Ni (%)	Cr (%)	Mo (%)	Cu (%)	Sn (%)	V (%)	Ceq (%)
0.10	0.50	0.14	0.013	0.012	0.02	0.03	0.000	0.01	0.003	0.040	0.20

Mechanical Tests:

Yield Strength Re (MPa)	Ultimate:Yield Rm/Re	Uniform Elong. Agt(%)	Bend Test	Rev. bend Test
361	1.19	16.1	Passed	Passed
345	1.24	16.0	Passed	Passed
345	1.24	15.8	Passed	Passed

Geometric Properties:

Rib Height h (mm)	Sum Gap (mm)	Longitud. Sp c (mm)	Proj Rib Area fr	Mass/m (Kg/m)
0.66	5.100	7.96	0.074	0.880

I certify that the above information is in accordance with the records of the company and conforms to the specifications as stated.

Pacific Steel Authorised Signatory:

Patrick Scanlon, Quality Manager

SEISMICMA A PACIFIC STEEL PRODUCT | WIREMARK NEW ZEALAND MADE BY PACIFIC STEEL

Fig. B-3 Certificate of origin of diameter 12 mm Grade 300E steel reinforcing bars.

PACIFIC STEEL
CERTAIN STRENGTH

259 James Fletcher Drive.
PO Box 22 201, Otahuhu
Auckland 1640, New Zealand

T. +64 9 276 1849
F. +64 9 270 4282
www.pacificsteel.co.nz

CERTIFICATE OF TEST

Cast Number:	91974-03
Specification:	AS/NZS 4671 D300E
Product:	ROUND L 25 MM
Certificate Number:	91974-03
Test Date:	17/03/2014
Mass of Test Unit:	00000000000001t

Chemical Analysis (% by mass):

C (%)	Mn (%)	Si (%)	S (%)	P (%)	Ni (%)	Cr (%)	Mo (%)	Cu (%)	Sn (%)	V (%)	Ceq (%)
0.18	0.85	0.24	0.030	0.016	0.08	0.10	0.013	0.24	0.018	0.003	0.37

Mechanical Tests:

Yield Strength Re (MPa)	Ultimate:Yield Rm/Re	Uniform Elong. Agt(%)	Bend Test
335	1.49	15.9	Passed
337	1.48	19.2	Passed
323	1.49	18.4	Passed

Geometric Properties:

Rib Height h (mm)	Sum Gap (mm)	Longitud. Sp c (mm)	Proj Rib Area fr	Mass/m (Kg/m)
1.70	7.900	15.85	0.096	3.820

Bar Mark:

I certify that the above information is in accordance with the records of the company and conforms to the specifications as stated.

Pacific Steel Authorised Signatory:

Patrick Scanlon, Quality Manager

SEISMICMA A PACIFIC STEEL PRODUCT | WIREMARK® NEW ZEALAND MADE BY PACIFIC STEEL

Fig. B-4 Certificate of origin of diameter 25 mm Grade 300E steel reinforcing bars.

PACIFIC STEEL
CERTAIN STRENGTH

259 James Fletcher Drive.
PO Box 22 201, Otahuhu
Auckland 1640, New Zealand

T. +64 9 276 1849
F. +64 9 270 4282
www.pacificsteel.co.nz

CERTIFICATE OF TEST

Cast Number:	99304-01
Specification:	AS/NZS 4671 D500E
Product:	ROUND L 25 MM
Certificate Number:	99304-01
Test Date:	07/02/2015
Mass of Test Unit:	00000000000050t

Chemical Analysis (% by mass):

C (%)	Mn (%)	Si (%)	S (%)	P (%)	Ni (%)	Cr (%)	Mo (%)	Cu (%)	Sn (%)	V (%)	Ceq (%)
0.18	1.32	0.32	0.024	0.013	0.06	0.07	0.009	0.18	0.023	0.107	0.45

Mechanical Tests:

Yield Strength Re (MPa)	Ultimate:Yield Rm/Re	Uniform Elong. Agt(%)	Bend Test
525	1.24	12.0	Passed
527	1.24	11.5	Passed
527	1.24	10.5	Passed

Geometric Properties:

Rib Height h (mm)	Sum Gap (mm)	Longitud. Sp c (mm)	Proj Rib Area fr	Mass/m (Kg/m)
1.72	6.200	16.81	0.094	3.810

Bar Mark:

I certify that the above information is in accordance with the records of the company and conforms to the specifications as stated.

Pacific Steel Authorised Signatory:

Patrick Scanlon, Quality Manager

SEISMIC MA A PACIFIC STEEL PRODUCT | WIREMARK® NEW ZEALAND MADE BY PACIFIC STEEL

Fig. B-5 Certificate of origin of diameter 25 mm Grade 500E steel reinforcing bars.